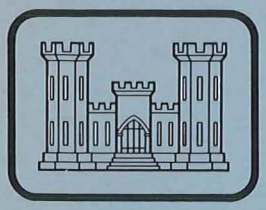

TECHNICAL REPORT GL-79-22

GEOTECHNICAL PROPERTIES OF OIL SHALE RETORTED BY THE PARAHO AND TOSCO PROCESSES

by

Frank C. Townsend, Richard W. Peterson

Geotechnical Laboratory
U. S. Army Engineer Waterways Experiment Station
P. O. Box 631, Vicksburg, Miss. 39180

November 1979
Final Report

Prepared for U. S. Department of Interior, Bureau of Mines
Spokane Mining Research Center
Spokane, Washington 99207

Under Contract No. H0262064

Destroy this report when no longer needed. Do not return it to the originator.

The findings in this report are not to be construed as an official Department of the Army position unless so designated by other authorized documents.

The contents of this report are not to be used for advertising, publication, or promotional purposes. Citation of trade names does not constitute an official endorsement or approval of the use of such commercial products.

Unclassified

SECURITY CLASSIFICATION OF THIS PAGE *(When Data Entered)*

REPORT DOCUMENTATION PAGE		READ INSTRUCTIONS BEFORE COMPLETING FORM
1. REPORT NUMBER Technical Report GL-79-22	2. GOVT ACCESSION NO.	3. RECIPIENT'S CATALOG NUMBER
4. TITLE *(and Subtitle)* GEOTECHNICAL PROPERTIES OF OIL SHALE RETORTED BY THE PARAHO AND TOSCO PROCESSES		5. TYPE OF REPORT & PERIOD COVERED Final report 6. PERFORMING ORG. REPORT NUMBER
7. AUTHOR(s) Frank C. Townsend Richard W. Peterson		8. CONTRACT OR GRANT NUMBER(s) Contract No. H0262064
9. PERFORMING ORGANIZATION NAME AND ADDRESS U. S. Army Engineer Waterways Experiment Station Geotechnical Laboratory P. O. Box 631, Vicksburg, Miss. 39180		10. PROGRAM ELEMENT, PROJECT, TASK AREA & WORK UNIT NUMBERS
11. CONTROLLING OFFICE NAME AND ADDRESS U. S. Department of Interior, Bureau of Mines Spokane Mining Research Center Spokane, Wash. 99207		12. REPORT DATE November 1979 13. NUMBER OF PAGES 272
14. MONITORING AGENCY NAME & ADDRESS*(if different from Controlling Office)*		15. SECURITY CLASS. *(of this report)* Unclassified 15a. DECLASSIFICATION/DOWNGRADING SCHEDULE

16. DISTRIBUTION STATEMENT *(of this Report)*

Approved for public release; distribution unlimited.

17. DISTRIBUTION STATEMENT *(of the abstract entered in Block 20, if different from Report)*

18. SUPPLEMENTARY NOTES

19. KEY WORDS *(Continue on reverse side if necessary and identify by block number)*

Compaction
Compositions
Consolidation
Geotechnical engineering
Oil shales
Shear strength

20. ABSTRACT *(Continue on reverse side if necessary and identify by block number)*

Waste disposal schemes using spent shale in embankments require a thorough knowledge of its geotechnical engineering properties for environmentally safe disposal. In this context, the objective of this laboratory investigation was to determine the physical properties, geotechnical properties, and composition of spent oil shale retorted by the PARAHO and TOSCO processes. Physical properties consisted of mechanical analyses, Atterberg

(Continued)

DD FORM 1 JAN 73 1473 EDITION OF 1 NOV 65 IS OBSOLETE

Unclassified

SECURITY CLASSIFICATION OF THIS PAGE *(When Data Entered)*

20. ABSTRACT (Continued)

limits, and specific gravity determinations. Geotechnical engineering properties were determined by compaction, maximum-minimum density, unconfined compression, triaxial compression, permeability, direct shear, K_o , cyclic triaxial, resonant column, and Los Angeles Abrasion tests. Petrographic, chemical, and scanning electron microscopy analyses were used to determine compositional features. Unprocessed shale is hard and durable and more properly described as a carbonate rock instead of shale. PARAHO is classified as a GP, while TOSCO classifies as an SM. PARAHO requires no moisture for compaction to maximum densities; however, TOSCO does. Retorting causes a loss in durability but creates self-cementing characteristics, which for PARAHO a 3- to 8-fold strength increase was observed, while for TOSCO the increase was 1.5 to 3 folds. The shear strength, compressibility, and dynamic properties of compacted PARAHO are comparable to those for sandy gravels. Compacted PARAHO is semipervious, while compacted TOSCO can be semipervious to impermeable.

FOREWORD

This report was prepared by the U. S. Army Engineer Waterways Experiment Station (WES), Vicksburg, Mississippi, under U. S. Bureau of Mines Contract No. H0262064. The contract was initiated under the Advancing Oil Shale Mining Technology program. It was administered under the technical direction of the Spokane Mining Research Center; Mr. Roger A. Bloomfield was the Technical Project Officer. Mr. David J. Askins was the contract administrator for the Bureau of Mines. This report is a summary of the work recently completed as a part of this contract during the period October 1976 to April 1979. This report was submitted by the authors on 15 May 1979.

Dr. F. C. Townsend, Research Group, Soil Mechanics Division (SMD), Geotechnical Laboratory (GL), was project leader during the study and prepared this report. Mr. R. W. Peterson, Soils Research Center, SMD, supervised and performed the majority of the strength testing program, while Mr. G. P. Hale, SMD, supervised other aspects. The assistance of Messrs. Paul Register, Jacob Major, and Patrick McCaffrey, GL, WES, and Mr. Mel Cohen of the Corps of Engineers South Pacific Division Laboratories are recognized. Mr. Alan Buck, Structures Laboratory, and Dr. D. M. Patrick, GL, performed and supervised, respectively, the chemical and compositional testing. The study was conducted under the general supervision of Mr. C. L. McAnear, Chief, SMD, and Messrs. J. P. Sale and R. G. Ahlvin, Chief and Assistant Chief, respectively, GL.

COL John L. Cannon, CE, and COL Nelson P. Conover, CE, were Directors of WES during the investigation and preparation of this report. Mr. F. R. Brown was Technical Director.

CONTENTS

CONTENTS (Concluded)

LIST OF FIGURES

LIST OF FIGURES (Continued)

LIST OF FIGURES (Continued)

LIST OF FIGURES (Continued)

LIST OF FIGURES (Concluded)

LIST OF TABLES

CHAPTER 1: SUMMARY

Problem Statement

Economic operation of a surface oil shale retort plant involves retorting an estimated 25,000 to 50,000 tons* of raw shale per day, which in turn creates approximately 20,000 to 40,000 tons of spent shale requiring disposal in a structurally and environmentally safe manner. Surface disposal requires information concerning geotechnical properties such as compaction, compressibility, strength, and permeability. To obtain this information and provide the oil shale industry with typical geotechnical properties for planning disposal schemes, the U. S. Bureau of Mines initiated this investigation on PARAHO and TOSCO retorted oil shales.

Scope of Work

The laboratory testing program conducted was divided into three categories: (a) physical properties, (b) engineering properties, and (c) compositional and durability characteristics. The physical properties tests consisted of typical classification tests for identifying and comparing the retorted shales with other materials. The engineering characterization investigated compaction, consolidation, shear strength, self-cementing tendencies, particle breakage and abrasion, and dynamic properties and earthquake resistance. Compositional tests consisted of X-ray diffraction, petrographic and scanning electron microscopy, differential thermal analyses, and chemical analyses.

Pertinent Results and Conclusions

The raw shale material is quite hard and resistant to abrasion and slaking, which is generally uncharacteristic of "shales." However, compositional analyses reveal that it is more properly described as a carbonate rock instead of shale. The PARAHO** retorted shale is classified as a nonplastic poorly graded sandy gravel (GP) with a trace of fines, while the TOSCO** is classified as a silty sand (SM). Both retorted shales are resistant to slaking as the plasticity index (PI) only increased from 0 to 5 after 18 months soaking. This observation is consistent with compositional analyses identifying a lack of clay minerals. Retorting essentially removes most of the hydrocarbons, and neither retorted shale has any indication of bitumen on surfaces, which could possibly have affected engineering results.

The PARAHO and TOSCO can be compacted in the laboratory to dry densities

---

* A table of factors for converting U. S. customary units of measurement to metric (SI) units is presented in Appendix D.

** For brevity, the terms PARAHO and TOSCO will be used throughout this report to refer to spent shale retorted by the PARAHO and TOSCO process.

of 95, 98, and 104 pcf, or 97, 99, and 104 pcf, respectively, for low (60 percent of standard), standard, and modified compaction efforts. In the case of PARAHO, these densities can be achieved without requiring water for compaction. Conversely, optimum water contents to achieve maximum densities of 97, 99, and 104 pcf range from 22 to 17 percent for TOSCO material. The maximum density achieved by laboratory vibration was only 89 pcf; however, Woodward-Clyde Consultants (1976) reported that vibratory compaction is the best method of field compaction and that densities ranged from 98 to 110 percent of standard depending upon lift thickness, number of passes, etc.

The compressibility of compacted PARAHO and TOSCO is comparable to that for dense rockfill or sands. Both PARAHO and TOSCO materials suffer particle breakage during consolidation; both materials experienced breakage values of approximately 28 percent for standard effort densities consolidated to 800-psi normal stress.

Both PARAHO and TOSCO possess self-cementing characteristics, which produce additional strength with time. PARAHO is more reactive than TOSCO exhibiting 3- to 8-fold strength gains over 28 days, while TOSCO only exhibits a 1.5- to 3-fold strength increase for comparable conditions. Cementing reactions under normal conditions are slow for PARAHO with increasing strength gains still indicated after 28 days, while TOSCO gains most of its strength within 3 days following compaction. Based upon chemical and petrographic analyses, the self-cementing characteristic is attributed to reformation of the carbonate minerals that decompose during the retort processing to remove the hydrocarbons (ongoing research on self-cementing properties is being investigated by Colorado School of Mines Research Institute under USBM Contract No. J0285001).

The shear strengths of both PARAHO and TOSCO are comparable to those for sandy gravels with respective effective angles of internal friction ϕ' of 33 deg and 37 to 43 deg, respectively. Despite high compaction efforts, both materials generally exhibit positive pore pressures when sheared. Special interface shear tests indicate the order of decreasing friction angle for raw shale and PARAHO is rubber belting, rusty steel, and stainless steel.

Compacted PARAHO can be considered as semipervious with permeability values of 10^{-3} and 10^{-4} cm/sec depending upon density. The finer grained TOSCO can be considered as semipervious to impermeable with permeability values of 10^{-6} to 10^{-7} cm/sec.

The dynamic characteristics of compacted PARAHO are comparable to those for dense sand and gravel. Cyclic triaxial test results show that at easily obtainable densities, the resistance to seismically induced failure is quite high.

Based upon the previously mentioned results, the PARAHO and TOSCO oil shales can be considered as possessing geotechnical properties characteristic of a GP and SM, respectively. In this context, properly engineered waste embankments of these materials should perform well. When both materials are compacted, they possess good strength values, which are enhanced by their self-cementing tendency. However, both are semipervious when compacted and could not be relied upon to perform as an impermeable barrier to seepage.

Recommendations

Analytical studies investigating typical embankment geometries for disposing spent shale should be conducted utilizing the properties of PARAHO and TOSCO determined in this investigation. Effects of internal drainage, seepage forces, and seismic resistance should be included. Performance and design predictions could subsequently be verified by geotechnical centrifugal models.

CHAPTER 2: INTRODUCTION

The current energy shortage and rapidly diminishing supply of petroleum have created an expanding search for alternative energy sources. These factors have spurred interests in developing oil shale as an energy source. Specifically, oil shale is a fine-grained, usually dark-colored sedimentary rock containing kerogen, a complex organic matter that decomposes upon heating to yield oil. Processing raw shale by heating involves use of surface retorts, in situ retorting, or combinations of both. However, to be commercially feasible and to operate economically, a surface operated oil shale retort plant should process an estimated 25,000 to 50,000 tons of raw shale per day. Most of the currently used surface retort processes produce retorted shale (spent shale, ash, etc.) for disposal at about 80 to 85 percent of total raw weight, which corresponds to approximately 40,000 tons of spent shale per day for a 50,000-ton per day plant or about 30,000 yd^3/day. As an alternative to surface retorting, in situ retorting would obviously reduce the volume of shale requiring surface disposal. However, since 20 percent by volume of the raw shale would be removed during in situ rubblization and subsequently processed in surface retorts, a sizeable volume of retorted shale still would require surface disposal.

Hence, one of the major problem areas of a commercial oil shale operation is the efficient disposal of the spent shale in a structurally and environmentally safe manner. Principal options available for the disposal of retorted oil shale from surface retorts are: (a) filling deep narrow canyons of the mine area with the spent shale, or (b) backfilling the mine cavities with spent shale as the raw shale is removed. Nevertheless, since the shale occupies about 20 percent greater volume after retorting, some of the material will have to be disposed in surface impoundments even if the main scheme is (b). In this context and in view of increasingly more rigid environmental restrictions, a thorough working knowledge of the geotechnical properties is essential. One of the first major studies in this area was "Disposal of Retorted Oil Shale--PARAHO Oil Shale Project" by Woodward-Clyde Consultants (WCC) (1976), which was sponsored by the U. S. Bureau of Mines.

Objectives

The objectives of this study were divided into two tasks: (a) a literature search and (b) material testing. The literature search was restricted to the Green River formation of oil shale in the tri-state area of Colorado (Piceance Basin), Utah (Uinta Basin), and Wyoming (Washakic and Green River Basins) and limited to physical and geotechnical properties. The purpose of the literature review was to provide a data base for comparisons with results obtained in task (b) and is documented by Snethen, et al. (1978) as U. S. Army Engineer Waterways Experiment Station (WES) Miscellaneous Paper S-78-3, "A Review of the Physical and Engineering Properties of Raw and Retorted Oil Shales from the Green River Formation" (Appendix A). The material testing was designed to furnish a complete characterization of the physical, geotechnical, and compositional properties of two retorted oil shales, PARAHO and TOSCO, for use in developing disposal schemes.

Scope

The testing program schematically diagrammed in Figure 1 is divided into four categories: (a) material processing, (b) physical properties, (c) engineering properties, and (d) composition and durability characteristics. The testing program was as follows:

Material processing

The PARAHO, TOSCO, and raw shale were received at the WES in 55-gal drums, from which subsamples were taken from randomly selected drums. Gradation analyses were performed on these subsamples to determine representative gradations and variability of the materials. Processing consisted of separating the material into various sieve fractions to facilitate reconstitution of uniform test specimens.

Physical properties

Physical property tests consisted of gradation analyses, Atterberg limits, and specific gravity.

a. Gradation analyses were performed to ascertain representative gradation and variability of the materials.

b. Atterberg limits were used to evaluate plasticity of PARAHO and TOSCO materials following three disaggregation procedures: (1) standard test on minus No. 40 material, (2) blenderized minus No. 40 material, and (3) material crushed to minus No. 40 sieve and subsequently blenderized. Plasticity of the raw shale was evaluated by the Corps of Engineers (CE) undried, air-dried, and blenderized methods used for shales. Plasticity changes due to inundation were evaluated after 9 and 18 months of inundation.

c. Specific gravity tests were performed on plus No. 4 and minus No. 4 fractions of retorted shale and the plus No. 4 fraction of raw shale.

Engineering properties

Engineering properties testing formed the bulk of the material testing program and was designed to determine the compaction, consolidation, shear strength, and permeability characteristics of compacted retorted shale under a variety of conditions.

a. Compaction tests were performed on PARAHO, TOSCO, and modeled PARAHO using three compaction efforts: (1) 60 percent of standard, (2) standard, and (3) modified. The PARAHO material was compacted in a 12-in.- (30.5-cm-) diam mold, while modeled PARAHO and TOSCO materials were compacted in a conventional 6-in.- (15.2-cm-) diam mold. Post-compaction gradation tests were performed to determine the extent of particle breakage during compaction.

b. Maximum-minimum density determinations were made on PARAHO and modeled PARAHO materials using an 11.0-in.- (28.2-cm-) diam mold and vibrating table.

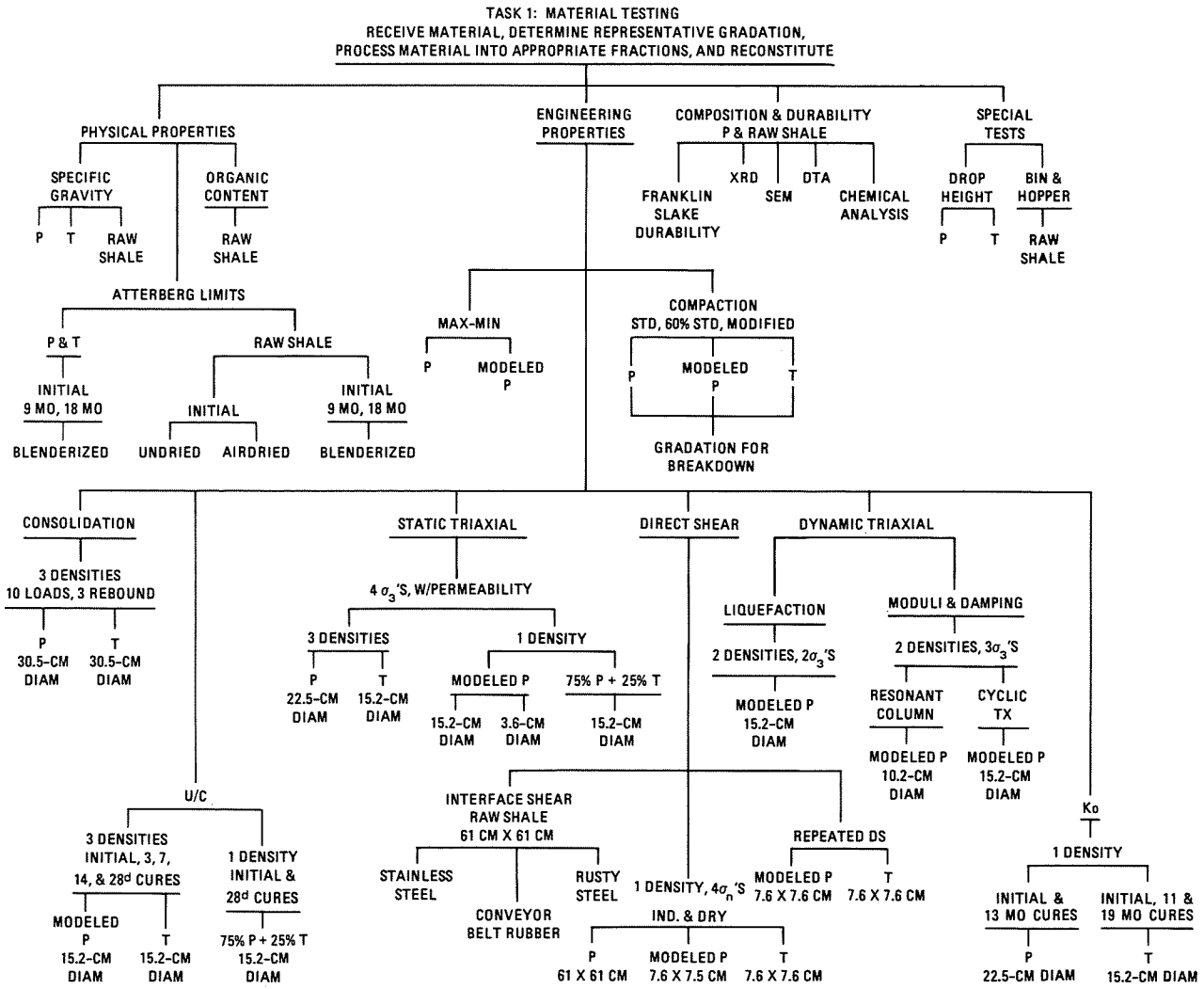

Figure 1. Flow diagram of testing program

c. Consolidation tests were conducted using 12-in.- (30.5-cm-) diam floating ring consolidometer specimens of PARAHO and TOSCO materials compacted to densities comparable to 60 percent of standard, standard, and modified compaction efforts. Maximum vertical stress applied was 800 psi (5.5 MPa), and postconsolidation gradations were determined to evaluate the effects of particle breakage during consolidation.

d. Unconfined compression tests were conducted on 6-in.- (15.2-cm-) diam specimens of modeled PARAHO and TOSCO materials compacted to densities comparable to 60 percent of standard, standard, and modified compaction efforts. Specimens were cured 0, 3, 7, 14, and 28 days to evaluate self-cementing tendencies. In addition, a mixture of 75 percent PARAHO plus 25 percent TOSCO compacted to a density corresponding to standard effort was tested after curing times of 0 and 28 days.

e. Consolidated-undrained $\bar{R}$* triaxial compression tests (with pore pressure measurements) or consolidated-drained S triaxial compression tests were performed on 9- and 6-in.- (22.9- and 15.2-cm-) diam specimens of PARAHO, modeled PARAHO, and TOSCO materials compacted to densities equivalent to 60 percent of standard, standard, and modified efforts. $\bar{R}$ tests were also performed on specimens of PARAHO fines, compacted to a density comparable to standard effort.

f. Permeability determinations were made on triaxial specimens (see e) after back-pressure saturation and consolidation, but prior to shearing.

g. Direct shear tests composed of two series of large-scale tests (2 by 2 by 1 ft (0.6 by 0.6 by 0.3 m)) performed on PARAHO compacted to a density equivalent to standard effort. One series was inundated, while the other was dry. Three interface shear tests were performed using raw shale on stainless steel, rusted steel, and conveyor-belt rubber using the large shear box (2 by 2 by 1 ft (0.6 by 0.6 by 0.3 m)). A series of conventional direct shear tests (3 by 3 in. (7.6 by 7.6 cm)) were performed on TOSCO, both inundated and dry, and on modeled PARAHO, inundated. A series of repeated direct shear tests to determine residual shear strength were also performed on 3- by 3-in. (7.6- by 7.6-cm) specimens of modeled PARAHO and TOSCO.

h. K_o tests were performed on 9-in.- (22.9-cm-) diam and 6-in.- (15.2-cm-) diam specimens of PARAHO and TOSCO, respectively, compacted to a density comparable to standard effort. PARAHO specimens were allowed to cure for 0 and 13 months, while TOSCO specimens cured for 0, 11, and 19 months prior to testing.

i. Cyclic triaxial tests were performed on 6-in.- (15.2-cm-) diam specimens of modeled PARAHO material compacted to densities corresponding to 60 percent relative density (D_r) at effective confining

* For convenience, symbols and unusual abbreviations are listed and defined in the Notation (Appendix E).

pressures of 14.5 and 29.0 psi (100 and 200 kPa) and to 60 percent of standard compaction effort at an effective confining pressure of 14.5 psi (100 kPa).

j. Dynamic properties tests that evaluate shear modulus G, Young's modulus E, and damping ratio λ were performed on 6-in.- (15.2-cm-) diam specimens of modeled PARAHO material using cyclic triaxial equipment. Complementary values of these parameters, but at lower strain levels, were determined on 4-in.- (10.2-cm-) diam specimens using the resonant column apparatus. All test specimens were compacted to densities equivalent to 60 percent of standard or modified compaction effort.

k. Drop height density determinations were made on PARAHO and TOSCO materials dropped from various heights up to 20 ft (6.1 m) to determine densities achieved from a free-fall condition.

l. Los Angeles abrasion tests were performed on various gradations of PARAHO, TOSCO, and raw shale to evaluate the abrasion resistance of these materials.

m. Bin and hopper analysis involved determining the flow rate for raw shale by Jenike and Johanson, Inc., to evaluate possible bin and hopper designs for handling raw shale materials.

Composition and durability characteristics

A series of petrographic and chemical tests were conducted to investigate possible physical and/or chemical changes that occur during curing and could account for the observed self-cementing tendencies. Accordingly, samples of raw shale and 28-day cured and uncured PARAHO were analyzed by the following tests.

a. X-ray diffraction (XRD).

b. Petrographic microscope of thin sections.

c. Scanning electron microscope (SEM).

Differential thermal analyses (DTA) and chemical analyses were performed on raw shale. The durability to alternate cycles of drying and slaking were evaluated on specimens of raw shale and cured and uncured PARAHO by Franklin slake durability tests.

CHAPTER 3: MATERIALS AND TESTING PROGRAM

Materials

The retorted oil shales tested in this program were retorted by the PARAHO and TOSCO processes and are designated as such in this report. In some instances, tests were performed on the raw shale and on mixtures of PARAHO and TOSCO.

PARAHO

The PARAHO retort is located at the Anvil Points Facility located near Rifle, Colorado. The retort shown schematically in Figure 2 basically is a vertical cylindrical vessel into which raw shale is introduced at the top where it is preheated by combustion gases as it travels downward by gravity. Air and recycling gas are injected at midheight and are burned, bringing the oil shale to the operating temperature of 1000° to 1200°F. The oil vapor is collected at tubes near the top. The shale obtained for this study was from the semiworks plant operating in the direct heating mode.

TOSCO

The TOSCO retort operated by the Colony Development Corporation is located in the Parachute Creek area near Rifle, Colorado. The retort shown schematically in Figure 3 is used to process the shale by mixing with preheated balls in a horizontal rotating kiln. This process can take a large amount of finely crushed shale particles, which are crushed further by the action of the balls.

Raw shale

The raw shale was from the Green River Formation and was that used in the PARAHO process.

Specimen Preparation

Generally, specimens were prepared in one of three ways. Compaction specimens were batched in three or five separate portions; each portion corresponded to a compaction lift. The appropriate amount of water was added to each portion of material to obtain the desired water content. Containers of material and water for each lift were then sealed and allowed to mellow for 16 hr before compaction. Specimens were then compacted using either a sliding weight rammer or a mechanical compactor, depending on the size of specimen to be compacted.

The second method, which was used for the large-scale direct shear tests, consisted of placing a lift of air-dried material into the test device. This air-dried material was loaded statically until the material was compressed to the desired dry density. This process was repeated for each lift.

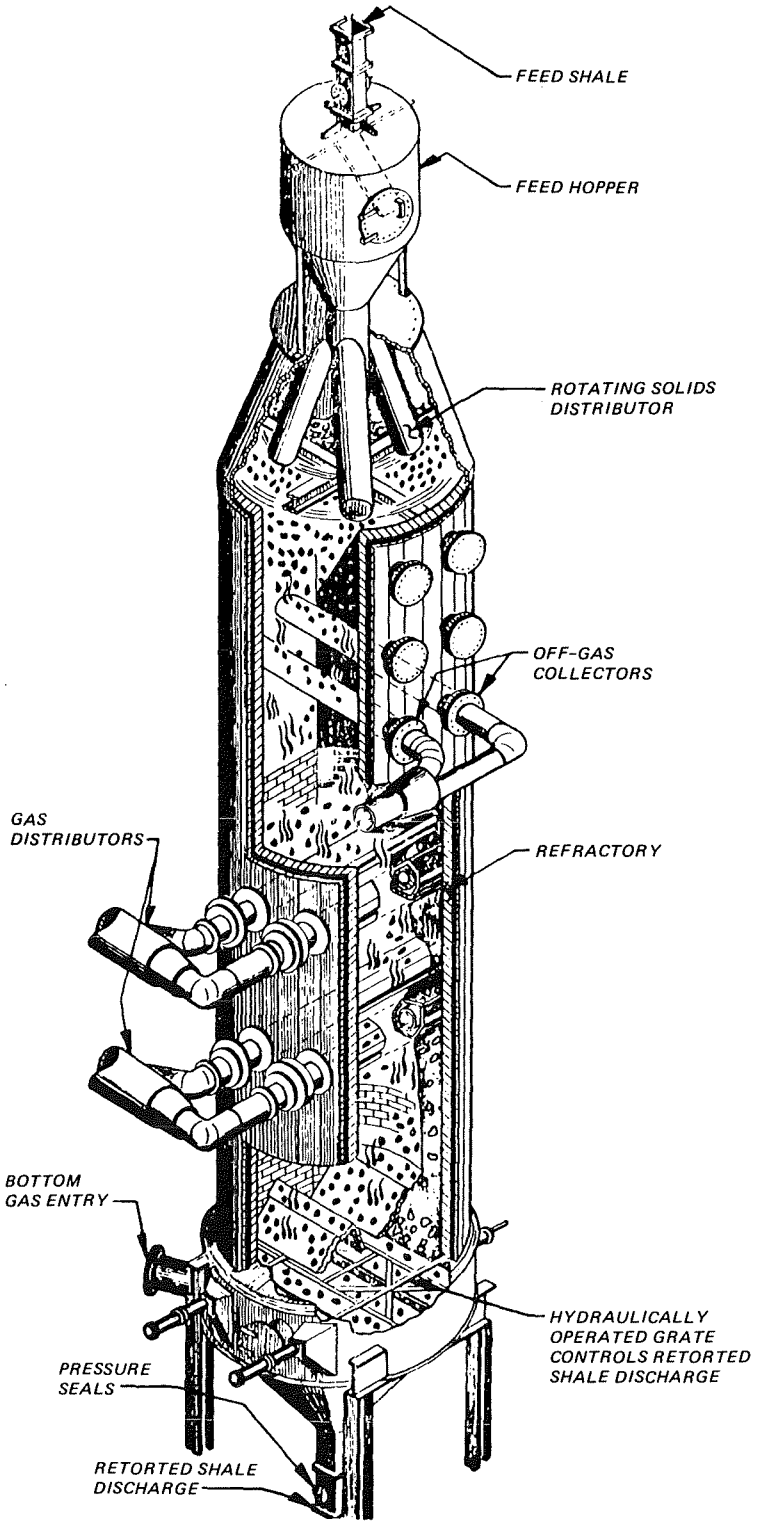

Figure 2. The PARAHO vertical retort (from WCC (1976), USBM Contract No. J0255004)

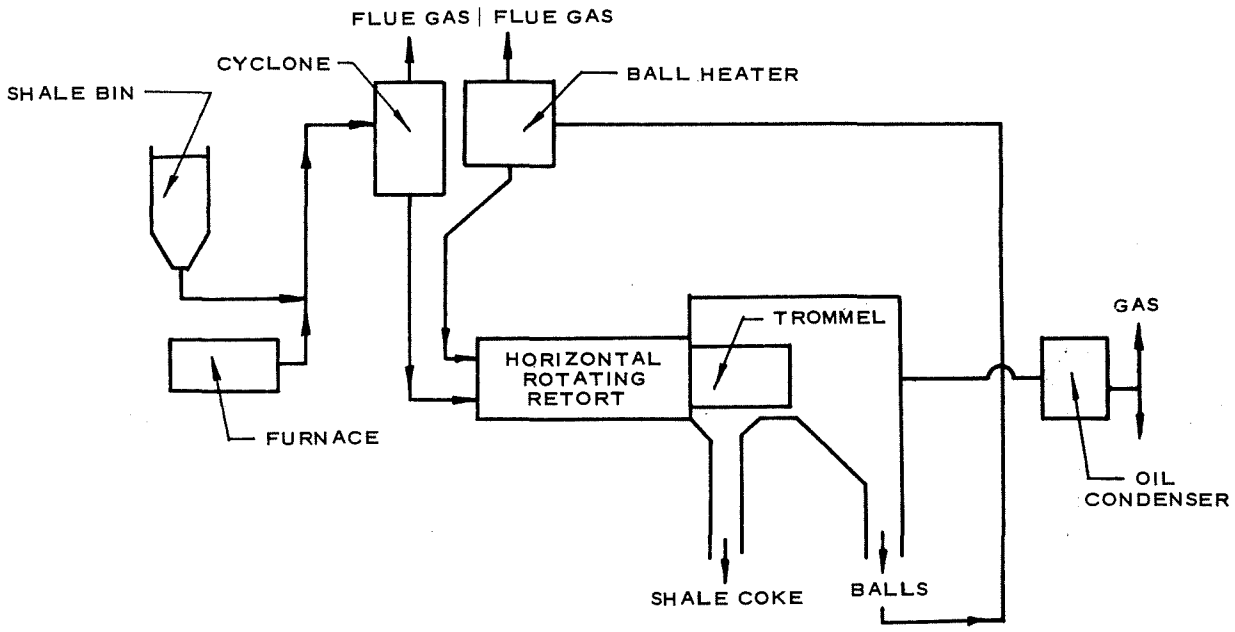

Figure 3. TOSCO process

Although static compaction produced a different structure from the impact compaction used for other strength tests, static compaction was the only practical method of preparing specimens for this device; since the materials were cohesionless, it was believed the effects of compaction method on strength would be small.

For all cylindrical-shaped strength specimens, i.e., unconfined compression, triaxial, resonant column, etc., the specimen preparation was as follows: each lift was batched separately to the appropriate gradation to minimize segregation and variation in gradation between lifts, and the appropriate amount of water added to achieve the desired water content. A procedure of undercompaction, in which each lower lift was compacted less dense than the succeeding lift, was used in an effort to achieve a more uniform density through the specimen. Approximately six to eight equal height lifts were used for each specimen.

The specimens were compacted inside a cardboard tube to the desired density using a sliding weight or a mechanical compactor. If the specimen was to be saturated, the top was sealed with wax; while specimens to be tested unsaturated were sealed with hydrostone. The sealed specimen was then put in a lard can with a small open jar of water and placed inside a 72°F environmental room until tested. Unless otherwise specified, the test specimens were usually cured 3 days prior to testing. This brief curing period was to take advantage of any self-cementing properties that would make the specimens less friable and easier to handle. Prior to testing, the cardboard tubes were cut and peeled away from the specimen.

Since size of laboratory equipment physically limits the maximum particle size of the material to be tested, often it is necessary to model the full-scale gradation. When modeled gradations were required, a scalping and replacing modeling technique was usually employed. This technique consisted

of removing the oversized particles (+3/4 in.(19 mm)) and replacing them with an equal weight of smaller fractions (3/4 in. (19 mm) to No. 4). The other two techniques, which were not used extensively, consisted of constructing a gradation parallel to the full-scale gradation, or merely scalping the oversized particles.

Tests and Test Methods

Material properties tests were performed in accordance to current CE procedures outlined in EM 1110-2-1906, "Laboratory Soil Testing" (Department of Army, 1970), which in most cases is compatible with American Society for Testing and Materials (ASTM) standards (ASTM, 1979). In cases where no standards were available, current research practice at the WES was followed, with necessary modifications to accommodate specific material property requirements.

Tests were conducted primarily on PARAHO and TOSCO retorted oil shale, with nominal testing conducted on mixtures of PARAHO and TOSCO, and on raw shale. The testing program has been presented in Figure 1 and is discussed below:

Physical properties

Gradation. Upon receipt of the PARAHO and TOSCO materials, particle-size distribution tests were conducted on representative samples to establish representative gradation of the materials. These tests were performed according to Appendix V of EM 1110-2-1906, which is compatible with ASTM D422. Wet sieving was performed on one sample each of PARAHO and TOSCO to disaggregate any possible clay lumps.

Specific gravity. Specific gravity analyses were performed on plus No. 4 and minus No. 4 fractions of PARAHO and TOSCO and plus No. 4 fraction of the raw shale. These tests were conducted in accordance with Appendix IV of EM 1110-2-1906.

Atterberg limits. Three procedures were followed to determine plasticity characteristics of the PARAHO, TOSCO, and raw shale; specifically, (a) standard test on minus No. 40 material, (b) blenderized minus No. 40 material, and (c) material crushed to minus No. 40 and then blenderized. These procedures were repeated after inundation for 9 and 18 months. Testing was in accordance with Appendix III of EM 1110-2-1906. Blenderization is a procedure described in this appendix and used for clay shale materials. It consists of one cycle of air-drying and slaking followed by disaggregation in a high-speed blender for 10 min.

Engineering properties

Compaction. Compaction tests were performed using three compaction efforts: (a) 60 percent of standard (7,425 ft-lb/ft^3), standard (12,375 ft-lb/ft^3), and modified (56,250 ft-lb/ft^3). Full-scale tests using a 12-in.-(30.5-cm-) diam mold were performed on PARAHO, while a conventional 6-in.-(15.2-cm-) diam mold was used for modeled PARAHO and TOSCO materials.

These compaction efforts are summarized as follows:

Compaction Effort	Mold Diameter in.	Hammer Weight lb	Drop Height in.	No. Blows/ Layer	No. Layers
60% Standard (7,425 ft-lb/ft^3)	6	5.5	12	34	3
(0.36 MJ/m^3)	12	24.7	24	39	3
Standard (12,375 ft-lb/ft^3)	6	5.5	12	56	3
(0.59 MJ/m^3)	12	24.7	24	65	3
Modified (56,250 ft-lb/ft^3)	6	10.0	18	56	5
(2.69 MJ/m^3)	12	24.7	24	179	5

The procedures for performing conventional 6-in.- (15.2-cm-) diam tests were according to Appendix VI of EM 1110-2-1906, which is similar to ASTM D698 for standard effort and D1557 for modified effort, with the exception that a sliding weight rammer instead of a sleeve rammer was used. The 60 percent of standard effort procedure used was merely the standard effort procedure, scaled to the appropriate number of blows. For modeling of the full-sized PARAHO material, a procedure of scalping the plus No. 3/4-in. (19.0-mm) material and replacing that percentage with an equal percentage of 3/4-in. (19.0-mm) to No. 4 sized material as described in Appendix VIA of EM 1110-2-1906 was generally used.

The large diameter (12-in.(30.5-cm)) compaction tests were performed using a Howard mechanical compactor (Figure 4). This equipment and procedures used for compacting large-diameter specimens are described by Donaghe and Townsend (1973 and 1975). The compactor is equipped with a 24.7-lb (11.2-kg) rammer having a face diameter of 6 in. (15.2 cm); the 12-in.- (30.5-cm-) diam mold is 12 in. (30.5 cm) high. A special harness for suspending the mold and specimen from a forklift was rigged with an electronic load cell sensitive to within 0.1 lb (0.5 kg) to obtain specimen-plus-mold weights. Batches for test specimens were prepared by thoroughly mixing by hand the appropriate air-dried portion (by weight) of material required from each sieve fraction with a measured quantity of water. Each layer was batched separately to minimize any variations in grading between layers. Each batch was stored in an airtight container after mixing and allowed to mellow for a period of at least 16 hr prior to compaction. Since compacted specimens could not be trimmed flush with the top of the mold without substantial disturbance, the specimen volume was determined by measuring from the top of the mold collar to specimen surface. The mold collar volume not occupied by the specimen was determined; hence, the specimen volume was then determined. The specimen was removed from the mold and oven-dried for water content determinations; selected samples were taken to determine particle breakdown during compaction.

Maximum-minimum density determinations. These were performed on PARAHO and modeled PARAHO in an 11.1-in.- (28.2-cm-) diam mold in accordance with Appendix XII of EM 1110-2-1906, which corresponds to ASTM D2049.

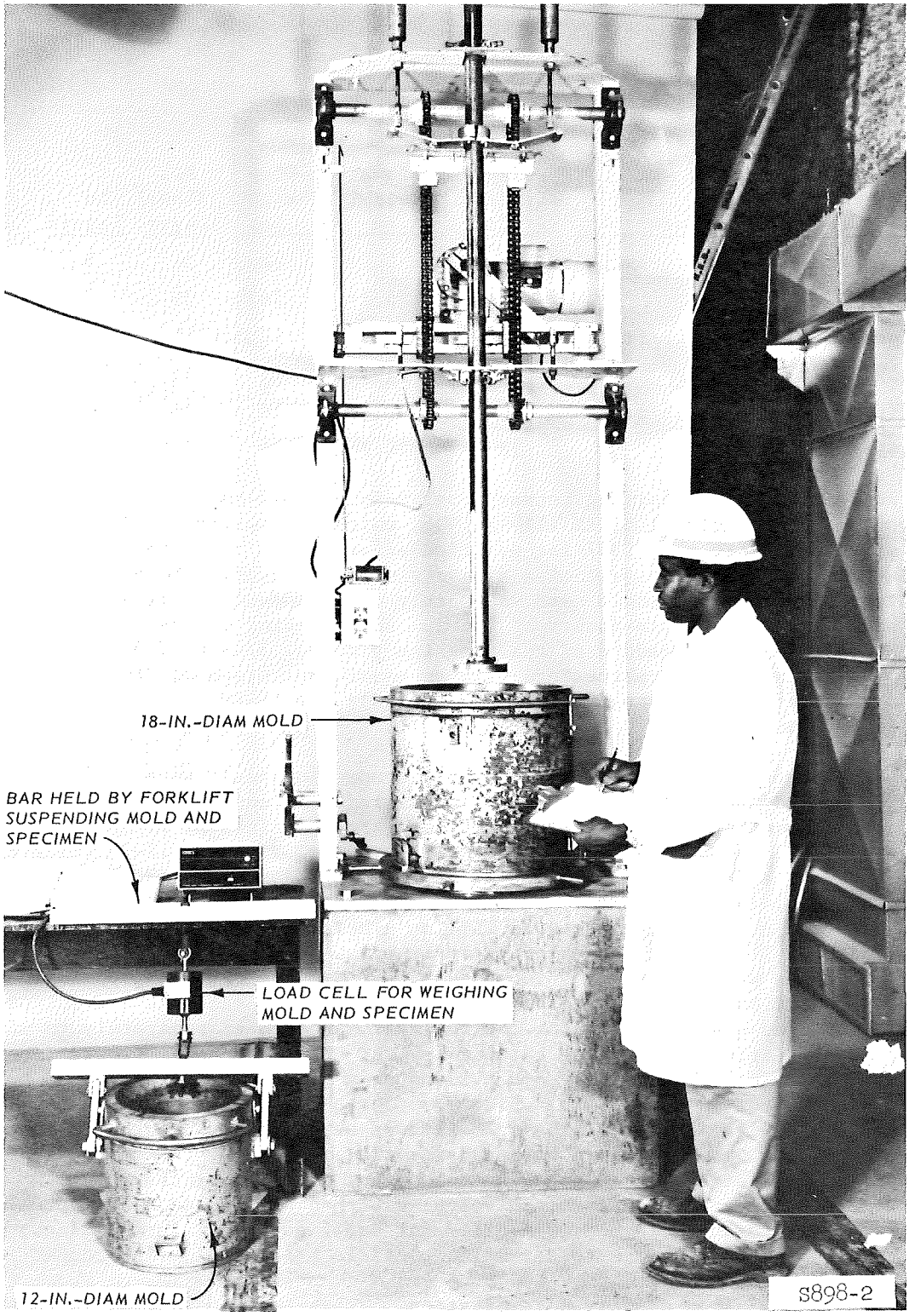

Figure 4. Howard mechanical compactor with 12-in.- (30.5-cm-) diam mold and load cell harness for weighing

Consolidation. Large diameter (12-in. (30.5-cm)) consolidation tests to 800-psi (5.5-MPa) vertical stress were performed on full-scale specimens of PARAHO and TOSCO materials compacted to densities corresponding to 60 percent of standard, standard, and modified efforts. These tests were performed at the South Pacific Division Laboratory (SPDL), CE, using a 12-in.- (30.5-cm-) diam floating ring consolidometer, which accommodates an 8.25-in.- (21.0-cm-) high specimen. Stresses were applied using a hydraulic ram, while deflections were monitored using four potentiometers located at quarter points. Consolidation stresses of 12.5, 25, 50, 100, 200, 400, 600, and 800 psi (86.2, 172.5, 345, 690, 1380, 2760, 4140, and 5520 kPa) with rebound stresses of 600, 200, 50, 12.5, and 0 (4140, 1380, 345, and 86.2 kPa) were each applied for a minimum of 24 hr. After rebounding, the specimen was oven-dried and a sieve analyses performed to determine particle breakage. Specimens were prepared by batching sufficient material with the appropriate gradation for 2- to 4-in.- (5- to 10-cm-) high lifts and compacting to the desired density with a 10-lb (4.5-kg) rammer.

Unconfined compression tests. Unconfined compression tests were performed on 6-in.- (15.2-cm-) diam specimens of modeled PARAHO and TOSCO materials compacted to densities corresponding to 60 percent of standard, standard, and modified compaction efforts. The specimens were then cured for 0, 3, 7, 14, and 28 days to evaluate their self-cementing properties. Unconfined compression tests were also performed on a mixture of 75 percent PARAHO and 25 percent TOSCO compacted to standard effort density and cured 0 and 28 days. Specimen preparation consisted of: (a) batching each appropriately graded layer to minimize segregation and variation in lift gradation, and (b) adding the required quantity of water and allowing the layer to mellow 1 hr prior to compaction. The specimens were compacted in six layers inside a 6-in.- (15.2-cm-) diam cardboard tube; the surface was leveled and sealed with hydrostone; and then the sealed specimen was placed inside a lard can containing a small jar of water and allowed to cure inside an environmental room at 72°F. Testing was according to Appendix XI of EM 1110-2-1906, which is compatible with ASTM D2166.

Triaxial compression tests. Consolidated-undrained (with pore pressure measurements) ($\bar{R}$) and/or consolidated drained (S) triaxial compression tests were performed on 9-in.- (22.9-cm-) and 6-in.- (15.2-cm-) diam specimens (depending upon maximum particle size) of PARAHO and TOSCO materials compacted to densities equivalent to 60 percent of standard, standard, and modified compaction efforts. $\bar{R}$ tests were also performed on 6-in.- (15.2-cm-) diam specimens of modeled PARAHO and on 1.4-in.- (3.6-cm-) diam specimens of PARAHO fines, all compacted to equivalent standard effort density. Effective confining pressures of 20, 40, 80, and 160 psi (138, 276, 552, and 1104 kPa) were used to isotropically consolidate the specimens. After back-pressure saturation, permeability determinations were made using falling head methods.

The axial load, chamber and pore pressures, and axial deformations were monitored electronically via a load cell, pressure transducers, and a linear variable differential transformer (LVDT), respectively, and recorded digitally on a multichannel recorder and/or an x-y-y' recorder. Testing procedures conformed to Appendix X of EM 1110-2-1906.

K_o triaxial tests. K_o tests were performed on 9-in.- (22.9-cm-) and 6-in.- (15.2-cm-) diam PARAHO and TOSCO specimens, respectively, compacted to equivalent standard effort density. In the case of PARAHO specimens, curing times were 0 or 13 months, while curing times for TOSCO were 0, 11, and 19 months. The principal of K_o testing is to determine the axial stress-deformation properties under conditions of zero lateral (horizontal) deformation. For PARAHO tests, the specimens were back-pressure saturated, and the null condition for no horizontal deformation was calculated from the axial deformation and volume of water expelled into a burette based upon the assumption that the specimen deformed as a right circular cylinder. For TOSCO tests, the horizontal and vertical deformations were monitored by a pair of LVDT clamps positioned at one-third points (Figure 5). The LVDT clamps eliminate the problem of membrane penetration affecting volume change measurements by directly monitoring the specimen diameter. (It is believed that errors due to membrane penetration on the volume of water measured by the burette in the tests on PARAHO were minimized due to the size of the specimens tested.) The axial load, deformation, and confining pressure were monitored electronically by a load cell, LVDT(s), and pressure transducer and recorded on an x-y-y' recorder.

Testing consisted of applying a small seating load, obtaining the null horizontal deformation, and then gradually increasing the axial stress. The chamber pressure was subsequently increased manually to maintain a null horizontal deformation value. Loading the specimen consisted of a series of load-rebound cycles to characterize the plastic and elastic components of deformation. Additional details concerning K_o testing and procedures used are described by Al-Hussaini and Townsend (1975 and 1975a).

Direct shear tests. Two series, inundated and dry, of large-scale (2- by 2- by 1-ft (0.6- by 0.6- by 0.3-m)) direct shear tests were performed on PARAHO material. The material was compacted in 3-in. (7.6-cm) lifts by placing the loading plate on the loose material and statically applying a load until the desired density (equivalent to standard effort) was achieved. Figure 6 shows a schematic drawing of the equipment. The normal stress is applied to the specimen by three hydraulic jacks and monitored by three load cells, all of which are mounted in the loading head. The shearing force is applied to the lower half of the specimen by three hydraulic jacks, which produce shear at the specimen midheight. This shearing force is determined from two load cells. Dial gages measure the normal and shear deformation of the box. Additional information on the apparatus is presented by Nicholson (1979). The tests were multistaged using ascending normal stresses of 2.5, 5.0, 10.0, and 20.0 tsf (239, 479, 958, and 1917 kPa) and allowing the specimen to reconsolidate under each normal stress.

Interface shear tests to determine material handling characteristics of PARAHO and raw shale were also performed using this equipment. For these tests, a plate to which either smooth stainless steel, rusty steel, or conveyor belt rubber was attached formed the top half of the specimen, thus providing an interface shear surface. Each material was loosely dumped in 3-in (7.6-cm) lifts into the lower half of the box as material handling would be for a loose state, and the only densification was due an applied normal

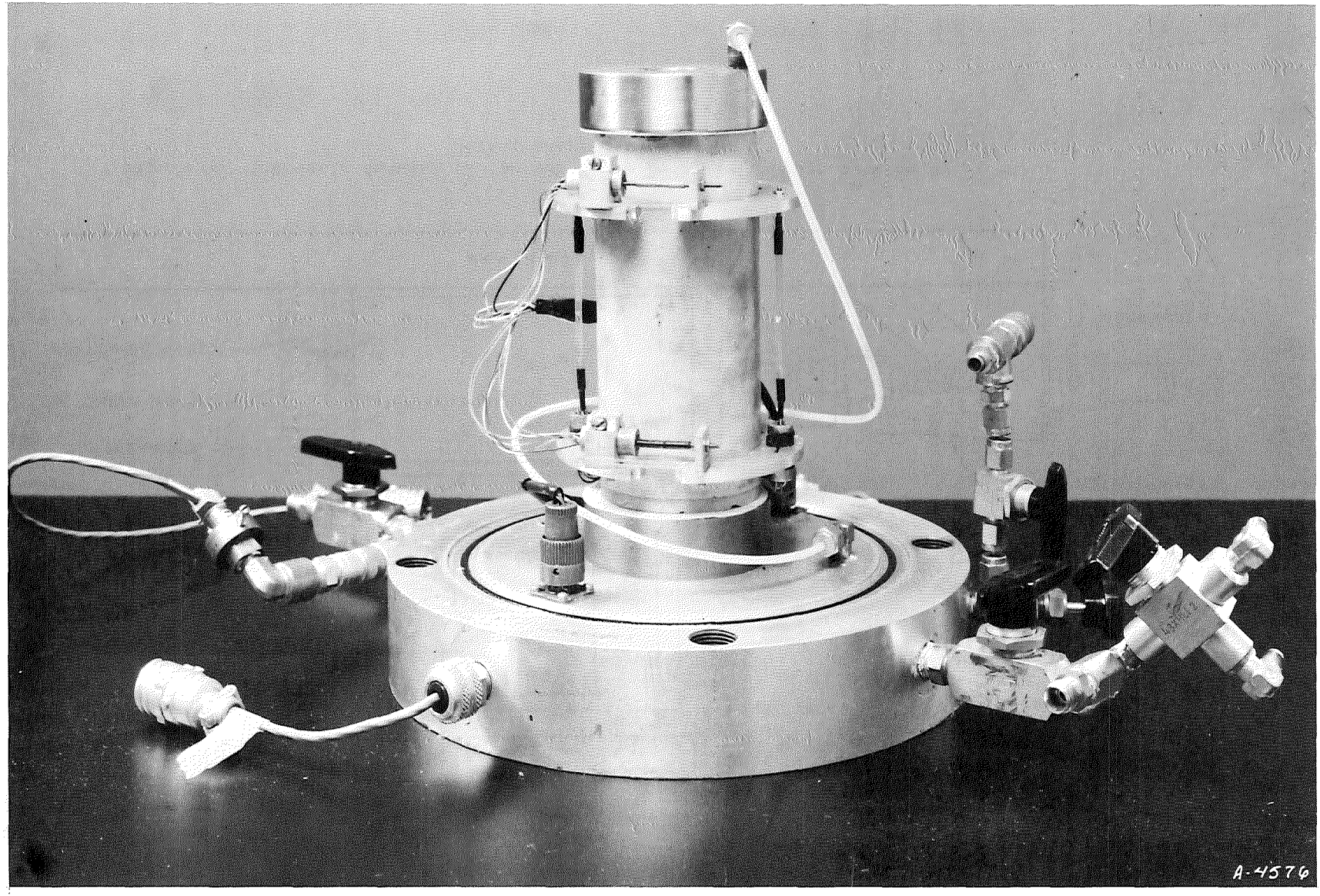

Figure 5. Specimen with the LVDT clamps

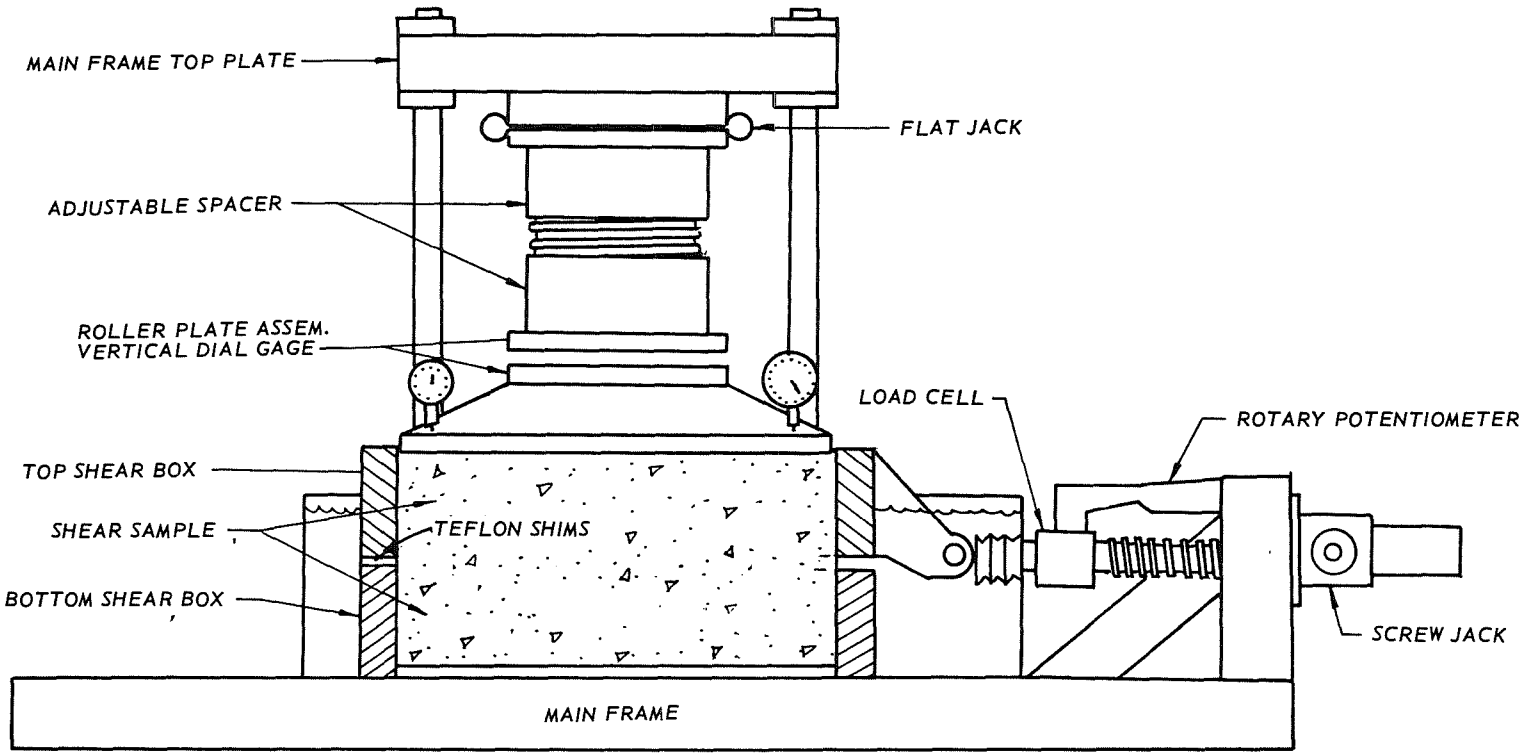

Figure 6. Schematic drawing of the WES 2- by 2- by 1-ft (0.6- by 0.6- by 0.3-m) direct shear apparatus

stress of 0.25 tsf (24 kPa). The tests were multistaged using ascending normal stresses of 0.25, 0.50, 1.0, and 2.0 tsf (24, 48, 96, and 192 kPa).

Conventional direct shear tests were also performed on 3- by 3-in. (7.6- by 7.6-cm) specimens of inundated modeled PARAHO and inundated and dry TOSCO. Specimens were trimmed from samples compacted in a 6-in.- (15.2-cm-) diam compaction mold using standard compaction effort. Testing was in accordance with Appendix IX of EM 1110-2-1906.

Repeated direct shear tests to establish residual shear strength were performed on 3- by 3-in. (7.6- by 7.6-cm) specimens of modeled PARAHO and TOSCO material trimmed from samples compacted in a 6-in.- (15.2-cm-) diam mold under standard compaction effort. The WES automated repeated direct shear machine (Figure 7) consists of a shear box, the top half of which is held stationary while the lower half is moved back and forth accumulating deformation until minimum resistance to shear is offered. The shear force and shear deformation are monitored electronically by a load cell and LVDT, respectively, and recorded on a strip chart recorder. The normal load is applied by an air cylinder. The tests were multistaged with increasing normal stresses applied after residual is achieved under a given normal stress. Testing was in accordance with Appendix IXA of EM 1110-2-1906.

Dynamic properties test. The dynamic properties of modeled PARAHO were evaluated by cyclic triaxial and resonant column equipment. Since resonant column equipment only applies small shear strains, i.e., 10^{-5} to 10^{-3} percent, and cyclic triaxial equipment is limited to 10^{-3} to 1 percent strain, both tests are required to completely characterize the dynamic properties.

a. Cyclic triaxial tests were performed on 6-in.- (15.2-cm-) diam specimens of modeled PARAHO compacted to equivalent 60 percent standard and modified effort density. An MTS closed-loop electrohydraulic system was used to apply a sinusoidal compression-extension wave form. The load-deformation hysteretic loop was monitored using a load cell and LVDT clamps positioned at one-third points on the specimen, respectively, and recorded using an x-y recorder. To ensure that the load and deformation responses did not exceed the recorder speed, testing was conducted at 0.5 Hz instead of 1.0 Hz as was used for the cyclic triaxial tests to evaluate earthquake response. To calculate the shear modulus G, using cyclic triaxial equipment, the equation, $G = E/2(1 + \nu)$, is used, which requires calculating Young's modulus E and either estimating or measuring deformations to obtain Poisson's ratio ν. For these tests, Poisson's ratio values were determined from axial and radial deformations using the LVDT clamps, which were recorded on a strip chart recorder. The tests were multistaged by applying 25 cycles of loading at each increasing strain level for each confining pressure. Each specimen was multistaged with respect to strains but not with respect to confining pressure.

b. Resonant column tests were performed on 4-in.- (10.2-cm-) diam specimens of modeled PARAHO with the same modeled gradation as used for

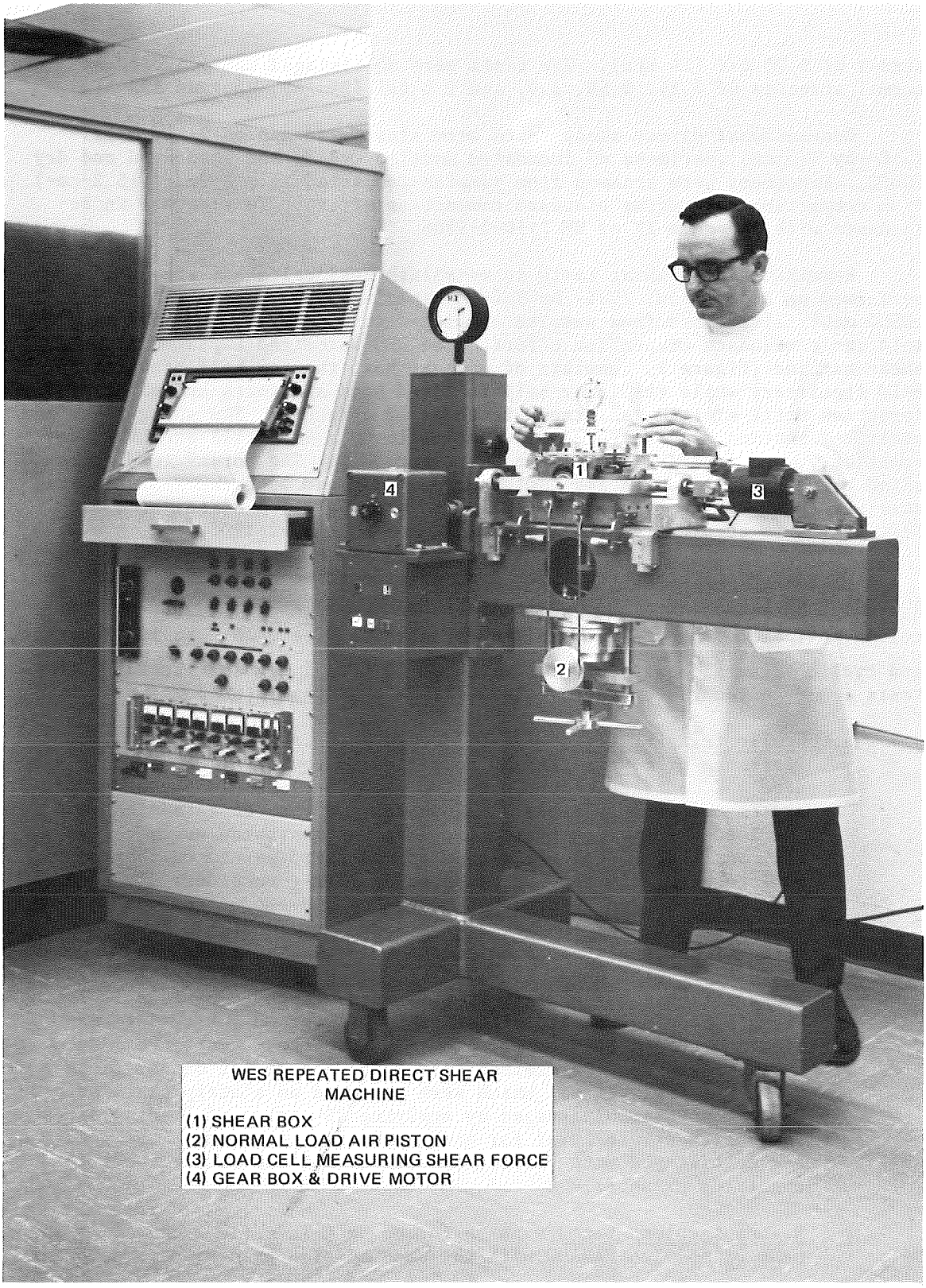

Figure 7. WES automated repeated direct shear machine

cyclic triaxial tests and compacted to equivalent 60 percent standard and modified effort density. Testing was with a Drnevich apparatus (Figure 8), which is a fixed-free type with torsional or longitudinal shearing stress applied to the specimen at the top using electrical coils or an electromagnet, respectively. The resulting Lissajous figure is monitored on an oscilloscope when resonance is established, and the shear modulus G and damping ratio λ are calculated from the resonant frequency, coil-power relationship, and accelerometer output. These tests were multistaged with respect to both strain level and confining pressure. Testing sequence was to increase strain level at a given confining pressure under the torsional mode, then return to a low strain value, and increase the strain level under the longitudinal mode. After specimen response was determined under both torsional and longitudinal excitations, the confining pressure was increased and the testing sequence repeated. Additional details concerning resonant column testing are described by Drnevich (1977 and 1978).

Cyclic triaxial tests. The earthquake resistance of modeled PARAHO material was evaluated by isotropically consolidated undrained cyclic triaxial tests on 6-in.- (15.2-cm-) diam specimens compacted to densities comparable to 60 percent of standard compaction effort and 60 percent relative density D_r. Testing was conducted using an MTS closed-loop electrohydraulic loading system, which applied a sinusoidal compression-extension wave at 1 Hz. The axial load, deformation, and confining and pore pressures were monitored electronically using a load cell, LVDT, and pressure transducers, respectively; their outputs were recorded on a six-channel strip chart recorder. Specimens at 60 percent D_r were prepared by moist tamping. Confining pressures used were 14.5 psi (100 kPa) for specimens compacted to 60 percent of standard effort, while confining pressures of 14.5 and 29.0 psi (100 and 200 kPa) were used for 60 percent D_r specimens. Testing procedures conformed to Appendix XA of EM 1110-2-1906.

Los Angeles Abrasion tests. These tests were performed in accordance with ASTM C131-76 and C535 on PARAHO and raw shale. ASTM gradings A, C, and 1 were used for the raw shale, while gradings A, C, and 2 were used for PARAHO.

Drop height density tests. These tests were performed on PARAHO and TOSCO materials to determine densities achieved from a free-fall condition. Testing was performed by placing the 11.1-in.- (28.2-cm-) diam D_r mold beneath a scaffold, dumping material from a known height into the mold, screeding, then weighing the mold plus material, and calculating the corresponding density. Drop heights of 0.7, 1.5, 4.5, 10.5, and 16.5 ft (0.2, 0.4, 1.4, 3.2, and 4.9 m) were used.

Bin and hopper tests. Flow tests were performed on samples of crushed raw shale (minus No. 8 sieve) by Jenike and Johanson, Inc. Tests were for continuous flow and for flow after 3 days storage at rest for three moisture contents: as received (1), 5.9, and 10.7 percent. In addition, compressibility, wall friction, and flow rate tests were also performed. Appendix B contains

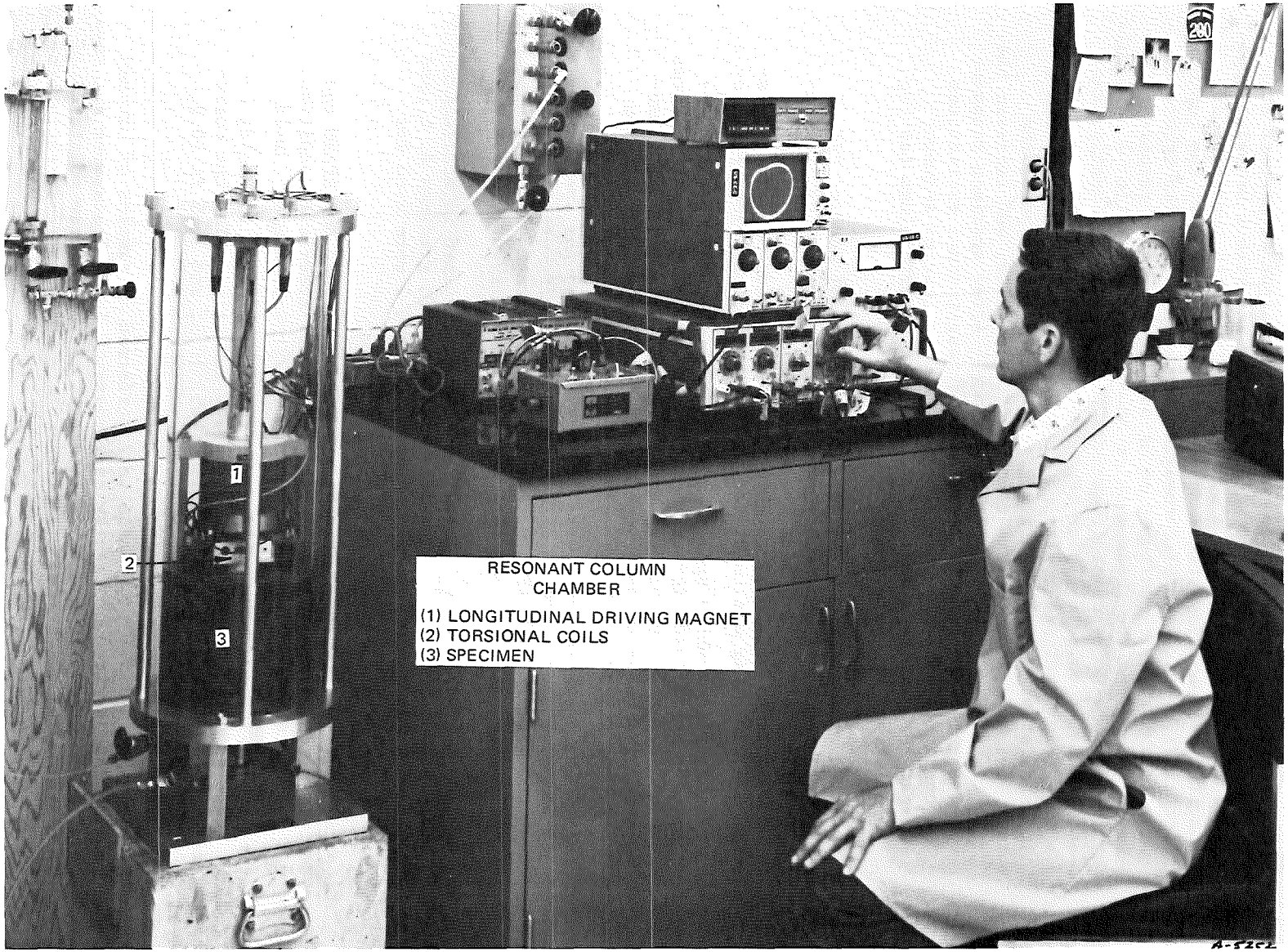

Figure 8. Drnevich LONG-TOR resonant column apparatus

details of the tests and data results furnished the WES.

Compositional and durability characteristics

Compositional characteristics. Various analyses were performed on samples of raw shale, PARAHO material, fragments of unconfined compression specimens of modeled PARAHO (28-day cure), and portions of retorted shale from Franklin slake durability tests. These analyses were performed to determine the mechanisms responsible for the observed self-cementing property of retorted oil shale and also included petrographic X-ray diffraction, scanning electron and steroscopic microscope examinations, differential thermal analyses, and chemical analyses.

Franklin slake durability tests. These tests were performed on fragments of raw shale, 1-1/2-in. and 3/4-in. PARAHO retorted shale, and the unconfined compression specimens. Testing consisted of duplicate specimens tumbled for 10 min inside a No. 10 sieve squirrel cage partially submerged in water, as described by Franklin and Chandra (1972).

CHAPTER 4: PRESENTATION AND DISCUSSION OF RESULTS

Physical Properties

Gradation

Upon receipt of the PARAHO material in 55-gal drums, 10 drums were randomly selected and subsectioned by quartering. Gradations were determined for five subsamples using the Gilson shaker, while one subsample was wet sieved and one dry sieved by hand. Figure 9 presents the results of these gradation analyses, plus those determined by WCC (1976). The results of tests on the five subsamples processed on the Gilson showed that the gradation of the PARAHO material was remarkably consistent; hence, Figure 9 shows only one curve representing a composite of these subsamples. A comparison between the hand-sieved and Gilson-sieved gradation results in Figure 9 also show that the PARAHO material is friable and experiences some breakdown by the Gilson shaker. The Gilson action produced approximately 10 percent more fines (minus No. 200 sieve) at the expense of coarser particles than the relatively less abrasive hand sieving. A comparison between the wet and dry hand-sieving gradation curves reveals that dry hand sieving better represents the gradation and probably more nearly represents the gradation of PARAHO material as it leaves the retort. This latter gradation was used as a basis for reconstituting PARAHO specimens.

A comparison of the gradations determined on the Gilson shaker with those of WCC (1976) reveals fairly close agreement in one case and a finer gradation obtained by WCC for another. Considering the variability of oil shale and gradations entering the retort, the agreement shown in Figure 9 is most likely a good representation of the gradation of PARAHO retorted shale.

Upon receipt of the TOSCO material in 55-gal drums, two drums were randomly selected and subsectioned by quartering. Gradations for these two subsections were determined using a Rotap shaker. The results of these gradation analyses presented in Figure 10 show excellent agreement between the two subsamples. Based upon this agreement, the drums of TOSCO material were combined. Figure 10 also shows the representative gradation of this combined material. Obviously, PARAHO processing produces a much coarser waste shale than TOSCO because of the large difference in raw shale particle sizes entering the retorts. The PARAHO material is classified as a poorly graded sandy gravel (GP), while TOSCO is classified as a silty sand (SM). These differences are reflected in the observed engineering properties.

Material processing

For the PARAHO material, processing consisted of dividing the material into various sieve sizes by passing the material through a Trommel rotating drum screen. The various sized fractions were then stored for reconstituting test specimens. The gradation determined by the hand sieving was selected as representing the PARAHO material.

For the TOSCO material, processing consisted of quartering the combined material into appropriate subsamples for preparing specimens. Based upon

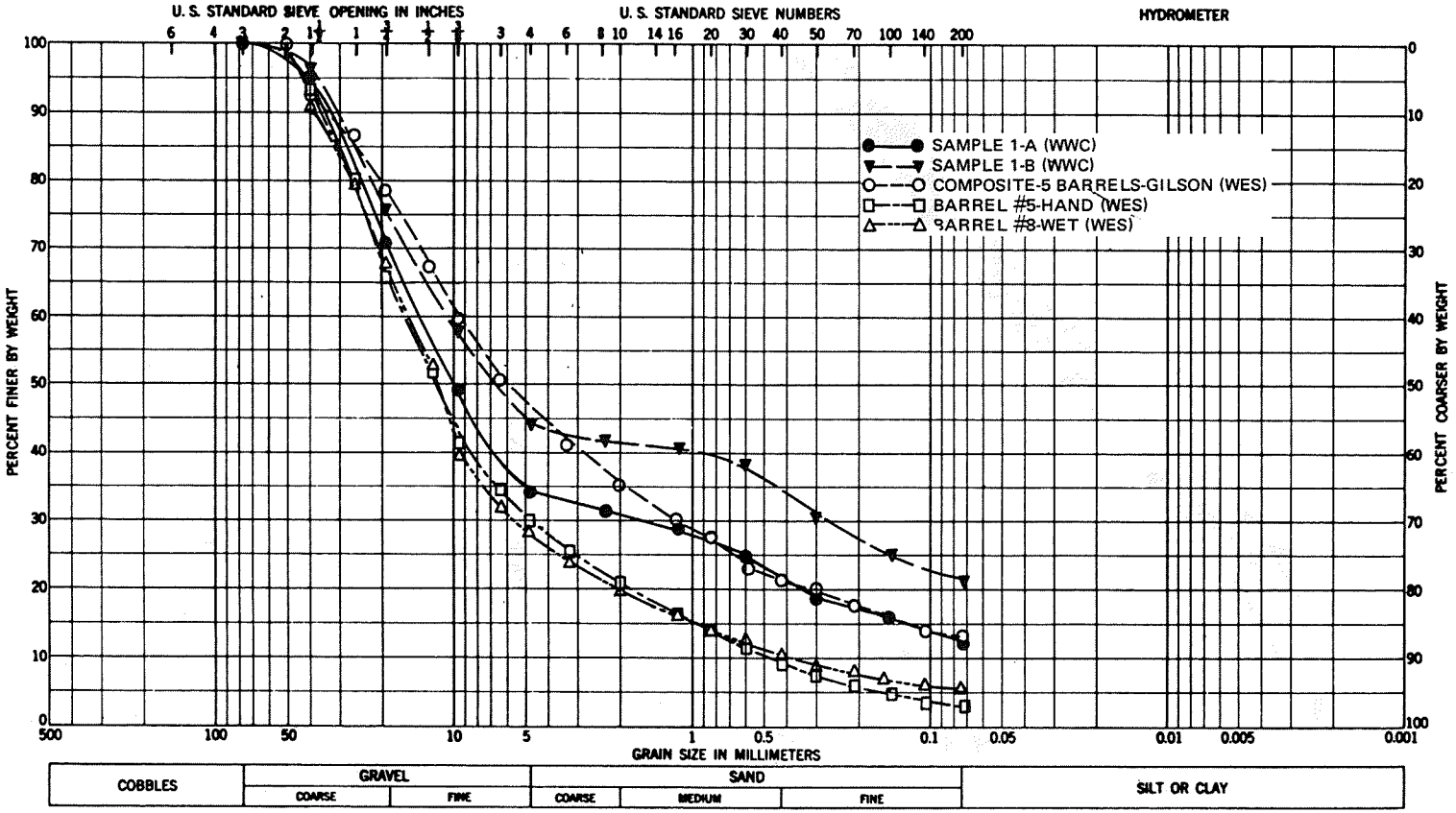

Figure 9. Comparison of gradation analyses for PARAHO retorted oil shale

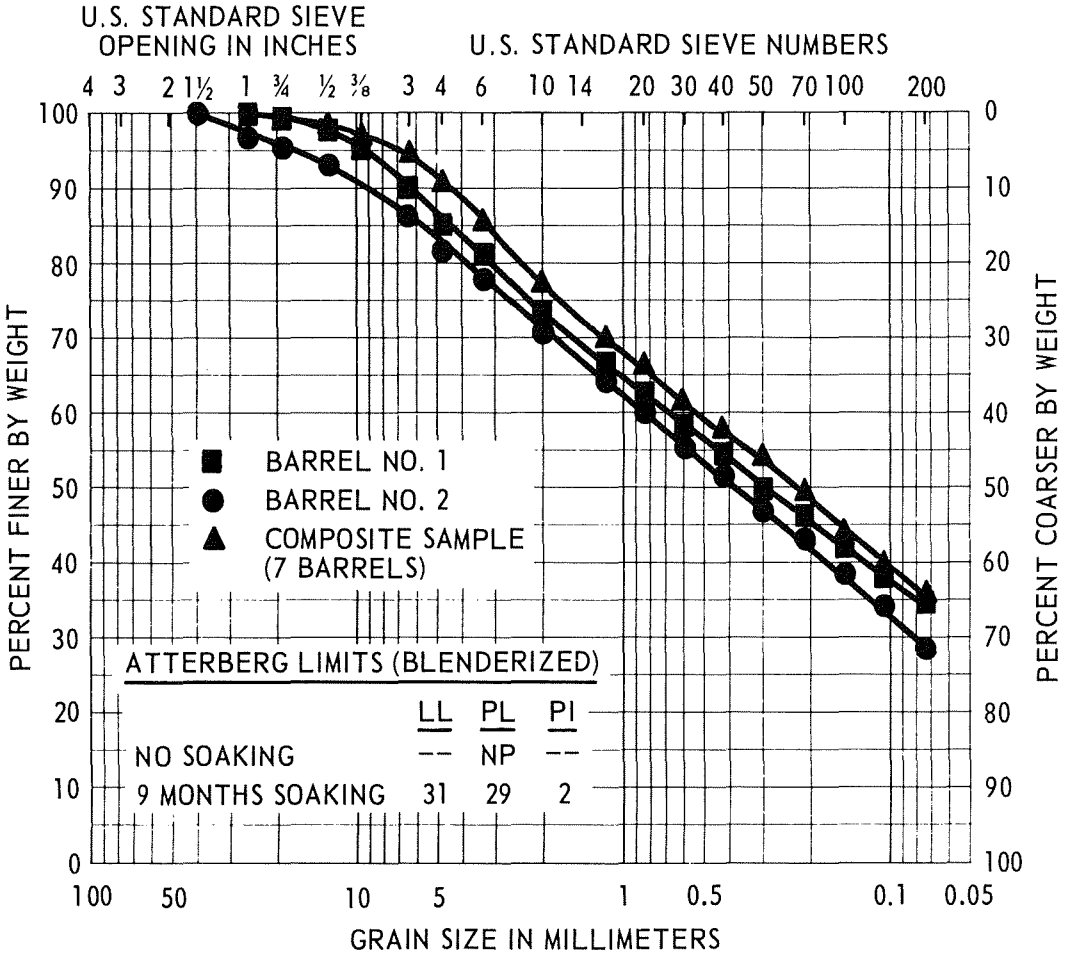

Figure 10. Summary of gradation analyses for TOSCO

gradations of Figure 10, the representative gradation of TOSCO material would be that corresponding to the composite material.

Atterberg limits and specific gravity

Table 1 presents a summary of the results of Atterberg limits tests and specific gravity analyses. These results show that the unprocessed shale is nonplastic even after inundation for 18 months. During initial undried, air-dried, and blenderized preparation procedures, the material proved to be extremely hard and difficult to process. Since blenderization produces the greatest amount of disaggregation and thus the highest plasticity, undried or air-dried processing would be fruitless on a material determined nonplastic (NP) by blenderized procedures. Both the PARAHO and TOSCO retorted oil shales initially were NP by blenderized procedures. However, after 18 months of inundation, both exhibited a PI of 5. While this is a low PI value, the increase indicates that some breakdown and softening of retorted shale can occur

Table 1

Summary of Atterberg Limits and Specific Gravities of Unprocessed, PARAHO, and TOSCO Oil Shales

Material	Fraction No.	LL*	PL*	PI*	G_s** Solids	G_a** Apparent	Remarks
Unprocessed shale	-40				2.19		Blenderized
	-40			NP†			Undried, air-dried, and blenderized
	-4 to +40			NP			Undried, air-dried, and blenderized
	-40			NP			Undried, air-dried, and blenderized, 9 months soak
	-40	32	31	1			Undried, air-dried, and blenderized, 18 months soak
PARAHO	-4				2.67		
	-40	29	29	NP			Blenderized
	-40	32	28	4			Blenderized, 9 months soak
	-40	37	32	5			Blenderized, 18 months soak
	+4					2.42	
TOSCO	-40			NP			Blenderized
	-40	31	29	2			Blenderized, 9 months soak
	-40	30	25	5			Blenderized, 18 months soak
	-4				2.61		
	+4					2.55	

* LL, PL, and PI = liquid limit, plastic limit, and plasticity index, respectively.
** G_s, G_a = specific gravity for solids and apparent specific gravity, respectively.
† NP = nonplastic.

with weathering. Dames and Moore (1974) reported PI values of 6 percent for TOSCO material, while WCC (1976) listed PI values of 3 percent for PARAHO; both of which agree well with values obtained in this investigation.

Specific gravity may be expressed in three forms: (a) the specific gravity of solids, which is applied to soils finer than a No. 4 sieve; (b) the apparent specific gravity; and (c) the bulk or mass specific gravity. Both the apparent and mass specific gravities are applied to soils coarser than the No. 4 sieve, with the apparent specific gravity being routinely used when dealing with coarse aggregate. Apparent specific gravity for raw shale was determined as 2.19. Average values of apparent specific gravity reported by Snethen et al. (1978) varied from 2.02 to 2.36.

The majority of apparent specific gravities, as reported by Snethen et al. (1978), for PARAHO material varied from 2.52 to 2.59. The value determined in this investigation was 2.42. Dames and Moore (1974) reported an apparent specific gravity value of 2.53 for TOSCO, as compared with 2.55 determined in this investigation. These values reported in the literature are comparable to those determined in this study, with values obtained for PARAHO being slightly lower and those for TOSCO being slightly higher.

Specific gravity of solids for PARAHO and TOSCO materials were determined as 2.67 and 2.61, respectively.

Engineering Properties

Compaction characteristics and maximum-minimum density

Figures 11 and 12, respectively, show the results of large-scale (12-in.-(30.5-cm-) diam) compaction tests using 60 percent of standard, standard, and modified compactive efforts performed on minus 2-in.- (50.8-mm-) diam PARAHO material, and companion tests performed on scalped and replaced minus 3/4-in. (19-mm) materials using a 6-in.- (15.2-cm-) diam mold. Vibrating table method maximum-minimum density tests were also performed on minus 2-in.- (50-mm-) and minus 3/4-in.- (19-mm-) diam PARAHO material using an 11.0-in.- (28.2-cm-) diam mold. Table 2 presents the the results of these tests plus a summary of the compaction test data.

The shapes of the water content-dry density curves in Figures 11 and 12 for both the full-scale and scalped and replaced PARAHO materials show the common condition that to achieve maximum dry density sufficient water to practically saturate the material is required. However, the effect of water contents less than optimum is markedly different between the full-scale and scalped and replaced materials. For the former, the addition of small quantities of water causes bulking of the material and corresponding low densities, which is common for these gradations. Conversely, for the scalped and replaced gradation, increasing water contents produced no bulking, but increasing densities. Nevertheless, despite this difference in water content effects and based upon the considerations that the full-scale tests are more representative of field conditions and that high water contents only produce a

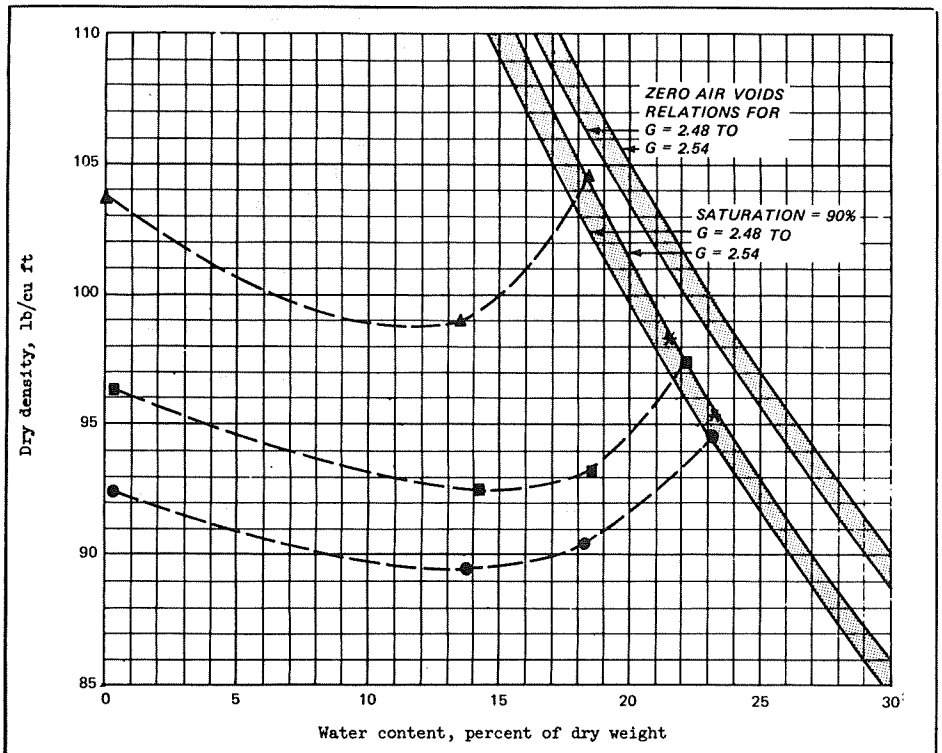

Sample No.	Elev or Depth	Classification	G	LL	PL	% > No. 4	% > 3/4 in.
		"AS BATCHED"	2.48		NP	72.5	33.5
●		60% STANDARD EFFORT	2.51		NP	63.0	28.5
■		STANDARD EFFORT	2.52		NP	58.0	25.5
▲		MODIFIED EFFORT	2.54		NP	49.0	19.5

Sample No.				
Natural water content, percent				
Optimum water content, percent				
Max dry density, lb/cu ft				

Remarks G_s = 2.67	Project OIL SHALE (PARAHO)
G_a = 2.42 NOTE: COULD NOT	12-IN.-DIAM COMPACTION TESTS
COMPACT MODIFIED EFFORT	Area
SAMPLE @ w = 23%.	Boring No. / Date MARCH 1977
* FREE WATER	**COMPACTION TEST REPORT**

ENG FORM 1 JUN 65 2091 PREVIOUS EDITIONS ARE OBSOLETE. (TRANSLUCENT)

Figure 11. Water content-density relationships for 12-in.- (30.5-cm-) diam compaction tests on PARAHO retorted oil shale

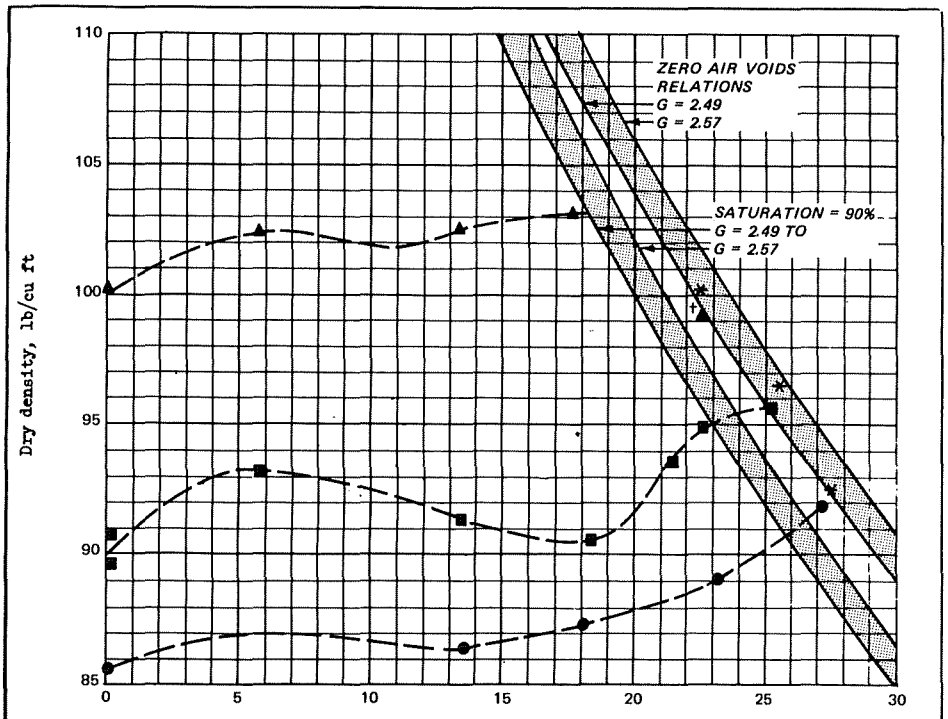

Sample No.	Elev or Depth	Classification	G	LL	PL	% > No. 4	% > 3/4 in.
		"AS BATCHED"	2.49		NP	72.0	0
●		60% STANDARD EFFORT	2.53		NP	52.0	0
■		STANDARD EFFORT	2.54		NP	50.0	0
▲		MODIFIED EFFORT	2.57		NP	38.5	0

Sample No.				
Natural water content, percent				
Optimum water content, percent				
Max dry density, lb/cu ft				

Remarks G_s = 2.67	Project OIL SHALE (PARAHO)
G_a = 2.42	6-IN.-DIAM COMPACTION TESTS
✳ FREE WATER	Area
†NOTE: TEST DATA MAY BE	Boring No. / Date MARCH 1977
QUESTIONABLE.	**COMPACTION TEST REPORT**

ENG FORM 2091 1 JUN 65 PREVIOUS EDITIONS ARE OBSOLETE. (TRANSLUCENT)

Figure 12. Water content-density relationships for 6-in.- (15.2-cm-) diam compaction tests on modeled PARAHO retorted oil shale

Table 2

Summary of Compaction Test Results on PARAHO Oil Shale

Gradation Size	Compaction Effort	Maximum Dry Density $\gamma_{d_{max}}$ pcf	Minimum Dry Density $\gamma_{d_{min}}$ pcf	Water Content w, %	Relative Density D_r, %
Original (-2 in. fraction)	Vibration	89.2	66.0	--	--
	60% of standard	94.6	--	23.3	116.2
	Standard	97.5	--	22.2	124.2
	Modified	104.4	--	18.4	141.4
Scalped and replaced (-3/4 in. fraction)	Vibration	81.8	62.9	--	--
	60% of standard	91.9	--	27.2	136.6
	Standard	95.7	--	25.3	148.3
	Modified	103.1	--	17.7	168.8
Parallel (-3/4 in. fraction)	Standard	88.9		0.2	
		88.0		22.8	
Scalped (-3/4 in. fraction)	Standard	88.7		0.2	
		92.5		23.1	

density slightly higher than that for dry material, compaction of PARAHO material in the as-retorted condition is feasible. This is particularly significant in that surface water is scarce in western Colorado and would have to be obtained at additional cost. Another obvious alternative to using water to increase density is to increase the compaction effort. The results presented in Figures 11 and 12 indicate that both full-scale and scalped and replaced materials produce significantly higher densities with increased compaction effort.

Since the zero air voids curve is a function of specific gravity, and the apparent specific gravity is lower than the specific gravity of the solids, the zero air voids curves presented in Figures 11 and 12 reflect the composite specific gravity values for the material. This composite was obtained by considering the percentage of a specific fraction and corresponding specific gravity.

Laboratory compaction test specifications limit the maximum allowable particle diameter to one fourth to one sixth of the corresponding mold diameter. Hence to test materials, such as PARAHO, which contain large particles, a modeling procedure that eliminates the oversized particles and allows testing with smaller more conventional size molds is required. Scalping and replacement was the primary modeling procedure used with some tests performed on parallel or scalped gradations. A comparison of the "as batched" gradations in Figures 13 and 14 shows the effect of modeling on gradation. A comparison of the results presented in Table 2 shows that the scalping and replacement procedure underestimates the maximum dry density and overestimates the optimum water content. These results are consistent with those of others who have observed that scalping and replacement modeling fails to achieve results comparable to full scale (Donaghe and Townsend, 1973 and 1975). Also presented in Table 2 are the results of compaction tests on parallel and on scalped (without replacement) gradations at zero and a water content assumed to be near optimum. These model gradations also underestimate the maximum dry density of the full-scale material. However, of the three model gradations tested, the scalped and replaced procedure more nearly approached the maximum density of the full-size material.

The gradation curves in Figures 13 and 14 demonstrate the extent of particle breakage during compaction for tests on full-scale and scalped and replaced gradations of PARAHO material, respectively. As shown in these figures, little difference in the magnitude of particle breakage exists for 60 percent of standard and standard compaction efforts. However, considerable breakage occurs when modified effort is applied, i.e., 4 to 5 times as many fines are produced by modified compaction effort than 60 percent of standard effort. This is logical considering that modified compaction effort represents 7.6 times more compaction effort than does 60 percent of standard. Marsal (1967) proposed a method for quantitatively describing the amount of particle breakage. In this method, the difference in the percent retained on each sieve before and after a test is obtained, and the sum of differences having the same sign is designated the breakage factor B. Table 3 summarizes the B values for the full-scale (12-in.- (30.5-cm-) diam) and scalped and replaced (6-in.- (15.2-cm-) diam) compaction tests on PARAHO material. A comparison of these B values shows a progressive increase with compaction effort.

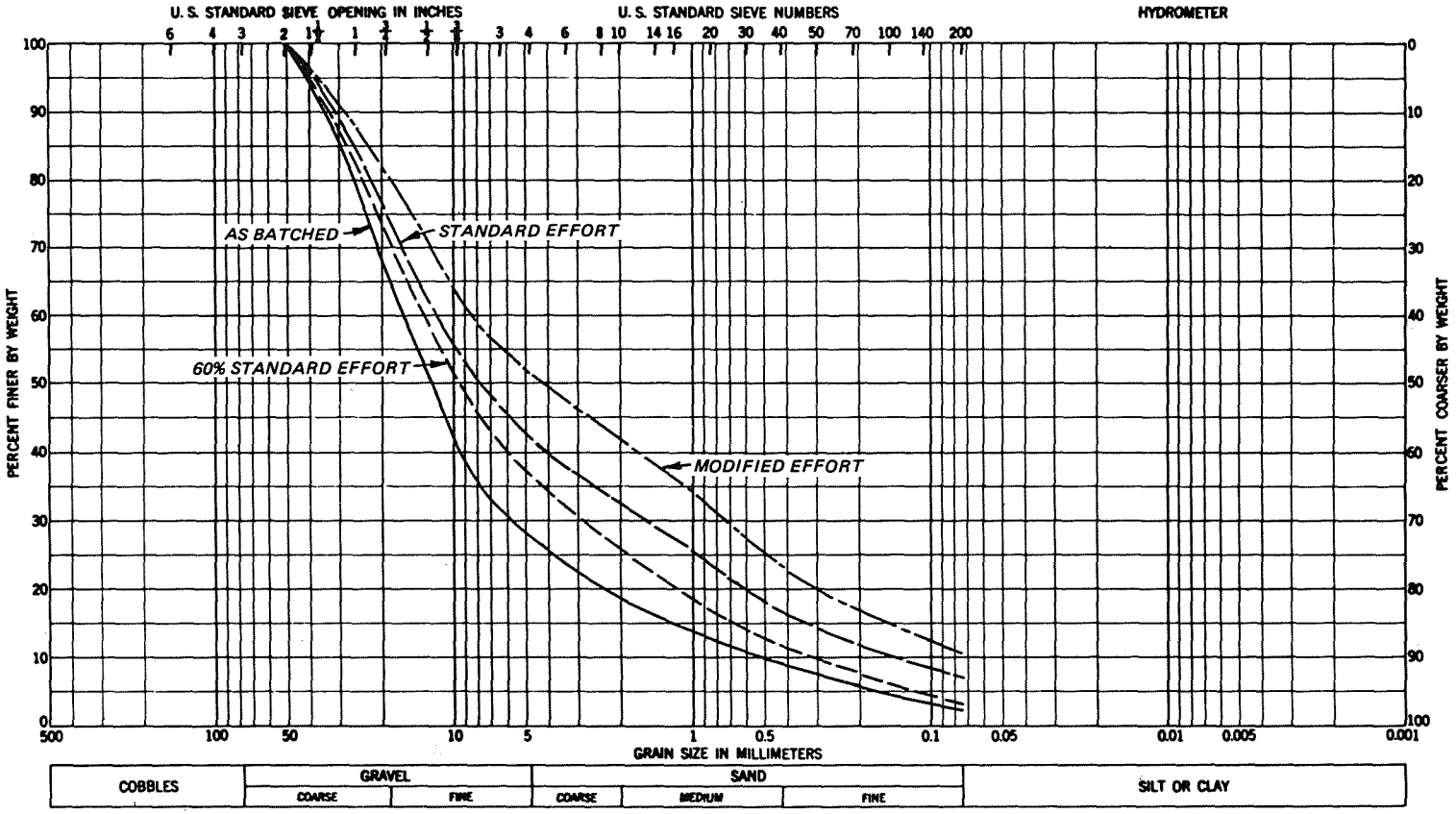

Figure 13. Effect of compaction effort on gradation for 12-in.- (30.5-cm-) diam compaction tests on PARAHO retorted oil shale

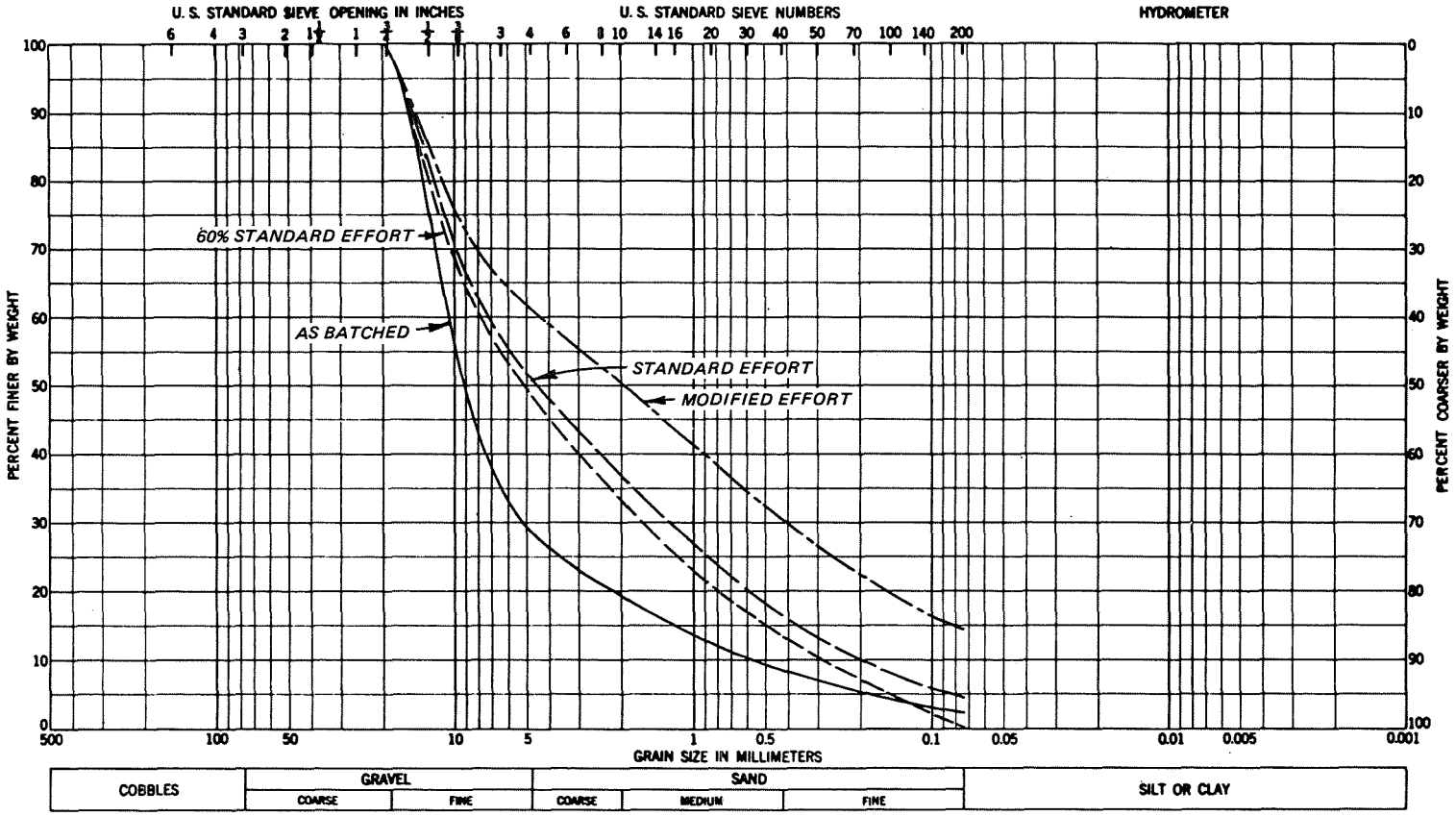

Figure 14. Effect of compaction effort on gradation for 6-in.- (15.2-cm-) diam compaction tests on PARAHO retorted oil shale

Table 3

Breakage Factors Due to Compaction of PARAHO Material

	Original											Scalped and Replaced									
	Initial		60% of Standard			Standard			Modified			Initial		60% of Standard			Standard			Modified		
Sieve Size	% Pass	% Retain	% Pass	% Retain	Diff Δ	% Pass	% Retain	Diff Δ	% Pass	% Retain	Diff Δ	% Pass	% Retain	% Pass	% Retain	Diff Δ	% Pass	% Retain	Diff Δ	% Pass	% Retain	Diff Δ
2+	100	0	100			100	0		100	0												
2 to 1-1/2	93	7	95	5	-2	96	4	-3	97	3	-4											
1-1/2 to 1	80	13	82	13	0	85	11	-2	90	7	-6											
1 to 3/4	67	13	73	9	-4	77	8	-5	82	8	-5	100	0	100	0		100			100		
3/4 to 1/2	50	17	58	15	-2	63	14	-3	71	11	-6	70	30	83	17	-13	83	17	-13	84	16	-14
1/2 to 3/8	40	10	51	7	-3	55	8	-2	63	8	-2	52	18	67	16	-2	70	13	-5	74	10	-8
3/8 to 4	27	13	37	14	+1	43	12	-1	52	11	-2	28	24	48	19	-5	52	18	-6	62	12	-12
4 to 10	18	9	27	10	+1	33	10	+1	42	10	+1	19	9	33	15	+6	37	15	+6	52	10	+1
10 to 20	13	5	17	10	+5	24	9	+4	32	10	+5	12	7	22	11	+4	24	13	+6	39	13	+6
20 to 40	9	4	13	4	0	17	7	+3	23	9	+5	8	4	13	9	+5	17	7	+3	30	9	+5
40 to 100	5	4	7	6	+2	11	6	+2	15	8	+4	4	4	5	8	+4	8	9	+5	19	11	+7
100 to 200	3	2	3	4	+2	8	3	+1	10	5	+3	3	1	4	1	0	5	3	+2	14	5	+4
		3		3	0		8	+5		10	+7		3		4	+1		5	+2		14	+11
"B" factor					11			16			25					20			24			34

The results also show that particles of the finer scalped and replaced gradation (6-in.- (15.2-cm-) diam mold) experienced greater breakage than did those of the coarser gradation, which is contrary to general trends that coarser particles generally experience a greater amount of particle breakage. One possible explanation for this anomaly is that the impact energy delivered by the hand-held rammer used with the 6-in.- (15.2-cm-) diam compaction tests is 688 ft-lb/ft^2 (10.0 kJ/m^2), while that for the full-scale mechanical compactor is only 252 ft-lb/ft^2 (3.8 kJ/m^2).

Due to the importance of compaction in disposing of spent shale, numerous laboratory compaction tests have been performed to evaluate the compaction characteristics of PARAHO material. The following tabulation from Snethen et al. (1978) summarizes the variability in compaction characteristics reported for this material.

Compaction Energy ft-lb/ft^3	ASTM Standard	Optimum Water Content w , %	Maximum Dry Density $\gamma_{d_{max}}$, pcf
6200	50% D698	18.5-23.7	77.0-99.2
12,375 (Standard)	D698	15.5-22.0	80.2-103.2
56,250 (Modified)	D1557	14.4-22.0	88.8-108.4

This variation is largely due to differences in gradation, particularly the amount of fines, and variability of the unprocessed shale and retorting mode (direct or indirect heat). A more valid comparison of previous data with data from this report would be for tests performed on PARAHO processed by direct heating in the semiworks retort as was the material used in this study. Accordingly, Figures 15 and 16 and Table 4 present the results of WCC (1976) for the pre- and post-compaction gradation analyses of minus 1-1/2-in. (38-mm) and minus 3/4-in. (19-mm) materials, while Table 5 compares results between this study and WCC (1976).

These comparisions show that the PARAHO material tested at the WES with its greater amount of coarse particles produced greater densities for both the minus 2-in. (50.8-mm) and minus 3/4-in. (19-mm) gradations than did the finer-grained WCC minus 1-1/2-in. and minus 3/4-in. gradations.

Both ASTM and CE criteria recommend using a vibratory table method to obtain the maximum dry density for materials containing less than 12 percent fines. Hence considering that the WES "as batched" gradations contained only 3 percent fines, densification by vibration should be more appropriate for achieving maximum density than impact compaction (Department of the Army, 1970; Townsend, 1972). Nevertheless, the maximum dry density achieved by vibration was only 89.2 and 81.8 pcf (1429 and 1210 kg/m^3) for full-scale (minus 2-in.- (minus 50.8-mm-) diam) and scalped and replaced (minus 3/4-in.- (minus 19-mm) diam) gradations, respectively, which is considerably lower than the maximum dry density achieved by 60 percent of standard compaction effort (Table 2). Similarly, WCC (1976) whose minus 1-1/2-in. (38.1-mm) and minus 3/4-in. (19-mm) gradations had 11 and 14 percent fines, respectively, presented results showing that vibratory densification produced lower densities than those

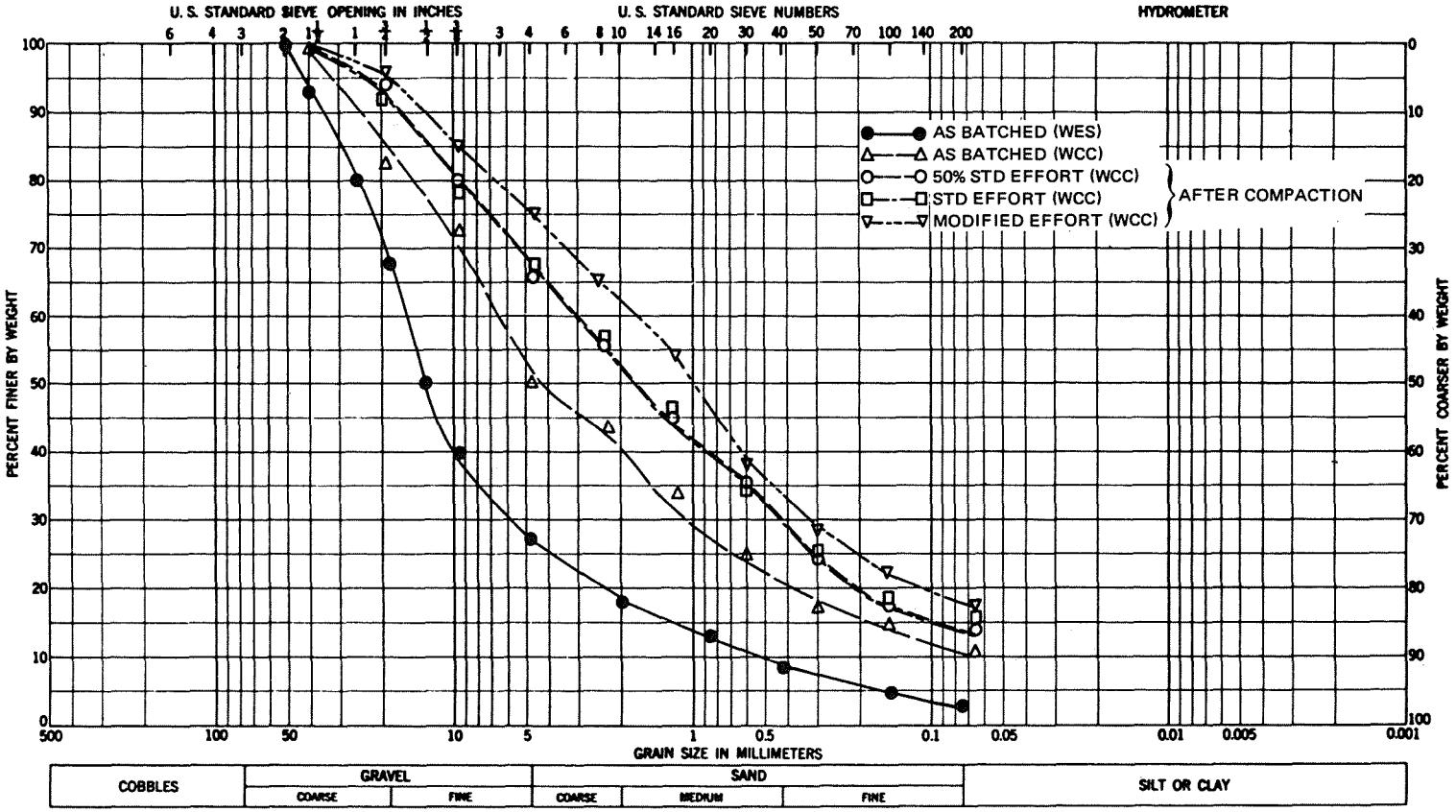

Figure 15. Effects of compaction effort on gradation for compaction tests by WCC (1976) on minus 1-1/2-in. (38.1-mm) PARAHO retorted oil shale

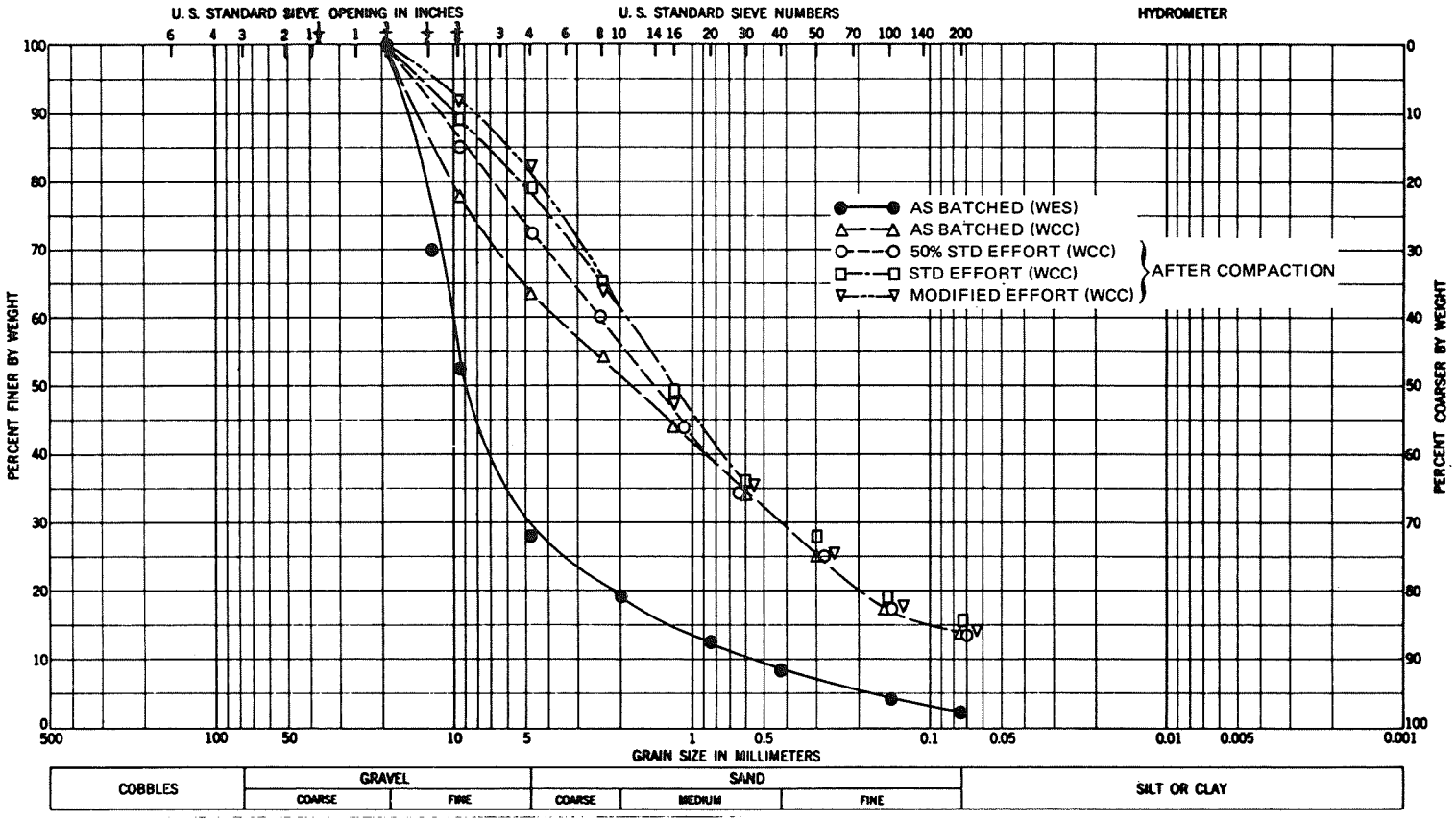

Figure 16. Effects of compaction effort on gradation for compaction tests by WCC (1976) on minus 3/4-in. (19-mm) PARAHO retorted oil shale

Table 4

Breakage Factors Due to Compaction of PARAHO Material Processed by Direct Heating

(from Appendix B of WCC, 1976)

	Initial		50% of Standard			Standard			Modified			Initial		50% of Standard			Standard			Modified		
Sieve Size	% Pass	% Retain	% Pass	% Retain	Diff Δ	% Pass	% Retain	Diff Δ	% Pass	% Retain	Diff Δ	% Pass	% Retain	% Pass	% Retain	Diff Δ	% Pass	% Retain	Diff Δ	% Pass	% Retain	Diff Δ
1-1/2+	100	0	100	0		100	0		100	0												
1-1/2 to 3/4	83	17	94	6	-11	93	7	-10	96	4	-13	100	0	100	0	-8	100	0		100	0	
3/4 to 3/8	72	11	80	14	+3	79	14	+3	85	11	0	77	23	85	15	-2	89	11	-12	92	8	-15
3/8 to 4	50	22	66	14	-8	68	11	-11	75	10	-12	62	15	72	13	+4	79	10	-5	82	10	-5
4 to 8	43	7	56	10	+3	56	12	+5	65	10	+3	54	8	60	12	+6	65	14	+6	64	18	+10
8 to 16	34	9	45	11	+2	46	10	+1	54	11	+2	44	10	44	16	0	49	16	+6	47	17	+7
16 to 30	25	9	36	9	0	35	11	+2	37	17	+8	34	10	34	10	0	36	13	+3	35	12	+2
30 to 50	17	8	24	12	+4	25	10	+2	28	9	+1	25	9	25	9	0	27	9	0	25	10	+1
50 to 100	15	2	18	6	+4	18	7	+5	22	6	+4	18	7	18	7	0	19	8	+1	18	7	0
100 to 200	11	4	14	4	0	15	3	-1	16	6	+2	14	4	14	4	0	15	4	0	14	4	0
-200		11		14	+3		15	+4		16	+7		14		14	0		15	+1		14	0
"B" Factor					19			22			25					10			17			20

Table 5

Comparison of Compaction Results on PARAHO

Compaction Effort ft-lb/ft^3	WES -2 in. Material w_{opt}* %	WES -2 in. Material $\gamma_{d_{max}}$ pcf	WES -2 in. Material Breakage B**	WCC -1-1/2 in. Material w_{opt} %	WCC -1-1/2 in. Material $\gamma_{d_{max}}$ pcf	WCC -1-1/2 in. Material Breakage B†	WES -3/4 in. Material w_{opt} %	WES -3/4 in. Material $\gamma_{d_{max}}$ pcf	WES -3/4 in. Material Breakage B†	WCC -3/4 in. Material w_{opt} %	WCC -3/4 in. Material $\gamma_{d_{max}}$ pcf	WCC -3/4 in. Material Breakage B**
6,200†† or 7,425‡ (50% or 60% of standard)	23.3	94.6	11	22	87.5	19	27.2	91.9	20	27.2	85.5	10
12,375 (standard)	22.2	97.5	16	22	94.8	22	25.3	95.7	24	25.2	90.2	17
56,250 (modified)	18.4	104.4	25	22	98.9	25	17.7	103.1	34	22.0	96.4	20

* w_{opt} = optimum water content.
** See Table 3.
† See Table 4.
†† WCC.
‡ WES.

achieved by impact compaction. From these observations, it might be concluded that PARAHO does not respond favorably to vibratory compaction. However, this conclusion is contrary to field compaction tests (WCC, 1976; Snethen, et al. 1978), which showed that the most economical compaction of PARAHO could be obtained using a vibrating drum roller. The results presented in Table 2 also show that modeling full-scale gradations by scalping and replacement will not duplicate corresponding estimates of maximum or minimum densities.

The results of 6-in.- (15.2-cm-) diam compaction tests using three compactive efforts on TOSCO material are presented and summarized in Figure 17, which shows the optimum water contents and densities obtained as 21 percent, 97 pcf (1554 kg/m^3), 19 percent, 99 pcf (1586 kg/m^3), and 18 percent, 104 pcf (1666 kg/m^3), respectively, for 60 percent of standard, standard, and modified compaction efforts. The shapes of the compaction curves show a marked effect of water content on density, quite unlike the PARAHO material, and water facilitates compaction. Hence, for this material, the economics of adding water versus increasing the compaction effort and compacting dry to achieve a specific density is much more critical than for the PARAHO. By comparison, compaction tests on TOSCO material by Dames and Moore (1974) show a range in maximum dry densities from 88 pcf (1410 kg/m^3) at 22 percent water content to 100 pcf (1602 kg/m^3) at 16 percent water content for standard compaction efforts; and for modified compaction efforts, densities ranged from 101 to 109 pcf (1618 to 1746 kg/m^2), while the corresponding optimum water contents varied from 19 to 15 percent, respectively.

Figure 18 demonstrates the extent of particle breakage during compaction. These results show the unusual event that during compaction the material became coarser or agglomerated. Although efforts were made to break down the test specimens into their appropriate fractions, the effort employed obviously was insufficient. This agglomeration is suggestive of some self-cementing as the TOSCO fines are noncohesive and ordinarily would readily disaggregate. Additional study of this is indicated.

The range of standard densities reported for TOSCO is slightly lower than typical results observed for a sandy soil, as TOSCO is classified.

Consolidation.

Figures 19 and 20 show the results of 12-in.- (30.5-cm-) diam consolidation tests to a maximum vertical stress of 800 psi (5.52 MPa) for each of the three compaction efforts for PARAHO and TOSCO, respectively. Appendix C presents the corresponding settlement-log time curves for the various applied vertical stresses. Table 6 summarizes the engineering consolidation parameters.

The total vertical strains, $\Delta e/(1 + e_o)$, when the vertical stress was 800 psi (5.52 MPa) varied from 4.7 to 10.0 percent for the PARAHO and 4.7 to 8.4 percent for TOSCO, with the higher compaction efforts exhibiting the smaller strains. By comparison, WCC (1975) obtained settlement values ranging from 2.2 to 11.3 percent for PARAHO for three comparable compaction efforts with a vertical stress of 1000 psi (6.9 MPa), which agrees quite well with the data presented. However, consolidation test results on TOSCO presented by

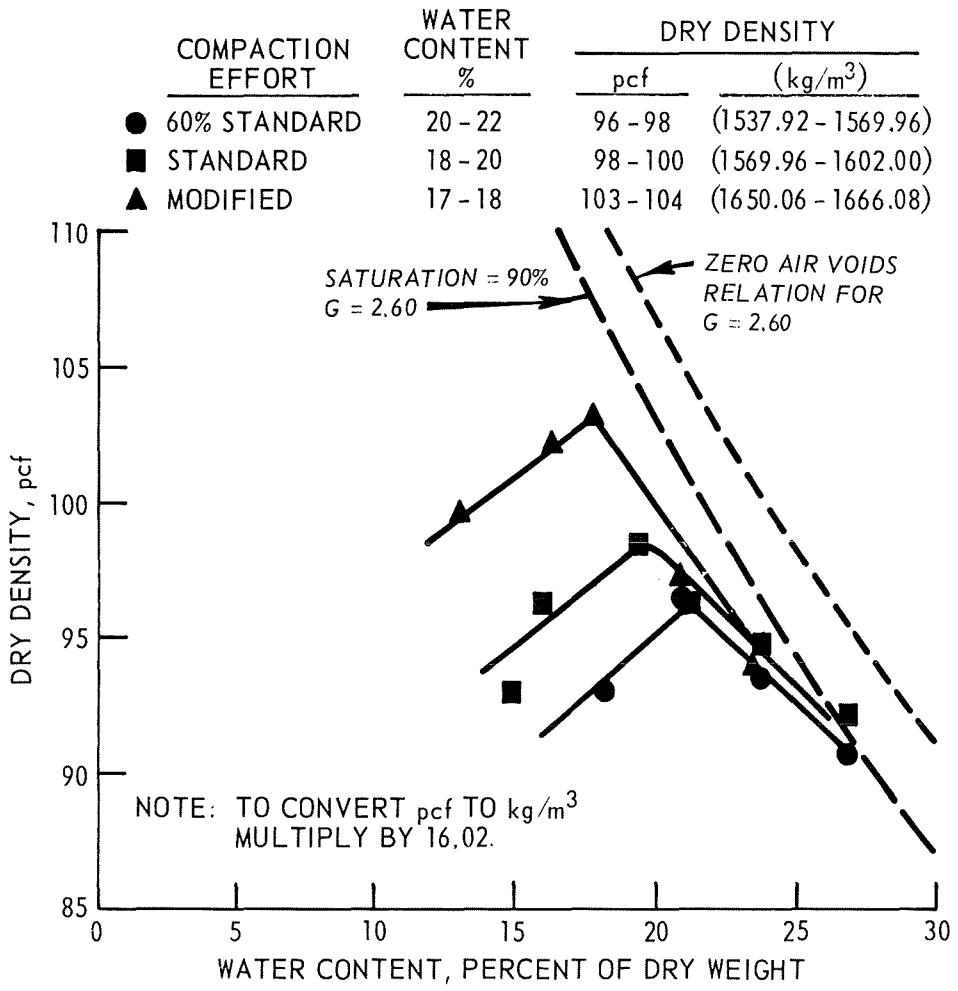

Figure 17. Compaction characteristics of TOSCO for 60 percent of standard, standard, and modified efforts

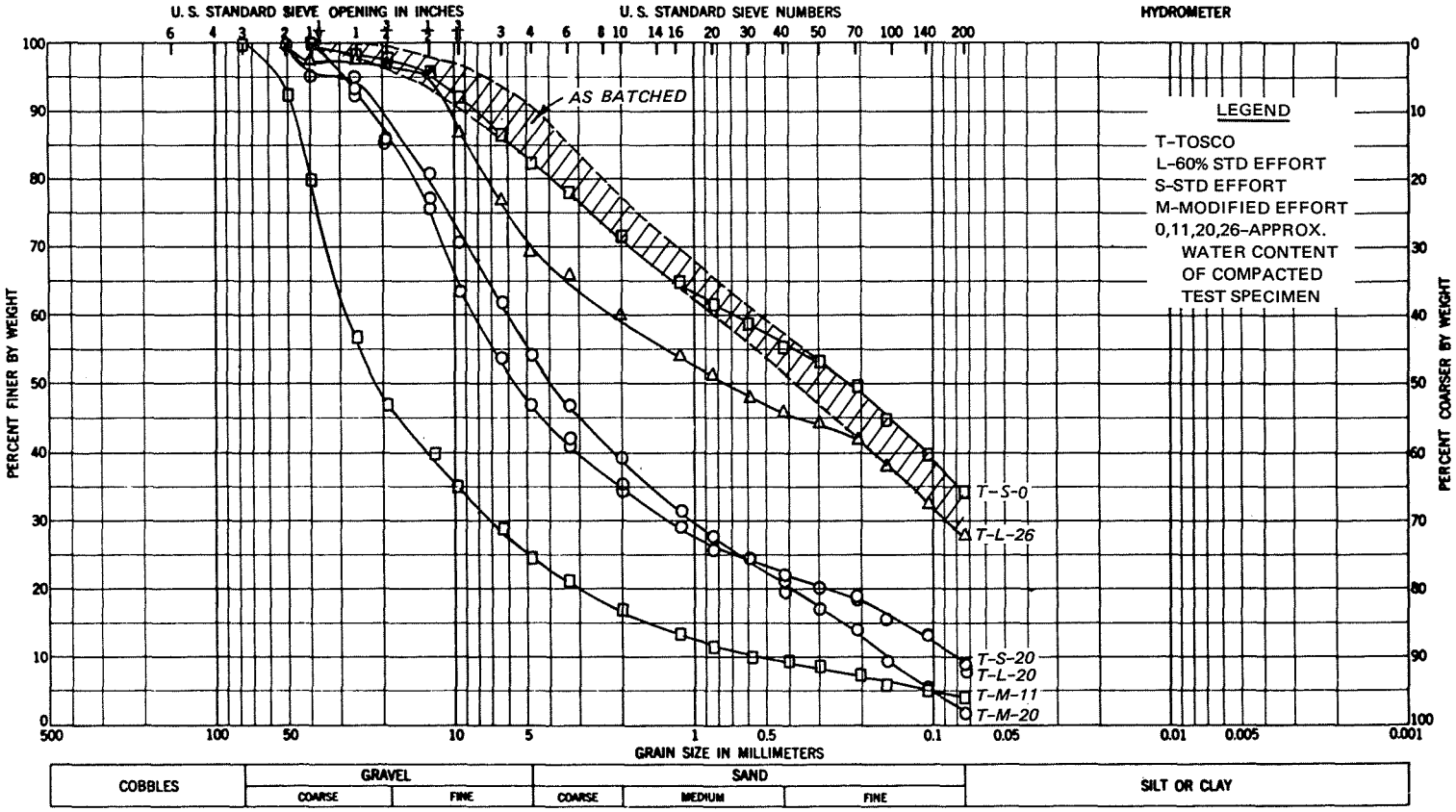

Figure 18. Effects of compaction effort on gradation for compaction tests on TOSCO retorted oil shale

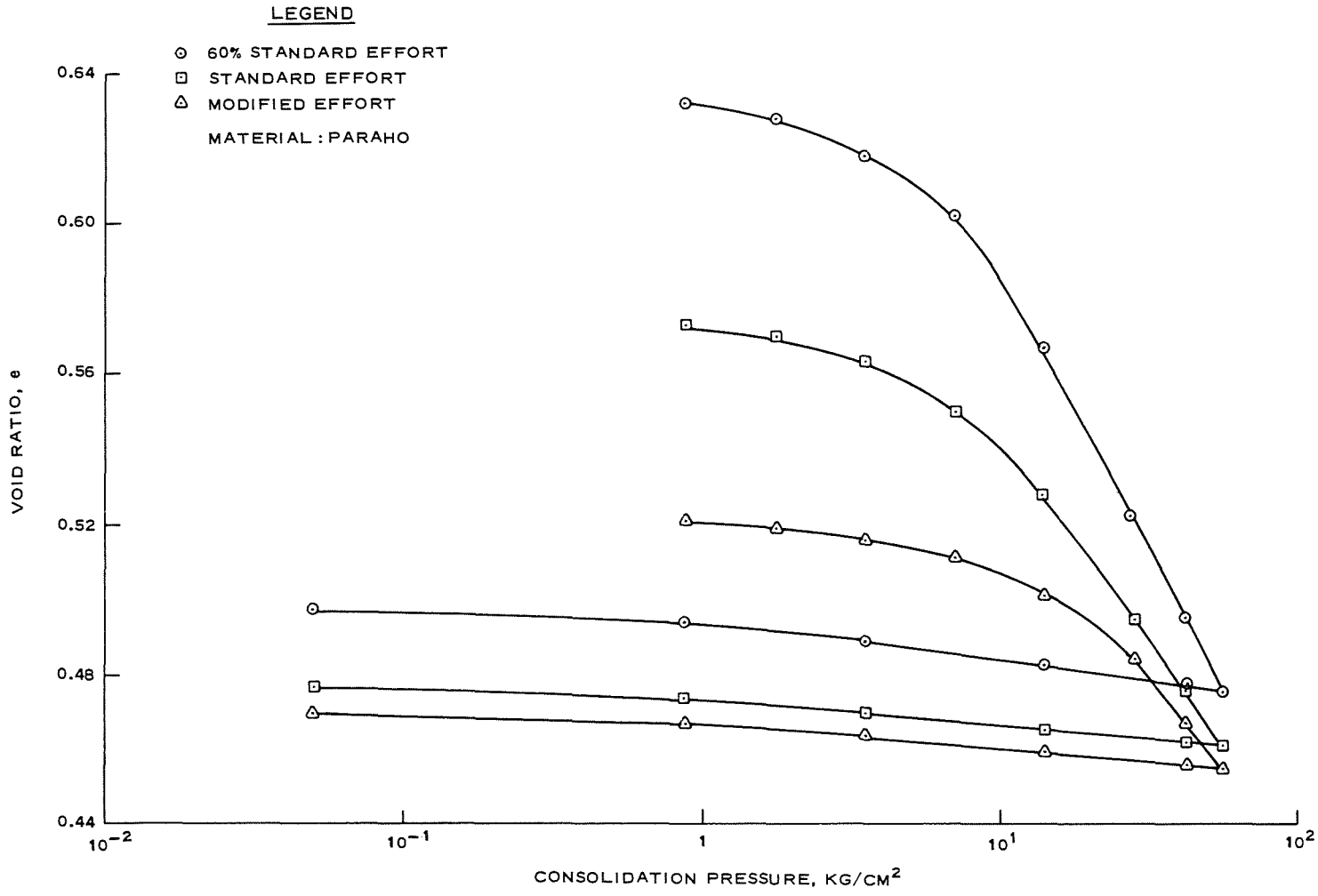

Figure 19. Consolidation characteristics of 12-in.- (30.5-in.-) diam consolidation tests on PARAHO retorted oil shale

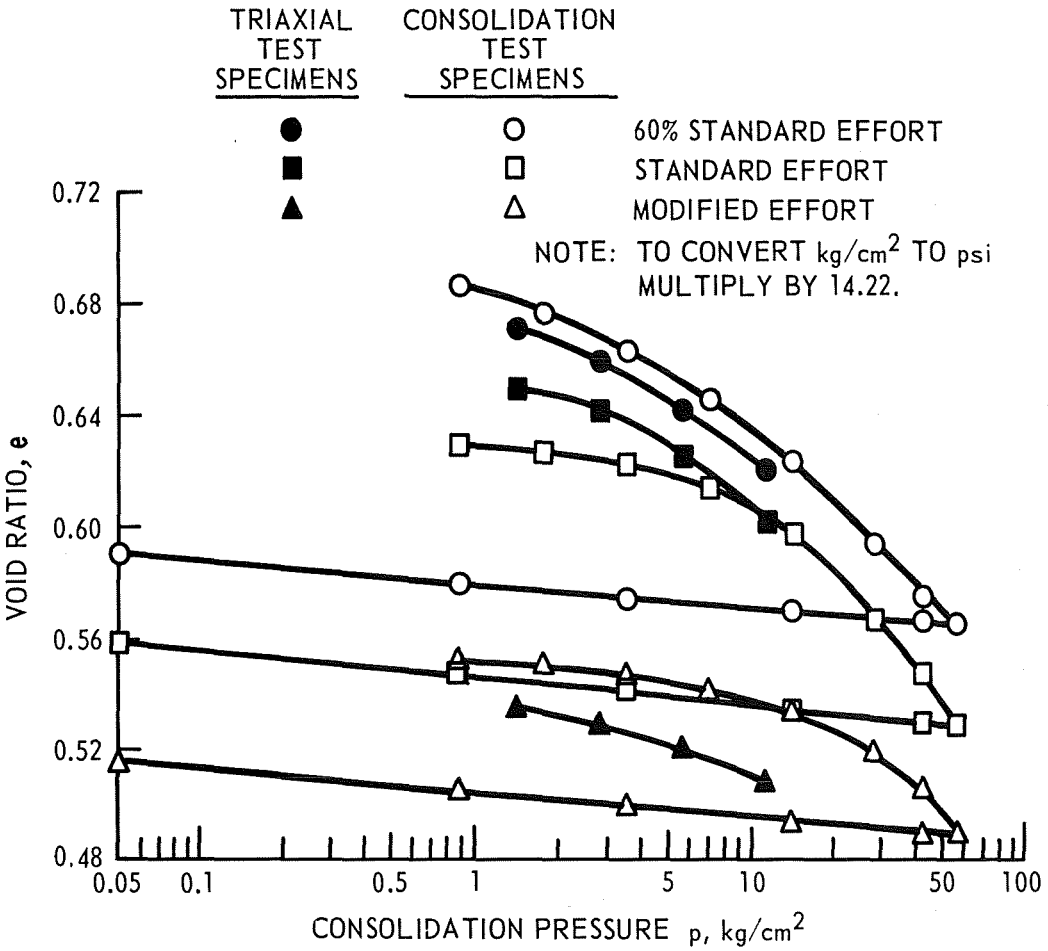

Figure 20. Consolidation characteristics of 12-in.- (30.5-cm-) diam consolidation tests and 6-in.- (15-cm-) diam triaxial specimens compacted to 60 percent of standard, standard, and modified compaction efforts on TOSCO retorted oil shale

Table 6

Consolidation Parameters for PARAHO and TOSCO Retorted Oil Shales at Maximum Applied Stress (800 psi)

Material/ Compaction Effort	Vertical* Strain, %	Coefficient of Compressibility $a_v = \Delta e/\Delta P$, cm^2/kg	Compression Index $C_c = \Delta e/\log P_2/P_1$, cm^2/kg	Coefficient of Consolidation $C_v = \frac{0.848H^2}{t_{90}}$, cm^2/sec	Permeability, k** $k = \frac{C_v a_v \gamma_w}{1 + e}$, cm/sec
PARAHO					
60% standard	10.0	0.00213	0.1495	0.293	4.2×10^{-7}
Standard	7.7	0.00154	0.1080	0.442	4.6×10^{-7}
Modified	4.7	0.00103	0.09634	0.4326	3.0×10^{-7}
TOSCO					
60% standard	8.4	0.00138	0.09634	0.358	3.1×10^{-7}
Standard	6.7	0.00135	0.1262	0.451	3.9×10^{-7}
Modified	4.7	0.00107	0.09966	0.352	2.5×10^{-7}

* $\varepsilon = \frac{\Delta e}{1 + e_o} = \frac{e_o - e_{800}}{1 + e_o}$

** Ft/yr = 0.97×10^{-6} cm/sec.

Dames and Moore (1974), where the applied vertical stress was 700 psi (4.8 MPa), had vertical strains varying from 16 to 25 percent. The apparent reason for the difference in results is that initial void ratios of the tests conducted at the WES ranged from 0.55 to 0.69, while those reported by Dames and Moore (1974) were much higher (lower dry density), 0.87 to 1.29. Figure 21 compares the compressibility of PARAHO and TOSCO with the data on dense rockfill materials summarized by Parkin (1977) and shows that both retorted oil shales are comparable to rockfill.

The permeability values presented in Table 6 generally exhibit the anticipated trend of decreasing with increasing compaction efforts and vertical stresses. The value obtained, 10^{-7} cm/sec, for both PARAHO and TOSCO indicate that these materials will be impermeable when compacted and subjected to sufficient vertical stress. By comparison, WCC (1975) reported permeabilities for PARAHO ranging from 1.7×10^{-6} to 8×10^{-8} cm/sec for three compaction efforts and a vertical stress of 200 psi (1.4 MPa). These low values of permeability for PARAHO are quite unexpected considering that this material generally contains less than 15 percent fines, and materials containing less than 12 percent fines are expected to be pervious.

Figures 22 and 23 present postconsolidation test gradation determinations for comparison with pretest batched gradations for PARAHO and TOSCO compacted to densities equivalent to 60 percent of standard and standard, respectively. Table 7 summarizes the corresponding breakage B values for these tests. These figures and table show that the PARAHO fines content increased from 3 to 12 percent during specimen compaction and subsequent consolidation testing, with no significant difference in particle breakage observed for the two densities; the corresponding breakage B value was 27 percent. For the TOSCO material, the fines content increased from 32 percent to 61 and 76 percent for standard and 60 percent of standard compaction efforts, respectively. The corresponding breakage B values were 29 and 44 percent, respectively.

These particle breakage results are a composite of breakage suffered during specimen compaction and application of the vertical stresses applied during consolidation. Breakage B values discussed previously in the compaction section indicate that breakage values of 11 and 16 percent occurred during compaction of the PARAHO specimens. This suggests that breakage in the magnitude of 16 percent for 60 percent of standard effort and 11 percent for standard compaction effort occurred during consolidation, although it must be noted that compaction equipment for the compaction tests was different from that used for preparing consolidation specimens. For comparison, isotropic consolidation of basalt to 650 psi (4.5 MPa) exhibited practically no particle breakage, i.e., $B < 5$ percent.

Postcompaction gradation determinations on TOSCO indicated that an agglomeration effect had occurred (i.e., the post-compaction gradations were coarser than the precompaction gradations). This unusual event precludes reasonable estimates of particle breakage during consolidation tests. Nevertheless, breakage B values of 29 and 44 percent for standard and 60 percent of standard compaction efforts, respectively, suggest considerable breakage occurred during compaction and/or consolidation for this material. It is most surprising that more particle breakage was observed for 60 percent of standard

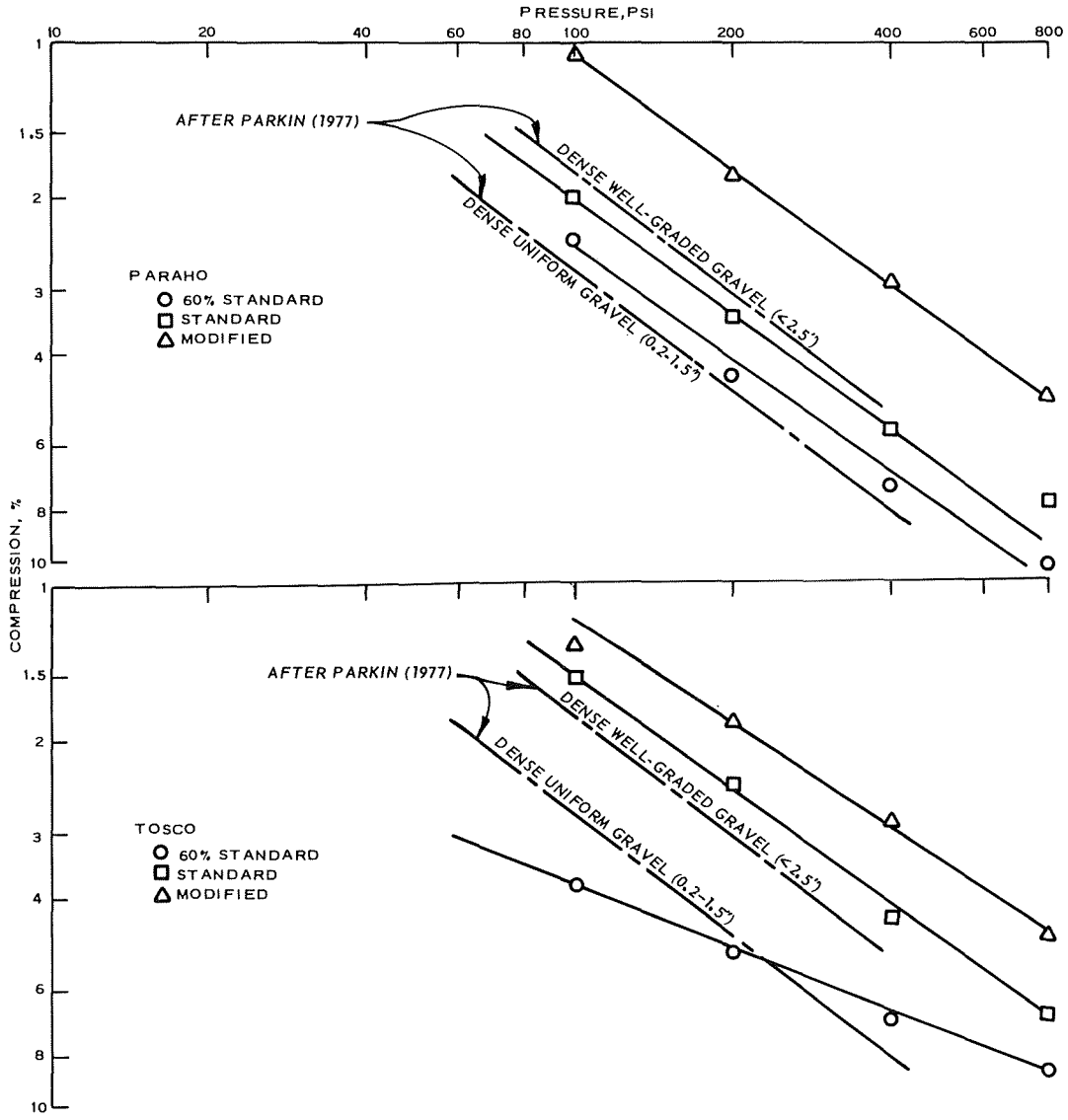

Figure 21. Comparison of the compressibility of compacted PARAHO and TOSCO with rockfill (after Parkin, 1977)

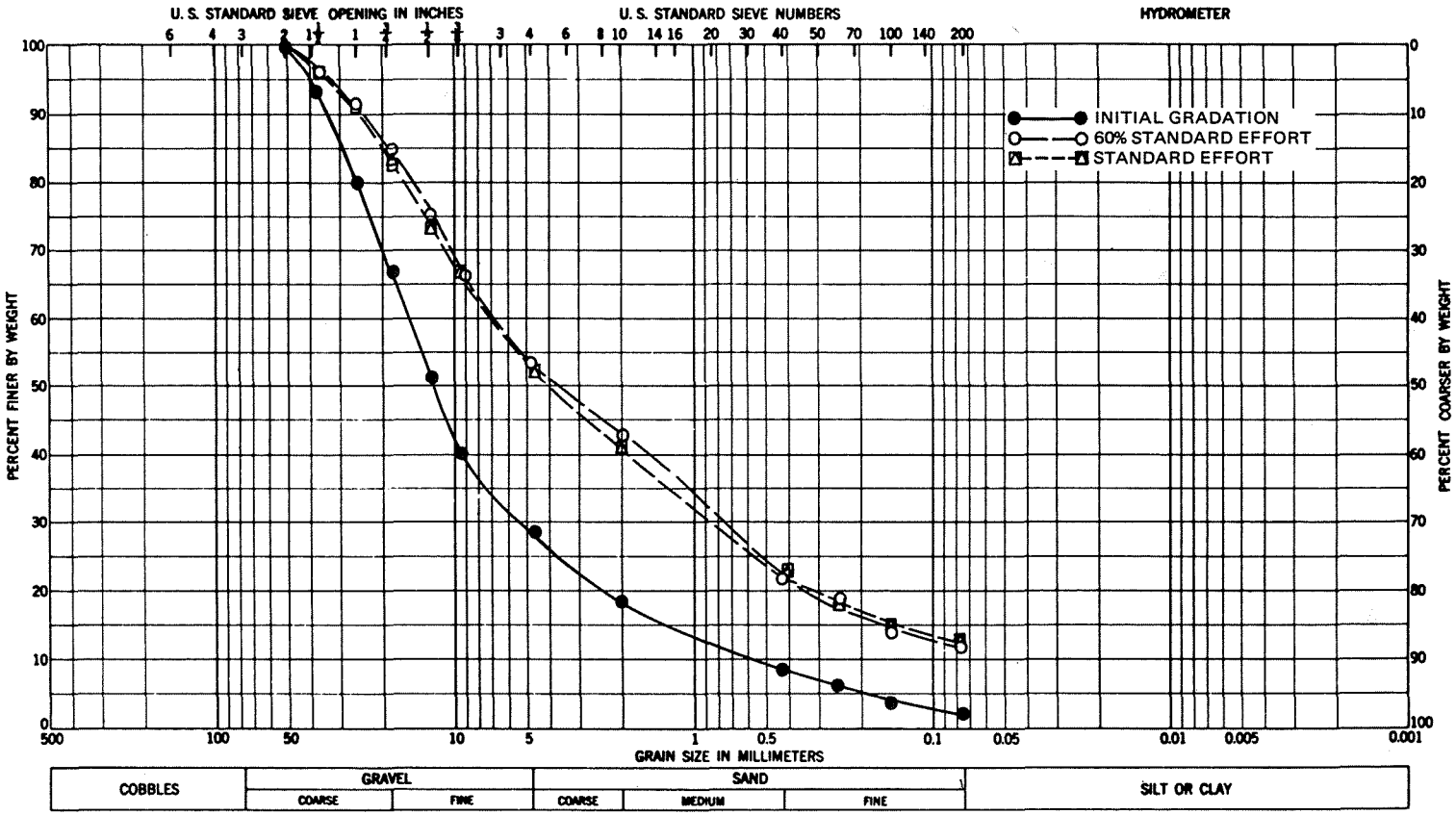

Figure 22. Effect of consolidation pressure to 800 psi (5.52 MPa) on gradation of PARAHO retorted oil shale

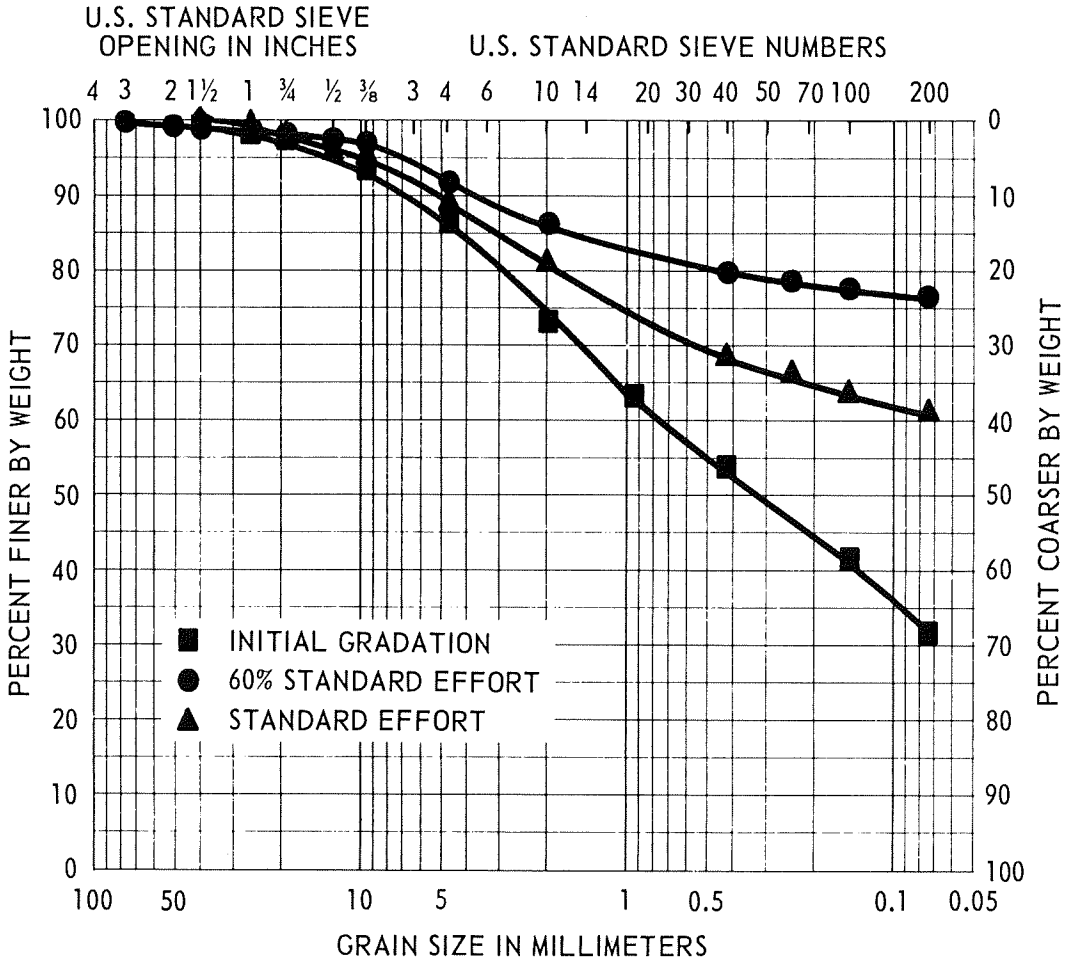

Figure 23. Effect of consolidation pressure to 800 psi (5.52 MPa) on gradation of TOSCO retorted oil shale

compaction effort than for standard compaction effort. Generally, it would be anticipated that more particle breakage would occur for the higher compaction effort. Perhaps the higher compaction effort contributed to better cementation due to closer association of the particles and, in turn, is expressed by less particle breakage. This explanation is more plausible considering Marachi's et al. (1969) triaxial test results in Pyramid Dam material, which indicated that density had little effect on breakage B value.

Unconfined compression

To investigate self-cementing characteristics, which had been reported by Snethen et al. (1978), Peterson et al. (1978), and WCC (1976) for spent oil shale, 6-in.- (15.2-cm-) diam unconfined compression tests were performed on specimens compacted using three compaction efforts and allowed to cure inside waxed cardboard tubes at ambient temperatures (approximately 72°F) for periods of 0 to 28 days. Figure 24 presents and Table 8 summarizes the unconfined compression results for PARAHO, and Figure 25 and Table 9 for TOSCO. Figure 26 compares the results for both PARAHO and TOSCO, i.e., a combination of both Figures 24 and 25. The following is a summary of the unconfined compressive strengths for PARAHO and TOSCO obtained in this study plus previous tests on PARAHO (WCC, 1976).

Table 7

Breakage Factors Due to Compaction and Consolidation of PARAHO and TOSCO Materials

	PARAHO					TOSCO							
	Original		60% of Standard and Standard			Original		60% of Standard			Standard		
Sieve Size	% Pass	% Retain	% Pass	% Retain	Diff Δ	% Pass	% Retain	% Pass	% Retain	Diff Δ	% Pass	% Retain	Diff Δ
2+	100		100			100							
2 to 1-1/2	93	7	96	4	-3	99	1	99	1	0	99	1	0
1-1/2 to 1	80	13	91	5	-8	98	1	98	1	0	98	1	0
1 to 3/4	67	13	85	6	-7	97	1	97	1	0	97	1	0
3/4 to 1/2	50	17	75	10	-7	96	1	97	0	-1	96	1	0
1/2 to 3/8	40	10	67	8	-2	93	3	97	0	-3	95	1	-2
3/8 to 4	27	13	54	13	0	87	6	92	5	-1	89	6	0
4 to 10	18	9	42	12	+3	73	14	87	5	-9	81	8	-6
10 to 20	13	5	32	10	+5	62	11	83	4	-7	73	8	-3
20 to 40	9	4	22	10	+6	53	9	80	3	-6	69	4	-5
40 to 100	5	4	15	7	+3	42	11	78	2	-9	64	5	-6
100 to 200	3	2	12	3	+1	32	10	76	2	-8	61	3	-7
		3		12	+9		32		76	+44		61	+29
"B" factor					27					44			29

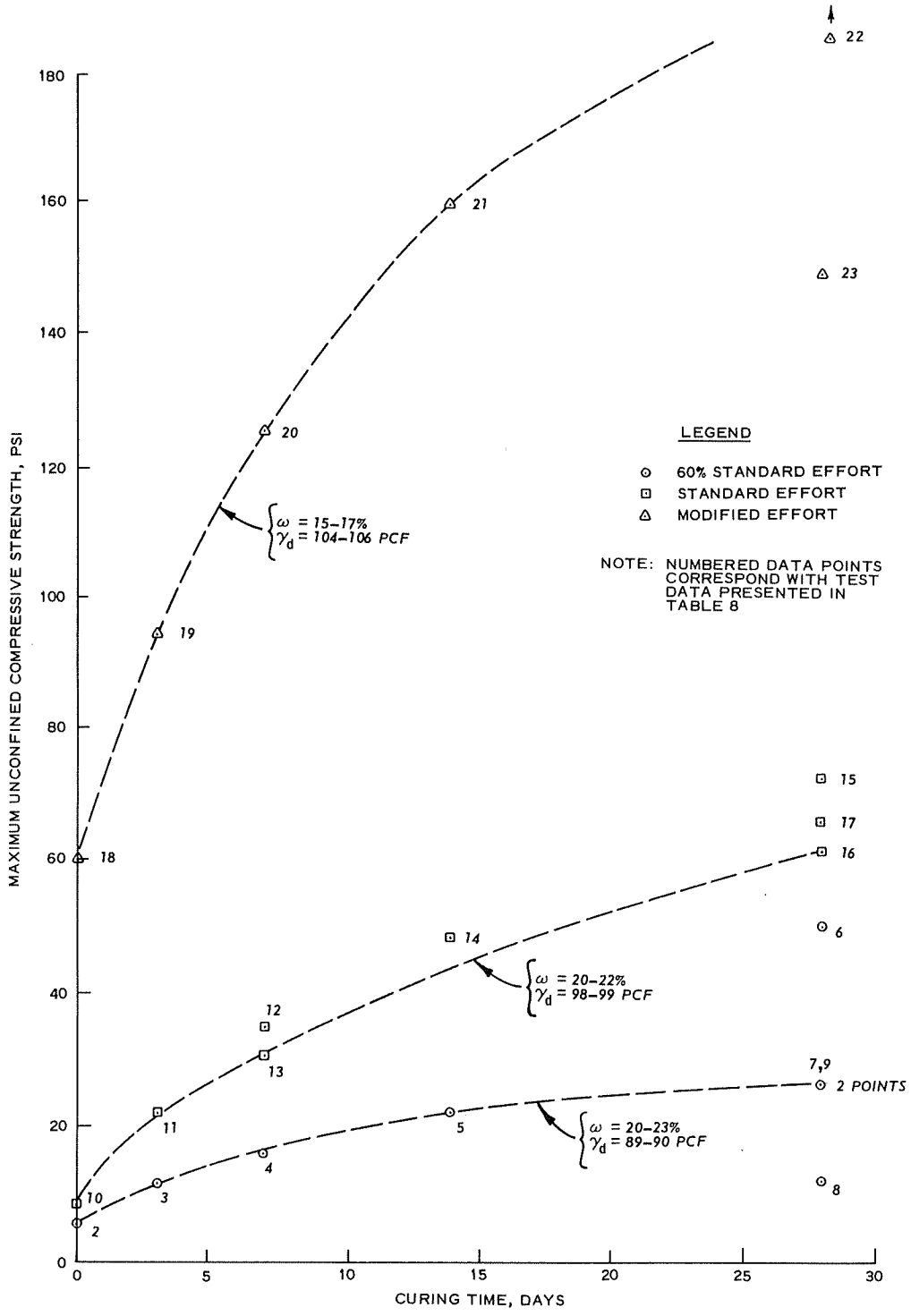

Figure 24. Effect of curing time on the unconfined compressive strength for compacted PARAHO (1 psi = 6.9 kPa)

Table 8

Summary of Unconfined Test Results on PARAHO Oil Shale

Symbol Number on Figure 24	Test No.	Compaction Effort	Curing Time days	As Tested: Water Content w, %	As Tested: Dry Density γ_d, pcf	Maximum Unconfined Strength: psi	Maximum Unconfined Strength: tsf	Secant Young's Modulus to 1/2 Maximum Unconfined Strength: psi	Secant Young's Modulus to 1/2 Maximum Unconfined Strength: tsf	Remarks
1	UC-L-0-9	60% standard	0	22.8	89.2	--	--	--	--	Questionable results
2	UC-L-0-9A		0	22.5	89.8	5.7	0.41	720	51.5	
3	UC-L-3-10		3	21.6	89.3	11.9	0.86	650	46.5	
4	UC-L-7-11		7	21.5	90.3	16.3	1.17	1,560	112.0	
5	UC-L-14-12		14	20.5	90.4	22.8	1.64	Not available		Initial strain data are questionable
6	UC-L-28-13		28	20.2	97.1	51.3	3.69	2,730	196.5	
7	UC-L-28-13A		28	23.0	93.0	27.4	1.97	1,180	85.5	Soaked overnight before test conducted
8	UC-L-28-13B		28	20.4	82.9	12.5	0.90	1,130	81.5	
9	UC-L-28-13C		28	20.4	90.5	27.4	1.97	1,840	132.5	
10	UC-S-0-5	Standard	0	20.7	99.6	8.2	0.59	510	37.0	
11	UC-S-3-6		3	21.4	99.0	22.4	1.61	890	64.0	
12	UC-S-7-1		7	21.3	98.0	35.6	2.56	950	68.5	Mellowed 16 hr before compacting
13	UC-S-7-4		7	21.3	98.2	31.1	2.24	1,430	103.5	
14	UC-S-14-7		14	20.3	100.9	49.3	3.55	2,230	160.5	
15	UC-S-28-2		28	20.4	98.3	73.6	5.30	3,640	262.0	Mellowed 16 hr before compacting
16	UC-S-28-3		28	22.1	98.1	62.3	4.49	2,740	197.0	Mellowed 16 hr before compacting; soaked overnight before test conducted
17	UC-S-28-8		28	19.5	101.2	66.8	4.81	2,630	189.0	
18	UC-M-0-14	Modified	0	17.2	104.4	61.3	4.41	4,100	295.0	
19	UC-M-3-15		3	16.6	105.8	95.6	6.88	4,240	305.0	
20	UC-M-7-16		7	15.6	105.2	127.0	9.14	8,170	588.0	
21	UC-M-14-17		14	15.7	105.5	161.6	11.64	12,000	864.0	
22	UC-M-28-18A		28	17.4	107.2	194.8	14.03	11,818	850.9	Soaked overnight before test conducted
23	UC-M-28-18B		28	15.1	106.5	151.4	10.90	11,818	850.9	

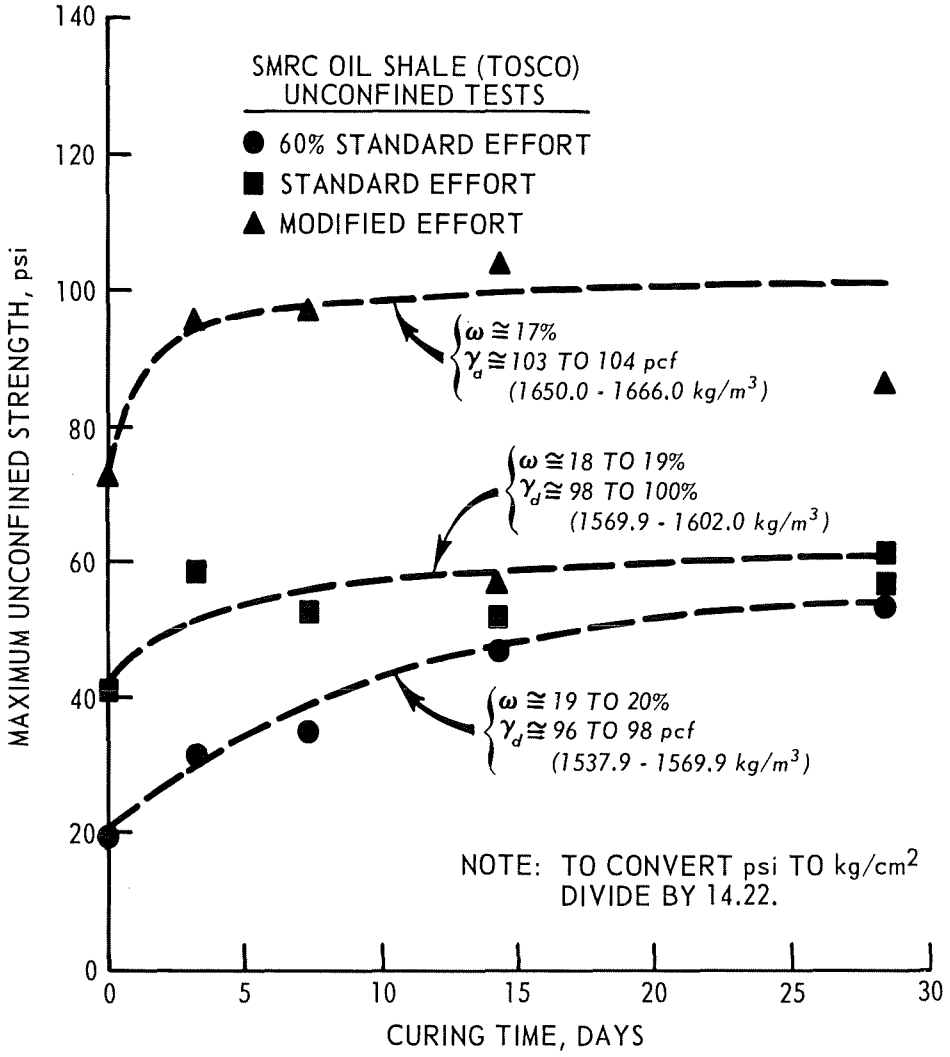

Figure 25. Effect of curing time on unconfined compressive strength for compacted TOSCO (1 psi = 6.9 kPa)

Table 9

Summary of Unconfined Test Results on TOSCO Oil Shale

Test No.	Compaction Effort	Curing Time days	As Tested Water Content %	As Tested Dry Density pcf	Maximum Unconfined Strength psi	Maximum Unconfined Strength tsf
		TOSCO Oil Shale				
UC-L-0	60% of	0	20.6	96.7	19.5	1.40
UC-L-3	Standard	3	19.9	97.5	31.7	2.28
UC-L-7	↓	7	20.0	97.6	35.1	2.53
UC-L-14		14	19.5	96.3	47.0	3.38
UC-L-28		28	18.6	95.5	53.7	3.87
UC-S-0	Standard	0	18.5	98.2	41.4	2.98
UC-S-3	↓	3	18.1	98.8	58.7	4.22
UC-S-7		7	18.1	100.9	52.5	3.78
UC-S-14		14	18.7	96.3	52.1	3.75
UC-S-28-1		28	18.0	97.5	57.1	4.11
UC-S-28-2		28	18.1	98.8	61.8	4.45
UC-M-0	Modified	0	17.2	103.7	72.4	5.21
UC-M-3	↓	3	17.4	101.6	95.5	6.88
UC-M-7		7	17.3	103.8	96.9	6.97
UC-M-14-1		14	17.3	103.1	57.1	4.11
UC-M-14-2		14	16.7	103.2	103.8	7.48
UC-M-14-3		14	17.2	104.1	104.0	7.49
UC-M-28		28	17.2	103.6	86.3	6.21
		75% PARAHO and 25% TOSCO Oil Shale				
UC-S-PT-0*	Standard	0	18.4	96.0	23.4	4.70
UC-S-PT-28*	Standard	28	17.3	96.2	65.9	4.74

* See Figure 26.

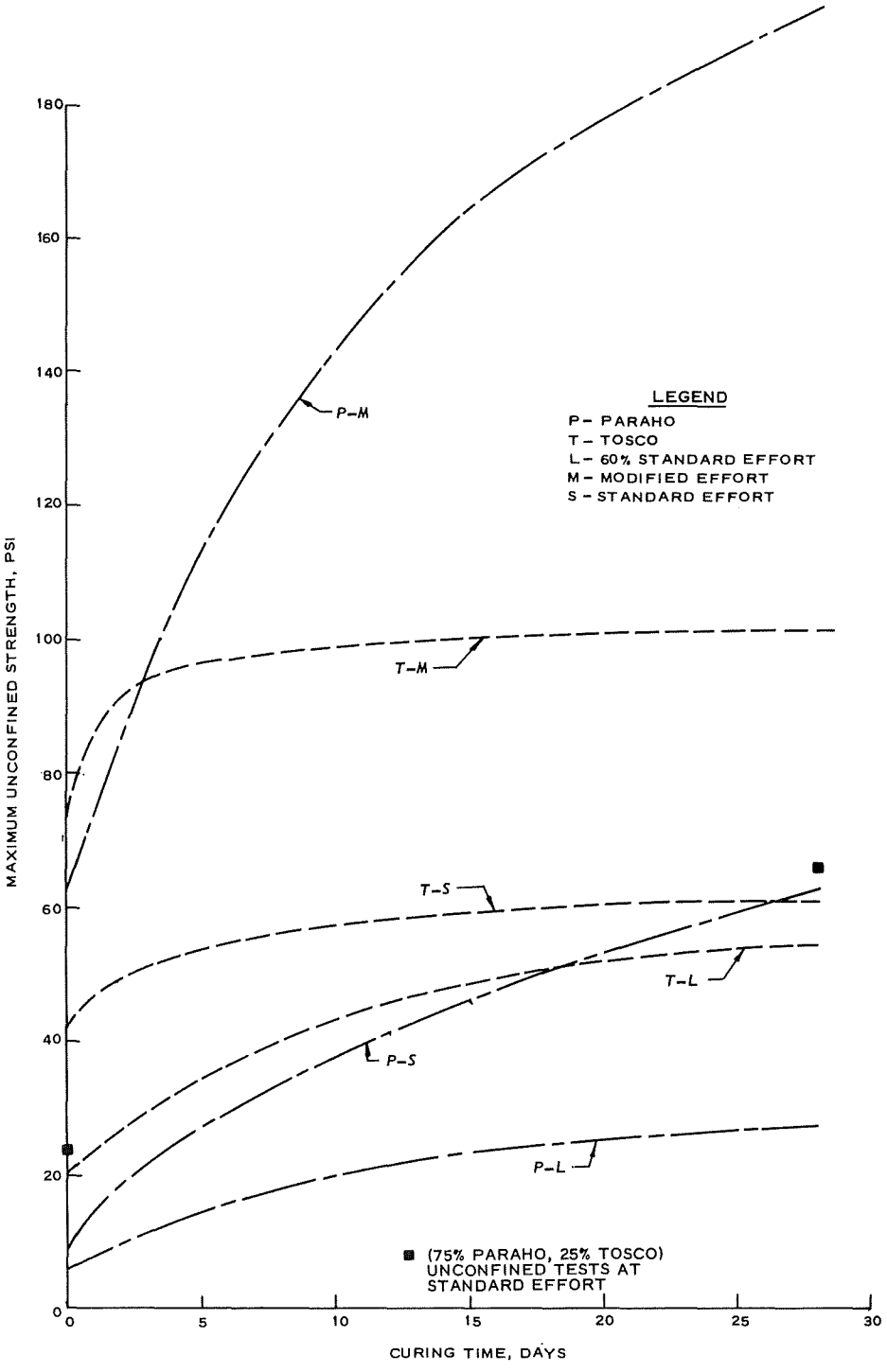

Figure 26. Comparison of unconfined compressive strengths for PARAHO and TOSCO retorted oil shales (1 psi = 6.9 kPa)

Compaction Effort	Unconfined Compressive Strength, psi				
	PARAHO		TOSCO		PARAHO (WCC, 1976)
	0^d	28^d	0^d	28^d	28^d at 123°F
60% of Standard	5.7	27.4	19.5	53.7	150-175
Standard	8.2	66.8	41.4	61.8	150-175
Modified	61.3	194.8	72.4	104	175-200

The unconfined compressive strength of a standard effort equivalent density specimen composed of 75 percent PARAHO plus 25 percent TOSCO mixture exhibited a strength increase from 23.6 psi for zero-day curing to 65.9 psi for 28-day curing (162.8 to 454.7 kPa) (Figure 26 and Table 9).

These results indicate self-cementing characteristics* since the unconfined compressive strength of retorted oil shale increases with curing time. The magnitude of cementation is dependent upon curing time and density and increases proportionally with these variables. The durability of the cementing action was verified for several 28-day cured PARAHO specimens by soaking them overnight (Table 8). These results also show that overnight soaking caused no strength loss; in fact, a slight strength gain was observed in two of the three specimens (low and modified compaction efforts). Hence, the observed self-cementing phenomenon is not due to capillary moisture tension, i.e., effective cohesion.

PARAHO specimens continued to gain strength throughout the 28-day curing time, and the shape of the curves in Figures 24 and 26 suggest that they are still gaining strength beyond these 28 days. Although higher densities produced greater strengths, percentagewise standard effort density specimens produced the greatest strength gains. For the TOSCO specimens, the major portion of the total strength gain occurred within three days after compaction. Perhaps the finer nature of the TOSCO material permits cementation reactions to be completed more rapidly than the coarser PARAHO material.

An examination of Figure 26 reveals PARAHO to be more reactive than TOSCO, for while TOSCO initial strengths are higher than corresponding PARAHO initial strengths, yet after 28 days, except for 60 percent of standard density specimens, the PARAHO specimens exhibit higher strengths. Also, the percent strength gains for PARAHO specimens are three to eight fold, while TOSCO specimens only register a 1.5- to 3-fold increase. The 75 percent PARAHO plus 25 percent TOSCO mixture at standard effort density performed practically the same as the comparable 100 percent PARAHO specimens. Whereas it would be anticipated that the finer nature TOSCO would be more reactive than coarser PARAHO, this is not the case. Perhaps the finer material deteriorates upon exposure to air more rapidly, thereby losing much of its self-cementing potential. If this is true, then the delay between retorting and fill placement becomes an important variable.

Previous unconfined compression tests by WCC (1976) on specimens of PARAHO processed at the semiworks plant by direct heating and cured 28 days at 125°F indicate strengths of 175-200 psi (1.2 to 1.4 MPa) and 150-175 psi

* Additional studies concerning self-cementing characteristics are being investigated by the Colorado School of Mines Research Institute under USBM Contract No. J0285001.

(1.0 to 1.2 MPa) for modified and standard effort density specimens, respectively. By comparison, strengths of 194.8 psi and 66.8 psi (1.3 MPa and 47 kPa) were obtained in this investigation for the same compacted efforts. Considering the differences in several key variables affecting cementing reactions, i.e., curing temperatures (125°F versus 72°F), percent fines and gradation differences (14-24 percent versus 3 percent), and the amount of time between retorting and compaction (approximately one week versus approximately six months) between WCC (1976) and this investigation, the agreement for the modified effort strengths is fortuitous. The differences between WCC (1976) and this investigation favor higher strengths for WCC specimens as observed.

Criteria for assessing stabilization response of soils treated with lime recommend an unconfined compressive strength increase of 50 psi (345 kPa) after 28-day curing at 72°F between standard effort density untreated and lime-treated specimens (Thompson, 1970). Durability criteria for nonfrost conditions recommend an unconfined compressive strength of 30 psi (207 kPa) after 28-day curing at 72°F followed by 24-hr immersion (Dunlap et al., 1975). Soil-lime specimens satisfying these two criteria are considered sufficiently strong and durable for use as base course material in pavements. Based upon these criteria, PARAHO would be judged as a suitable stabilized material, while TOSCO fails to satisfy these criteria. Perhaps the fine-grained nature of TOSCO makes self-cementing components susceptible to deterioration upon prolonged exposure to air, while PARAHO breaks down during compaction and exposes fresh surfaces for reaction.

An important construction consideration for stabilized soils is time between mixing and compaction, termed "mellowing time." The results presented in Table 8 show that mellowing times up to 16 hr had no effect on resulting unconfined compressive strengths. Based upon these considerations several important design and construction guidelines are evident if self-cementing is desired:

a. PARAHO and TOSCO both possess self-cementing properties producing additional strength with time. However, PARAHO satisfies recommended criteria for lime-stabilized soils, but TOSCO does not.

b. Increased density produces higher strengths. Hence, areas where additional strength is required, i.e., adjacent to structures, surfaces exposed to erosion, etc., can be accommodated by providing additional compaction.

c. Mellowing times up to 16 hr have little effect on self-cementing of PARAHO. Nevertheless, experience dictates this time should be kept to a minimum. However, if this is not possible, increased compaction effort can be substituted to obtain greater strengths if the expense of increased compaction effort is justified.

d. For PARAHO, the self-cementing components do not deteriorate significantly due to exposure to air after retorting. However, for TOSCO this apparently is not the case, as it is less reactive, although finer grained. Nevertheless, logic suggests that exposure time between retorting and placement should be minimized to maximize self-cementation.

e. The self-cementing characteristics of PARAHO are retained, i.e., specimens not affected by immersion.

f. Cementing reactions under normal curing conditions for PARAHO are slow, with strength gains still indicated after 28 days. Hence, heavy equipment should be restricted from tracking compacted areas for at least 7-14 days following compaction. Conversely, TOSCO gains most of its strength within 3 days following compaction, and equipment routing can be done accordingly.

Triaxial compression tests

Strength parameters for the three compactive efforts were determined by performing a series of consolidated-drained S triaxial compression tests and consolidated-undrained $\bar{R}$ triaxial compression tests with pore pressure measurements on 9-in.- (22.9-cm-) diam specimens of PARAHO material. Supplementary $\bar{R}$ tests were performed on 6-in.- (15.2-cm-) and 1.4-in.- (3.6-cm-) diam specimens of modeled PARAHO and PARAHO fines, respectively, prepared at equivalent standard effort density. A series of $\bar{R}$ tests on 6-in.- (15.2-cm-) diam specimens of TOSCO compacted to three different densities were used to determine the strength of this material. Effective confining pressures used for these tests were 20, 40, 80 psi (138, 276, 552 kPa) and 160 psi (1.1 MPa).

Interpretation of shear strength parameters based upon total stresses from $\bar{R}$ test envelopes is influenced by several factors: (a) curved failure envelopes, (b) negative pore pressures, and (c) criteria selecting maximum deviator stress. Typically the failure envelope based upon total stresses is curved, particularly in the overconsolidated range of normal stresses. Thus the parameters, angle of internal friction ϕ and cohesion c , are often reported only for the higher confining stresses, i.e., the normally consolidated range. In undrained tests, reduced pore pressures due to the tendency for dilation during shear creates tension in the pore water, which can cause measured deviator stresses to be unusually high and to correspondingly affect the failure envelope. Because these high induced negative pore pressures, $u - u_o$, may not develop in the field, the deviator stress corresponding to the maximum effective stress ratio, σ_1'/σ_3' , is used for determining the strength envelope. Since $\sigma_1'/\sigma_3' = \tan^2 (45 + \phi'/2)$, this provides the maximum value for the effective angle of friction ϕ' . Alternatively, the effective stress path, which is the locus of stress states, can provide indications of dilation and the influence of pore pressure on strength. Typically, the stress path will curve upward or down the failure envelope, thereby assisting in determining values of ϕ' and effective cohesion c' . For these reasons, Tables 10 through 12 list values for maximum deviator stress and stress ratio.

Figures 27 through 34 present the effective stress paths, Mohr's circles based upon maximum effective principal stress ratio, and the total and effective stress envelopes for both PARAHO and TOSCO materials where applicable. The following tabulation summarizes and compares the total and effective stress parameters for PARAHO and TOSCO; the values shown ignore failure envelope curvature and are based upon "best-fit" straight-line envelopes:

Material and Compaction Effort	Maximum Particle Size, in.	Total Stress		Effective Stress	
		ϕ, deg	c, kg/cm^2	ϕ', deg	c', kg/cm^2
PARAHO					
9-in.-diam, 60% of Standard	1-1/2			33.0	0.9
Standard	1-1/2	14.5	1.3	32.7	0.8
Modified	1-1/2	31.0*	0	32.3	1.9
Modeled PARAHO					
9-in.-diam, Standard*	3/4			38.0	0
6-in.-diam, Standard	3/4	17.1	1.7	37.9	1.1
PARAHO Fines					
1.4-in.-diam, Standard		23.2	1.7	33.6	2.3
TOSCO					
6-in.-diam, 60% of Standard	3/4	20.2	0.3	36.7	0.1
Standard	3/4	18.4	0.3	35.0	0.1
Modified	3/4	24.5	1.4	43.0	0

* Based upon single test.

Typically well-graded compacted gravels have effective angles of internal friction ranging from 40 to 45 deg for these confining stresses (Donaghe and Cohen, 1978; Becker et al., 1972); hence, while PARAHO possesses adequate strength, it is slightly weaker than similarly graded gravels. These results show that except for a higher cohesion intercept for specimens compacted using modified effort, increased compaction effort does not noticeably improve PARAHO's shear strength parameters.

These results also show that modeling by scalping and replacement techniques (compare 6-in.- (15.2-cm-) diam with 9-in.- (22.9-cm-) diam, standard effort density) overestimate the effective angle of internal friction by 5.2 deg and cohesion intercept by 0.3 kg/cm^2. The tests on the PARAHO fines provide conflicting conclusions, as the 1.4-in.- (3.6-cm-) diam tests show higher strengths (ϕ' = 33.6 deg) than the full-scale 9-in.- (22.9-cm-) diam specimens (ϕ' = 32.3 to 33.0 deg), yet lower strengths than the 6-in.- (15.2-cm-) diam modeled specimens (ϕ' = 37.9 deg). Nevertheless, due to the small quantity of fines in the large specimens, it is doubtful that the fines control the strength of this material. Concerning effects of modeling technique, Donaghe and Cohen (1978) have shown that model gradations having a constant uniformity coefficient C_u (parallel gradation) or variable C_u, (scalped only) provide the same estimates of the angle of internal friction for clean gravels at single confining stresses. Marachi et al. (1969) also has shown that for constant C_u modeling (parallel), reasonable estimates of friction angle can be obtained using smaller specimens. Hence, from these considerations, use of scalping and replacement as a modeling technique is not recommended for PARAHO material.

The S triaxial compression tests on 6-in.- (15.2-cm-) diam specimens of 1-1/2-in. (38-mm) maximum particle-sized PARAHO material at standard

Table 10

Summary of Consolidated-Drained (S) and -Undrained ($\bar{R}$) Triaxial Compression Tests on PARAHO Material

Test No.*	Compaction Effort**	Specimen Conditions: Initial: Water Content w, %	Initial: Dry Density γ_d pcf	Initial: Saturation S, %	Initial: Void Ratio e	After Consolidation: Dry Density γ_d pcf	After Consolidation: Void Ratio e	Maximum B Before Consolidation $B = \Delta u/\Delta\sigma_3$	Permeability cm/sec	At Maximum Effective Stress Ratio, $\bar{\sigma}_1/\bar{\sigma}_3$: Principal Stress Difference $\sigma_1 - \sigma_3$ kg/cm^2	Induced Pore Pressure $u - u_o$ kg/cm^2	Volumetric Strain $\Delta V/V_o$ %	Effective Minor Principal Stress $\bar{\sigma}_3$ kg/cm^2	Effective Stress Ratio $\bar{\sigma}_1/\bar{\sigma}_3$	Pore Pressure Parameter, A $A = \frac{u - u_o}{\sigma_1 - \sigma_3}$	Strain ε %
S-P-9-L-20-1	(1)	17.0	90.1	57.8	0.738	90.9	0.724	0.97	1.5×10^{-2}†	6.23	N/A	2.65	1.66	4.75	N/A	15.02
S-P-9-L-40-1		18.3	89.3	62.2	0.753	91.4	0.714	0.97	1.0×10^{-2}†	8.95	N/A	4.81	3.04	3.94	N/A	13.2
S-P-9-L-80-1		23.3	89.2	79.1	0.756	92.2	0.700	0.97	5.8×10^{-3}	14.29	N/A	6.29	5.86	3.44	N/A	14.2
S-P-9-L-160-1		17.8	88.7	60.6	0.765	95.4	0.643	0.96	2.7×10^{-3}	27.54	N/A	7.61	11.35	3.43	N/A	15.2
$\bar{R}$-P-9-S-20-1	(2)	18.7	95.1	72.8	0.654	95.9	0.640	0.97	4.6×10^{-3}	4.03	0.68	N/A	0.80	6.02	0.17	1.5
$\bar{R}$-P-9-S-40-1		17.3	95.1	67.2	0.654	96.6	0.629	0.98	1.9×10^{-3}	6.13	1.59	N/A	1.38	5.45	0.26	2.0
$\bar{R}$-P-9-S-160-1		17.5	95.2	68.2	0.652	98.1	0.604	0.96	5.2×10^{-4}	10.61	8.65	N/A	2.73	4.89	0.81	5.1
S-P-9-S-80SR-1		18.1	96.5	70.6	0.629	98.0	0.618	0.97	6.8×10^{-4}	18.79	N/A	1.80	5.72	4.28	N/A	7.8
S-P-9-S-80-2		18.6	94.6	72.7	0.662	97.0	0.622	0.97	6.2×10^{-4}	14.81	N/A	4.20	5.69	3.60	N/A	14.24
S-P-9-M-20-1	(3)	13.1	98.7	51.5	0.606	99.5	0.594	0.98	5.9×10^{-4}	10.34	N/A	0.48	1.57	7.58	N/A	1.5
S-P-9-M-40-1		12.9	100.3	50.6	0.581	101.2	0.567	0.97	7.6×10^{-4}	14.35	N/A	0.57	2.95	5.86	N/A	1.8
$\bar{R}$-P-9-M-80-1		13.0	100.3	51.2	0.581	101.8	0.558	0.97	4.6×10^{-4}	12.32	3.56	N/A	2.22	6.55	0.29	1.0
S-P-9-M-160-1		12.8	98.5	50.4	0.601	101.7	0.559	0.99	5.7×10^{-4}	32.23	N/A	2.24	11.33	3.84	N/A	7.0

* S = consolidated-drained; $\bar{R}$ = consolidated-undrained; P = PARAHO; SR = scalped and replaced gradation; 9 = 9-in. diam; 6 = 6-in. diam; L, S, and M = low, standard, or modified compaction effort; 20, 40, 80, or 160 = confining pressure; 1 or 2 = specimen number. Example: S-P-9-L-20-1 = 9-in.-diam PARAHO specimen, low compaction effort, 20-psi confining pressure, test specimen No. 1.

** (1) indicates 60% of standard (G_s = 2.51); (2) standard (G_s = 2.52); and (3) modified (G_s = 2.54).

† Permeability data may be questionable.

Table 11

Summary of Consolidated-Undrained Triaxial Compression Tests with Pore Pressure Measurements on Modeled PARAHO and PARAHO Fines

Test No.*	Compaction Effort	Specimen Condition: Water Content w, %	Specimen Condition: Dry Density γ_d pcf	Specimen Condition: Saturation S, %	Specimen Condition: Void Ratio e	Maximum B Before Consolidation $B = \Delta u/\Delta\sigma_3$	Permeability k, cm/sec $\times 10^{-6}$	Rate of Strain %/min	Principal Stress Difference $\sigma_1 - \sigma_3$ kg/cm^2	Induced Pore Pressure $u - u_o$ kg/cm^2	Effective Minor Principal Stress $\bar{\sigma}_3$ kg/cm^2	Effective Stress Ratio $\bar{\sigma}_1/\bar{\sigma}_3$	Pore Pressure Parameter $A = \frac{u - u_o}{\sigma_1 - \sigma_3}$	Strain ε %
		Initial								At Maximum Effective Stress Ratio, $\bar{\sigma}_1/\bar{\sigma}_3$				
$\bar{R}$-P-6-S-20-1	Standard	21.3	99.6	91.5	0.592	0.90	0.16	0.05	5.65	0.66	0.75	8.54	0.12	2.51
$\bar{R}$-P-6-S-20-2	↓	21.4	98.4	88.9	0.612	1.03	52	0.08	5.59	0.81	0.59	10.55	0.15	2.02
$\bar{R}$-P-6-S-40-1	↓	20.7	99.3	88.2	0.596	0.85	5.3	0.11	10.21	1.40	1.33	8.69	0.14	3.54
$\bar{R}$-P-6-S-80-1	↓	21.7	96.7	86.1	0.640	1.02	23	0.12	9.54	4.03	1.53	7.25	0.42	2.14
$\bar{R}$-P-6-S-160-1	↓	21.9	96.5	86.6	0.643	1.02	6.8	0.11	13.83	8.14	3.12	5.43	0.59	2.74
$\bar{R}$-P-6-L-40-1	60% of Standard	21.5	91.4	74.8	0.727	0.96	49	--	--	--	--	--	--	--
$\bar{R}$-P-1.4-S-20-2	Standard	24.3	80.4	60.6	1.073	1.00	13	--	7.11	1.37	0.04	205.8	0.19	0.67
$\bar{R}$-P-1.4-S-40-1	↓	23.4	82.3	60.8	1.026	1.00	8.5	--	10.88	2.55	0.27	41.85	0.23	0.92
$\bar{R}$-P-1.4-S-80-1	↓	23.3	82.0	60.1	1.034	1.01	12	--	10.95	3.73	1.90	6.77	0.34	1.24
$\bar{R}$-P-1.4-S-160-1	↓	23.0	83.0	61.0	1.008	1.01	8.3	--	19.96	6.65	4.60	5.34	0.33	2.41
		After Consolidation							At Maximum Principal Stress Difference, $\bar{\sigma}_1 - \bar{\sigma}_3$					
$\bar{R}$-P-6-S-20-1	Standard	--	100.2	--	0.583	0.90	0.16	0.05	12.92	-2.08	3.49	4.71	-0.16	13.14
$\bar{R}$-P-6-S-20-2	↓	24.0	99.6	102.9	0.592	1.03	52	0.08	12.12	-1.95	3.35	4.62	-0.16	13.44
$\bar{R}$-P-6-S-40-1	↓	22.1	102.4	102.2	0.549	0.85	5.3	0.11	16.31	-1.02	3.75	5.35	-0.06	14.69
$\bar{R}$-P-6-S-80-1	↓	23.7	100.6	104.7	0.576	1.02	23	0.12	15.38	1.57	3.98	4.86	0.10	14.49
$\bar{R}$-P-6-S-160-1	↓	23.0	101.7	104.6	0.559	1.02	6.8	0.11	17.64	6.77	4.69	4.76	0.37	8.70
$\bar{R}$-P-6-L-40-1	60% of Standard	28.5	93.4	104.2	0.692	0.96	49	--	--	--	--	--	--	--
$\bar{R}$-P-1.4-S-20-2	Standard	38.6	80.9	97.3	1.060	1.00	13	--	12.10	0.32	1.09	12.10	0.03	1.92
$\bar{R}$-P-1.4-S-40-1	↓	38.4	83.5	102.9	0.996	1.00	8.5	--	13.43	0.77	2.04	7.59	0.06	2.51
$\bar{R}$-P-1.4-S-80-1	↓	37.1	83.7	100.0	0.990	1.01	12	--	13.23	3.19	2.43	6.44	0.24	2.25
$\bar{R}$-P-1.4-S-160-1	↓	35.7	86.1	101.9	0.935	1.01	8.3	--	20.69	6.47	4.78	5.33	0.31	3.21

* $\bar{R}$ = consolidated-undrained; P = PARAHO; 6 = 6-in. diam; L, S, and M = low, standard, or modified compaction effort; 20, 40, 80, or 160 = confining pressure; 1 or 2 = specimen number. Example: R-P-6-L-20-1 = 6-in.-diam PARAHO specimen, low compaction effort, 20-psi confining pressure, test specimen No. 1.

Table 12

Summary of Consolidated-Undrained Triaxial Compression Tests with Pore Pressure Measurements on TOSCO

Test No.*	Compaction Effort	Specimen Conditions: Water Content w, %	Specimen Conditions: Dry Density γ_d, pcf	Specimen Conditions: Saturation S, %	Specimen Conditions: Void Ratio e	Maximum Pore Pressure Parameter Before Consolidation $B = \Delta u/\Delta\sigma_3$	Coefficient of Consolidation $C_v = \frac{0.2H^2}{t_{50}}$ cm^2/sec	Coefficient of Permeability k cm/sec $\times 10^{-6}$	Rate of Strain %/min	Principal Stress Difference $\sigma_1 - \sigma_3$ kg/cm^2	Induced Pore Pressure $u - u_o$ kg/cm^2	Effective Minor Principal Stress $\bar{\sigma}_3$ kg/cm^2	Effective Stress Ratio $\bar{\sigma}_1/\bar{\sigma}_3$	Pore Pressure Parameter $A = \frac{u - u_o}{\sigma_1 - \sigma_3}$	Strain ε %
		Initial									At Maximum Effective Stress Ratio, $\bar{\sigma}_1/\bar{\sigma}_3$				
R-T-6-L-20-1	60% of Standard	18.8	95.5	69.5	0.706	1.00	1.83	5.0	0.10	2.94	0.55	0.82	4.58	0.19	1.17
R-T-6-L-40-1	↓	20.2	95.6	74.9	0.704	1.04	1.19	2.9	0.09	3.75	1.73	1.17	4.21	0.46	4.29
R-T-6-L-80-1	↓	18.5	95.8	68.9	0.701	1.00	0.88	2.7	0.08	6.31	3.47	2.06	4.06	0.55	2.69
R-T-6-L-80-2	↓	20.6	96.3	77.7	0.692	0.97	0.72	2.1	0.12	6.90	2.79	2.78	3.48	0.40	5.48
R-T-6-L-160-1	↓	20.7	96.0	77.5	0.697	1.05	0.52	1.3	0.14	12.67	7.07	4.13	4.07	0.56	5.82
R-T-6-S-20-1	Standard	18.7	97.9	73.4	0.665	1.00	0.56	3.4	0.07	2.19	0.74	0.66	4.32	0.34	1.20
R-T-6-S-40-1	↓	19.1	97.4	74.1	0.672	0.99	0.69	2.7	0.06	5.27	1.14	1.66	4.17	0.22	3.11
R-T-6-S-40-2	↓	18.9	98.5	75.3	0.655	1.06	1.15	2.3	0.09	5.12	1.48	1.31	4.90	0.29	1.81
R-T-6-S-80-1	↓	18.5	96.0	69.2	0.697	1.00	0.76	2.3	0.11	7.25	4.65	2.52	3.88	0.64	3.51
R-T-6-S-160-1	↓	18.4	96.8	70.2	0.684	1.02	0.62	1.9	0.10	11.27	6.90	4.11	3.74	0.61	5.63
R-T-6-M-20-1	Modified	19.0	103.1	85.5	0.580	1.04	0.35	0.88	0.14	5.88	0.16	1.25	5.70	0.03	2.08
R-T-6-M-20-2	↓	17.3	104.4	80.5	0.561	1.02	0.45	0.73	0.10	6.15	0.33	1.09	6.66	0.05	1.10
R-T-6-M-20-3	↓	19.3	104.2	89.3	0.564	1.02	0.49	0.82	0.015	10.39	-0.78	2.13	5.89	-0.08	1.88
R-T-6-M-40-1	↓	18.3	103.0	82.1	0.582	1.07	0.33	0.68	0.10	8.68	0.74	2.21	4.92	0.09	3.84
R-T-6-M-80-1	↓	17.5	105.3	83.5	0.547	0.98	0.83	0.58	0.09	16.31	2.41	3.22	6.07	0.15	2.32
R-T-6-M-160-1	↓	18.4	103.1	82.8	0.580	1.01	0.60	0.67	0.10	20.33	5.96	5.29	4.85	0.29	2.95
		After Consolidation									At Maximum Principal Stress Difference, $\bar{\sigma}_1 - \bar{\sigma}_3$				
R-T-6-L-20-1	60% of standard	26.2	95.8	97.6	0.700	1.00	1.83	5.0	0.10	3.97	-0.01	1.38	3.88	0.00	15.00
R-T-6-L-40-1	↓	25.7	96.9	98.2	0.682	1.04	1.19	2.9	0.09	4.67	1.23	1.67	3.80	0.26	15.00
R-T-6-L-80-1	↓	25.4	97.7	99.3	0.668	1.00	0.88	2.7	0.08	7.19	2.89	2.64	3.73	0.40	13.96
R-T-6-L-80-2	↓	24.3	99.2	98.7	0.643	0.97	0.72	2.1	0.12	8.12	2.02	3.56	3.28	0.25	15.00
R-T-6-L-160-1	↓	23.5	100.5	99.0	0.621	1.05	0.52	1.3	0.14	14.62	6.12	5.07	3.88	0.42	15.00
R-T-6-S-20-1	Standard	24.4	98.2	96.5	0.659	1.00	0.56	3.4	0.07	2.92	0.25	1.15	3.53	0.08	15.00
R-T-6-S-40-1	↓	25.0	98.5	99.6	0.655	0.99	0.69	2.7	0.06	6.58	0.33	2.47	3.67	0.05	15.00
R-T-6-S-40-2	↓	24.2	99.4	98.6	0.639	1.06	1.15	2.3	0.09	7.38	0.21	2.58	3.86	0.03	15.00
R-T-6-S-80-1	↓	24.8	98.5	98.7	0.654	1.00	0.76	2.3	0.11	8.44	3.99	3.18	3.65	0.47	15.00
R-T-6-S-160-1	↓	23.6	101.7	102.4	0.602	1.02	0.62	1.9	0.10	11.87	6.28	4.74	3.50	0.53	15.00
R-T-6-M-20-1	Modified	21.3	103.8	97.9	0.569	1.04	0.35	0.88	0.14	12.28	-1.60	3.00	5.09	-0.13	4.50
R-T-6-M-20-2	↓	21.1	105.1	100.8	0.545	1.02	0.45	0.73	0.10	21.44	-3.81	5.23	5.10	-0.18	4.04**
R-T-6-M-20-3	↓	21.3	104.9	100.4	0.553	1.02	0.49	0.82	0.015	19.06	-3.57	4.92	4.88	-0.19	4.30**
R-T-6-M-40-1	↓	20.9	105.9	102.5	0.552	1.07	0.33	0.68	0.10	19.87	-3.60	6.56	4.03	-0.18	11.86**
R-T-6-M-80-1	↓	19.9	108.3	103.1	0.504	0.98	0.83	0.58	0.09	31.46	-3.56	9.18	4.43	-0.11	7.67**
R-T-6-M-160-1	↓	20.4	108.0	104.7	0.508	1.01	0.60	0.67	0.10	35.34	-1.40	12.65	3.79	-0.04	15.00

* $\bar{R}$ = consolidated-undrained; T = TOSCO; 6 = 6-in. diam; L, S, and M = low, standard, or modified compaction effort; 20, 40, 80, or 160 = confining pressure; 1 or 2 = specimen number. Example: R-T-6-L-20-1 TOSCO specimen, low compaction effort, 20-psi confining pressure, test specimen No. 1.

** Test terminated at approximately -3.5 kg/cm^2 induced pore pressure.

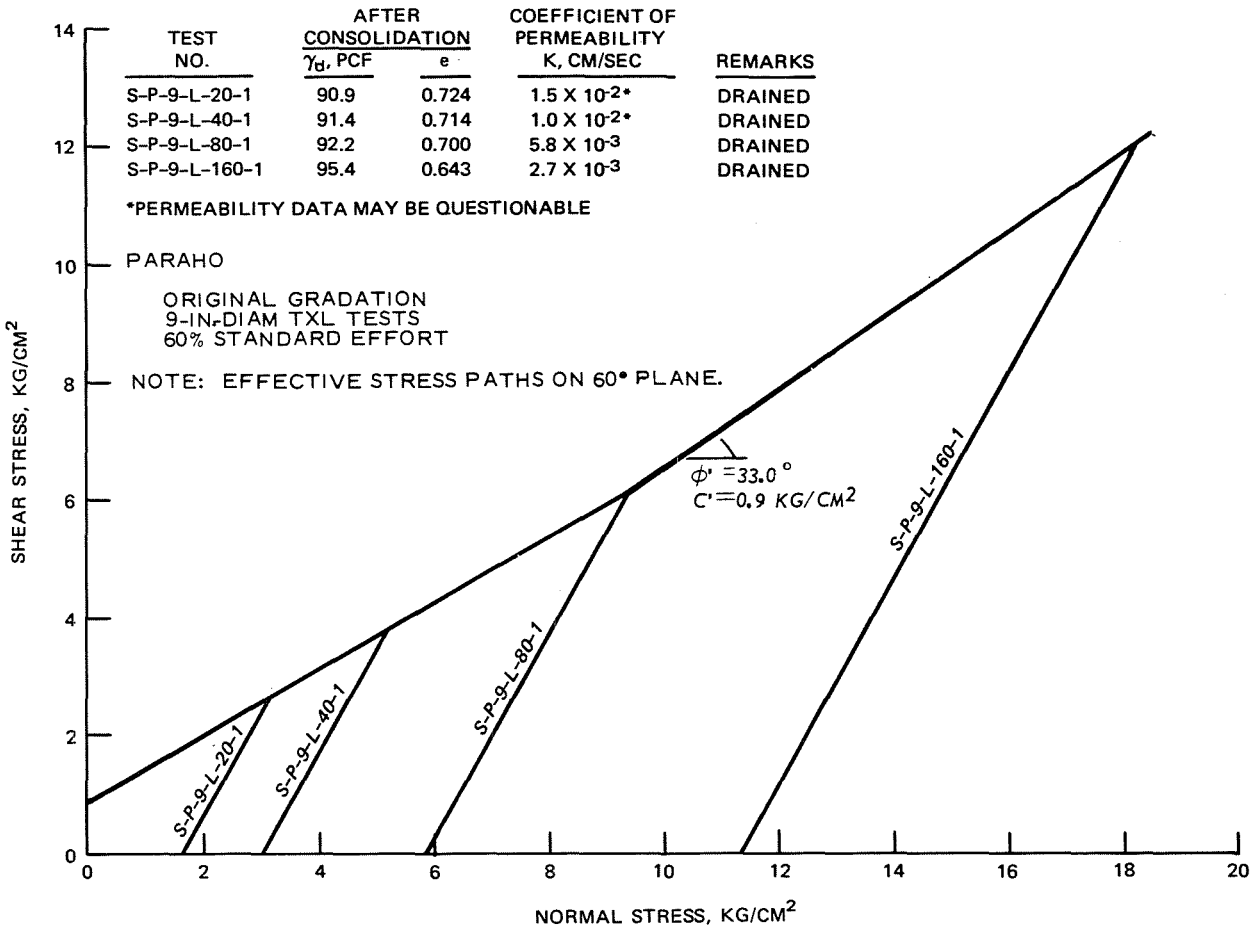

Figure 27. Effective stress envelope for PARAHO compacted to 60 percent of standard effort density

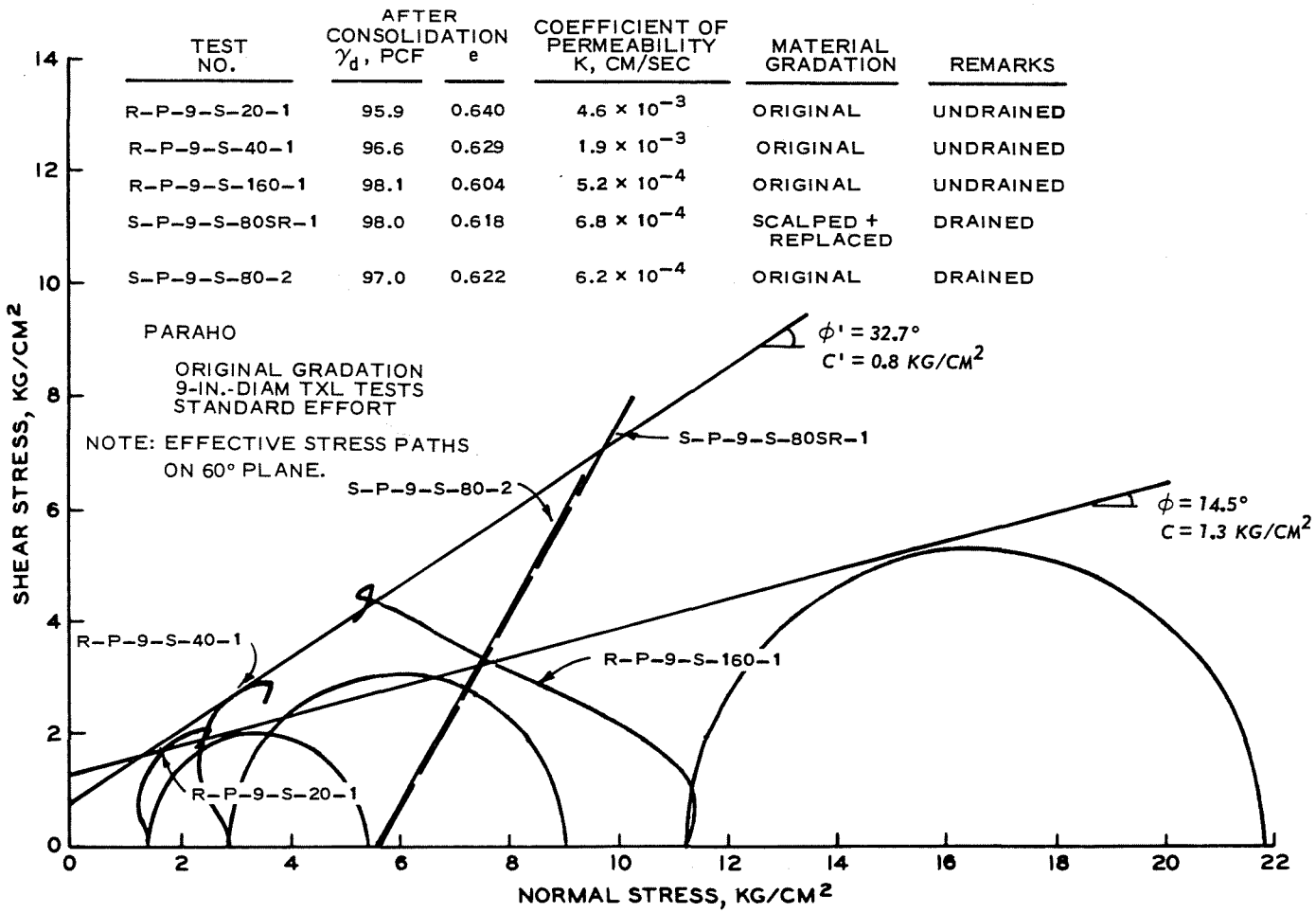

Figure 28. Total and effective stress envelopes for PARAHO compacted to standard effort density

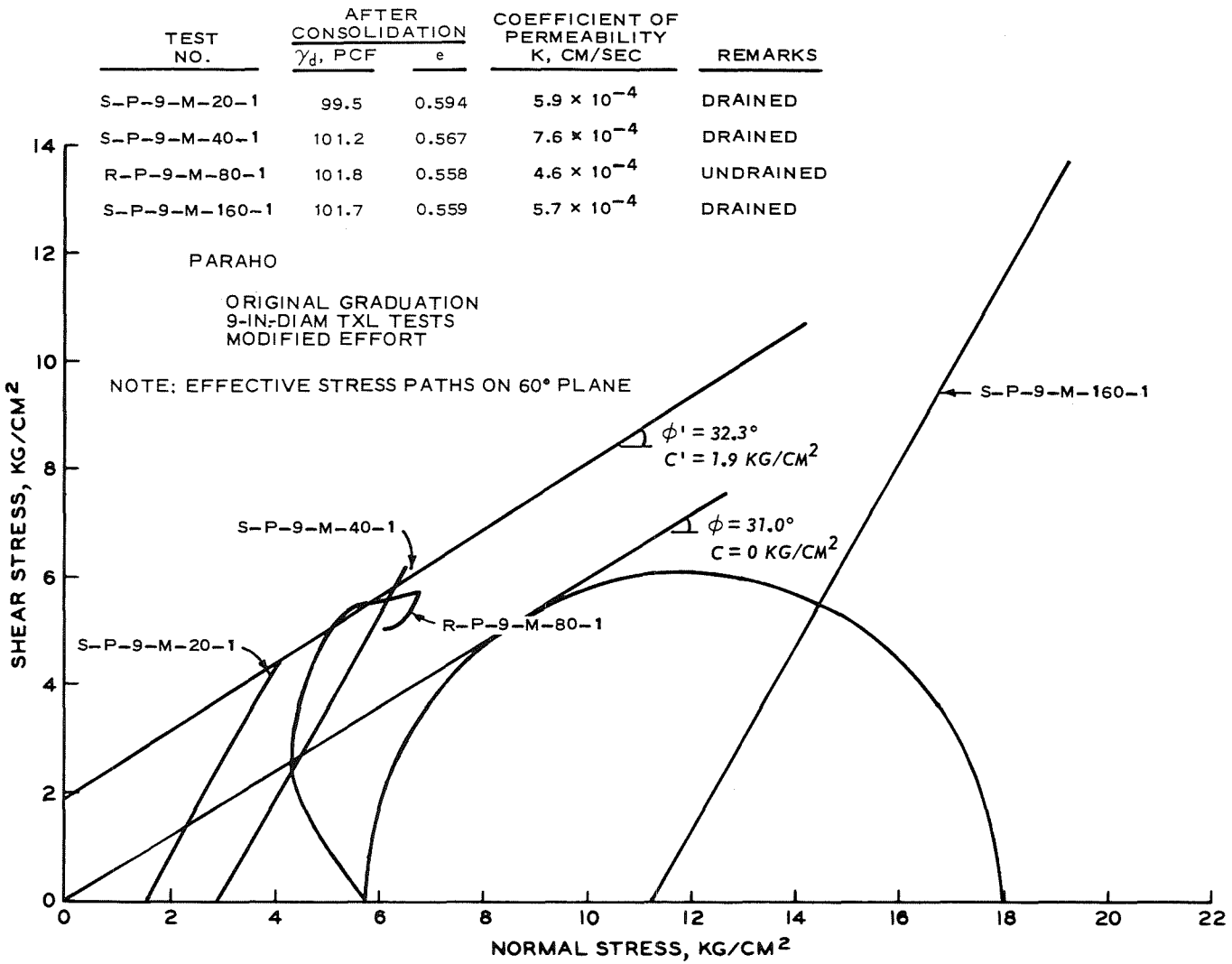

Figure 29. Effective stress envelope for PARAHO compacted to modified effort density

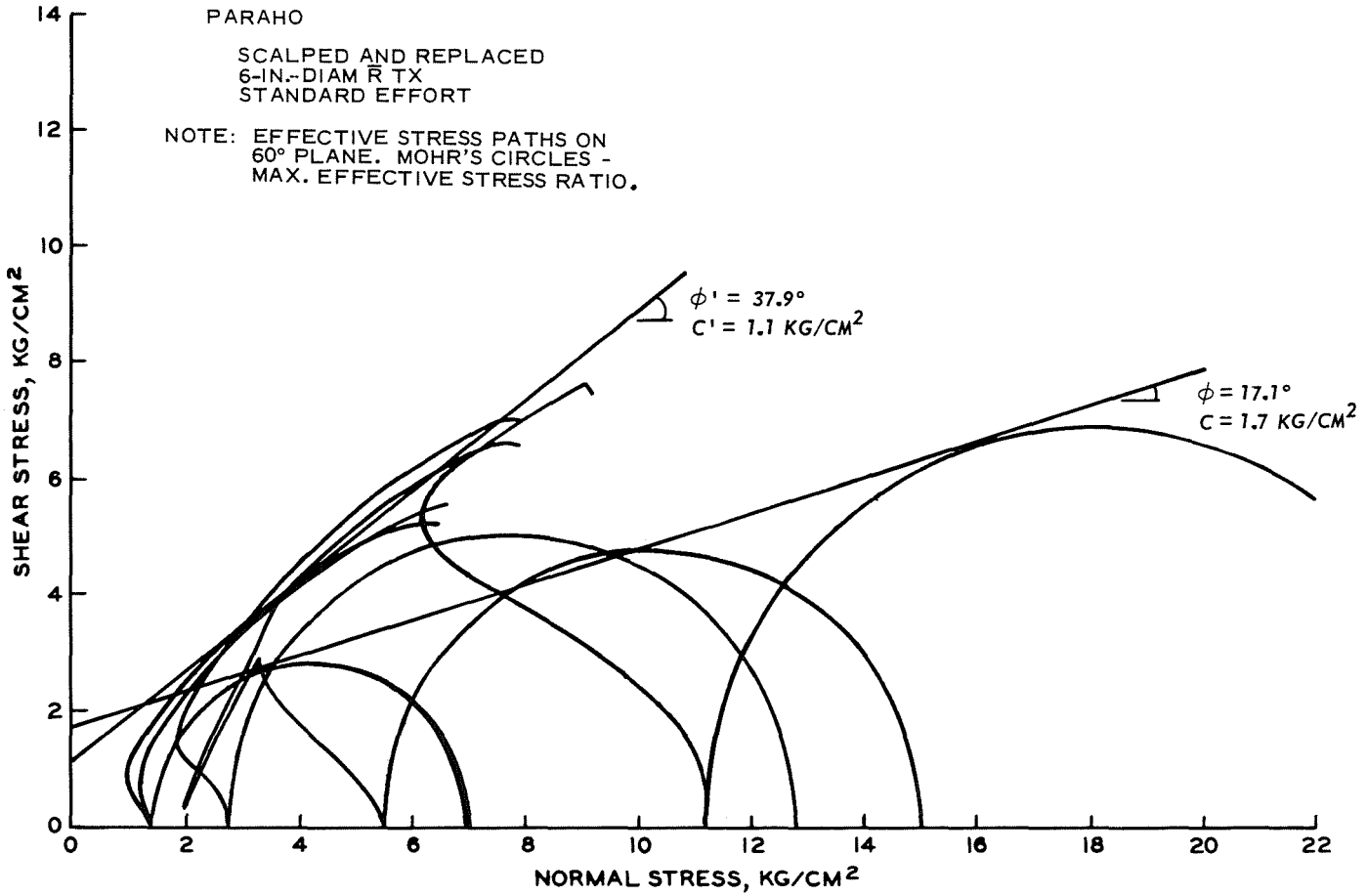

Figure 30. Total and effective stress envelopes for modeled PARAHO compacted to standard effort density

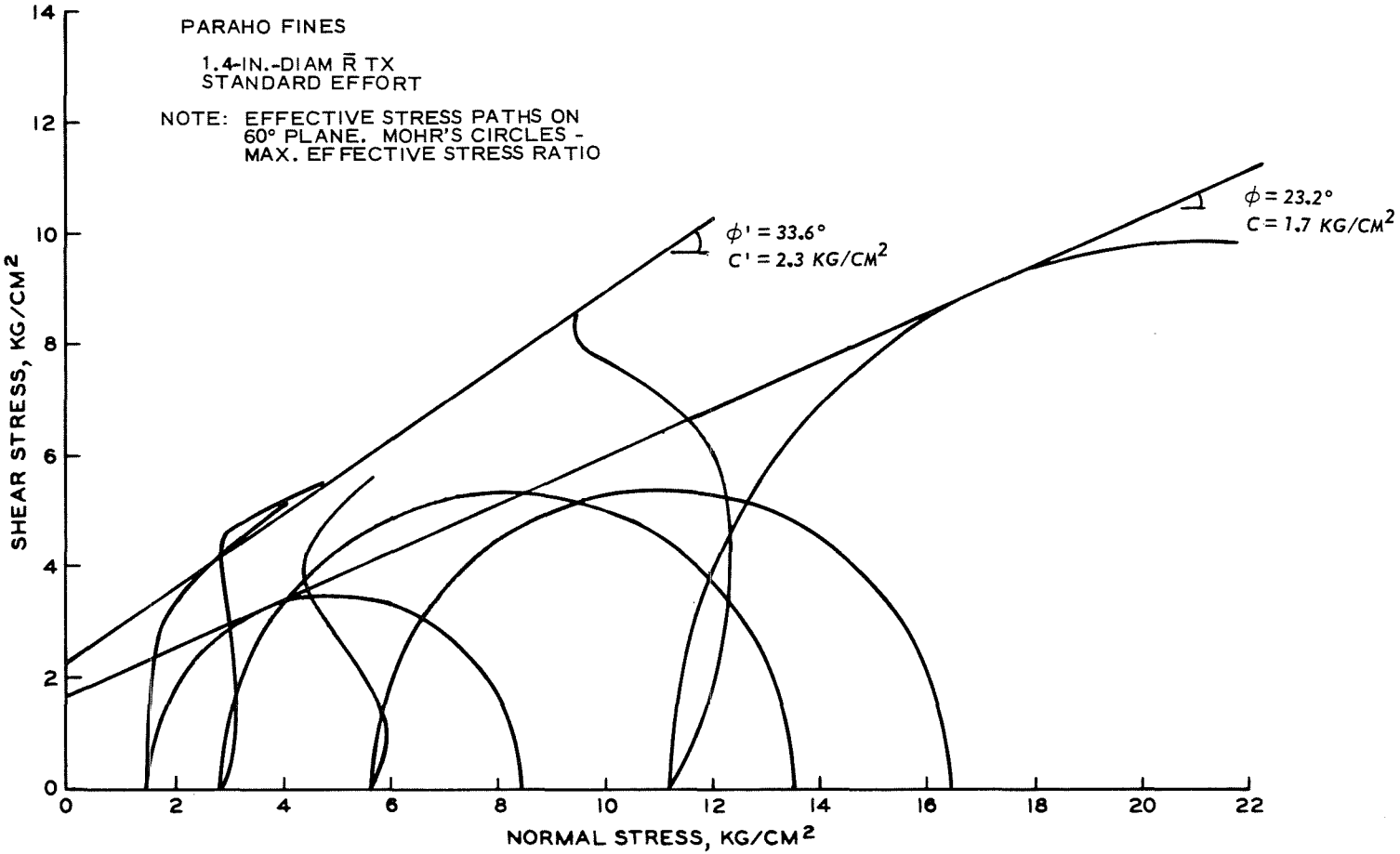

Figure 31. Total and effective stress envelopes for PARAHO fines compacted to standard effort density

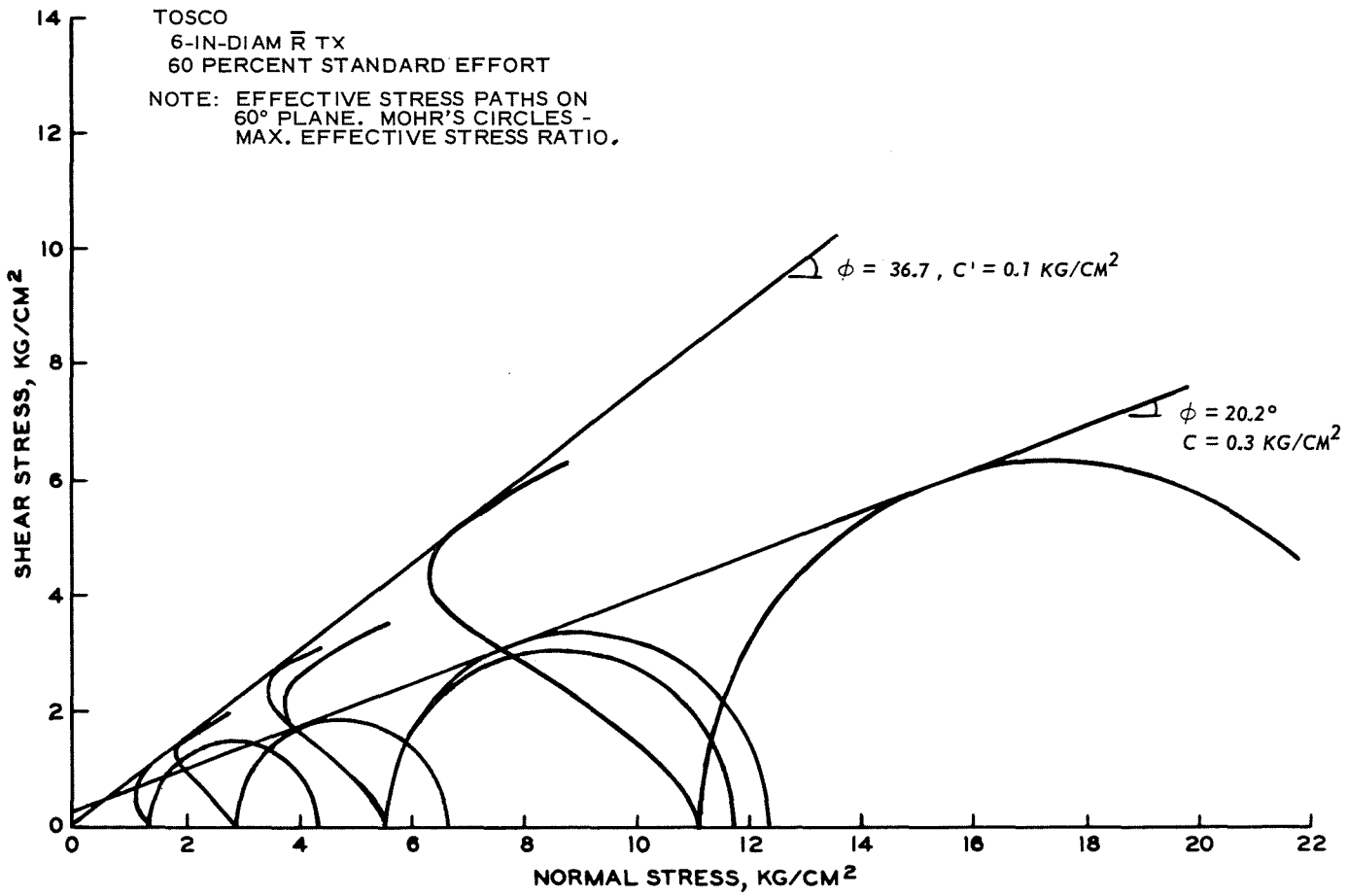

Figure 32. Total and effective stress envelopes for TOSCO compacted to 60 percent of standard effort density

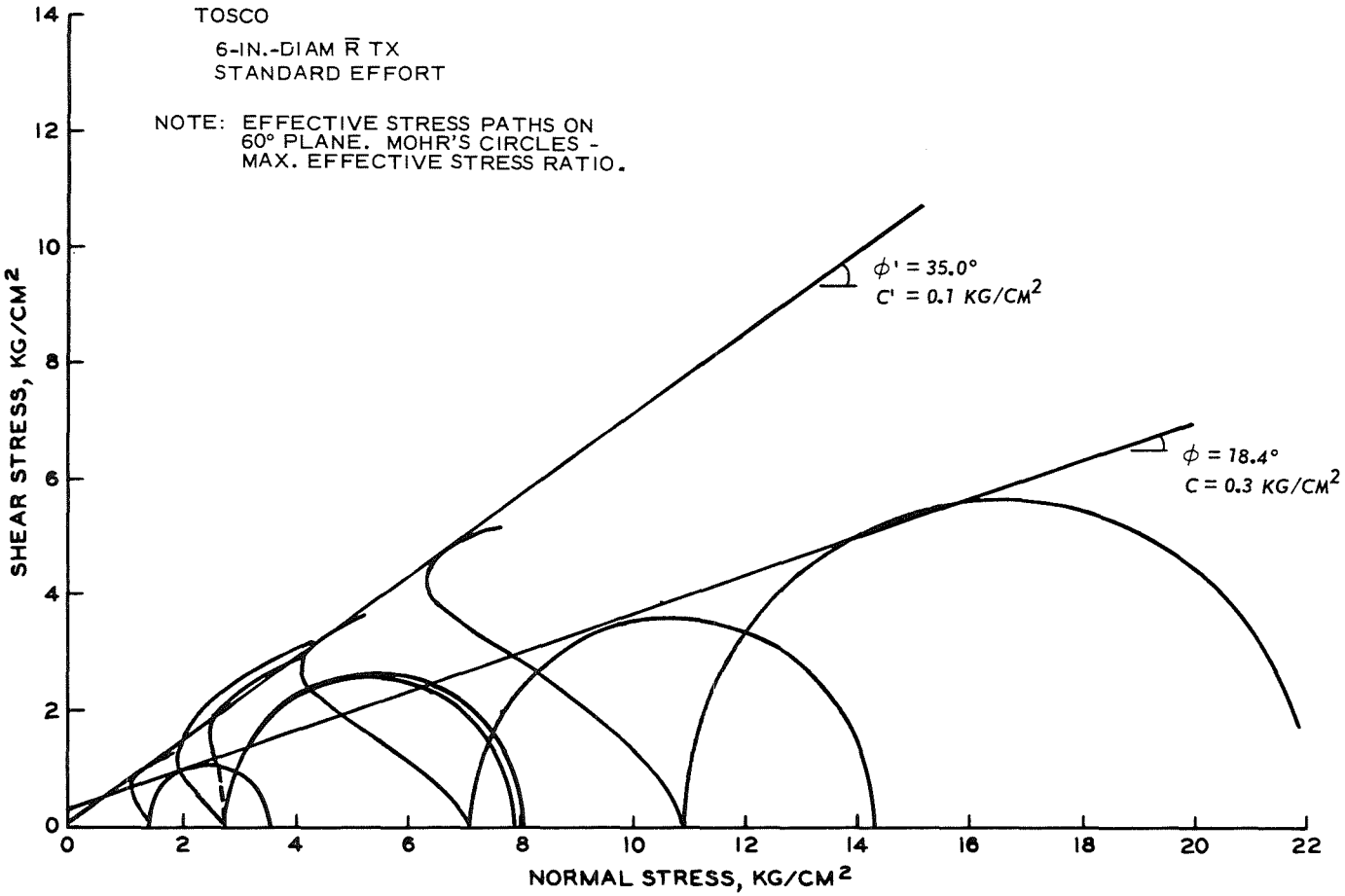

Figure 33. Total and effective stress envelopes for TOSCO compacted to standard effort density

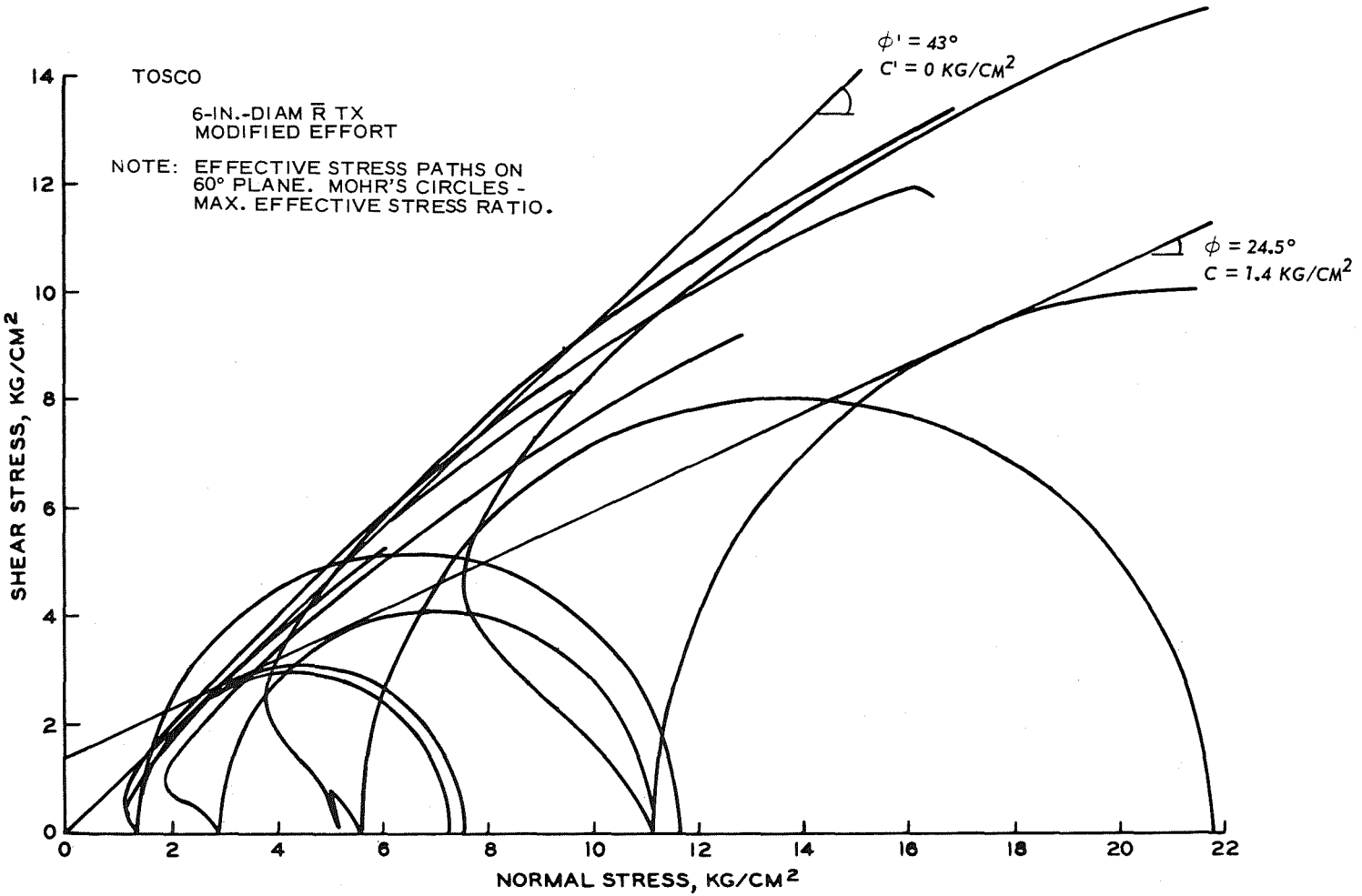

Figure 34. Total and effective stress envelopes for TOSCO compacted to modified effort density

density conducted by WCC (1976) provided strength parameters of $c' = 1.95$ kg/cm^2 and $\phi' = 34.2$ deg. These values agree quite well with those obtained in this investigation.

The TOSCO strength parameters summarized in the preceding tabulation show that modified compaction effort is required to significantly increase the strength, and little improvement will occur using only standard effort. Nevertheless, these results show TOSCO is amenable to increased strength with increased compaction effort, while PARAHO is not.

The strength parameters listed for TOSCO are quite reasonable when compared with those for a dense sand, i.e., $\phi' = 40$ deg. The $\bar{R}$ triaxial compression tests reported by Dames and Moore (1974) for specimens with dry densities of 85 to 90 pcf gave total stress parameters of $c = 0$ and $\phi = 20$ deg. These values agree quite well with the total stress data obtained in this investigation ($\phi = 18.4$ to 24.5 deg).

Figure 35 presents the volumetric strain versus normal stress on 60-deg plane for the 9-in.- (22.9-cm-) diam S triaxial compression tests on PARAHO material. These results show that only at modified compaction equivalent densities and low confining pressures is the material dilative (i.e., curves 2 and 4), and that the materials are contractive for all other conditions. Hence, positive pore pressures could be anticipated for undrained conditions.

Permeability

Figures 36 and 37 presented the results of permeability measurements preceding shear of triaxial compression tests on specimens of PARAHO and TOSCO materials compacted to densities comparable to 60 percent of standard, standard, and modified compaction efforts. For comparison, permeability values based upon calculations using consolidation data presented previously are also shown in these figures. Both sets of data are consistent and show decreasing permeabilities with decreasing void ratios (higher densities). Generally, the permeabilities for PARAHO decreased from 10^{-3} cm/sec for 60 percent of standard effort densities to 10^{-4} cm/sec for modified effort densities. In the case of TOSCO material, the coefficient of permeability decreased from 10^{-6} cm/sec to 10^{-7} cm/sec as the compaction effort increased from 60 percent of standard to modified effort. The lower permeability values for TOSCO as compared with PARAHO reflect its finer gradation.

The permeabilities determined from consolidation tests reflect lower values due to lower void ratios achieved from higher consolidation stresses. By comparison, permeability values determined by WCC (1975) on 8-in.- (20-cm-) diam specimens of 1-1/2-in. (38-mm) PARAHO material are also presented in Figure 36. These results also show decreasing permeabilities with increased compaction effort. However, for comparable void ratios, they obtained considerably lower permeabilities. This is due to the greater amount of fines (approximately 30-35 percent after compaction) for the WCC material than the WES material (approximately 8-15 percent fines after compaction).

Generally, materials are classified as impervious if they exhibit

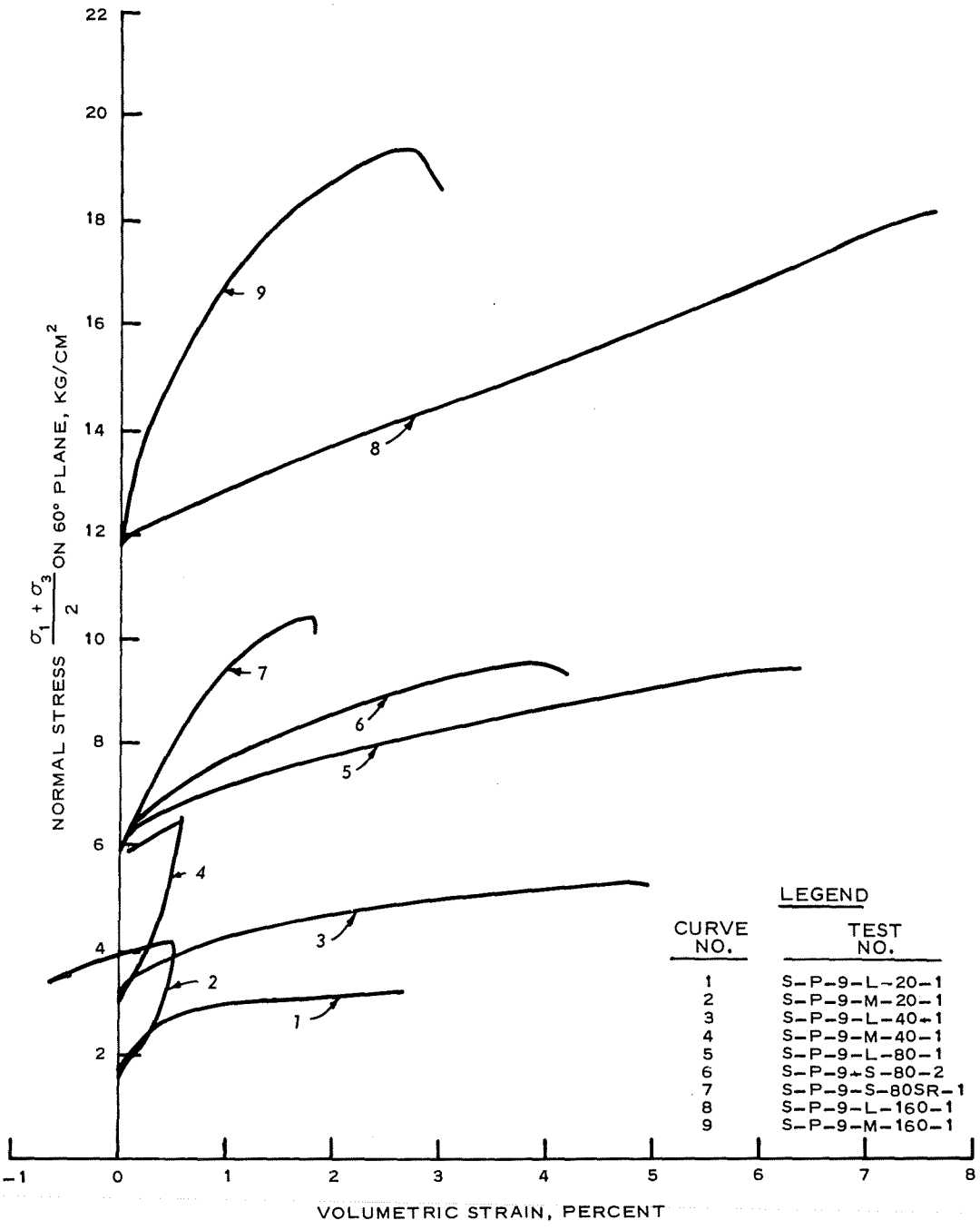

Figure 35. Normal stress-volumetric strain relationships for S triaxial compression tests on 9-in.- (22.9-cm-) diam specimens of PARAHO

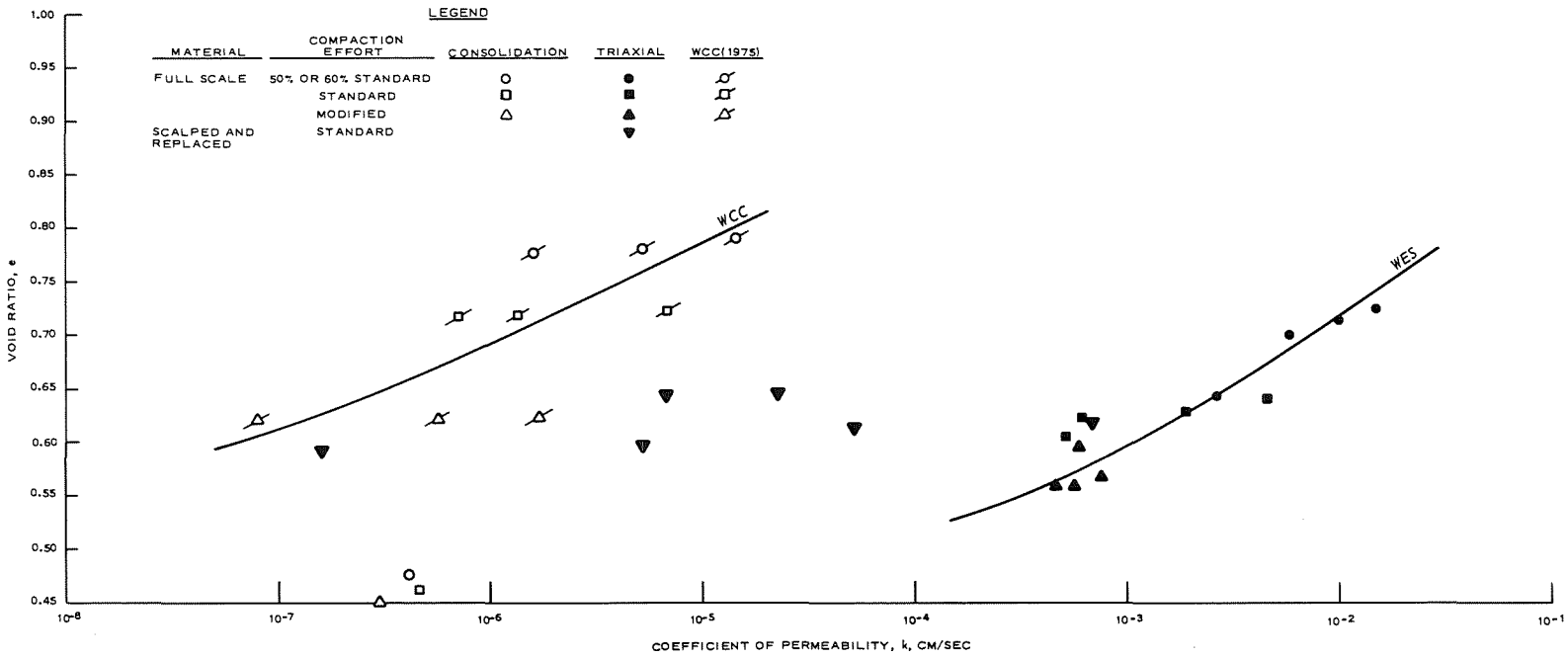

Figure 36. Permeability-void ratio relationships for compacted PARAHO retorted oil shale

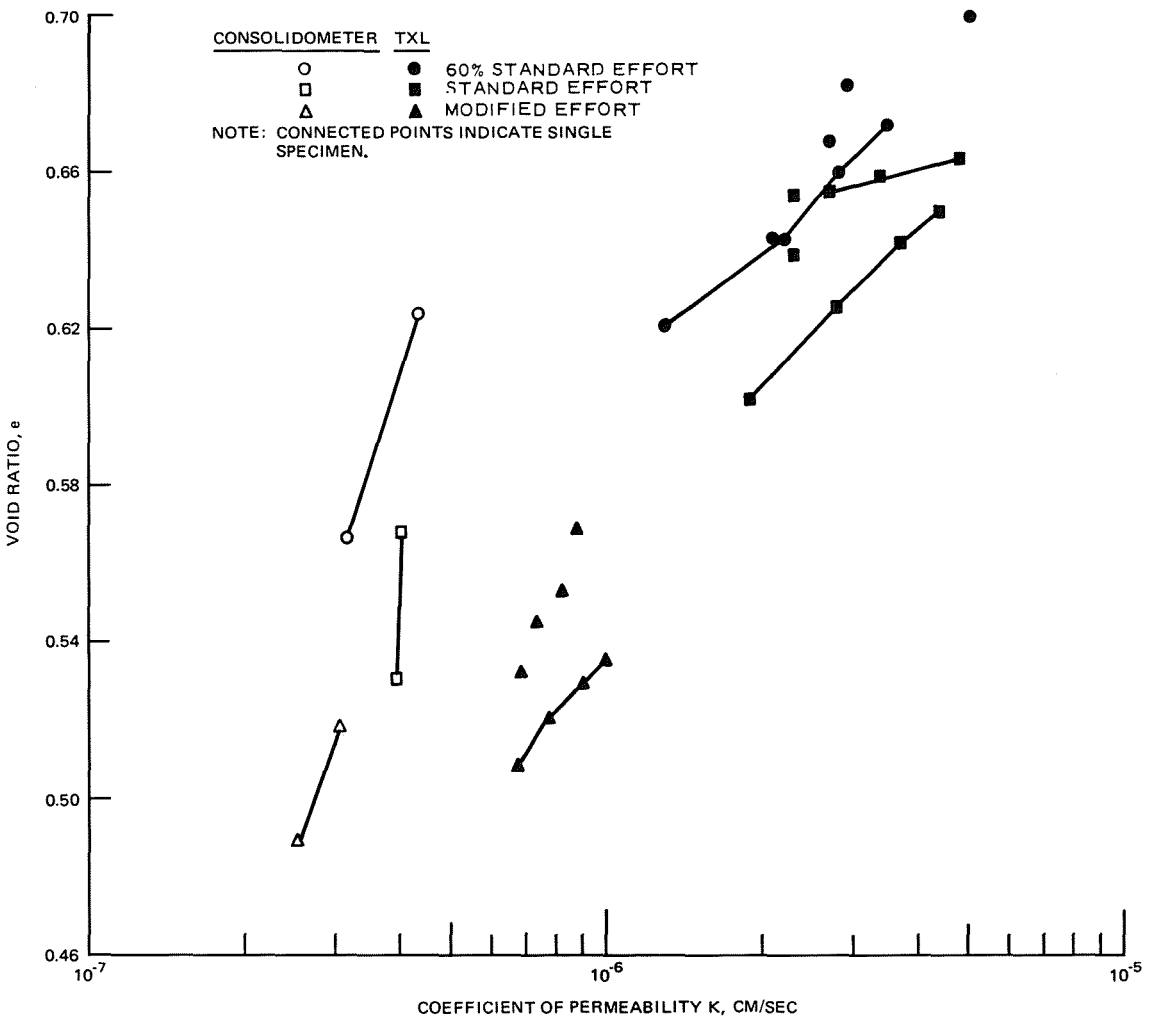

Figure 37. Permeability-void ratio relationships for compacted TOSCO retorted oil shale

permeability values less than 10^{-6} cm/sec and as pervious if they exhibit permeability values greater than 10^{-4} cm/sec. Hence, depending upon compaction effort, PARAHO and modeled PARAHO can be considered as semipervious to pervious, while in the case of TOSCO only modified compaction effort will produce an impermeable material. For construction of impermeable barriers using retorted oil shale, material selection would be more critical than compaction effort. That is to say, materials with sufficient fines can be just as impervious as modified effort compacted PARAHO. However, based upon these tests, neither PARAHO or TOSCO materials would perform well as impermeable materials.

Direct shear tests

Figure 38 presents the results of multistaged S direct shear tests on dry and inundated 2- by 2- by 1-ft (0.6- by 0.6- by 0.3-m) specimens of full-sized PARAHO material statically compacted to equivalent standard effort density. Comparison S direct shear tests were performed on 3- by 3-in. (7.6- by 7.6-cm) specimens of modeled PARAHO compacted to equivalent standard effort density with the results also shown in Figure 38. Table 13 summarizes and compares these results.

The shear stress τ_{ff} envelope for the 2- by 2-ft (0.6- by 0.6-m) full-scale PARAHO specimens is shown markedly curved in Figure 38, and the selection of the cohesion intercept and angle of internal friction is quite dependent upon normal stress σ_n. In Figure 39, the friction angle ϕ' decreases from 57 to 32 deg and 45 to 28 deg as the normal stress increases from 2.5 to 15 tsf (0.2 to 1.4 MPa) for dry and inundated specimens, respectively. Both Figures 38 and 39 show that inundation causes a reduction in strength, which is most pronounced at the lower normal stresses. Also presented in these figures are the results of 3- by 3-in. (7.6- by 7.6-cm) S direct shear tests on modeled PARAHO. For this material, normal stress has very little effect on the friction angle. A comparison of shear strengths shows that the strength of the modeled material is considerably lower than that of the full-sized material except at the highest normal stress (14 tsf).

Also presented in Figures 38 and 39 are the shear stress, τ_{ff}, and friction angle ϕ', respectively, versus normal stress σ_{ff} for triaxial compression tests on PARAHO and modeled PARAHO. These results show that for the coarse fraction reasonable agreement is obtained between the 9-in.-(22.9-cm-) diam triaxial and 2- by 2-ft (0.6- by 0.6-m) inundated direct shear results, which are the gradations most alike. Conversely, in the case of the modeled PARAHO, considerable divergence in results was obtained.

The results of S direct shear tests on 3- by 3-in. (7.6- by 7.6-cm) dry and inundated specimens of TOSCO material compacted to standard effort densities and tested under a maximum normal stress of 14 kg/cm^2, as presented in Figure 40, are summarized in the following table:

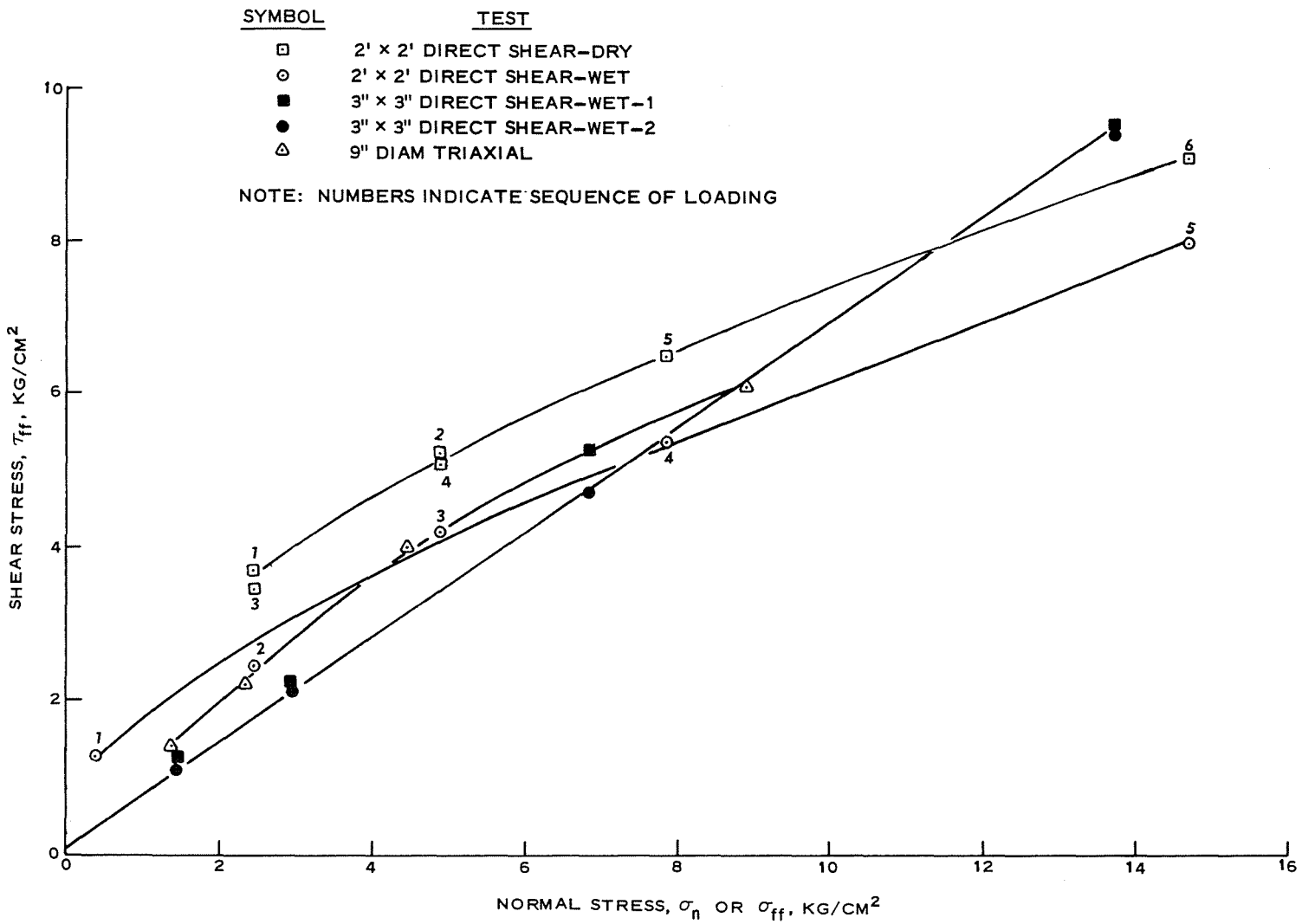

Figure 38. Failure envelopes for direct shear tests on PARAHO retorted oil shale

Table 13

Summary of Direct Shear Tests on PARAHO at Standard Effort Density

Material	Specimen Size in.	Initial Specimen Conditions: Water Content w, %	Initial Specimen Conditions: Dry Density γ_d, pcf	Normal Stress σ_n: psi	Normal Stress σ_n: tsf	Apparent Cohesion c': psi	Apparent Cohesion c': tsf	Apparent Angle of Internal Friction, ϕ', deg
Dry	24 by 24	Dry	96.2	208	15	0*	0*	31.6*
Inundated	24 by 24	Dry	96.2	208	15	0*	0*	28.4*
Modeled	3 by 3	19.8-20.1	89.2-93.3	195	14	1.4	0.1	34.6
inundated		19.7-20.0	90.5-91.9	195	14	1.4	0.1	34.6

* Failure envelope is markedly curved; values are for maximum normal stress.

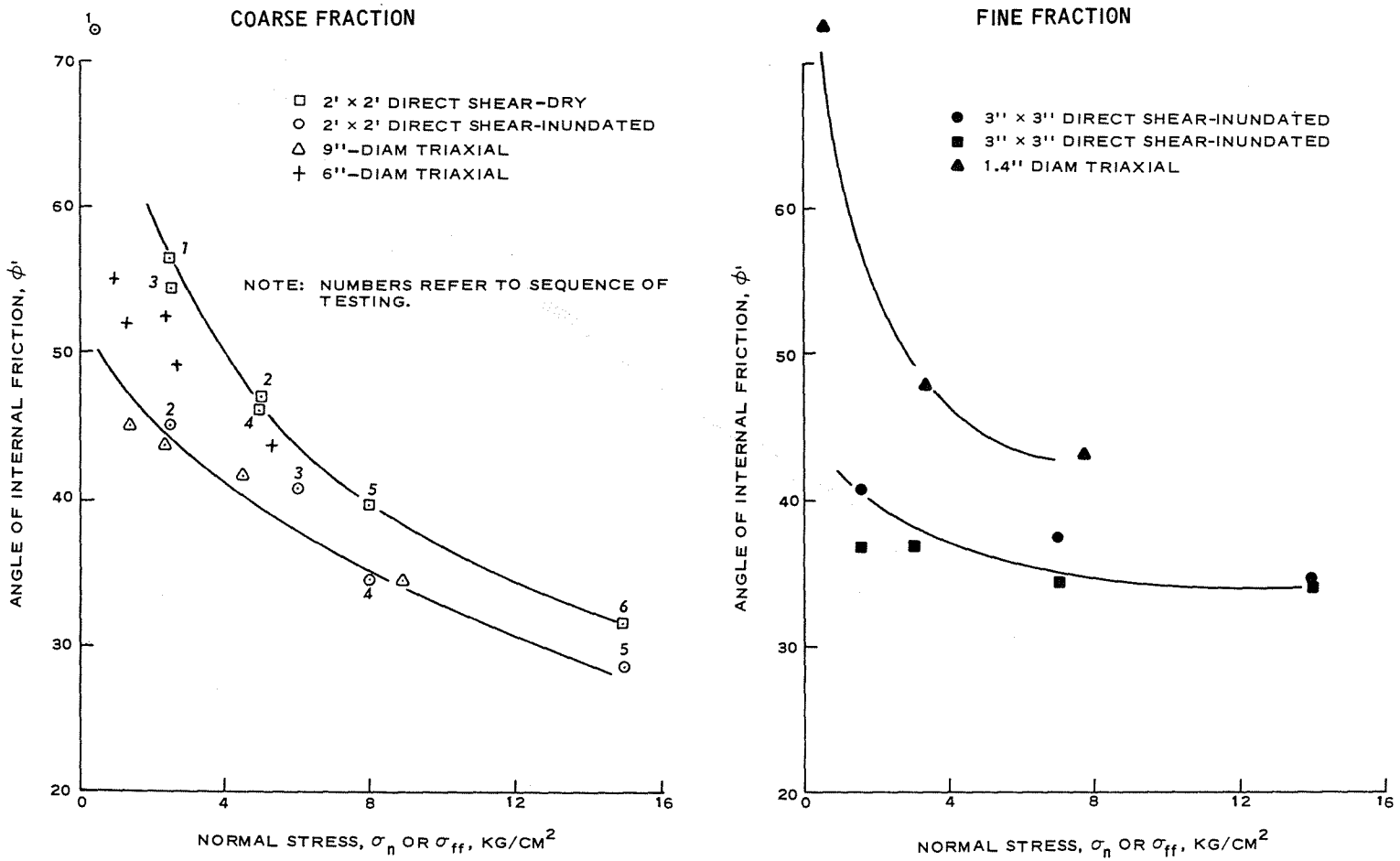

Figure 39. Comparison of friction angles for coarse and fine fractions of PARAHO retorted oil shale

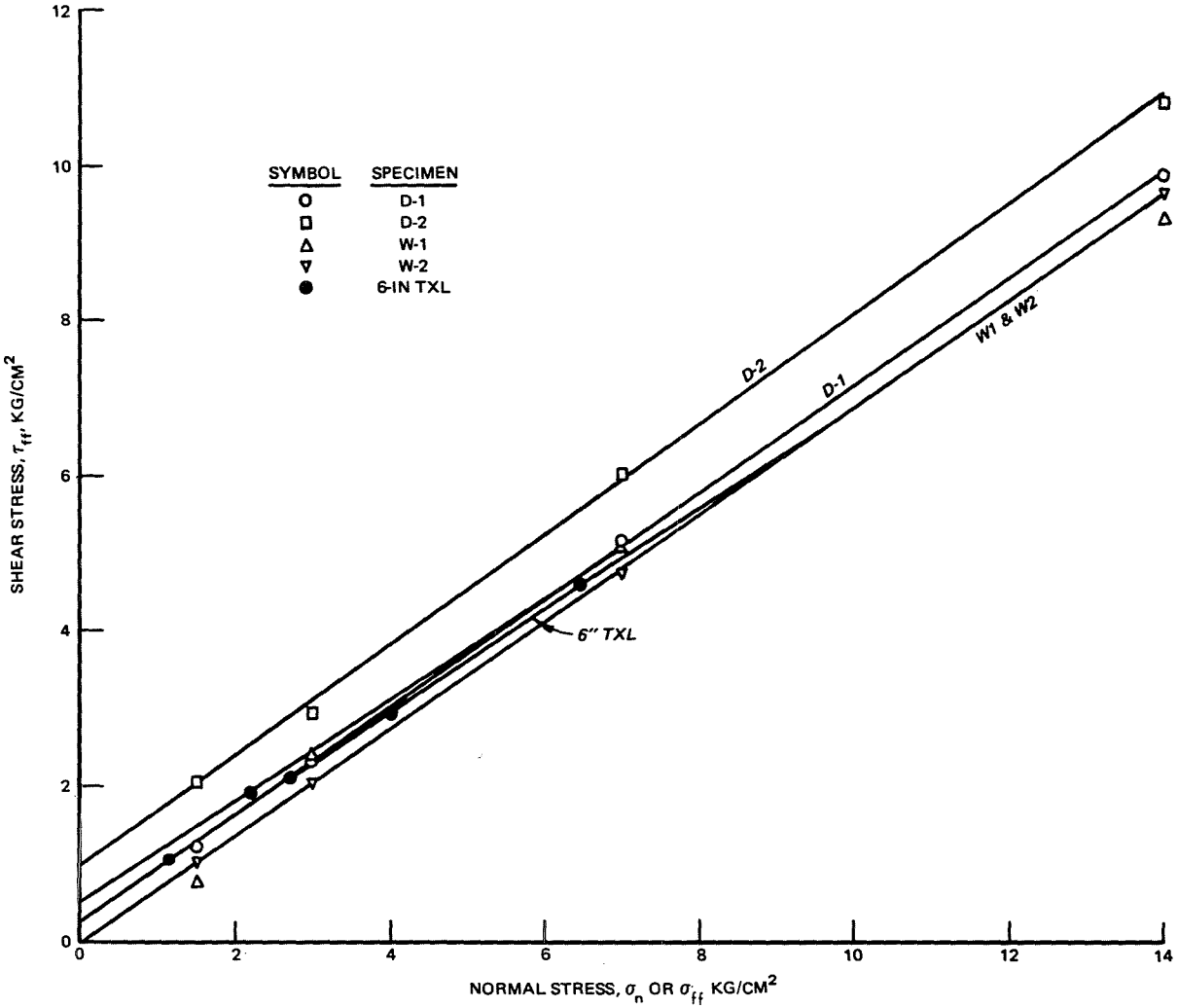

Figure 40. Failure envelopes for direct shear tests on TOSCO retorted oil shale

Condition	Initial Specimen Conditions: Water Content w, %	Initial Specimen Conditions: Dry Density γ_d, pcf	Apparent Cohesion, c': psi	Apparent Cohesion, c': kg/cm^2	Apparent Angle of Internal Friction ϕ', deg
Dry	20.1-20.2	92.8-93.3	14	1.0	36
Inundated	20.2-20.7	92.4-93.3	0	0	34
Inundated	20.0-20.1	92.6-93.0	3	0.2	34

As in the case with PARAHO, these results show that inundation causes a decrease in shear strength. For comparison, the failure envelope, presented in Figure 40, for 6-in.- (15.2-cm-) diam triaxial tests on TOSCO, shows remarkable agreement with the direct shear results.

Interface shear tests. Figures 41 and 42, respectively, present the results of 2- by 2-ft (0.6- by 0.6-m) interface direct shear tests on raw shale and PARAHO against rubber belting, rusty steel, and smooth stainless steel. The following tabulation summarizes these results. For these tests, the material was placed in an "as-dumped" loose condition and only small normal loads were applied, the intention being to duplicate field material handling operations. For comparison, also listed below are simulated interface shear tests by WCC (1976a) on raw shale using plates of interface material inserted along assumed failure planes in 6-in.- (15.2-cm-) diam triaxial specimens compacted to standard effort density.

Material	Shear Surface	Density γ_d, pcf	Maximum Normal Stress, σ_n: psi	Maximum Normal Stress, σ_n: tsf	Apparent Cohesion, c': psi	Apparent Cohesion, c': tsf	Apparent Internal Friction ϕ', deg
PARAHO	Rubber Belting	70.0	28	2.00	0	0	39
(Air-Dried)	Rusty Steel	70.0	28	2.00	0	0	32
	Stainless Steel	70.0	28	2.00	0	0	24
Raw Shale	Rubber Belting	60.0	28	2.00	0	0	31
(Air-Dried)	Rusty Steel	60.0	28	2.00	0	0	30
	Stainless Steel	60.0	28	2.00	0	0	14
Raw Shale*	Raw Shale	88.3	80	5.75	23.0	1.65	35
	Steel	88.3	80	5.75	6.2	0.45	19
	Hard Rubber	88.3	80	5.75	9.0	0.65	35
	Soft Rubber	88.3	80	5.75	5.6	0.45	27

* From WCC (1976a).

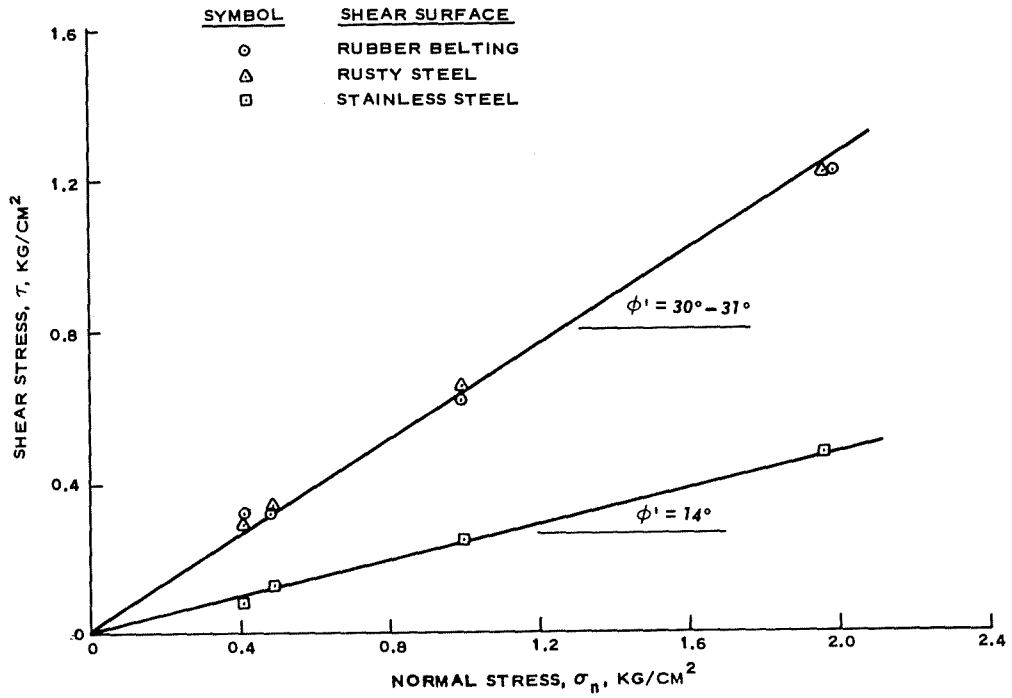

Figure 41. Friction envelopes for interface direct shear tests on raw oil shale

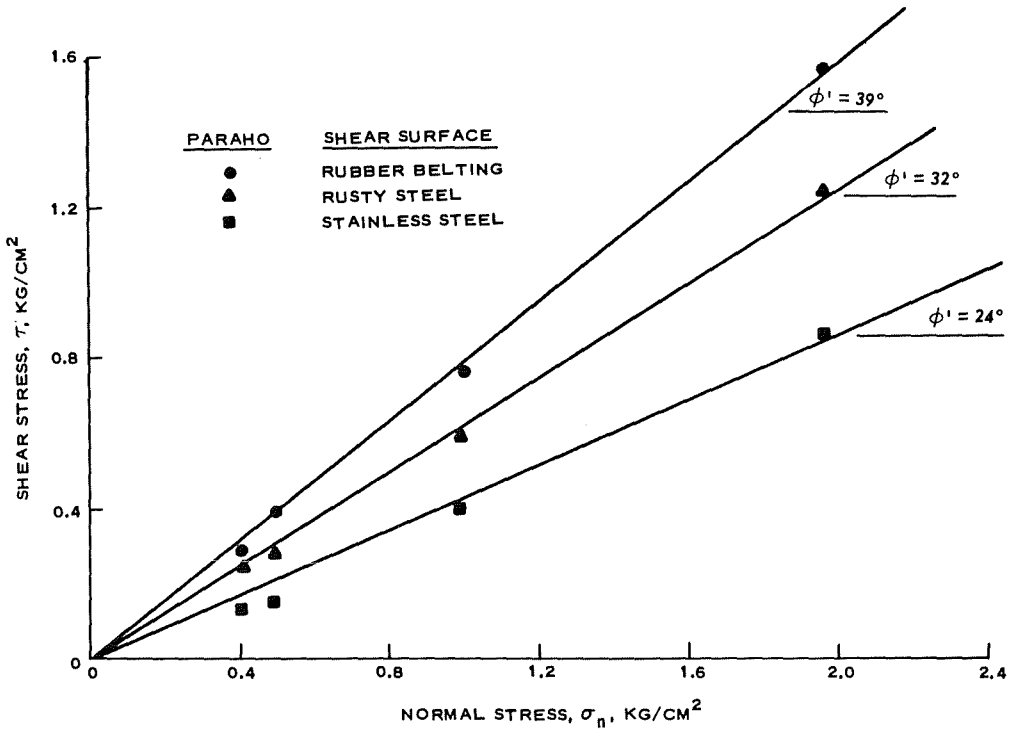

Figure 42. Friction envelopes for interface direct shear tests on PARAHO retorted oil shale

These results show the decreasing order of friction angles to be rubber belting, rusty steel, and stainless steel for both the PARAHO and raw shale. Despite testing differences, WCC (1976a) results also indicate that higher friction angles exist with rubber than with steel and the values of friction angles are somewhat similar.

Repeated direct shear tests

The results of 3- by 3-in. (7.6- by 7.6-cm) repeated direct shear tests on modeled PARAHO and TOSCO compacted to equivalent standard effort densities and sheared under a maximum normal stress of 14 kg/cm^2 are presented in Figure 43 and summarized in the following tablulation:

Material	Initial Conditions: Water Content w, %	Initial Conditions: Dry Density γ_d, pcf	Apparent Cohesion, c': psi	Apparent Cohesion, c': tsf	Apparent Angle of Internal Friction ϕ', deg
PARAHO	19.8	91.1-94.4	0	0	35.5
TOSCO	20.0	95.9-96.1	0	0	34.5

These values of residual strength are practically identical to those for conventional direct shear tests: 35.5 versus 34.6 deg for modeled PARAHO and 34.5 versus 34.0 deg for TOSCO. Thus, these materials do not develop significant losses in frictional strength with large displacements as overconsolidated clays do, because cohesionless granular materials lack platey particles that become oriented with displacement resulting in lower shear strengths.

K_o tests

Table 14 and Figures 44 through 55 present the results of K_o tests on 9-in.- (22.9-cm-) diam triaxial specimens of PARAHO and 6-in.- (15.2-cm-) diam specimens of TOSCO compacted to equivalent standard effort densities and allowed to cure 0 and 13, and 0, 11, and 19 months, respectively. Also included are the results of two tests on 6-in.-diam specimens of modeled PARAHO compacted to 60 percent of standard and modified equivalent densities. These latter two tests were performed on specimens used for dynamic properties tests.

For full-scale PARAHO, the normally consolidated values of K_o range from 0.19 to 0.38, which correspond to Poisson's ratio values of 0.16 to 0.28, for specimens with only 3-day curing. For comparable specimens cured 13 months, the values of K_o (loading) range from 0.20 to 0.40, which correspond to Poisson's ratio values of 0.17 to 0.29. The normally consolidated constrained moduli ranged from 553 to 1358 kg/cm^2 for specimens cured 3 days and from 318 to 1141 kg/cm^2 for specimens cured 13 months. From these comparisons, no improvement in stiffness was observed with increased curing times. Jaky (1948) experimentally derived the relationship, $K_o = 1-\sin \phi'$ for estimating values of K_o. Utilizing $\phi' = 32.7$ deg (see Triaxial compression tests section), the corresponding value of K_o would be 0.46, which overestimates the experimentally obtained results.

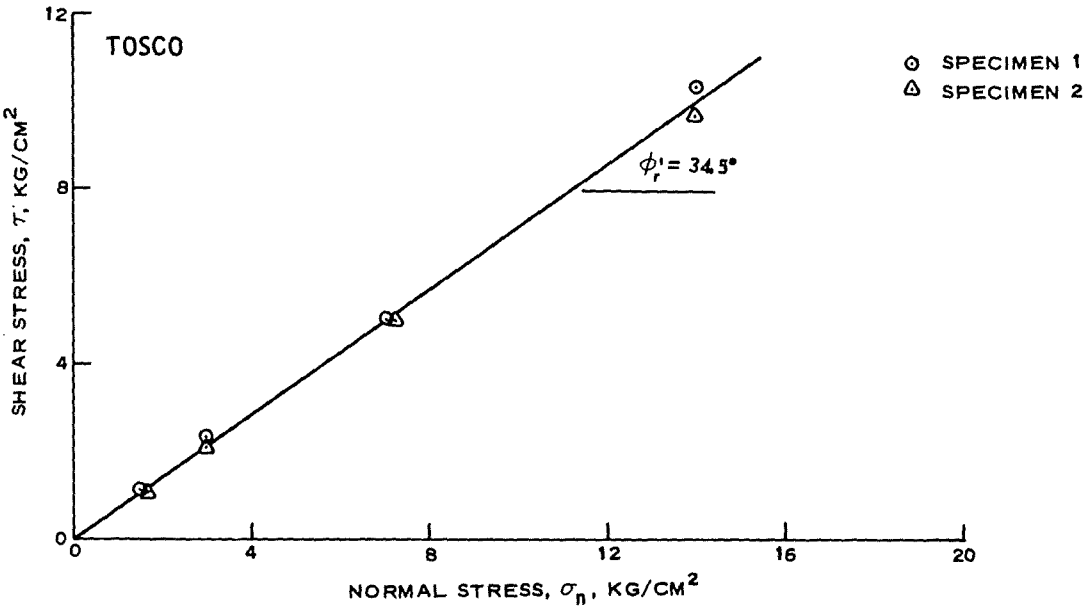

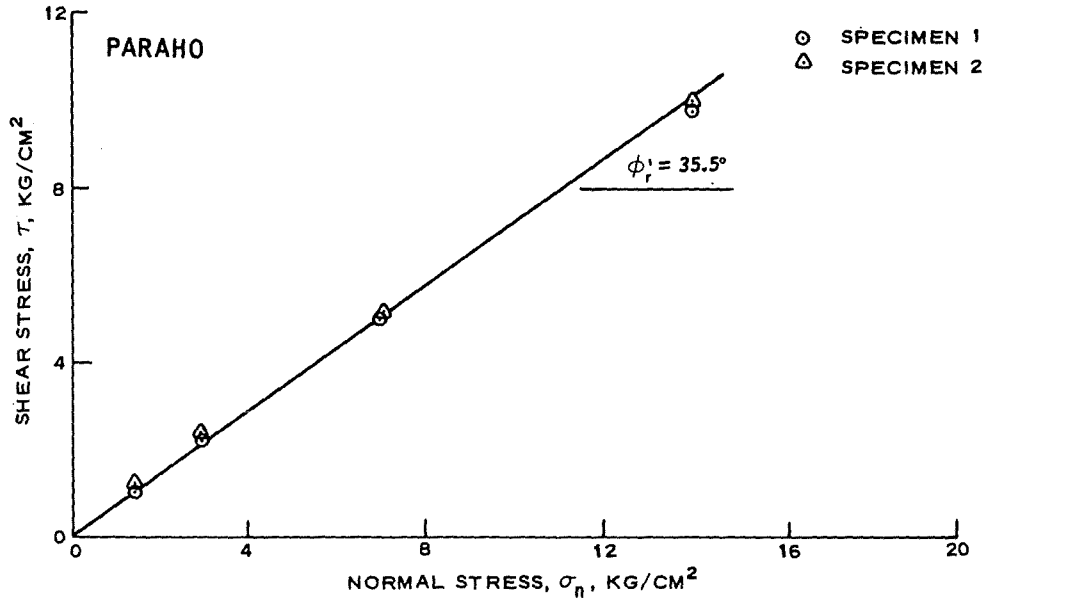

Figure 43. Residual strength envelopes for repeated direct shear tests on modeled PARAHO and TOSCO retorted oil shales

Table 14

Summary of K_o Tests on PARAHO and TOSCO Retorted Oil Shales

Test Specimen No.*	Radial Stress σ_3 kg/cm^2	Axial Stress σ_1 kg/cm^2	Axial Strain ε_1 %	OCR**	Stress† Ratio σ_3/σ_1	Poisson's†† Ratio ν	Secant Values‡ K_o $\Delta\sigma_3/\Delta\sigma_1$	Secant Values‡ $\nu = K_o/(1 + K_o)$	Secant Values‡ Constrained Modulus, $D = \Delta\sigma_1/\Delta\varepsilon_1$, kg/cm^2
K-P-9-S-0-1	0	0	0	0	0	0			
	1.4	6.4	1.03	1.0	0.22	0.18	0.22	0.18	620
	0.1	0.6	0.91	11.3	0.19	0.16	0.23	0.19	4,772
	3.0	11.5	1.95	1.3	0.25	0.20	0.26	0.20	1,050
	1.2	2.2	1.78	5.1	0.54	0.35	0.19	0.16	5,400
	6.2	18.7	3.13	1.0	0.33	0.25	0.30	0.23	1,220
	1.9	2.8	2.90	6.6	0.66	0.40	0.27	0.21	6,824
	12.0	31.1	4.98	1.0	0.38	0.28	0.36	0.26	1,358
	2.6	3.5	4.68	9.0	0.75	0.43	0.34	0.25	9,106
K-P-9-S-0-2	0	0	0	0	0	0			
	1.4	7.2	1.30	1.0	0.20	0.16	0.20	0.16	553
	0.8	1.9	1.21	3.8	0.42	0.30	0.12	0.10	5,817
	2.8	11.1	2.05	1.0	0.25	0.20	0.22	0.18	1,096
	1.3	2.3	1.91	4.8	0.56	0.36	0.17	0.15	6,134
	5.7	17.4	3.30	1.0	0.33	0.25	0.29	0.22	1,082
	2.2	3.1	3.11	5.6	0.71	0.41	0.24	0.20	7,640
	11.6	29.9	5.42	1.0	0.38	0.28	0.35	0.26	1,164
	2.8	3.7	5.07	8.1	0.77	0.43	0.33	0.25	7,667

(Continued)

* Specimen number: K = K_o test; P or T = PARAHO or TOSCO; 9 or 6 = diam of specimen, in.; S, M, or L = standard, modified, or 60 percent of standard (low) compaction effort; 0, 9, or 18 = months of curing time; 1-4 = specimen number of series. Example: K-P-9-S-0-1 = K_o test on 9-in.-diam PARAHO specimen compacted to standard effort density with no curing time, specimen No. 1 of this condition.

** OCR based upon σ_1, i.e., overburden pressure.

† Stress ratio, σ_3/σ_1, may be considered as K_o.

†† Based upon stress ratio K_o, where $\nu = K_o/(1 + K_o)$.

‡ Actual values of K_o, ν, and D based upon secant points of load-unload relationships.

Table 14 (Continued)

Test Specimen No.	Radial Stress σ_3 kg/cm^2	Axial Stress σ_1 kg/cm^2	Axial Strain ε_1 %	OCR	Stress Ratio σ_3/σ_1	Poisson's Ratio ν	Secant Values: K_o $\Delta\sigma_3/\Delta\sigma_1$	Secant Values: $\nu = K_o/(1 + K_o)$	Secant Values: Constrained Modulus, D = $\Delta\sigma_1/\Delta\varepsilon_1$, kg/cm^2
K-P-9-S-12-2	0	0	0	0	0	0			
	1.4	6.7	2.10	1.0	0.21	0.17	0.21	0.17	318
	0.3	1.2	1.94	5.5	0.24	0.19	0.21	0.17	3,603
	2.8	10.3	3.03	1.0	0.27	0.21	0.27	0.21	841
	0.8	1.9	2.86	5.5	0.42	0.29	0.24	0.19	5,049
	5.6	16.6	4.62	1.0	0.34	0.25	0.33	0.24	833
	1.4	2.4	4.38	7.0	0.57	0.36	0.30	0.23	5,972
	11.4	28.3	6.87	1.0	0.40	0.29	0.39	0.28	1,042
	2.2	3.1	6.52	9.1	0.70	0.41	0.36	0.27	7,213
K-P-9-S-12-3	0	0	0	0	0	0			
	1.5	7.3	2.29	1.0	0.20	0.17	0.20	0.17	320
	0.4	1.5	2.15	4.9	0.25	0.20	0.19	0.16	4,267
	2.9	11.2	3.24	1.0	0.26	0.20	0.26	0.21	893
	0.8	1.9	3.07	5.8	0.44	0.30	0.22	0.18	5,538
	5.8	17.8	4.79	1.0	0.32	0.24	0.31	0.24	923
	1.6	2.6	4.54	6.9	0.61	0.38	0.27	0.21	5,992
	11.4	29.5	6.90	1.0	0.39	0.28	0.36	0.27	1,141
	2.5	3.4	6.57	8.6	0.75	0.42	0.34	0.25	7,892
PR-P-6-L-14.5-2##	0	0	0	0	0	0			
	3.0	6.6	1.05	1.0	0.45	0.31	0.45	0.31	634
	2.0	3.0	1.00	2.2	0.67	0.40	0.27	0.21	7,428
	5.9	13.0	2.61	1.0	0.45	0.31	0.39	0.28	622
	2.8	4.0	2.43	3.2	0.70	0.41	0.34	0.25	5,071
PR-P-6-M-14.5-1##	0	0	0	0	0	0			
	5.7	15.5	0.61	1.0	0.37	0.27	0.37	0.27	2,524
	2.7	3.9	0.56	2.6	0.69	0.41	0.25	0.20	23,100

(Continued)

Cyclic triaxial properties tests subjected to K_o test.

Table 14 (Continued)

Test Specimen No.	Radial Stress σ_3 kg/cm^2	Axial Stress σ_1 kg/cm^2	Axial Strain ε_1 %	OCR	Stress Ratio σ_3/σ_1	Poisson's Ratio ν	Secant Values K_o $\Delta\sigma_3/\Delta\sigma_1$	Secant Values $\nu = K_o/(1 + K_o)$	Secant Values Constrained Modulus, $D = \Delta\sigma_1/\Delta\varepsilon_1$, kg/cm^2
K-T-6-S-0-3	0	0	0	0	0	0			
	5.8	13.6	2.35	1.0	0.42	0.30	0.42	0.30	580
	3.3	5.2	2.30	2.6	0.62	0.38	0.30	0.23	17,071
K-T-6-S-0-4	0	0	0	0	0	0			
	1.9	5.0	0.74	1.0	0.38	0.27	0.38	0.27	689
	1.0	2.4	0.70	2.1	0.45	0.31	0.31	0.24	8,356
	3.7	9.6	1.41	1.0	0.39	0.28	0.37	0.27	1,017
	1.9	3.3	1.30	2.9	0.59	0.37	0.29	0.22	5,493
	7.4	18.0	2.43	1.0	0.41	0.29	0.37	0.27	1,303
	2.4	3.5	2.20	5.1	0.69	0.41	0.34	0.25	6,312
	15.2	35.4	3.95	1.0	0.43	0.30	0.40	0.29	1,818
	4.4	5.9	3.62	6.0	0.75	0.43	0.37	0.27	8,972
K-T-6-S-9-1	0	0	0	0	0	0			
	2.1	6.7	0.69	1.0	0.31	0.24	0.31	0.24	969
	0.3	1.3	0.59	5.0	0.24	0.19	0.33	0.25	5,395
	4.0	11.8	1.21	1.0	0.34	0.25	0.35	0.26	1,680
	0.7	1.8	1.01	6.5	0.39	0.28	0.33	0.25	5,076
	7.2	19.8	1.98	1.0	0.36	0.27	0.36	0.26	1,857
	1.3	2.6	1.70	7.6	0.51	0.33	0.34	0.25	6,156
	14.9	37.3	3.51	1.0	0.40	0.28	0.39	0.28	1,922
	3.6	5.0	3.15	7.4	0.72	0.42	0.35	0.26	8,967
	16.2	40.7	3.75	1.0	0.40	0.28	0.35	0.26	5,893

Table 14 (Concluded)

Test Specimen No.	Radial Stress σ_3 kg/cm^2	Axial Stress σ_1 kg/cm^2	Axial Strain ε_1 %	OCR	Stress Ratio σ_3/σ_1	Poisson's Ratio ν	Secant Values: K_o $\Delta\sigma_3/\Delta\sigma_1$	Secant Values: $\nu = K_o/(1 + K_o)$	Secant Values: Constrained Modulus, D = $\Delta\sigma_1/\Delta\varepsilon_1$, kg/cm^2
K-T-6-S-9-2	0	0	0	0	0	0			
	2.0	4.6	1.35	1.0	0.43	0.30	0.43	0.30	342
	0.8	1.7	1.35	2.6	0.47	0.32	0.40	0.29	?
	4.1	9.4	2.21	1.0	0.44	0.30	0.43	0.30	893
	1.7	2.5	2.13	3.7	0.69	0.41	0.34	0.25	8,328
	8.6	20.0	3.51	1.0	0.43	0.30	0.39	0.28	1,263
	4.1	5.1	3.35	3.8	0.80	0.44	0.30	0.23	9,009
	16.4	38.4	5.03	1.0	0.42	0.30	0.36	0.27	1,973
	3.8	3.8	4.65	10.0	0.98	0.50	0.36	0.27	9,009
	5.6	7.6	4.79	5.0	0.74	0.42	0.35	0.26	12,431
K-T-6-S-18-1	0	0	0	0	0	0			
	1.4	4.1	0.42	1.0	0.35	0.26	0.35	0.26	966
	0.3	0.3	0.37	11.2	0.92	0.48	0.30	0.23	7,921
	2.8	7.9	0.85	1.0	0.35	0.26	0.32	0.24	1,611
	0.8	1.3	0.75	6.0	0.64	0.39	0.29	0.23	7,044
	6.6	18.2	1.79	1.0	0.36	0.27	0.34	0.25	1,634
	1.4	1.9	1.55	9.7	0.76	0.43	0.32	0.24	6,968
	9.6	26.0	2.40	1.0	0.37	0.27	0.34	0.25	2,859
	2.0	2.4	2.11	10.8	0.82	0.45	0.32	0.24	8,386
K-T-6-S-18-2	0	0	0	0	0	0			
	1.4	3.5	0.59	1.0	0.39	0.28	0.40	0.28	592
	0.6	0.8	0.57	4.1	0.74	0.43	0.29	0.22	11,158
	2.9	6.8	0.97	1.0	0.43	0.30	0.39	0.28	1,468
	1.2	1.6	0.90	4.1	0.74	0.42	0.33	0.25	7,222
	5.6	13.2	1.47	1.0	0.42	0.30	0.38	0.28	2,026
	1.8	2.2	1.38	6.0	0.81	0.45	0.35	0.26	11,612
	11.4	26.8	2.38	1.0	0.42	0.30	0.39	0.28	2,460
	3.1	3.5	2.19	7.7	0.90	0.47	0.35	0.26	12,213

(Sheet 4 of 4)

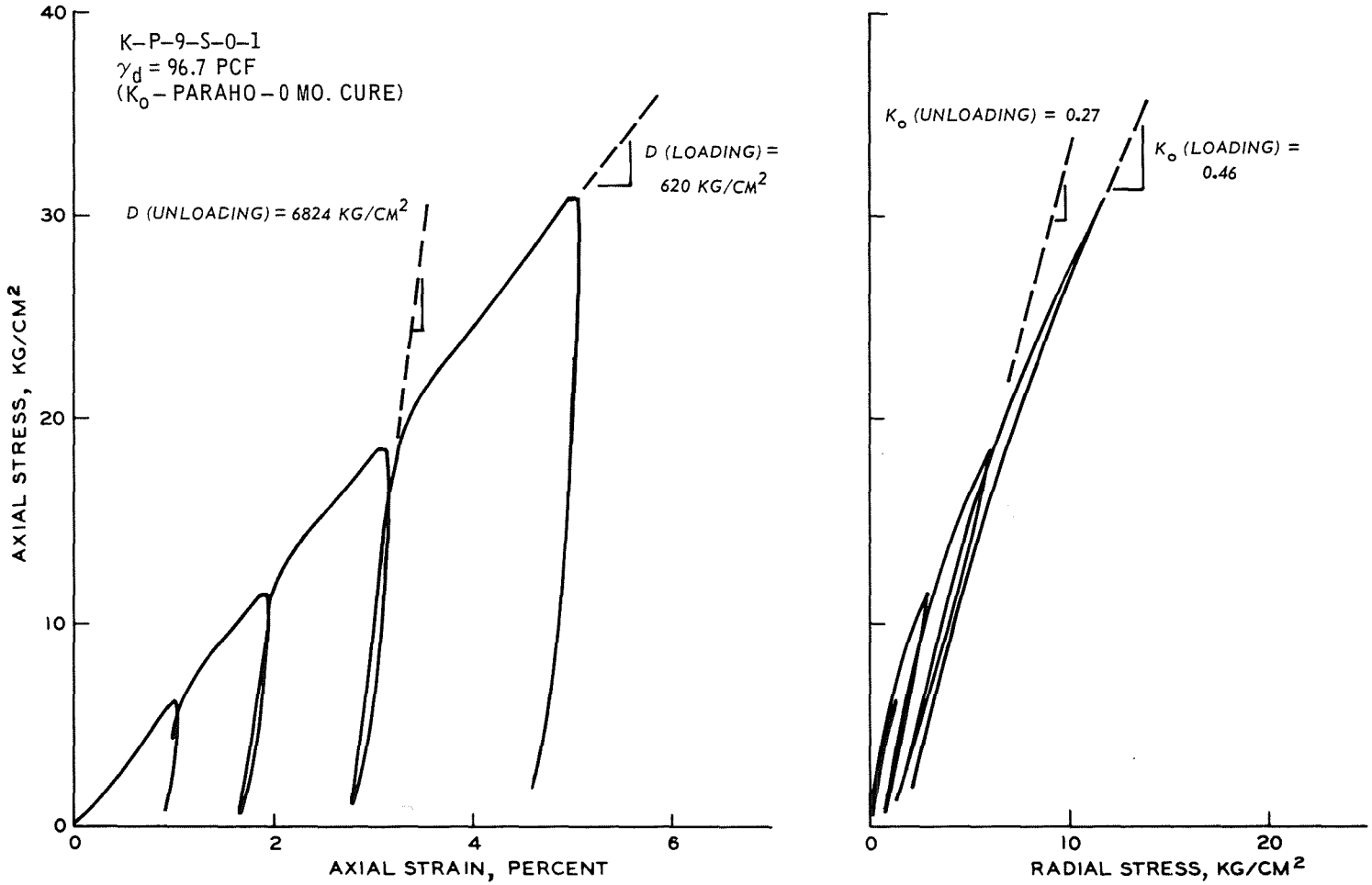

Figure 44. Stress-strain relationships for 9-in.- (22.9-cm-) diam K_o tests on PARAHO compacted to standard effort density, 0-month cure, test specimen K-P-9-S-0-1

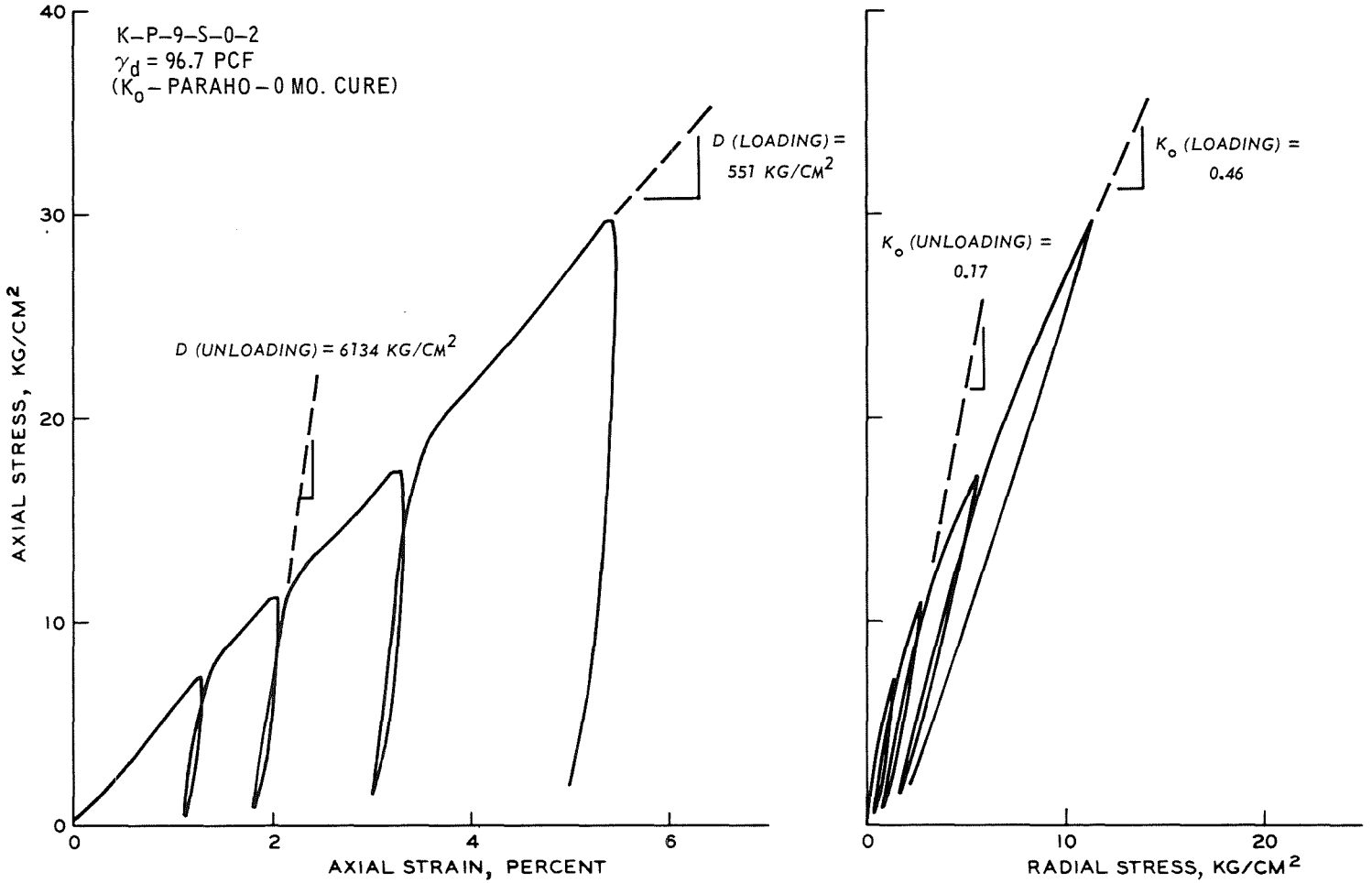

Figure 45. Stress-strain relationships for 9-in.- (22.9-cm-) diam K_o tests on PARAHO compacted to standard effort density, 0-month cure, test specimen K-P-9-S-0-2

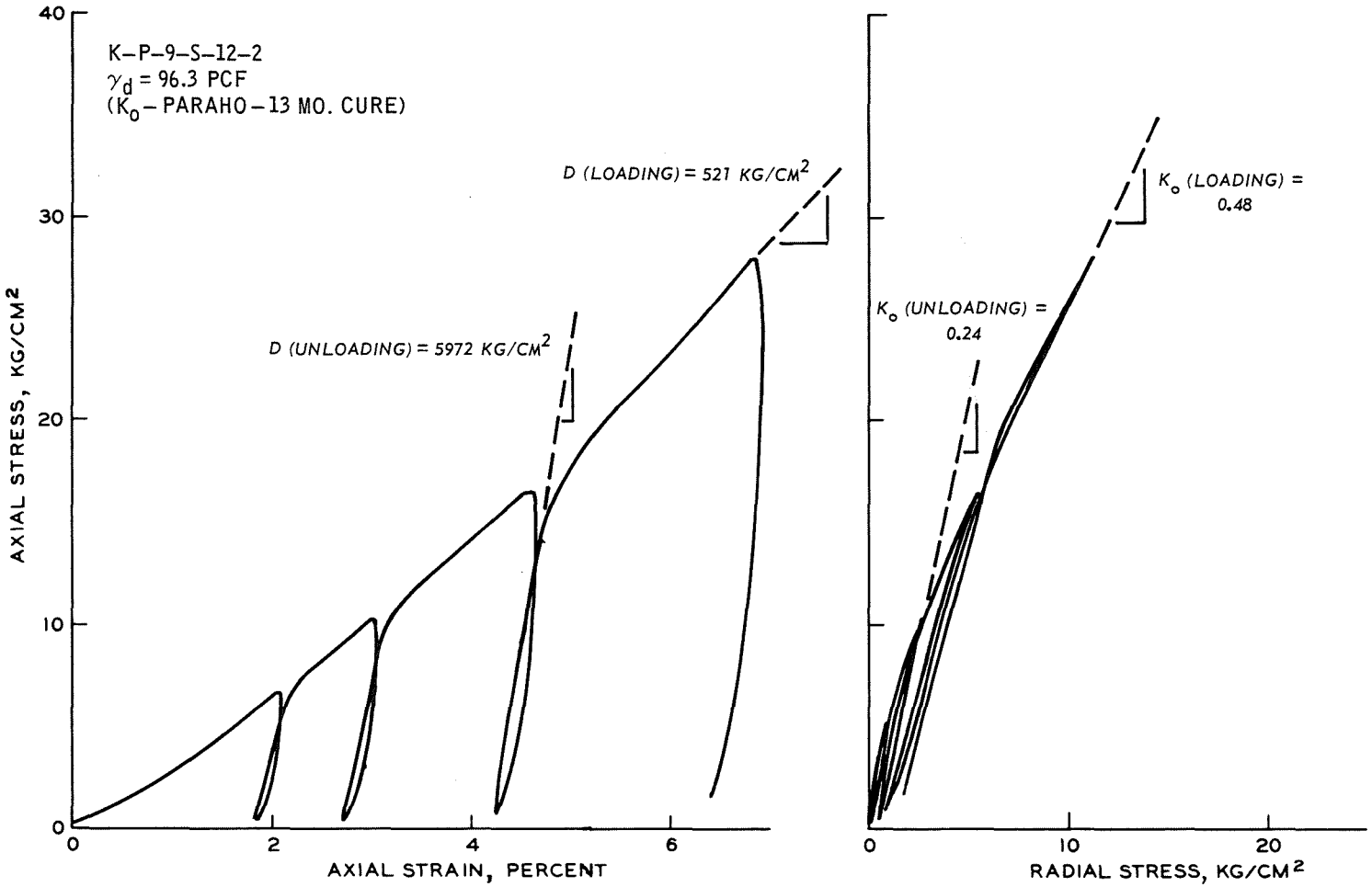

Figure 46. Stress-strain relationships for 9-in.- (22.9-cm-) diam K_o tests on PARAHO compacted to standard effort density, 13-month cure, test specimen K-P-9-S-12-2

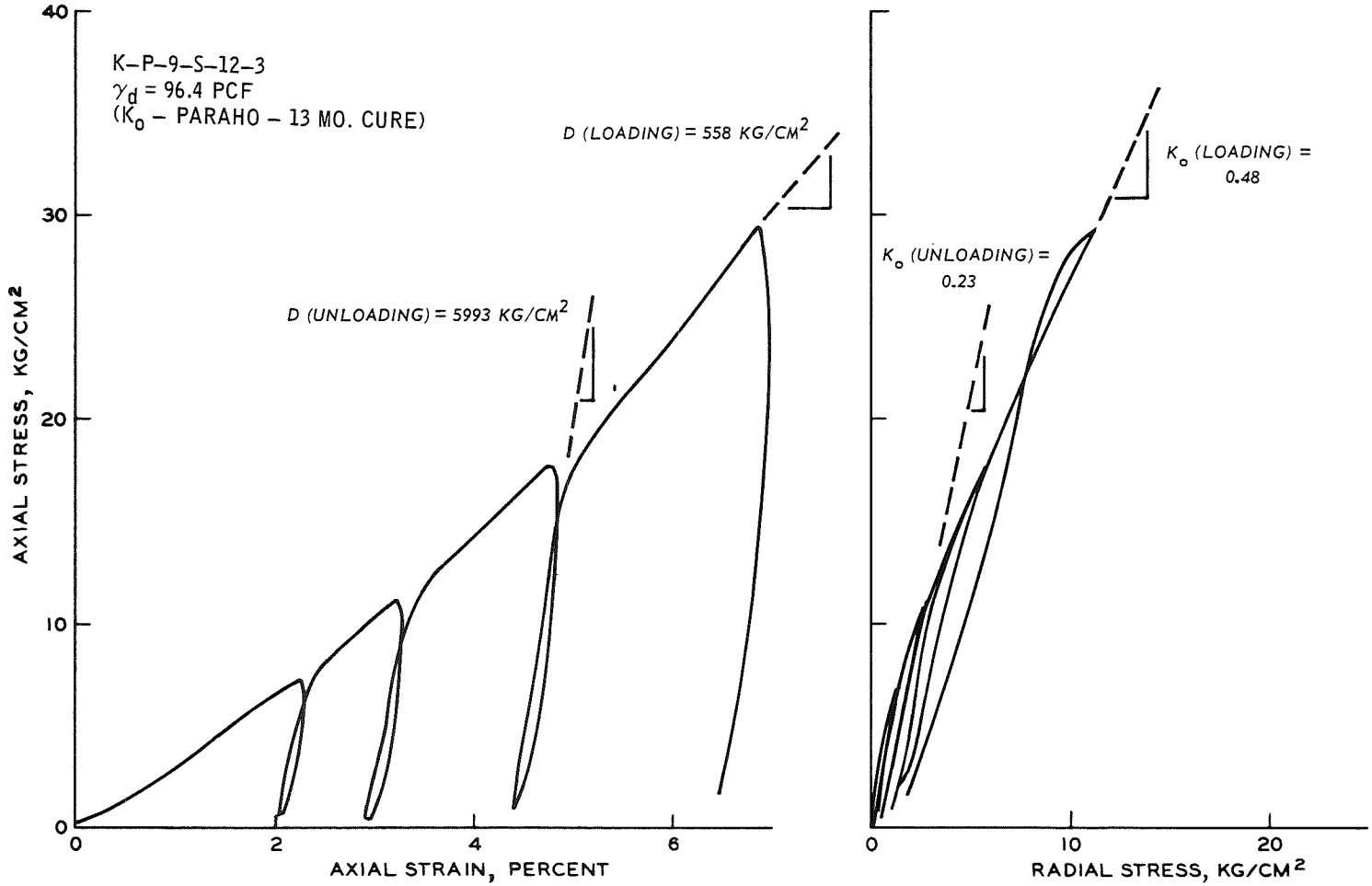

Figure 47. Stress-strain relationships for 9-in.- (22.9-cm-) diam K_o tests on PARAHO compacted to standard effort density, 13-month cure, test specimen K-P-9-S-12-3

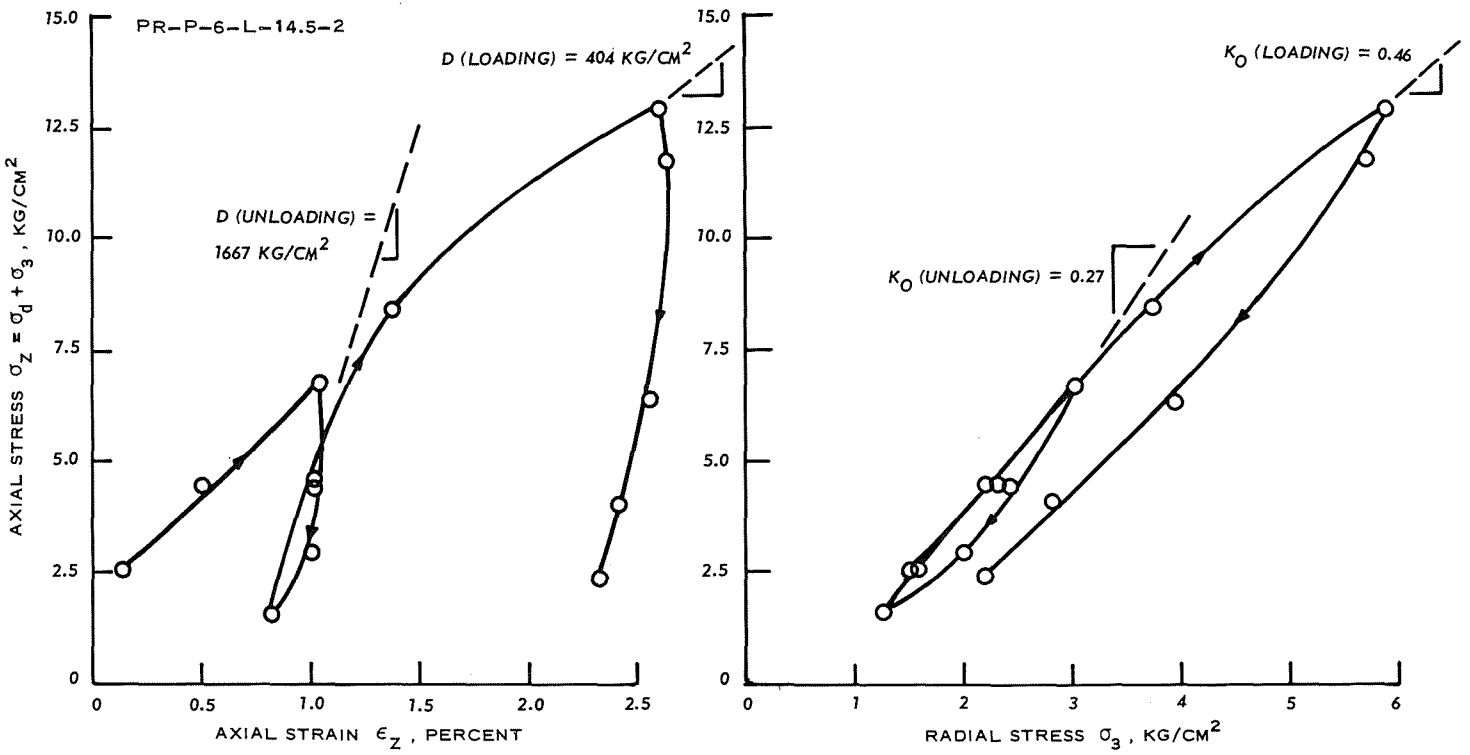

Figure 48. Stress-strain relationships for 6-in.- (15.2-cm-) diam K_o tests on modeled PARAHO compacted to 60 percent of standard effort density, test specimen PR-P-6-L-14.5-2

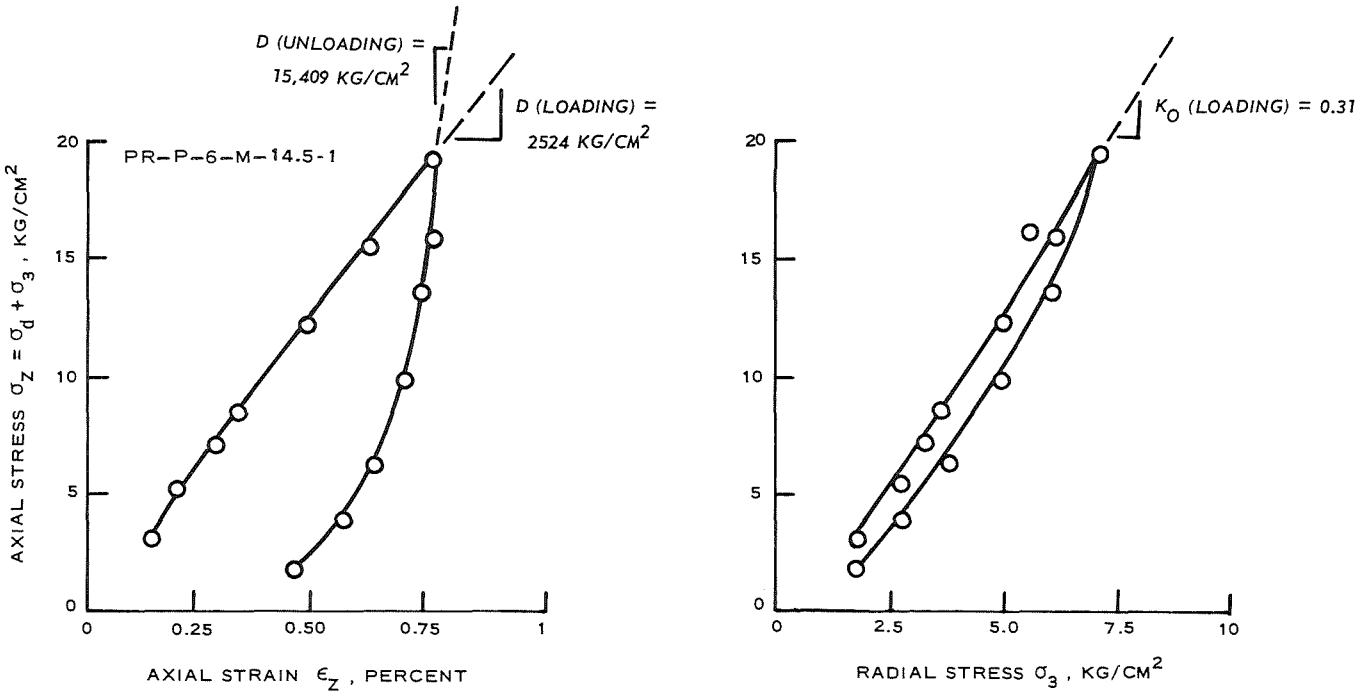

Figure 49. Stress-strain relationships for 6-in.- (15.2-cm-) diam K_o tests on modeled PARAHO compacted to modified effort density, test specimen PR-P-6-M-14.5-1

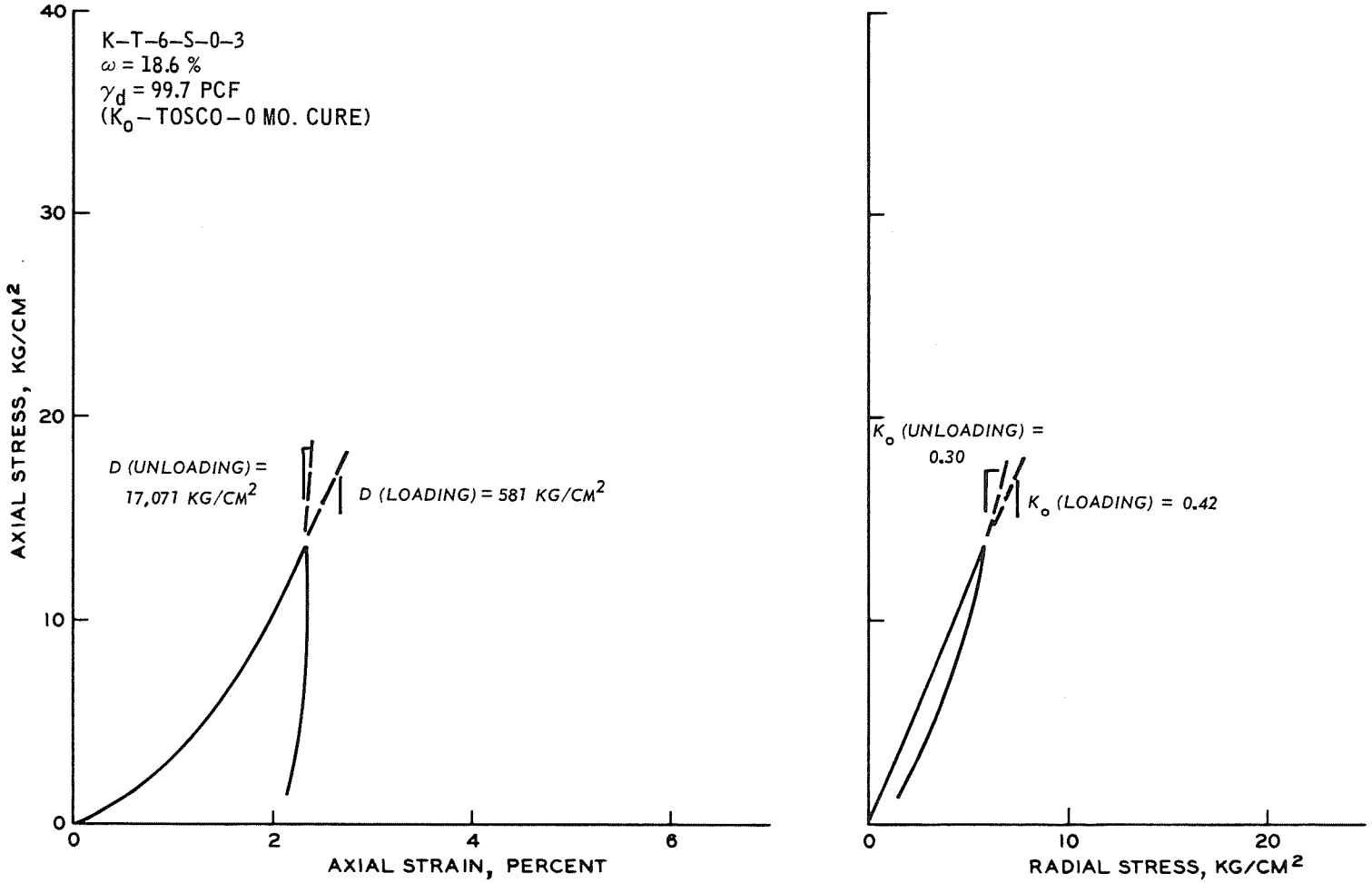

Figure 50. Stress-strain relationships for 6-in.- (15.2-cm-) diam K_o test on TOSCO compacted to standard effort density, 0-month cure, test specimen K-T-6-S-0-3

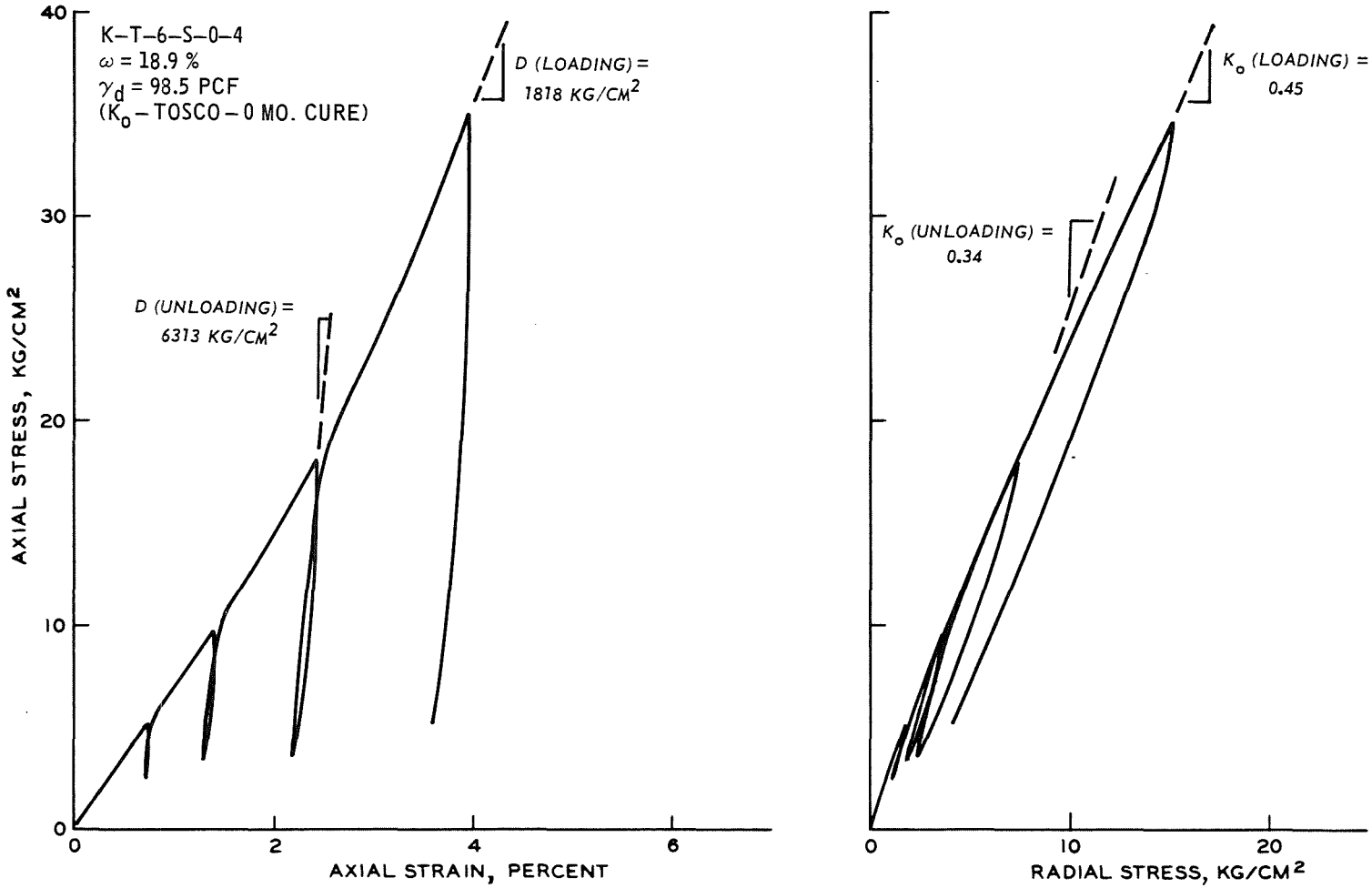

Figure 51. Stress-strain relationships for 6-in.- (15.2-cm-) diam K_o tests on TOSCO compacted to standard effort density, 0-month cure, test specimen K-T-6-S-0-4

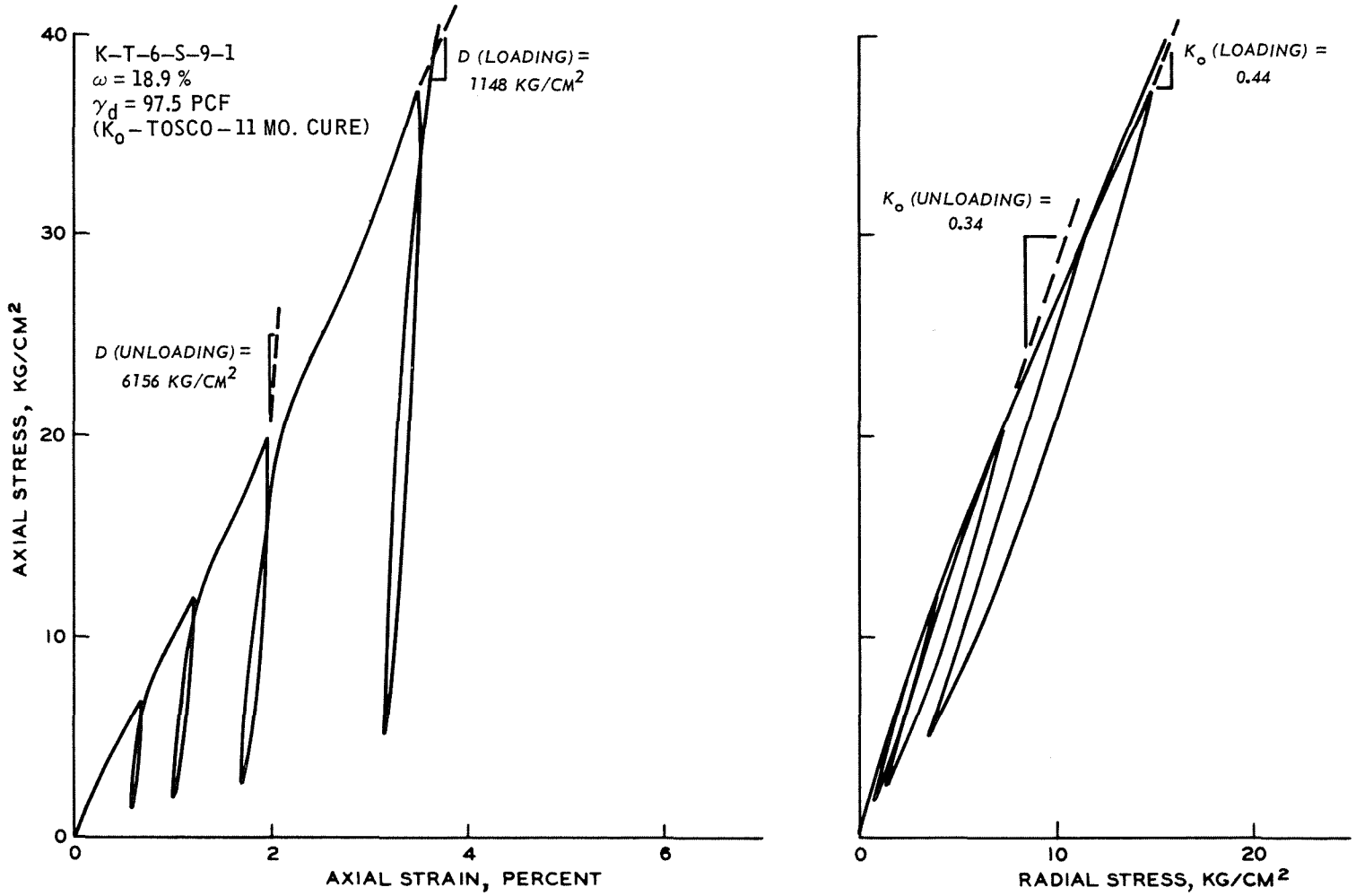

Figure 52. Stress-strain relationships for 6-in.- (15.2-cm-) diam K_o tests on TOSCO compacted to standard effort density, 11-month cure, test specimen K-T-6-S-9-1

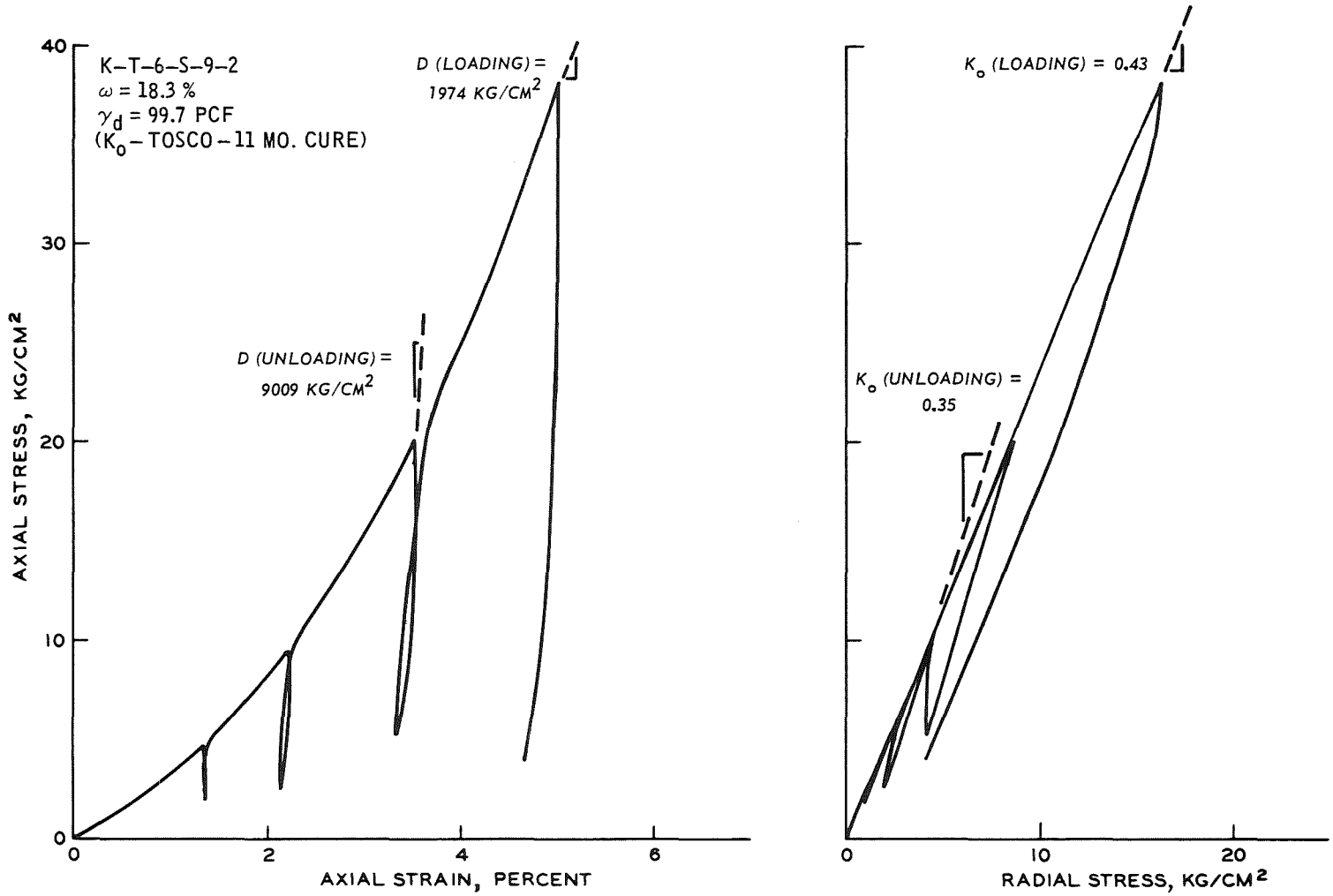

Figure 53. Stress-strain relationships for 6-in.- (15.2-cm-) diam K_o tests on TOSCO compacted to standard effort density, 11-month cure, test specimen K-T-6-S-9-2

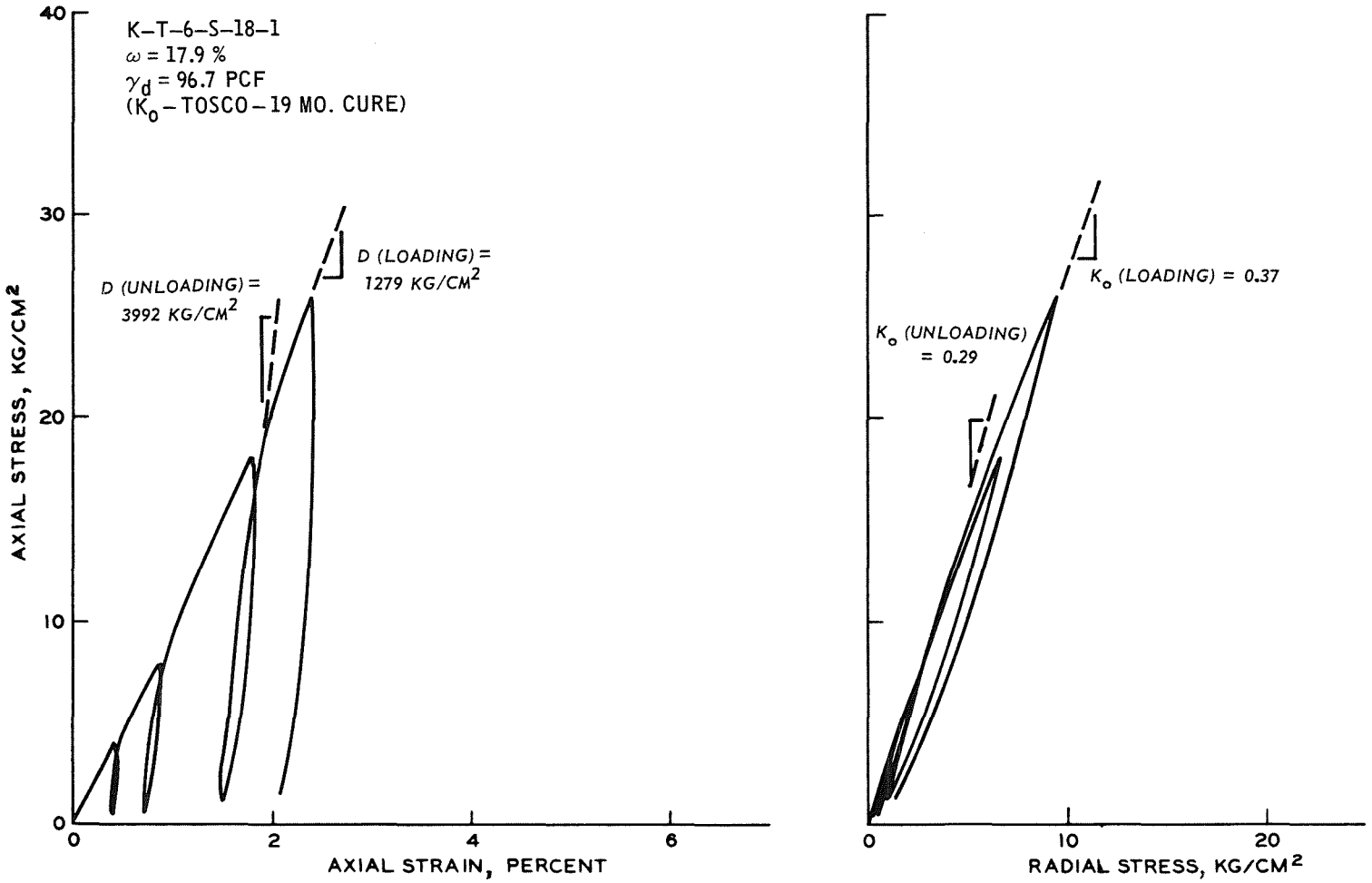

Figure 54. Stress-strain relationships for 6-in.- (15.2-cm-) diam K_o tests on TOSCO compacted to standard effort density, 19-month cure, test specimen K-T-6-S-18-1

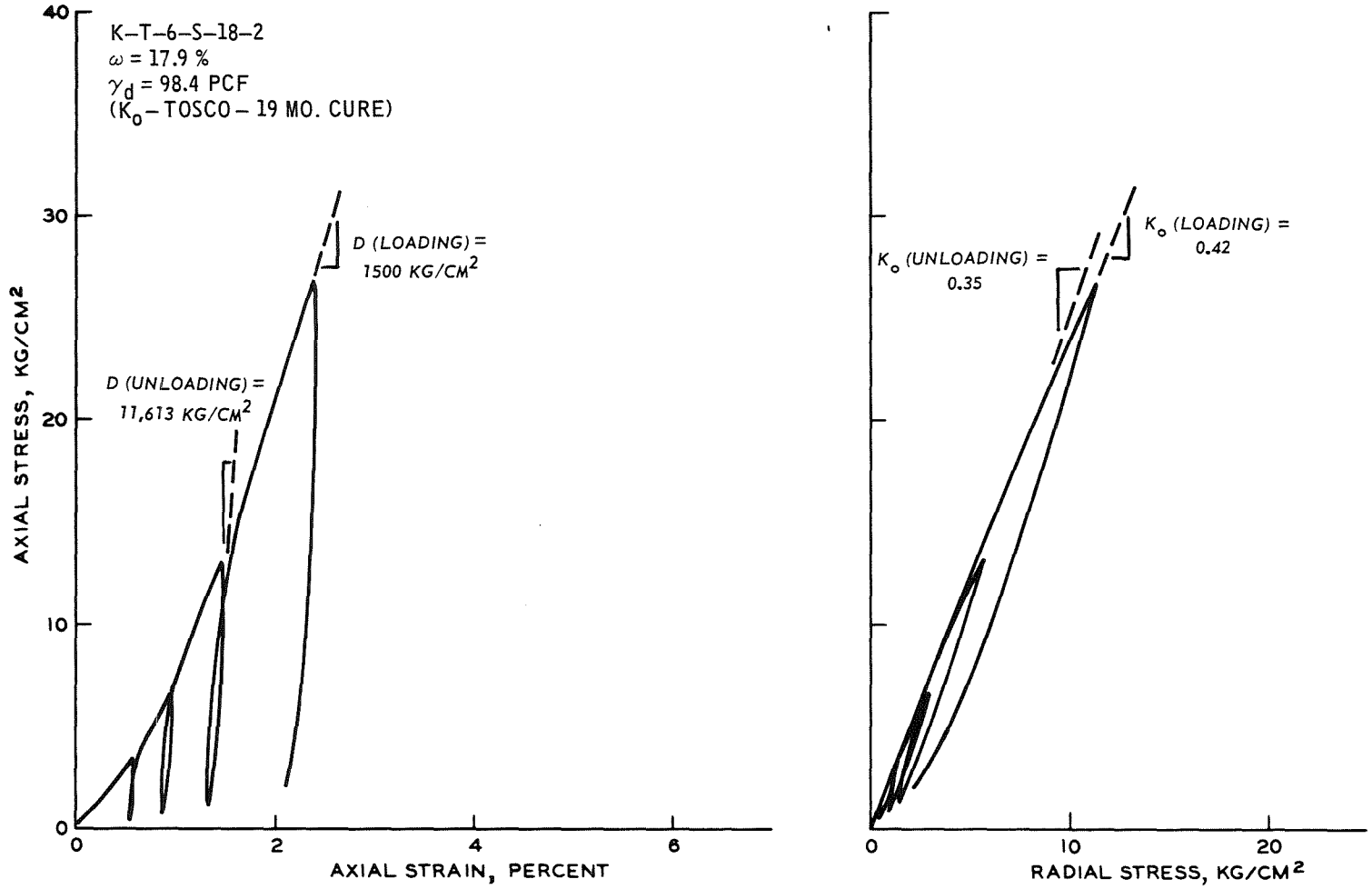

Figure 55. Stress-strain relationships for 6-in.- (15.2-cm-) diam K_o tests on TOSCO compacted to standard effort density, 19-month cure, test specimen K-T-6-S-18-2

Normally consolidated K_o values on modeled PARAHO were 0.45 and 0.37 for 60 percent of standard and modified compaction efforts, respectively. The corresponding normally consolidated constrained moduli D values were 634 kg/cm^2 and 2524 kg/cm^2, respectively. Thus, increased compaction effort resulted in stiffer specimens. For these specimens, an estimate of ϕ' is 37.9 deg (see tabulation in the Triaxial compression tests section), which using Jaky's (1948) expression gives a K_o value of 0.39 and in turn closely approximates the experimentally observed values. By comparison, WCC (1976) reported average normally consolidated K_o values of 0.41 to 0.43 and 0.43 to 0.45 for low compaction effort density 6-in.- (15.2-cm-) diam specimens cured 28 and 60 days, respectively. For modified compaction effort densities, they reported K_o values of 0.36 and 0.38 for 28 and 60 days curing, respectively. They also reported Young's moduli values E_d under K_o conditions of 427 to 466 kg/cm^2 and 1651 to 1431 kg/cm^2 for 28- and 60-day cured low and modified compaction efforts, respectively. These E_d values correspond to D values of 575 to 627 kg/cm^2 and 1788 to 2063 kg/cm^2, where $D = (1 - \nu - 2\nu^2)\ E_d$ for Poisson's ratio ν values of 0.30 and 0.27, respectively. These values of K_o and D are in remarkably good agreement with results obtained in this investigation. The WCC (1976) results also show that curing time has little effect on K_o or D values, and compaction results in stiffer specimens.

For TOSCO, the normally consolidated K_o values range from 0.38 to 0.43, from 0.32 to 0.44, and from 0.35 to 0.43 for specimens cured 3 days, 11 months, and 19 months, respectively. These correspond to ν values from 0.27 to 0.30, from 0.24 to 0.30, and from 0.26 to 0.30, respectively. The normally consolidated D values ranged from 580 to 1818 kg/cm^2, from 342 to 1973 kg/cm^2, and from 592 to 2859 kg/cm^2 for specimens cured 3 days, 11 months, and 19 months, respectively. Hence, although D values for 19 months are slightly higher, for practical purposes, increased curing times had very little effect on K_o or D values as was the case for PARAHO. Utilizing Jaky's (1948) expression, $K_o = 1 - \sin \phi'$, and a value of $\phi' = 35$ deg, the corresponding K_o value would be 0.43, which is consistent with the experimental values.

Figures 56 through 65 present the effects of σ_1 (overburden pressure) and overconsolidation ratio (OCR) on K_o, which can be used to obtain estimates of K_o for field situations. Table 14 lists these effects with normally consolidated values. These results show that the value of K_o increases with increasing axial stress level and overconsolidation ratio. Similar results concerning effect of stress history on K_o have been reported by Al-Hussaini and Townsend (1975 and 1975a). Although not indicated by all specimens tested, the general trend is that K_o is independent of the loading cycle. Similarly, the constrained modulus D increases with increasing stress level, with a

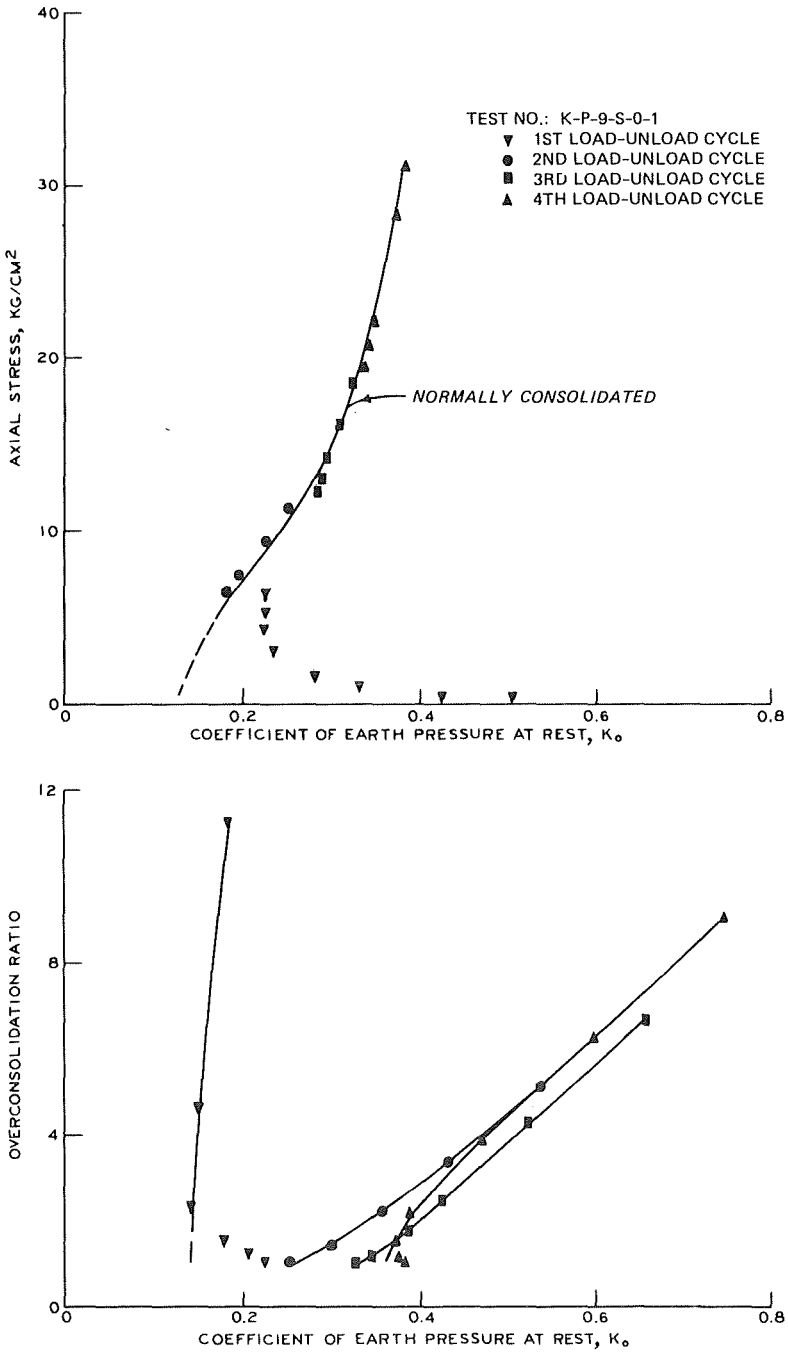

Figure 56. Relationship between axial stress and overconsolidation ratio on K_o values for PARAHO compacted to standard effort density, 0-month cure test specimen K-P-9-S-0-1

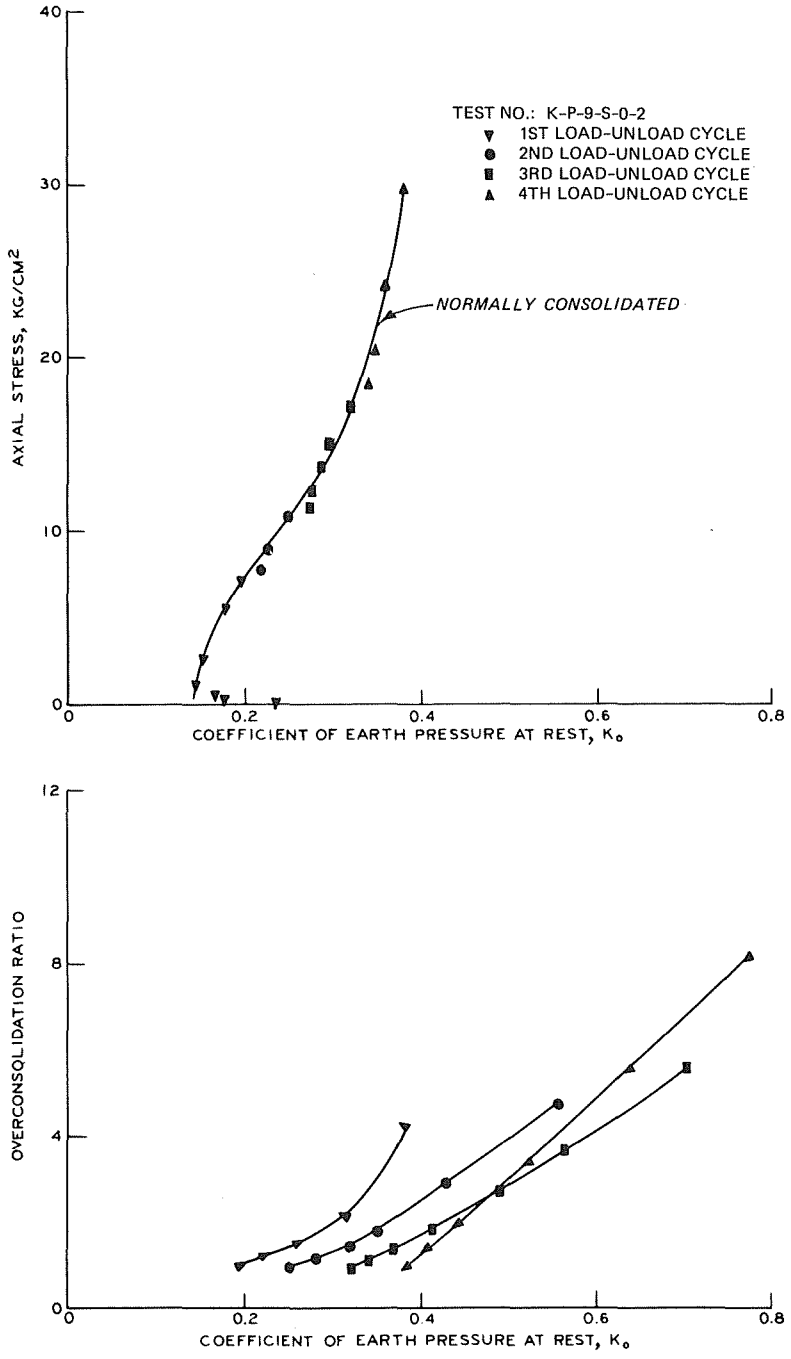

Figure 57. Relationship between axial stress and overconsolidation ratio on K_o values for PARAHO compacted to standard effort density, 0-month cure, test specimen K-P-9-S-0-2

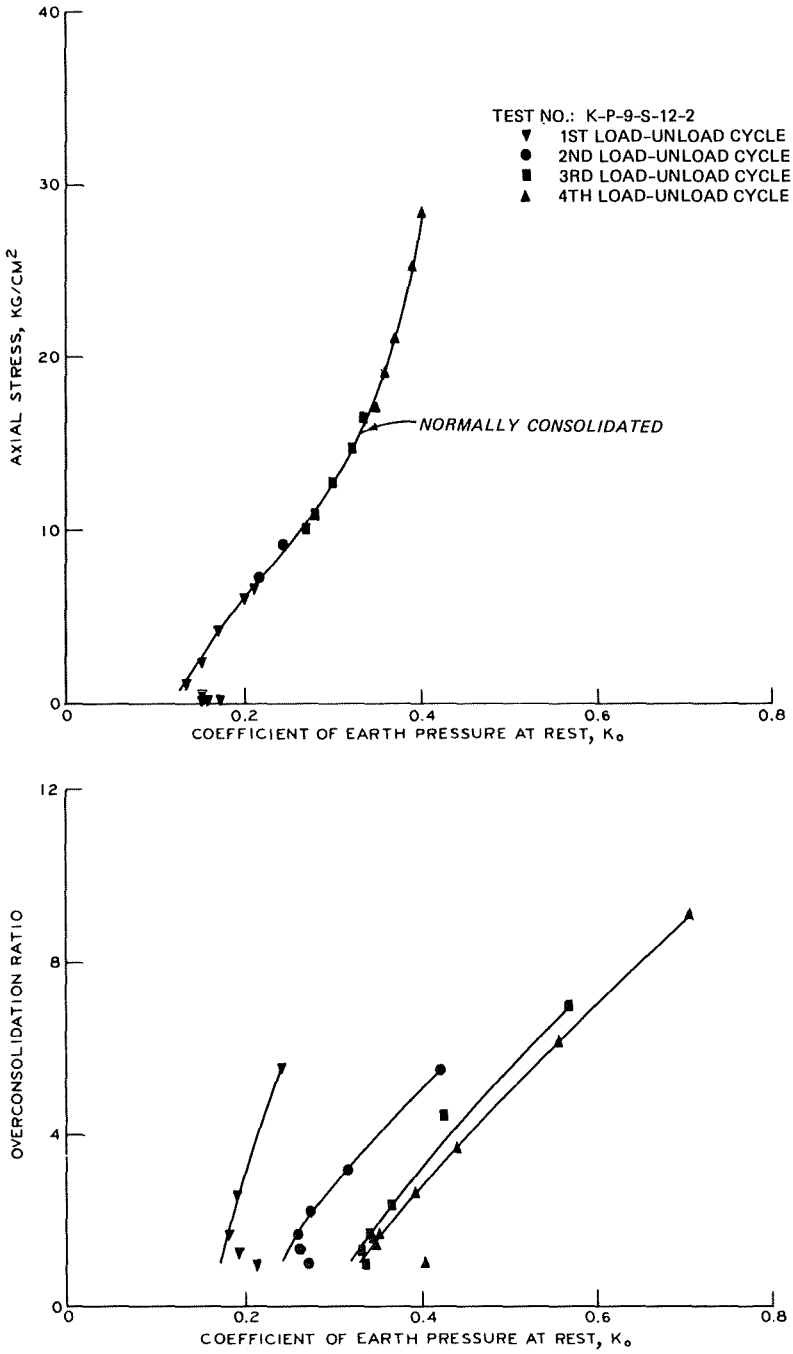

Figure 58. Relationship between axial stress and overconsolidation ratio on K_o values for PARAHO compacted to standard effort density, 13-month cure, test specimen K-P-9-S-12-2

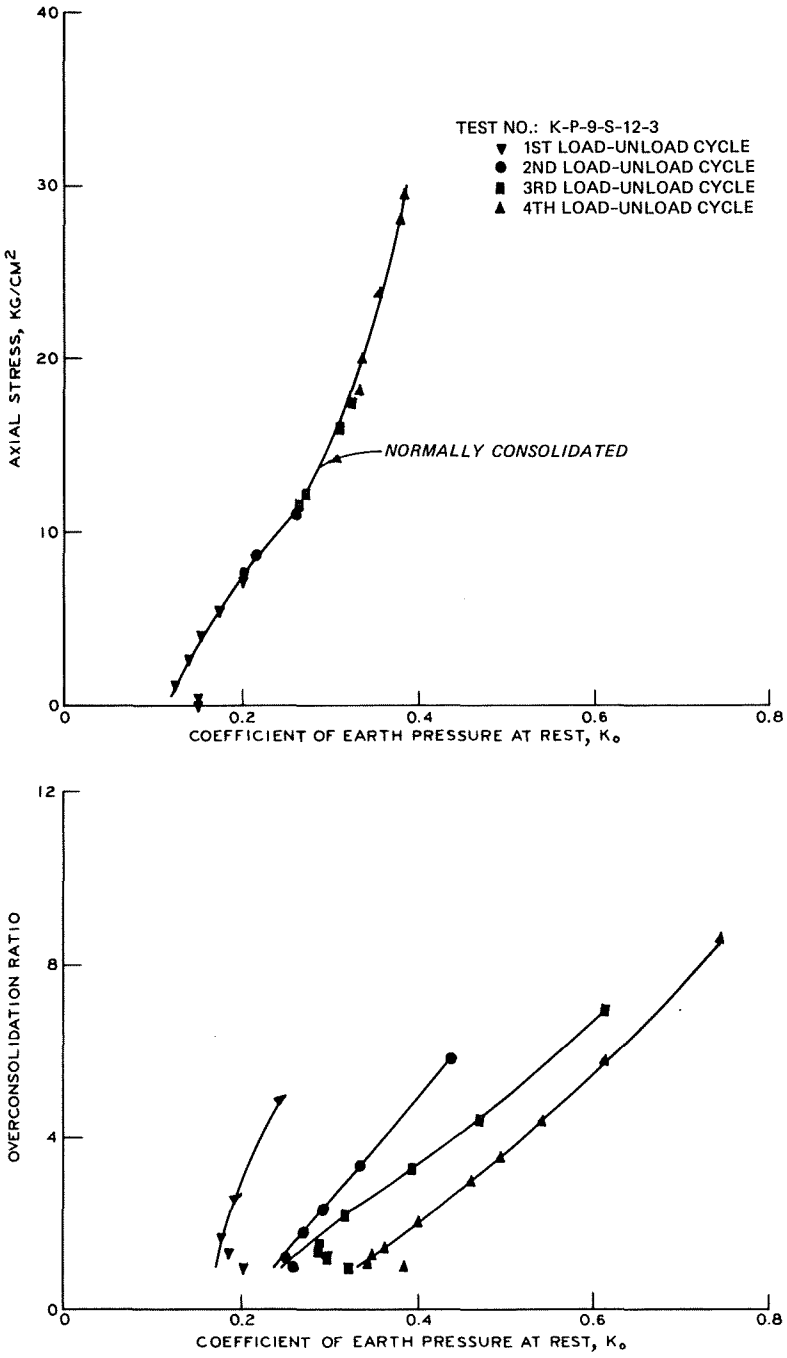

Figure 59. Relationship between axial stress and overconsolidation ratio on K_o values for PARAHO compacted to standard effort density, 13 test specimen K-P-9-S-12-3

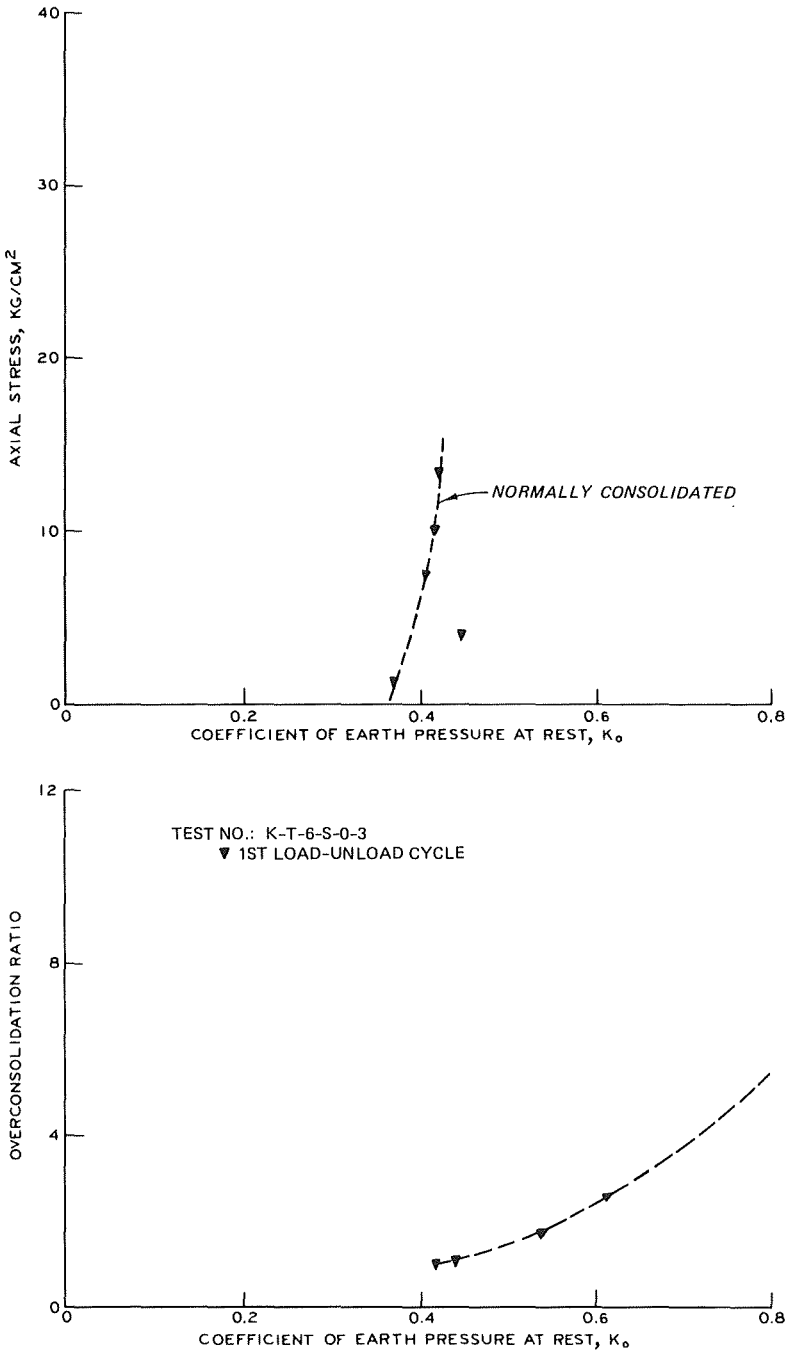

Figure 60, Relationship between axial stress and overconsolidation ratio on K_o values for TOSCO compacted to standard effort density, 0-month cure, test specimen K-T-6-S-0-3

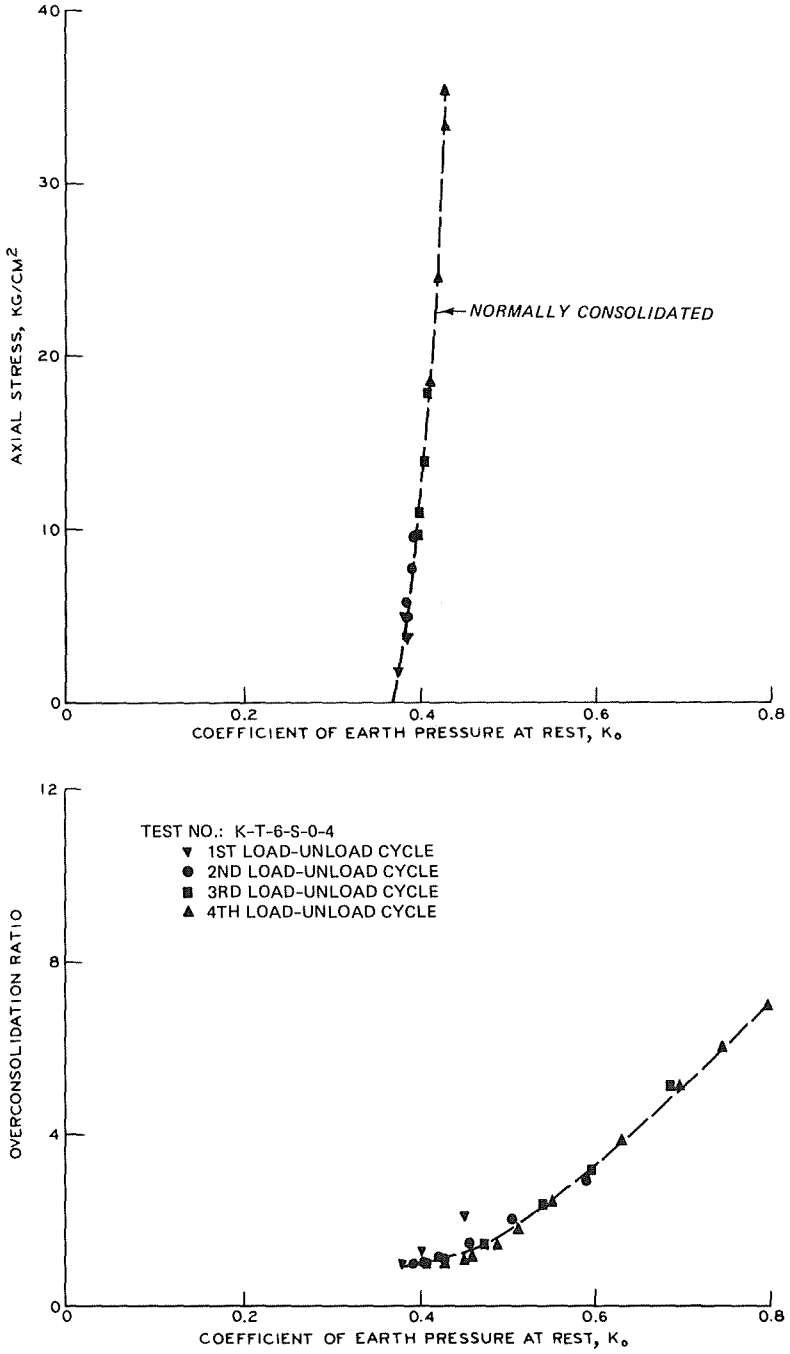

Figure 61. Relationship between axial stress and overconsolidation ratio on K_o values for TOSCO compacted to standard effort density, 0-month cure, test specimen K-T-6-S-0-4

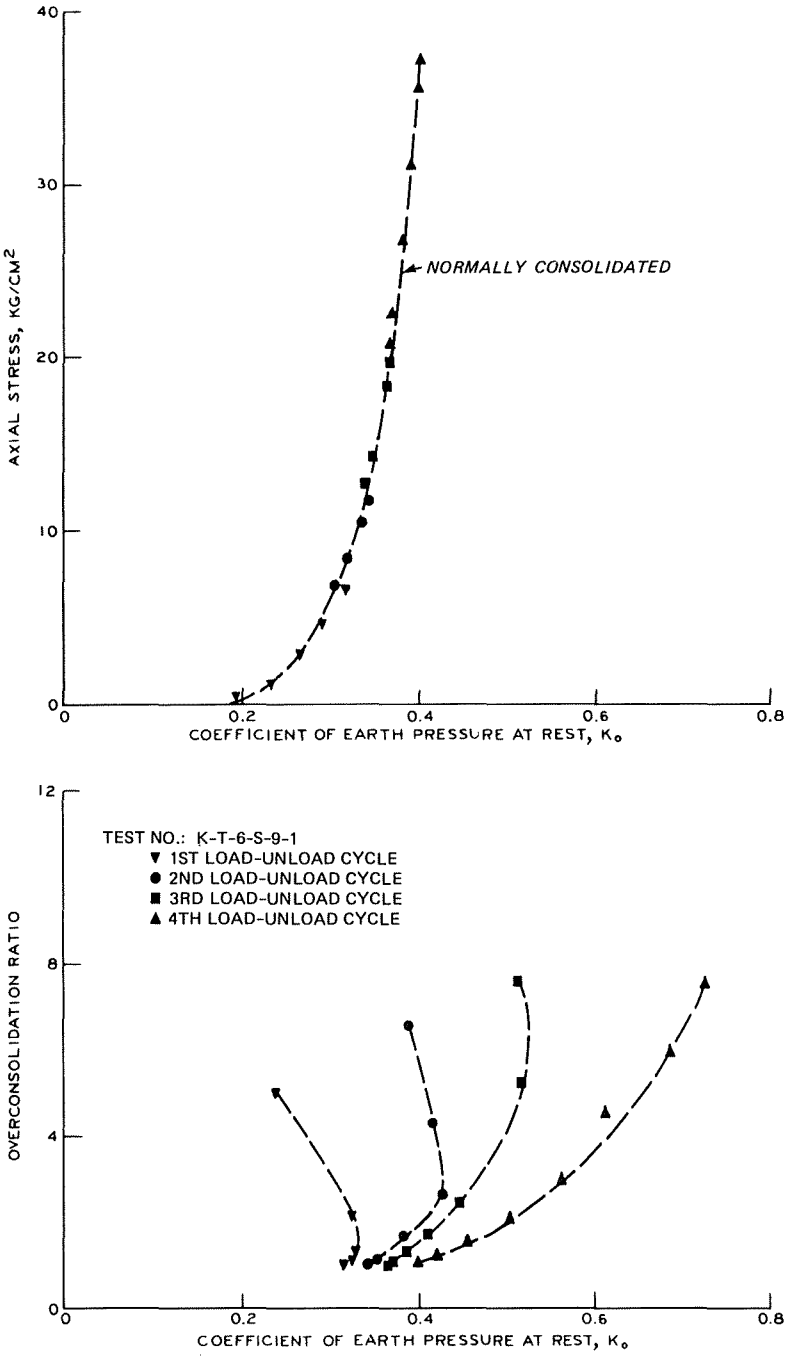

Figure 62. Relationship between axial stress and overconsolidation ratio on K_o values for TOSCO compacted to standard effort density, 11-month cure, test specimen K-T-6-S-9-1

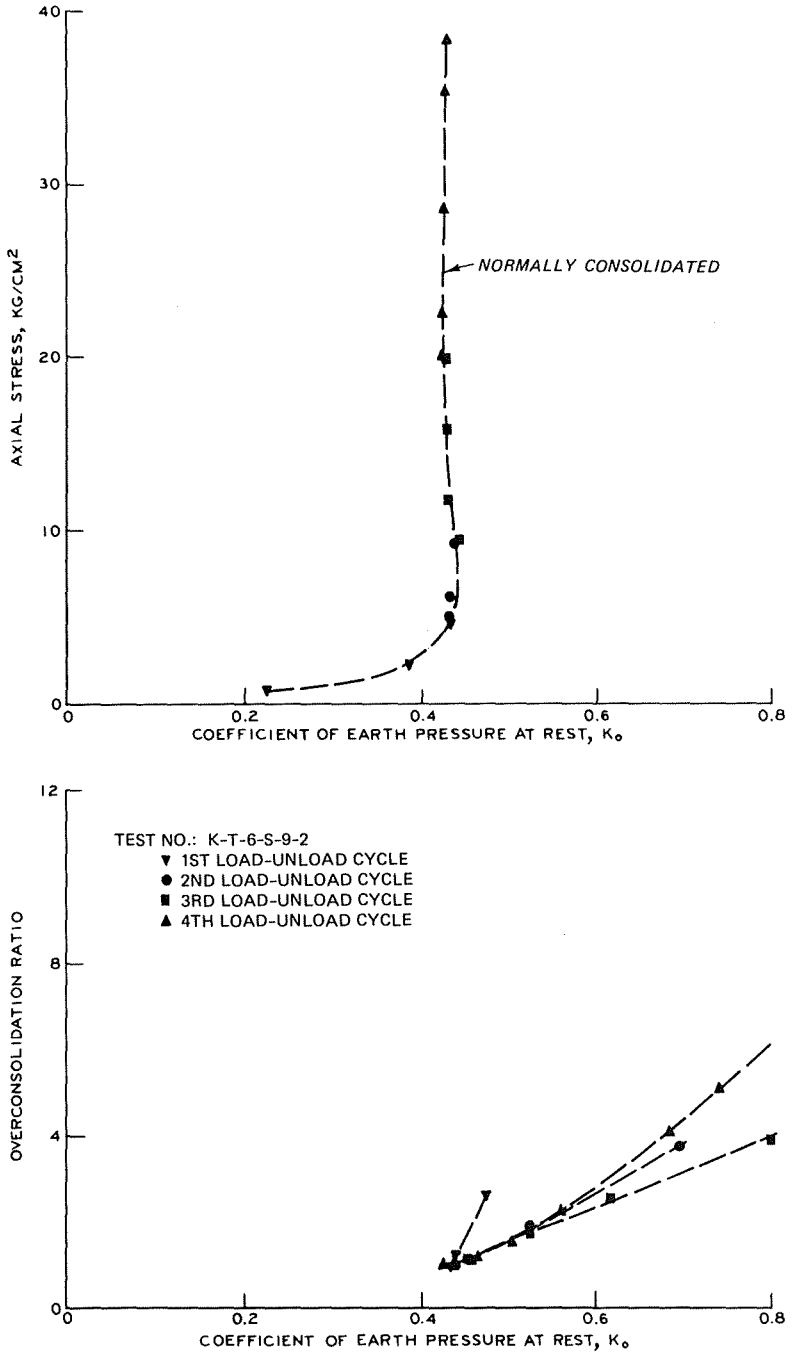

Figure 63. Relationship between axial stress and overconsolidation ratio on K_o values for TOSCO compacted to standard effort density, 11-month cure, test specimen K-T-6-S-9-2

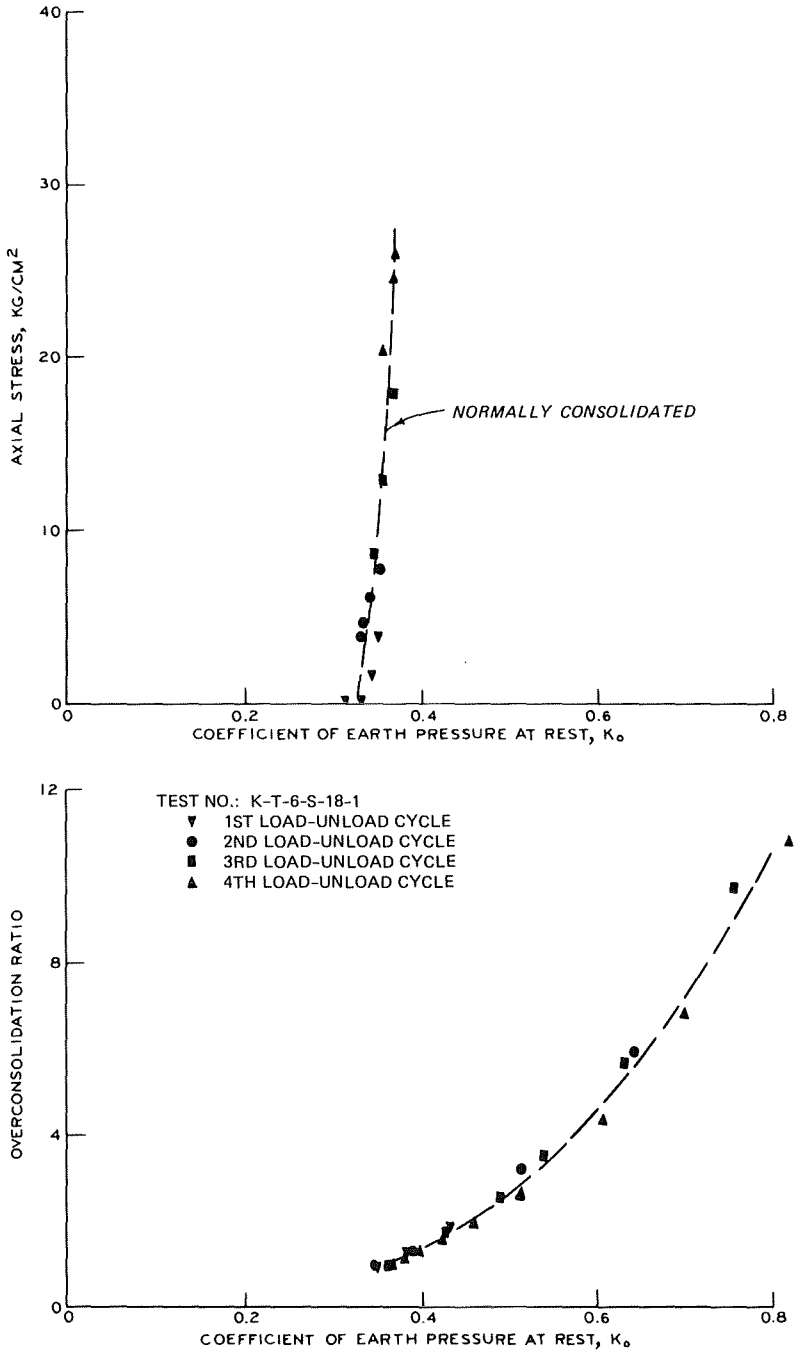

Figure 64. Relationship between axial stress and overconsolidation ratio on K_o values for TOSCO compacted to standard effort density, 19-month cure, test specimen K-T-6-S-18-1

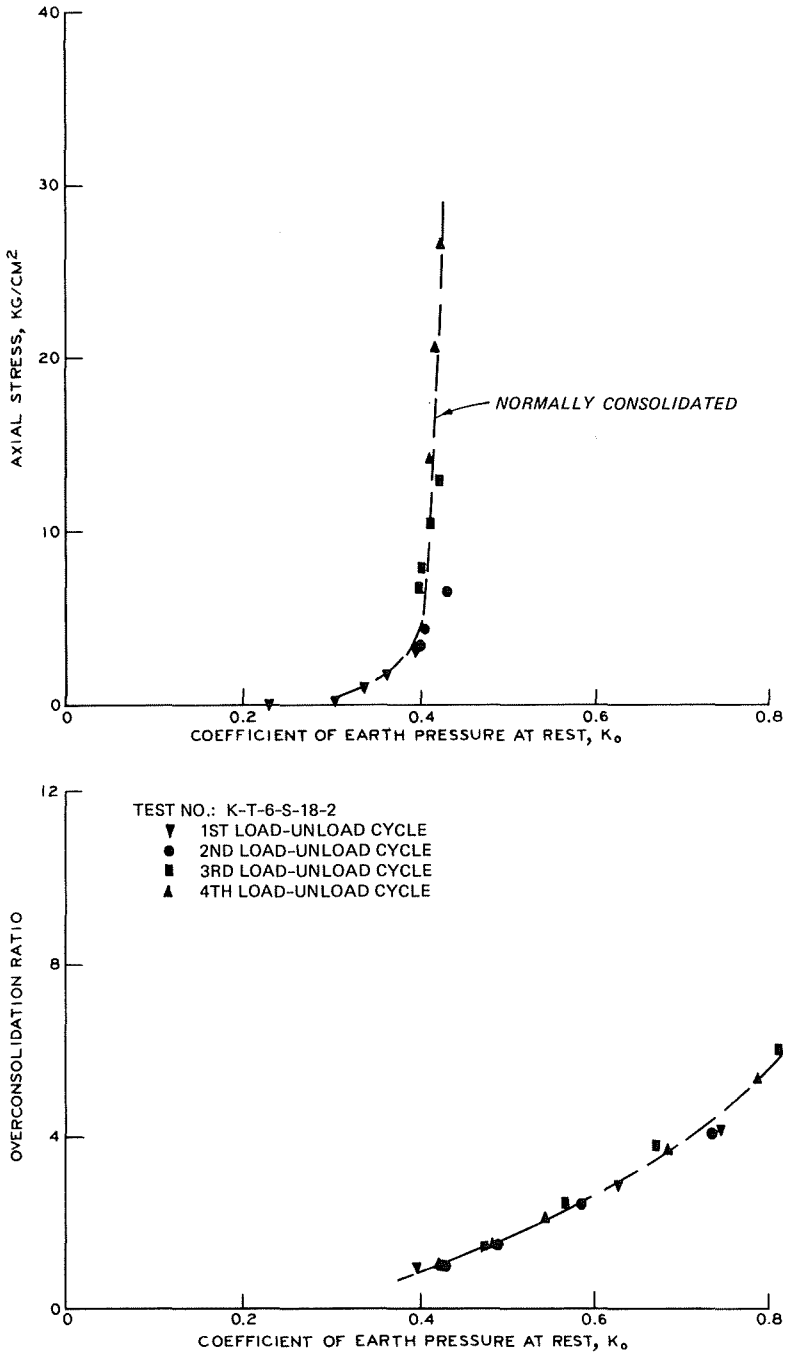

Figure 65. Relationship between axial stress and overconsolidated ratio on K_o values for TOSCO compacted to standard effort density, 19-month cure, test specimen K-T-6-S-18-2

tendency to become constant at higher stress levels. The D value is much higher upon unloading, and exhibits an increase with increasing OCR.

Cyclic triaxial tests

Figure 66 and Table 15 show the results of cyclic triaxial tests to assess the resistance of compacted modeled PARAHO to seismically induced ground failure. The first test series, performed on specimens compacted to 60 percent of standard density, shows that even at this low compaction effort, the material is quite resistant to cyclic loading as high stress ratios and large numbers of cycles were required to produce 100 percent pore pressure response (PPR). Hence, succeeding tests, performed on moist tamped specimens compacted to 60 percent D_r to evaluate PARAHO with other materials, show that at this abnormally low density for field conditions, cyclic loading could be a problem. For example, a stress ratio of 0.39 causes 100 percent PPR in 10 cycles for Monterey No. 0 sand moist tamped compacted to 60 percent D_r (Silver et al., 1976), while only a stress ratio of 0.21 is required to cause 100 percent PPR for modeled PARAHO. These results also show that the cyclic stress ratio required to cause 100 percent PPR decreases with increasing confining pressure, but the practical effect is small. Similar results have been reported by Townsend (1977).

For comparison, Wong et al. (1975) has shown that a cyclic stress ratio of 0.29 was required to cause 5.0 percent double amplitude strain in 30 cycles for various soils with a mean grain size D_{50} similar to modeled PARAHO at 60 percent D_r. The results in Figure 66 indicate that a cyclic stress ratio of 0.16 would be required for comparable conditions. From this standpoint, the modeled PARAHO at 60 percent D_r appears to be weaker than similarly graded materials. Nevertheless, seismically induced ground failure of a waste embankment is deemed an unlikely event as 100 percent saturation will probably never occur, nor will the materials be deposited in such a loose condition.

Dynamic properties tests

Since the dynamic properties, E, G, and λ, of soils are strongly dependent upon shear strain amplitude γ, characterization requires testing at various strain amplitudes, i.e., 10^{-4} to 1 percent strains. Since, currently no single apparatus is capable of applying strains over this range, typically resonant column methods are used for applying small strain amplitudes and cyclic triaxial tests for applying larger strain amplitudes. This approach implies that the small strain theory is applicable and the materials are linearly elastic. Hence, shear moduli G and torsional strain, $\gamma = 2r\theta/3L$, values based upon resonant column excitation are presumed compatible and are combined with longitudinal triaxial tests via the relationship $G = E/2(1 + \nu)$, and $\gamma = \varepsilon_1(1 + \nu)$ with Poisson's ratio either determined or assumed. For these tests, Poisson's ratio was dynamically determined from lateral and axial strain measurements using LVDT clamps on triaxial specimens.

Both resonant column and cyclic triaxial tests were performed on modeled PARAHO specimens compacted to densities equivalent to 60 percent of standard and modified efforts. Confining pressures of 14.5, 43.5, and 72.5 psi (100,

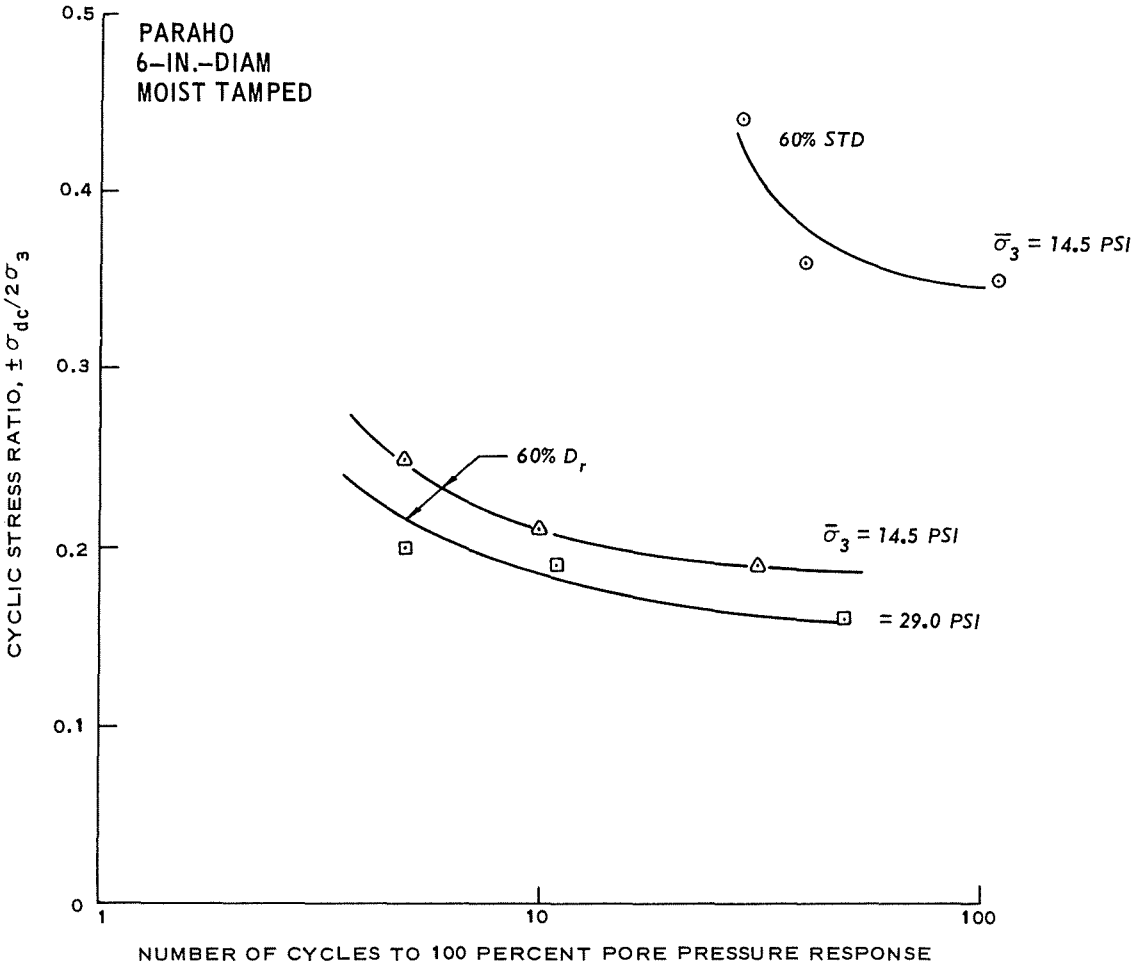

Figure 66. Cyclic triaxial response of compacted PARAHO retorted oil shale

Table 15

Summary of Cyclic Triaxial Tests on 6-in.-diam Specimens of Modeled PARAHO

Test Specimen*	Dry Density** γ_d, pcf	Effective Confining Stress σ'_3, psi	B	Cyclic Deviator Stress $\pm\sigma_{dc}$ psi	Cyclic Stress Ratio $\pm\sigma_{dc}/2\sigma'_3$	No. of Cycles	
						100% Pore Pressure Response Ni	10% Double Amplitude Strain N ± 5%
P-6-L-14.5-1	92.5†	14.5	0.96	12.72	0.44	29	53
P-6-L-14.5-3	97.9	14.5	0.94	10.71	0.36	40	123
P-6-L-14.5-4	100.3†	14.5	0.93	10.14	0.35	101	155
P-6-60-14.5-1	74.4	14.5	0.94	5.41	0.19	31	††
P-6-60-14.5-2	73.7	14.5	0.98	7.16	0.25	5	6
P-6-60-14.5-3	74.0	14.5	0.98	6.17	0.21	10	9
P-6-60-29.0-1	77.4	29.0	0.98	11.83	0.20	5	5
P-6-60-29.0-2	77.2	29.0	0.97	11.04	0.19	11	11
P-6-60-29.0-3	76.8	29.0	0.97	9.12	0.16	49	51

* P = PARAHO; 6 = 6-in.-diam specimen; L = low compaction effort or 60 = 60% D_r; 14.5 or 29.0 = confining pressure, psi; number 1, 2, 3, or 4 = number of test in series.

** Dry density after consolidation.

† Estimated.

†† Load fell off before achievement of double amplitude strain.

300, and 500 kPa) were used. In the case of resonant column tests, both longitudinal and torsional excitation modes were possible; therefore, both E and G values were determined on single specimens subjected to multistage confining pressures and multistage strain levels. In the case of cyclic triaxial specimens, only multistage strain levels were varied for a given confining pressure.

Table 16 summarizes the resonant column test data for the maximum and minimum dynamic strain conditions. Also listed for comparison are estimated values of G_{max} calculated from the equation for sands (Hardin and Black, 1969) $G_{max} = 1230(2.973\text{-}e)^2\sqrt{\sigma_3'}/(1 + e)$, where σ_3' and G_{max} are in pounds per square inch. An examination of these estimations reveals that experimental G_{max} values for tests RC-P-4-L-2 and RC-P-4-M-1 are as much as three times greater than predicted values. Thus, it appears that this equation is not appropriate for this gradation of material.

Table 17 summarizes the cyclic triaxial test data. The values of Poisson's ratio listed range from 0.1 to 0.3, which are slightly lower than the average value of 0.25 obtained from static K_o tests. However, the strain levels for the cyclic tests are substantially lower than those for K_o tests.

Figures 67 and 68 present the Young's moduli values, while Figures 69 and 70 present the shear moduli values for the respective two densities. One testing difficulty is readily apparent: the specimen stiffness exceeded tolerable limits of the resonant column apparatus for both the longitudinal and torsional modes, which is especially evident for modified compaction effort density and high confining pressures for both densities. As a result, the resonant column derived moduli values are too low and damping ratios too high.

For the low compaction effort, reasonable compatibility was obtained between the resonant column and cyclic triaxial tests (Figures 67 and 69). The strong dependence of modulus on confining pressure, strain amplitude, and density is readily evident in these figures. This dependence is more clearly summarized in Figure 71, in which values from cyclic triaxial tests for k from the expression, $G = 1000\ k(\sigma_3)^{1/2}$, where σ_3 is in pounds per square foot, are presented versus single amplitude shear strain γ . For comparison, values for k reported by Seed and Idriss (1970) are also shown. These comparisons suggest that well-compacted modeled PARAHO exhibits properties similar to those for dense sand and gravel.

Figure 72 presents damping ratio λ values versus single amplitude shear strain. A somewhat reasonable data band is apparent if the resonant column data for modified compaction efforts are disregarded because of exceeding the apparatus capabilities and thereby experiencing damping contributed by the device. This band suggests that λ increases with strain amplitude, but is independent of density and confining pressure. For comparison, the range of damping ratio values for sands summarized by Seed and Idress (1970), are also shown in Figure 72.

Table 16

Summary of Resonant Column Tests on PARAHO

Test Identification*	σ'_3 psi	Void Ratio e	Excitation Mode	Minimum** Dynamic Strain $\times 10^{-4}$	Maximum† Dynamic Modulus psf $\times 10^5$	Damping Ratio at Minimum Strain λ, %	Maximum** Dynamic Strain $\times 10^{-4}$	Minimum† Dynamic Modulus psf $\times 10^5$	Damping Ratio at Maximum Strain λ, %	Calculated†† G_{max} psf $\times 10^5$
RC-P-4-L-2-S1	14.5	0.801	Torsional	0.001	42.0	5.80	0.153	40.2	8.10	17.7
			Longitudinal	0.001	111.4	6.32	0.031	105.4	6.35	
RC-P-4-L-2-S2	43.5	0.772	Torsional	0.001	51.2	6.14	0.118	48.8	9.90	31.9
			Longitudinal	<0.001	193.7	4.77	0.015	197.0	4.09	
RC-P-4-L-2-S3	72.5	0.742	Torsional	0.002	55.1	5.31	0.126	51.0	5.98	43.1
			Longitudinal	<0.001	227.3	2.35	0.017	224.5	3.32	
RC-P-4-L-2-S4	14.5	0.751	Torsional	0.002	46.5	31.28	0.110	42.8	37.34	19.0
			Longitudinal	<0.001	114.8	9.83	0.035	96.2	10.85	
RC-P-4-M-1-S1	14.5	0.544	Torsional	0.003	72.3	3.35	0.247	59.4	2.95	25.8
			Longitudinal	<0.001	209.0	2.95	0.022	196.4	3.39	
RC-P-4-M-1-S2	43.5	0.533	Torsional	0.002	62.7	8.99	0.080	59.6	16.89	45.4
			Longitudinal	<0.001	246.2	2.91	0.021	233.3	2.74	
RC-P-4-M-1-S3	72.5	0.524	Torsional	0.002	65.7	15.40	0.092	60.7	28.38	59.6
			Longitudinal	<0.001	272.4	2.35	0.012	241.7	2.74	
RC-P-4-M-1-S4	14.5	0.529	Torsional	0.002	59.3	6.18	0.087	65.6	5.13	26.3
			Longitudinal	<0.001	207.8	4.06	0.015	190.5	5.05	

* RC = resonant column, P = PARAHO; 4 = 4-in.-diam specimen; L or M = low or modified compaction effort; 1 or 2 = specimen No. 1 or 2; S1-S4 = stage sequence.

** Maximum dynamic strain will be γ_{max} for torsional mode or ε_{max} for longitudinal mode, similarily for minimum dynamic strain.

† Maximum dynamic modulus will be G_{max} for torsional mode or E_{max} for longitudinal mode, similarily for minimum dynamic modulus.

†† From Hardin and Black (1969), $G_{max} = 1230 \frac{(2.973 - e)^2}{1 + e} \sqrt{\sigma'_3}$, $\times 144$ where σ'_3 is in psi.

Table 17

Summary of Cylic Triaxial Properties Tests on PARAHO

Test Identification	σ'_3 psi	Single Amp. Axial Strain $\pm\varepsilon_a$, %	Single* Amp. Shear Strain $\pm\gamma$, %	Poisson's Ratio ν	Cyclic Deviator Stress $\pm\sigma_{dc}$, psi	Young's Modulus E, psf $\times 10^5$	Shear Modulus G, psf $\times 10^5$	K	λ
L-14.5-1	14.5	0.02	0.02	0.14	3.9	27.6	12.1	26.5	
		0.05	0.06	0.12	5.9	16.3	7.2	15.9	
		0.08	0.09	0.13	7.5	13.7	6.1	13.3	
		0.10	0.12	0.14	9.1	12.4	5.5	12.0	
		0.23	0.26	0.14	12.8	8.1	3.5	7.8	
		0.50	0.56	0.14	18.3	5.3	2.3	5.1	
L-14.5-2	14.5	0.004	0.004	0.11	1.7	65.2	29.3	64.2	23.8
		0.01	0.01	0.09	3.5	37.0	16.9	37.1	15.0
		0.02	0.03	0.14	5.3	29.0	12.7	27.9	13.3
		0.04	0.05	0.15	7.3	23.2	10.1	22.1	12.2
		0.07	0.08	0.17	9.1	18.9	8.1	17.8	11.6
		0.10	0.12	0.17	10.8	15.2	6.5	14.2	11.7
		0.15	0.18	0.17	12.8	12.1	5.1	11.3	9.9
		0.18	0.21	0.17	13.5	10.5	4.5	9.9	10.1
L-43.5-1	43.5	0.006	0.007	0.07	3.6	82.2	38.5	48.7	11.4
		0.01	0.02	0.10	7.3	65.5	29.7	37.5	8.8
		0.04	0.05	0.15	14.4	47.3	20.5	25.9	10.1
		0.09	0.10	0.17	21.4	34.5	14.8	18.7	11.4
		0.20	0.23	0.12	28.6	20.0	8.9	11.3	11.3
		0.25	0.31	0.22	35.4	20.0	8.2	10.4	11.8
L-72.5-1	72.5	0.003	0.003	0.16	3.5	197.0	84.7	83.0	19.1
		0.01	0.01	0.10	10.5	106.0	48.0	47.0	14.0
		0.03	0.03	0.15	17.7	80.1	34.8	34.1	12.5
		0.06	0.07	0.16	27.0	59.0	25.4	24.8	11.6
		0.10	0.12	0.21	35.5	50.8	21.0	20.6	13.3
		0.19	0.22	0.19	46.6	35.7	14.9	14.6	12.9
M-14.5-1	14.5	0.005	0.006	0.17	3.5	100.9	43.3	94.8	13.1
		0.01	0.01	0.08	5.3	75.7	34.9	76.5	11.1
		0.02	0.02	0.10	9.0	51.5	23.4	51.2	11.4
		0.05	0.05	0.12	12.3	35.7	16.0	35.0	10.8
		0.05	0.06	0.12	13.4	35.7	15.9	34.8	10.0
		0.05	0.06	0.15	14.9	41.2	17.9	39.2	11.5
		0.08	0.09	0.17	17.6	31.5	13.5	29.6	11.0
		0.13	0.16	0.21	25.5	27.1	11.2	24.5	11.3
		0.18	0.23	0.26	32.5	25.2	10.0	21.9	11.3
		0.22	0.29	0.29	41.7	26.6	10.2	22.5	10.9
M-43.5-1	43.5	0.002	0.003	0.35	5.2	315.7	117.0	147.9	27.4
		0.002	0.003	0.35	5.2	316.1	117.2	148.1	31.2
		0.009	0.01	0.09	10.8	171.6	78.6	99.3	19.5
		0.03	0.03	0.13	21.1	96.4	42.6	53.8	15.8
		0.07	0.08	0.15	32.0	62.5	27.2	34.4	14.6
		0.11	0.13	0.15	39.0	48.7	21.1	26.7	13.0
M-72.5-1	72.5	0.001	0.002	0.33	3.5	403.8	151.7	148.5	21.6
		0.003	0.004	0.13	7.1	326.9	144.3	141.3	17.4
		0.009	0.01	0.07	14.5	229.6	107.0	104.7	12.6
		0.02	0.03	0.13	28.9	150.5	66.4	65.0	12.0
		0.06	0.07	0.13	43.3	101.2	44.5	43.6	11.2
		0.11	0.13	0.15	57.8	72.6	31.5	30.8	11.4
		0.20	0.22	0.15	69.9	50.5	22.0	21.5	10.7

* $\gamma = \varepsilon_a(1 + \nu)$.

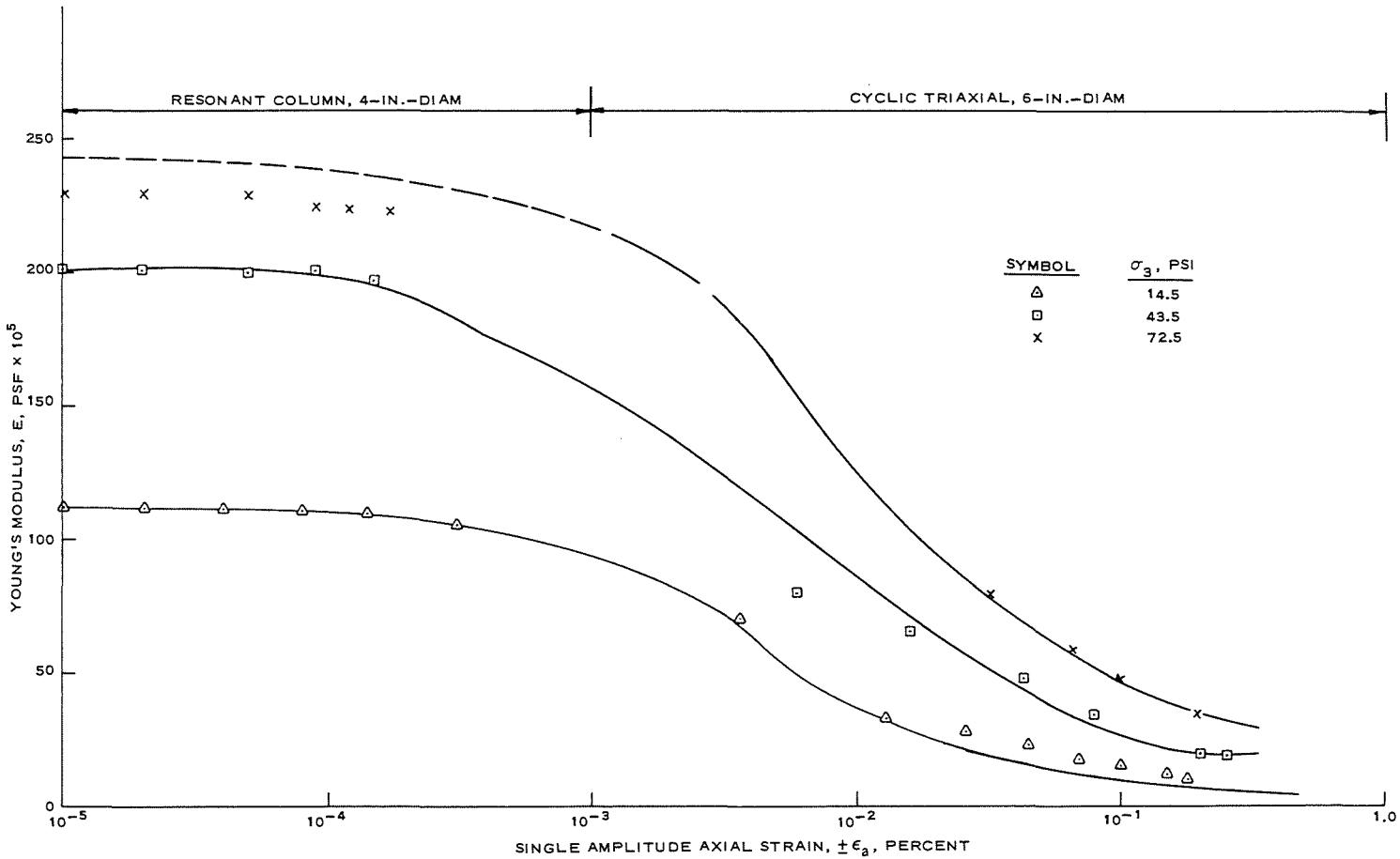

Figure 67. Dynamic Young's moduli values for PARAHO compacted to 60 percent of standard effort density

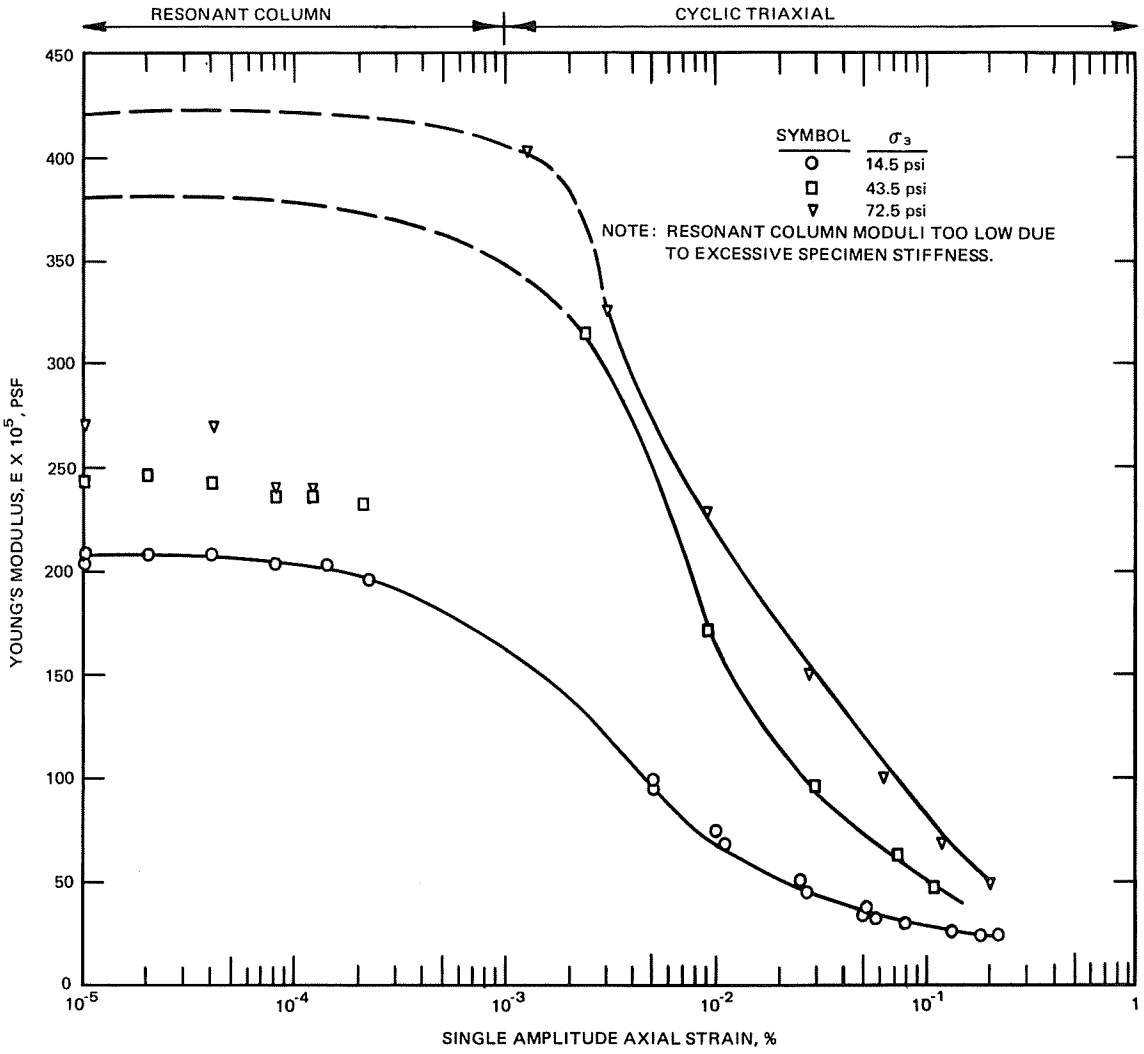

Figure 68. Dynamic Young's moduli values for PARAHO compacted to modified effort density

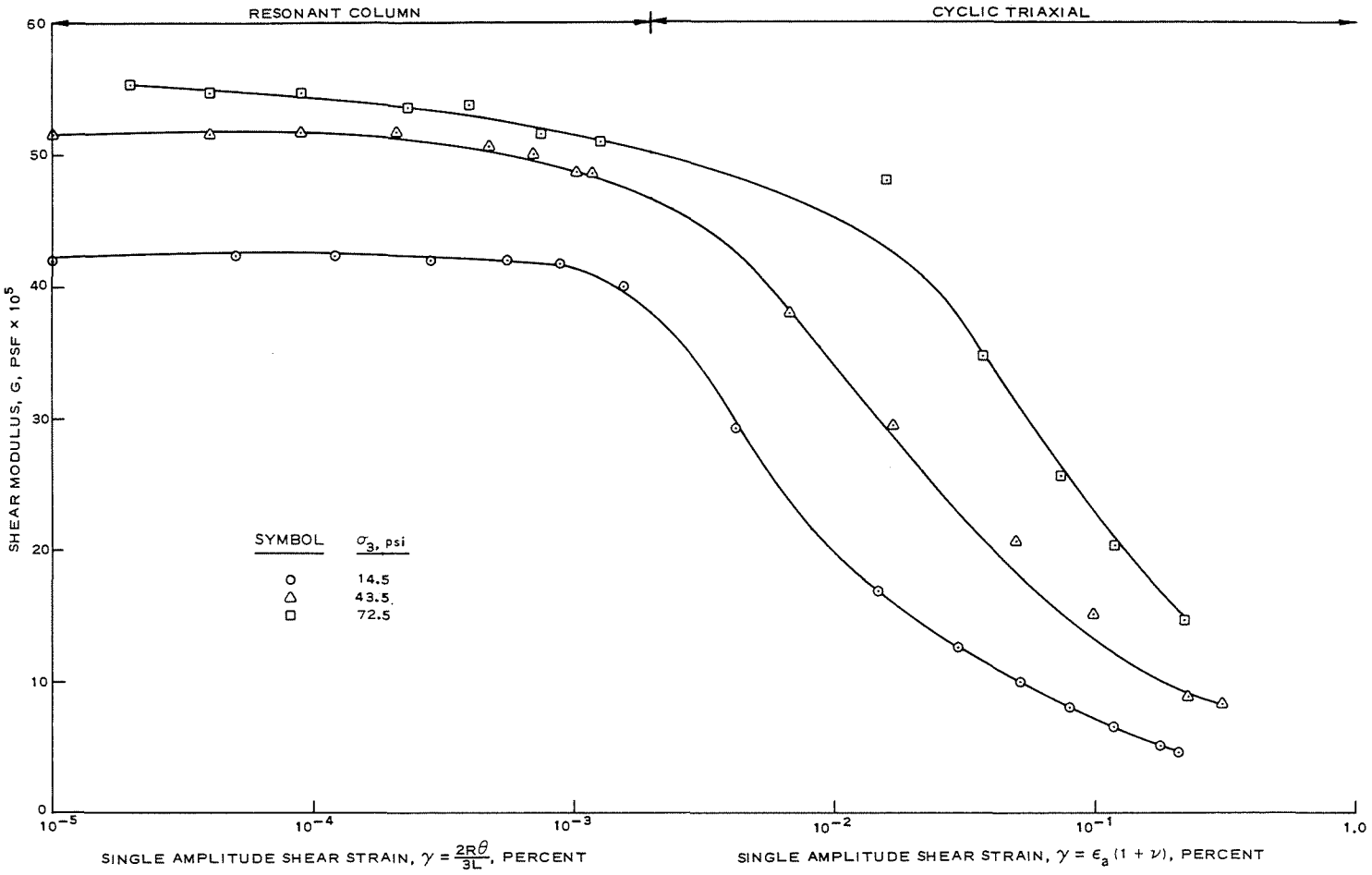

Figure 69. Dynamic shear moduli values for PARAHO compacted to 60 percent of standard effort density

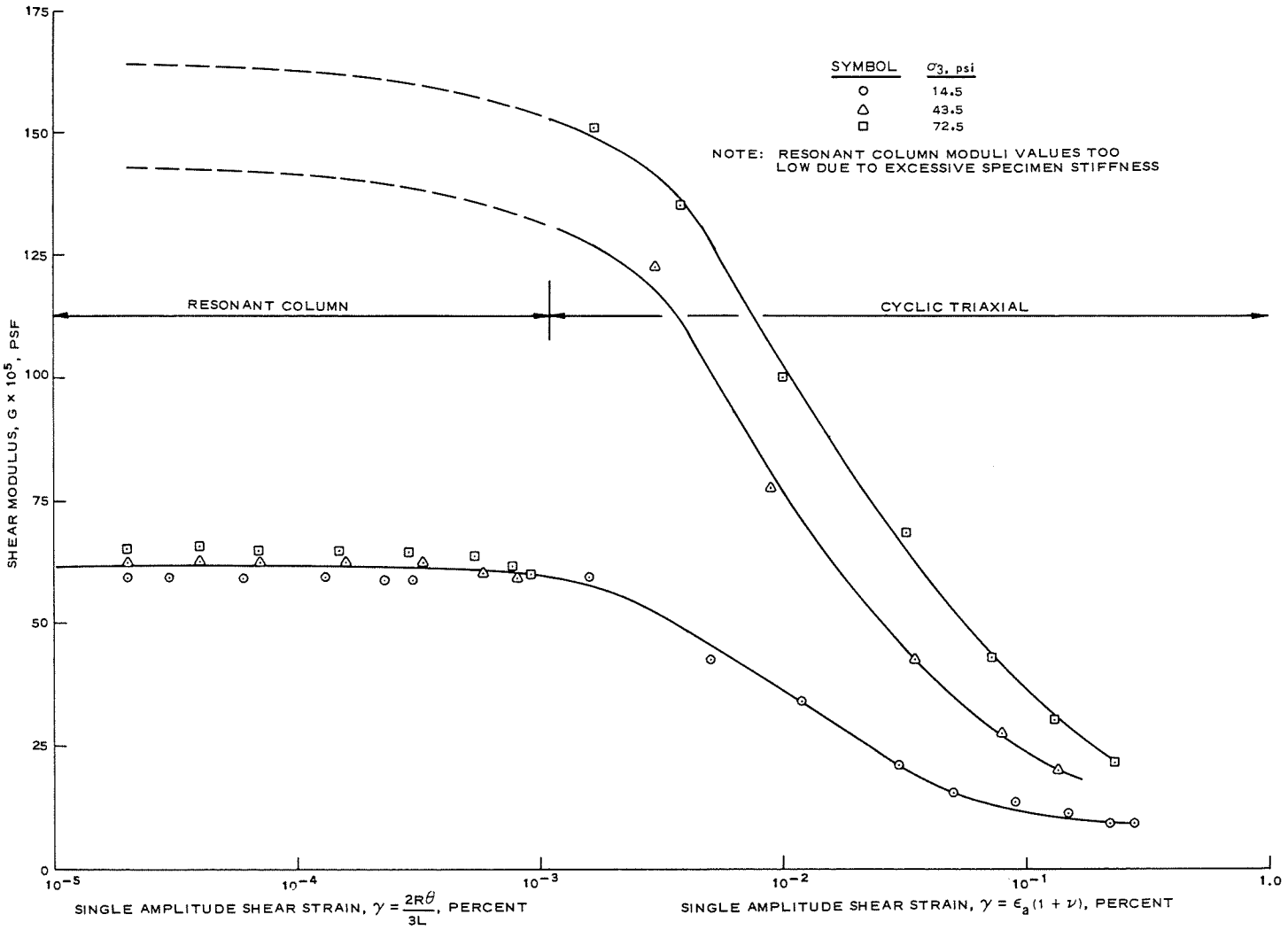

Figure 70. Dynamic shear moduli values for PARAHO compacted to modified effort density

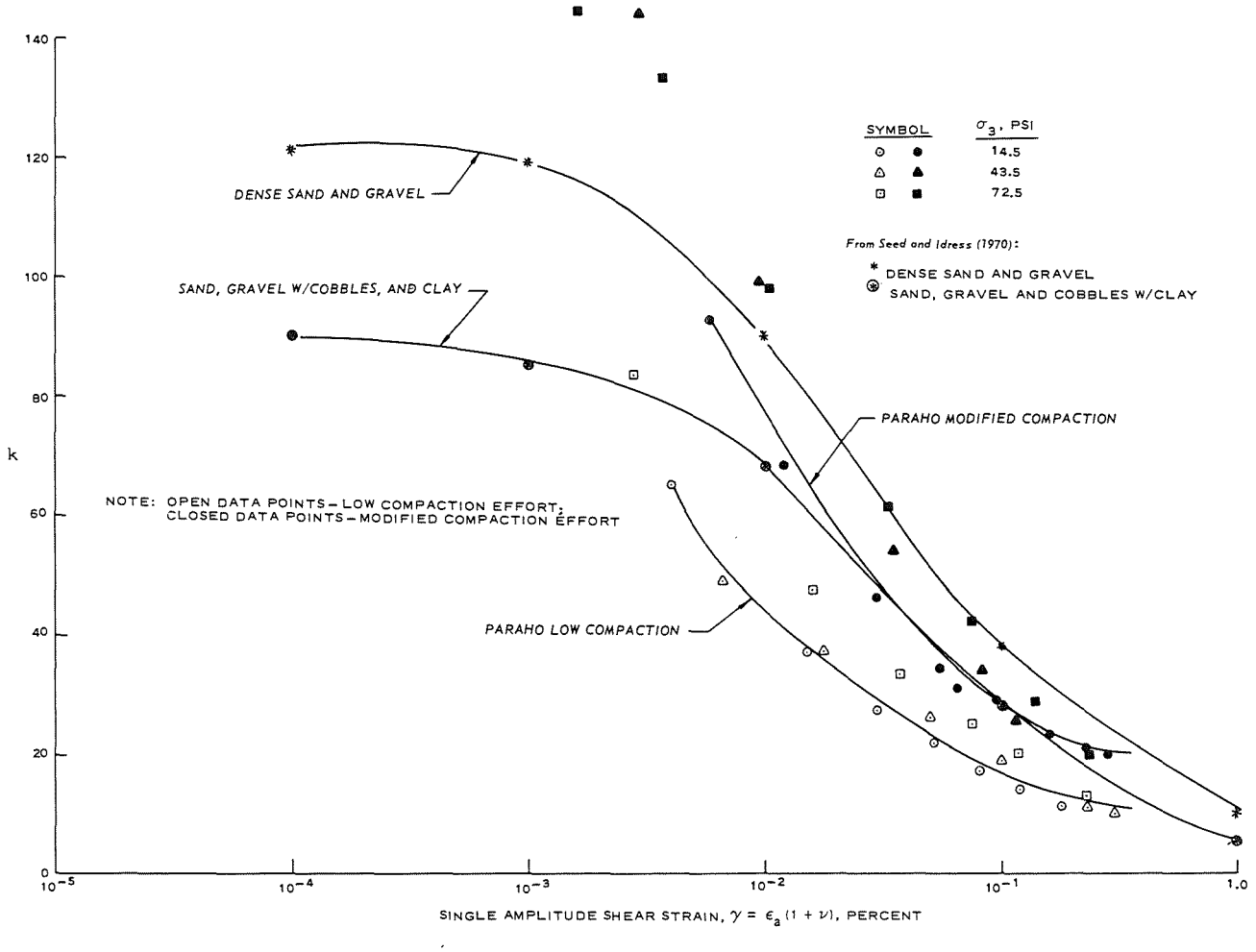

Figure 71. Comparison of dynamic shear moduli from cyclic triaxial tests for PARAHO and gravels

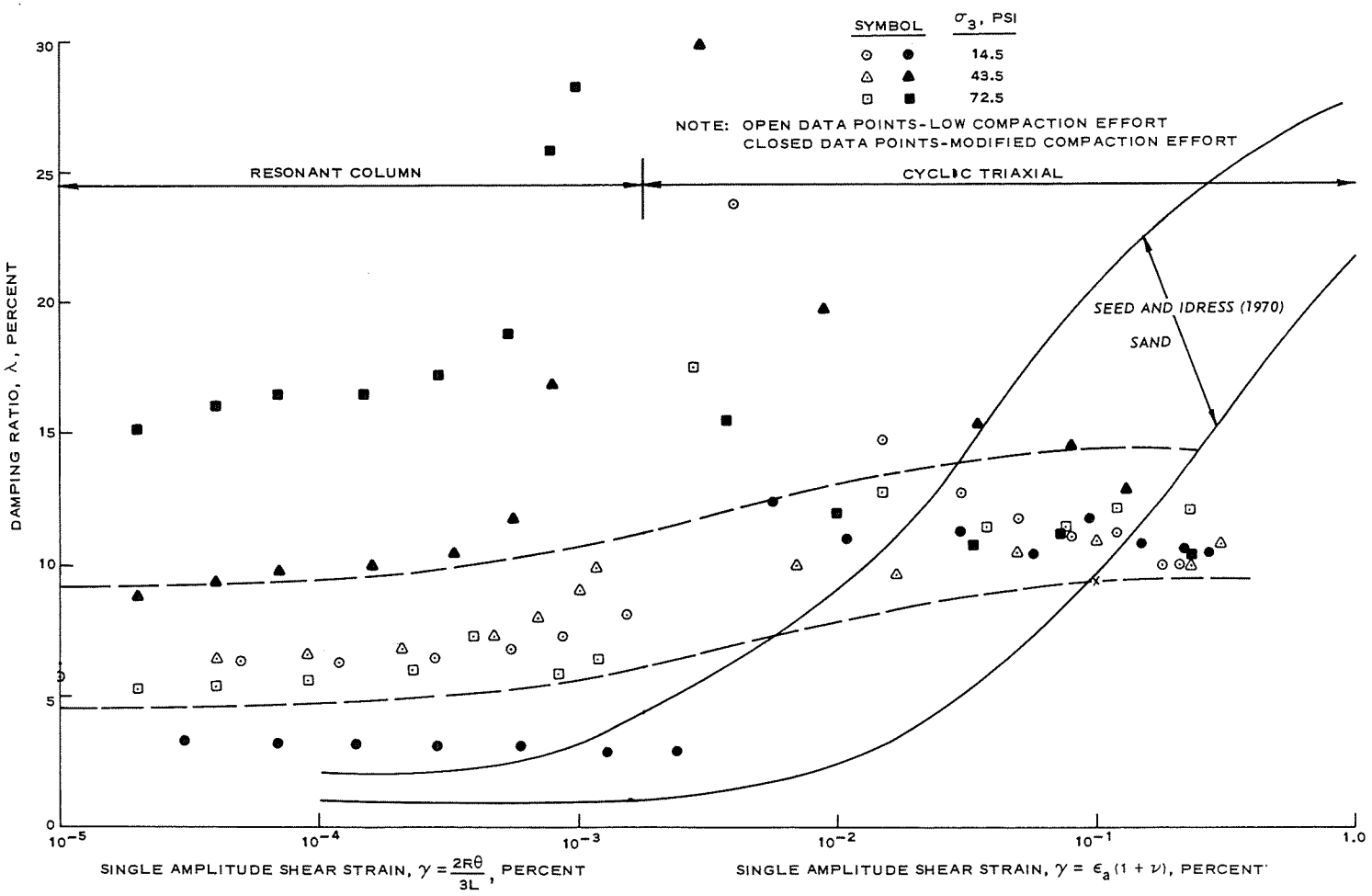

Figure 72. Damping ratio values for PARAHO compacted to 60 percent of standard and modified effort densities

Table 18

Summary of Drop Height Tests on PARAHO and TOSCO Oil Shales

Material	Height of Drop ft	Density* pcf
PARAHO (-2 in. fraction)	0.7	73.8
	1.5	74.1
	4.5	79.8
	10.5	82.0
	16.5	83.0
TOSCO	0.7	77.0
	1.5	77.1
	4.5	78.0
	10.5	82.4
	16.5	86.3

* Air-dry material. (The water contents of the PARAHO and TOSCO fractions are about 0.1 and 1.2 percent, respectively.)

Table 19

Summary of Los Angeles Abrasion Test Results on PARAHO and Raw Oil Shales

Material	ASTM Designation	Grading	Sieve Size, in.	Percentage Wear
PARAHO	C131-76	A	- 1-1/2 to + 1	79.7
			- 1 to + 3/4	
			- 3/4 to + 1/2	
			- 1/2 to + 3/8	
PARAHO	C131-76	C	- 3/8 to + No. 3	80.1
			- No. 3 to + No. 4	
PARAHO	C535-69	2	- 2 to + 1-1/2	66.7
			- 1-1/2 to + 1	
Raw shale	C131-76	A	- 1-1/2 to + 1	13.2
			- 1 to + 3/4	
			- 3/4 to + 1/2	
			- 1/2 to + 3/8	
Raw shale	C131-76	C	- 3/4 to + No. 3	12.2
			- No. 3 to + No. 4	
Raw shale	C535-69	1	- 3 to + 2-1/2	18.4
			- 2-1/2 to + 2	
			- 2 to + 1-1/2	

per minute; one burned portion that had been in moist storage for 3 days was also ground and examined by DTA. A thin section of one raw shale fragment was made and examined with a polarizing microscope.

PARAHO retorted shale. Samples of 1-1/2-in. (38-mm) and 3/4-in. (19-mm) fragments were selected for analyses and examined with a stereoscopic microscope. A piece from each sample was ground to pass the 45-μm (No. 325) sieve and subsequently examined by X-ray diffracton. A 1-1/2-in. (38-mm) fragment of shale was used to make a thin section and then examined with a polarizing microscope. A freshly cut interior of this piece was also examined by X-ray diffraction as a slab in an inert atmosphere containing hot barium hydroxide to prevent carbonation. This slab was again X-rayed after soaking in water for several days to determine if any detectable changes had occurred.

The dense and the vesicular 3/4-in (19-mm) fragments were examined by a scanning electron microscope (SEM) after coating with a layer of carbon and a layer of gold palladium. Crystals from a dense 3/4-in. (19-mm) fragment were concentrated by gently crushing and grinding of the pieces, coated as above, and examined by SEM.

Unconfined compressive strength samples of PARAHO retorted shale. Portions of samples UC-L-28-13C (oven-dried), UC-S-28-8, and UC-M-28-18B (Table 8), all of which had been cured 28 days prior to shearing, were allowed to dry in air, ground, and examined by X-ray diffraction. It was observed that small white crystals formed on the surface of sample UC-M-28-18B, after the wax coating was removed. A sample of these white crystals was obtained by hand picking and examined by X-ray diffration, A piece of UC-M-28-18B was coated, as described earlier, and examined by SEM.

Disaggregated PARAHO retorted shale from Franklin slake test. A portion of 1-1/2-in (38-mm) fragment from UC-M-28-18B that had been subjected to the Franklin slake test was ground and examined by X-ray diffraction in the manner described earlier. Some of the fine material also from this sample and not oven-dried was sedimented on a glass slide and examined by X-ray diffraction when dried.

Chemical analyses

Portions of the six pieces of raw shale examined by X-ray diffraction were composited to provide a sample for chemical analysis. A portion of the PARAHO retorted fragment from UC-S-28-8, which had been examined by X-ray diffraction, was also selected for chemical analysis. Each sample was analyzed after drying to 105°C. Companion portions were burned until a constant weight was achieved at 500° and 900°C. The original analysis was recalculated to take account of the weight loss at 900°C.

Tests results of petrographic and chemical analyses

Raw shale. The raw shale consists of fragments tabular to blocky in shape. It has a yellowish-gray (color 5Y 7/2 based upon National Research Council, 1963) dusty surface. Fresh surfaces are alternating thin layers of black (N1) to brownish-black (color 5YR 2/1) material. When a fresh surface is scratched, the scratch is light colored like older surfaces; the same is

true when the rock is ground to a powder. The X-ray examination showed that the light-colored surface coating had the same composition as the bulk of the rock and that the six pieces were not uniform in composition. While all six pieces examined contained dolomite, quartz, plagioclase feldspar, and clay mica, only four of the six pieces were found to contain calcite. Four of the six pieces were found to contain analcime ($NaAlSi_2O_6.H_2O$), which is usually described with zeolite minerals because it behaves as such, but strictly speaking it is not actually a zeolite (Hay, 1966). Obviously, the noncrystalline hydrocarbons were not detected by X-ray diffraction. Clay-mica, a minor constituent, was the only clay mineral that was detected by the X-ray examinations. In this content, a rock having this composition is not properly described as a shale. Heady (1952), during a study of Colorado oil shale by DTA and X-ray diffraction, found the same minerals observed in this study, namely, analcime, quartz, feldspar, clay-mica, dolomite, calcite, and iron sulfide. Petrographic analyses performed by the Department of Interior's Bureau of Reclamation and presented by WCC (1976) list dolomite, calcite, feldspar, and quartz as the major constituents of raw shale, with trace amounts of siderite (iron carbonate), analcite, and clay-mica.

The thin section of raw shale showed that the carbonates (dolomite and calcite) were present as fine-grained matrix material. Quartz, feldspar, and analcime were all present as larger grains scattered through the matrix. These grains were generally anhedral in shape with the analcime containing cracks. Rare grains of clay-mica or mica were recognizable. Considerable amounts of opaque material were also evident; these grains appeared to be an iron sulfide when examined in reflected light. Examination of the thin section from the 1-1/2-in. (38-mm) fragment of dense PARAHO rock showed a significant difference from the thin section of raw shale. For the retorted oil shale, the carbonite grains are larger and many of the rhombs contain overgrowths of carbonate. However, the X-ray diffraction examination of a fresh surface of this same retorted fragment before and after storage in water did not show any detectable changes.

The experiments to simulate the retorting process by heating unprocessed shale at 540°C and then hydrating it by moist storage showed the development of anhydrous calcium sulfate, which hydrated to gypsum ($CaSO_4.2H_2O$) in the presence of water. It is not clear whether gypsum was already present but widely scattered in the shale; thus it was not present in the pieces of raw shale examined by X-ray diffraction, but possibly was present in the pieces heated at 540°C, where it would have been dehydrated to anhydrite and then rehydrated in water. This seems to be the most likely hypothesis. It is also possible that during the heating and burning, pyrite (iron sulfide, FeS_2) released SO_2 which combined with CaO from calcite that had lost CO_2 and with oxygen to make $CaSO_4$ that hydrated to gypsum in water. Since gypsum was not found in the retorted and the compressive strength samples, the laboratory simulation was regarded as unsuccessful, and so no further description of it will be given.

The DTA patterns of four of the raw shale fragments showed endothermic peaks at 460°C and one to two endothermic peaks in regions from 700° to 760°C

and from 800° to 810°C. The lack of a 460°C peak in material from a piece that had been burned 45 min at 540°C and then placed in moist storage showed that the 460°C peak was due to distillation of the hydrocarbons in the inert atmosphere in this temperature range. The wide range of magnitude of the 460°C peak between four of the pieces indicated a similar range in hydrocarbon content. The peak or peaks in the 700° to 810°C range were due to breakdown of the carbonate mineral or minerals. The fine-grain size probably accounts for the lower than usual temperature of these reactions. Since X-ray diffraction showed that there was dolomite in each of these four pieces, there should have been two peaks for the decomposition of dolomite. The lack of two peaks in some cases may have been due to lack of sensitivity of the DTA unit at the settings used.

PARAHO retorted shale. Examination of the PARAHO retorted fragments showed that most were dense rock while a few pieces had become vesicular during the retorting. All of the pieces were black and dirtied the hands during handling. The changes that were apparent were: (a) all surfaces were now blackish, (b) some of the rock had been heated enough to become vesicular, and (c) the dense particles showed slight development of parting planes. The mineralogical composition was similar to what it had been before the rock was retorted. The dense pieces sometimes contained more calcite than dolomite. This reversal did not occur in the six pieces of unprocessed shale that were examined by X-ray diffraction to represent unprocessed rock. The 1-1/2-in. (38-mm) fragments contained detectable analcime, while the samples of 3/4-in. (19-mm) fragments usually did not contain detectable analcime. The complex mineral assemblage of quartz, feldspar, dolomite, clay-mica, and usually analcime and calcite tended to mask peaks of possible reaction products, such as CaO, MgO, $Ca(OH)_2$, or $Mg(OH)_2$, that would be possible constituents if retorting had broken down the carbonate phase or phases. MgO and calcium sulfate were probably present in some X-ray diffraction patterns of the dense retorted material. X-ray diffraction examination of a vesicular piece of retorted shale from the 3/4-in. (19-mm) fragments showed no detectable dolomite, probably MgO, and considerable calcite in addition to quartz, feldspar, and probably siderite ($FeCO_3$). A piece of vesicular shale from the 3/4-in. (19-mm) fragments showed no detectable dolomite. X-ray diffraction analyses of PARAHO retorted shale by the Bureau of Reclamation (WCC, 1976) lists dolomite, calcite, feldspar, and quartz as the major constituents with siderite, analcite, iron oxide, and mica-illite (clay-mica) as minor constituents. These analyses also identified the presence of analcime, a type of zeolite, which was also detected in this present investigation.

Figures 74 through 77 illustrate the use of scanning electron micrographs in petrographic analyses. In Figure 74, the micrographs show three views of a piece of dense retorted rock from a sample of 3/4-in. (19-mm) retorted shale. In Figure 75, the micrographs present three views of a piece of vesicular retorted rock from the same sample. In Figure 76, the micrographs present four views of two portions of the compressive strength specimen UC-M-28-18B. In Figure 77, the micrograph shows some crystals concentrated from a dense retorted particle of the 3/4-in. (19-mm) sample.

When the waxed sample of the compressive strength specimen UC-M-28-18B

a. Micrograph at 18X

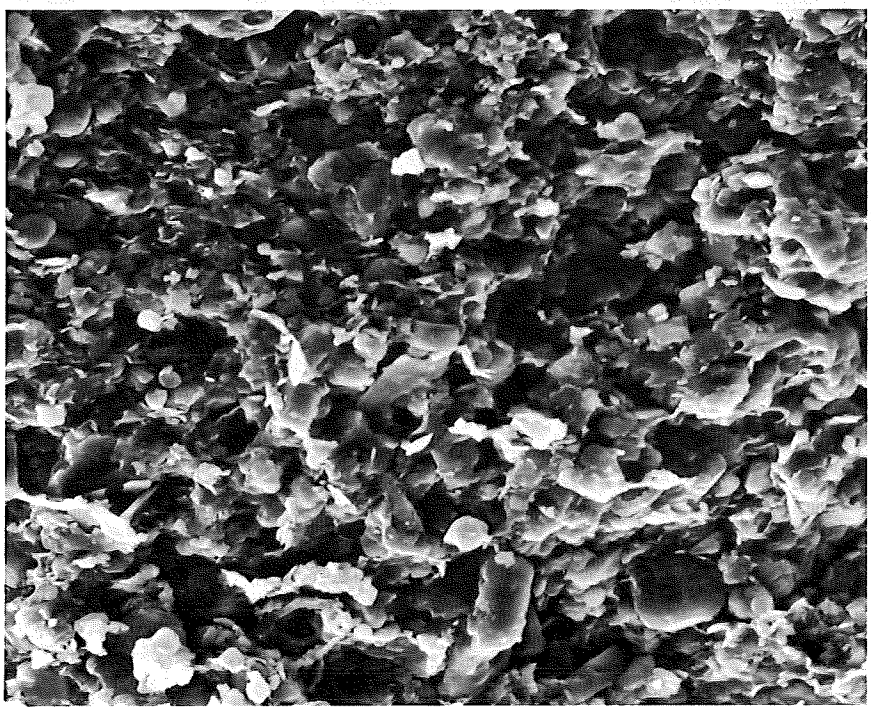

b. Portion of micrograph a at 1800X

Figure 74. Scanning electron micrographs of a dense particle of PARAHO retorted oil shale from a sample of 3/4-in. (19-mm) fragments (Sheet 1 of 2)

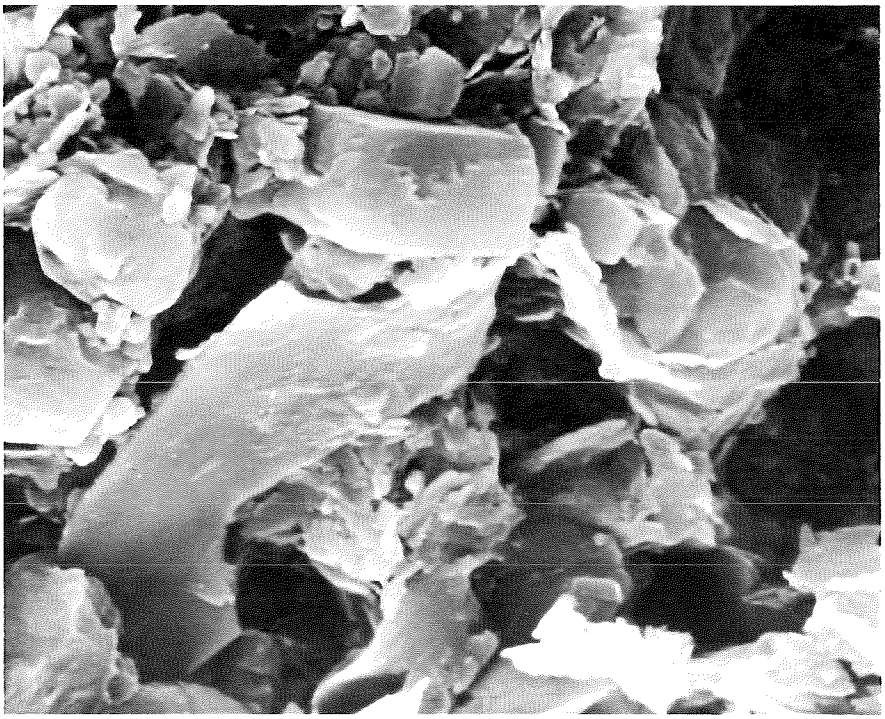

c. Central portion of micrograph c at 9000X. (Note sharp edges and lack of vermicular material)

Figure 74. (Sheet 2 of 2)

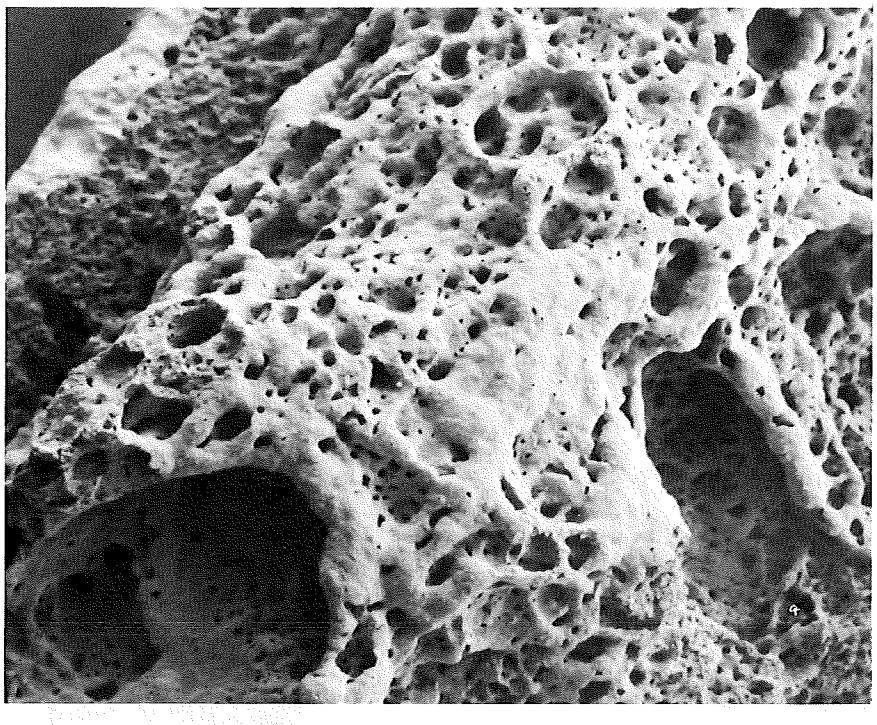

a. Micrograph at 21X

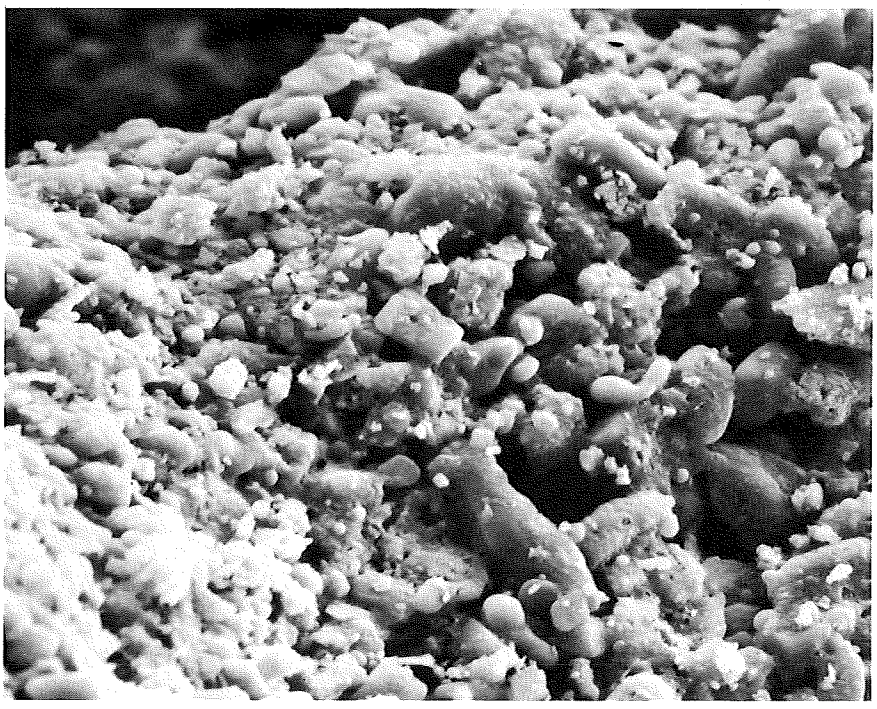

b. Portions of micrograph a at 2120X

Figure 75. Scanning electron micrographs of a vesicular particle of PARAHO retorted shale from a sample of 3/4-in. (19-mm) fragments (Sheet 1 of 2)

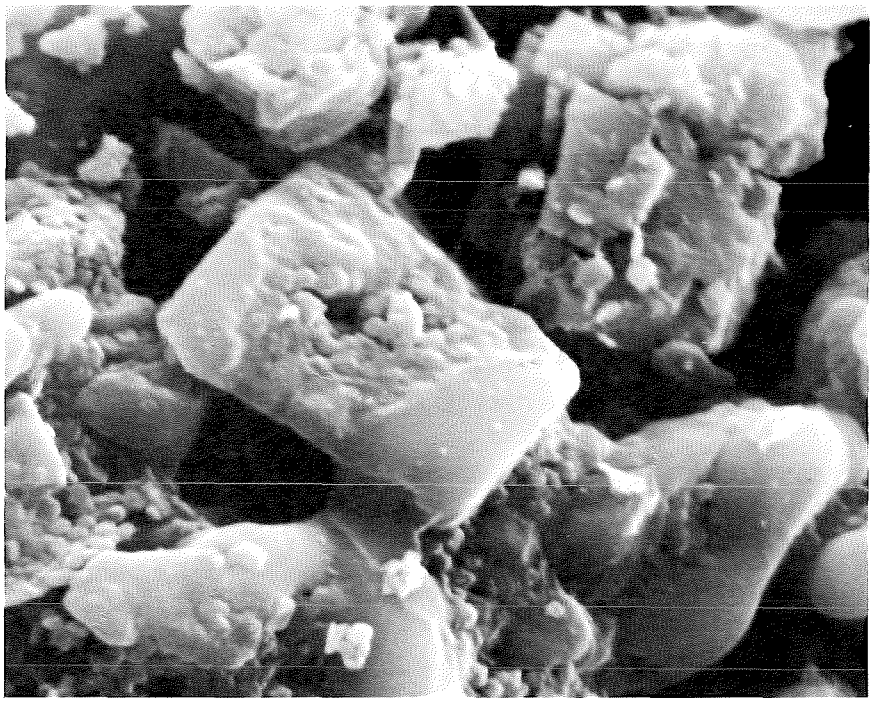

c. Central portion of micrograph b at 10,600X. (Note bridging between grains in left central area and smaller grains on surface in left part of picture)

Figure 75. (Sheet 2 of 2)

a. Micrograph at 19X

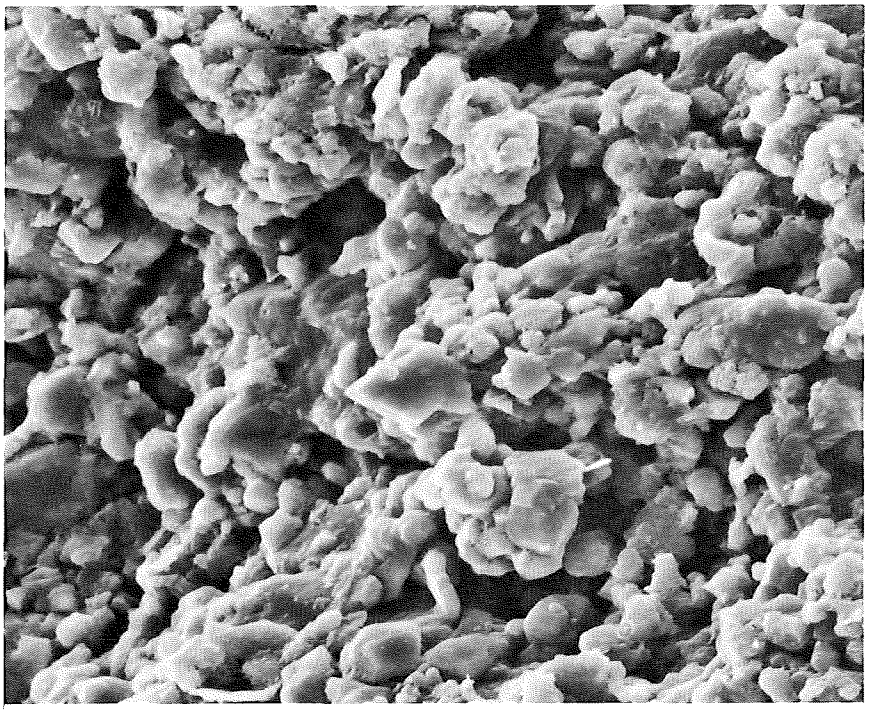

b. Portion of micrograph a at 1920X

Figure 76. Scanning electron micrographs of unconfined compression test specimen UC-M-28-18B of PARAHO retorted oil shale (Sheet 1 of 2)

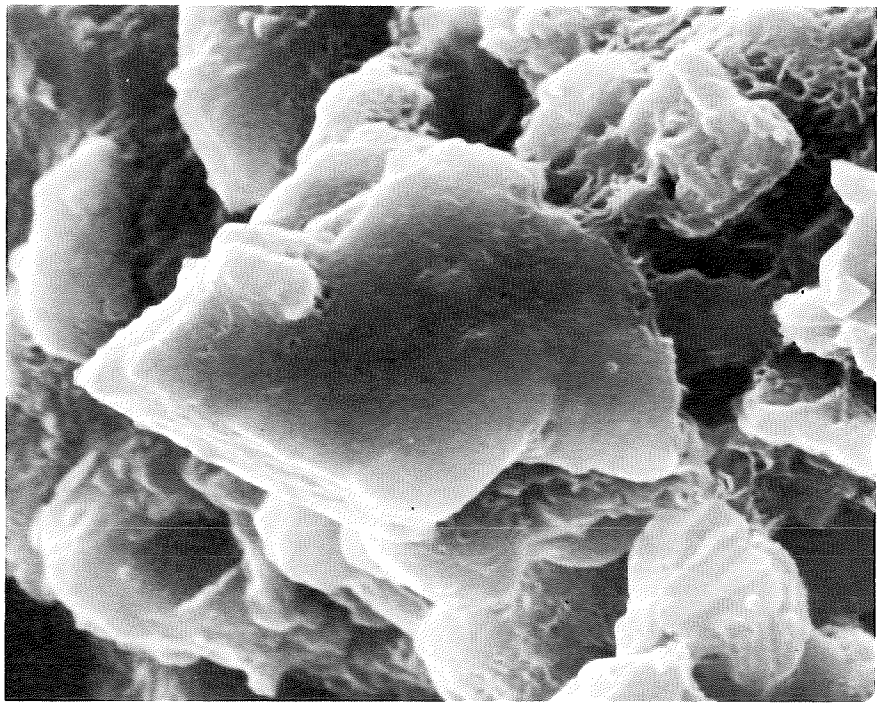

c. Central portion of micrograph b at 9600X. (Note abundance of vermicular material)

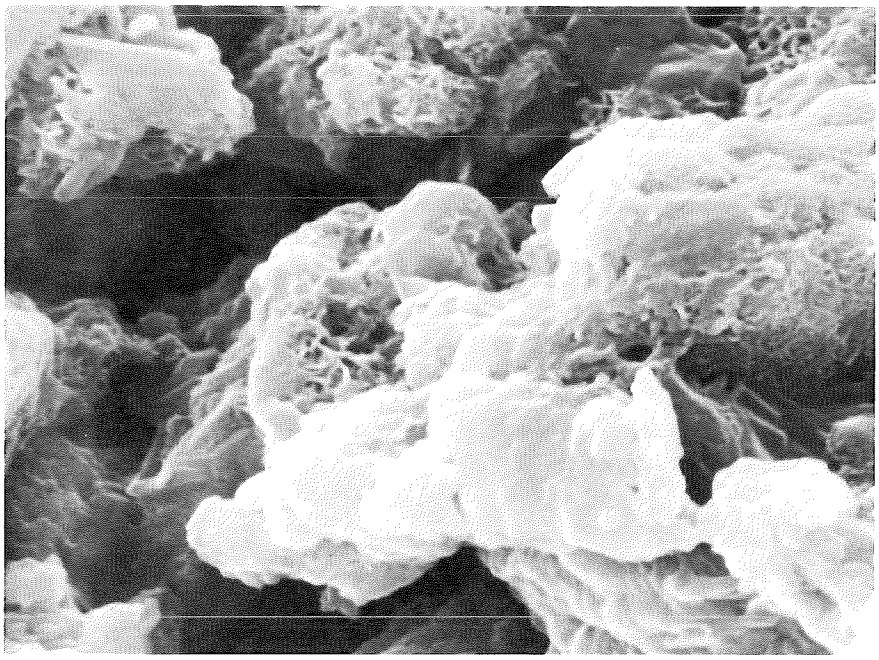

d. A different area in a piece of UC-M-18B at 9600X. (Note abundance of vermicular material)

Figure 76. (Sheet 2 of 2)

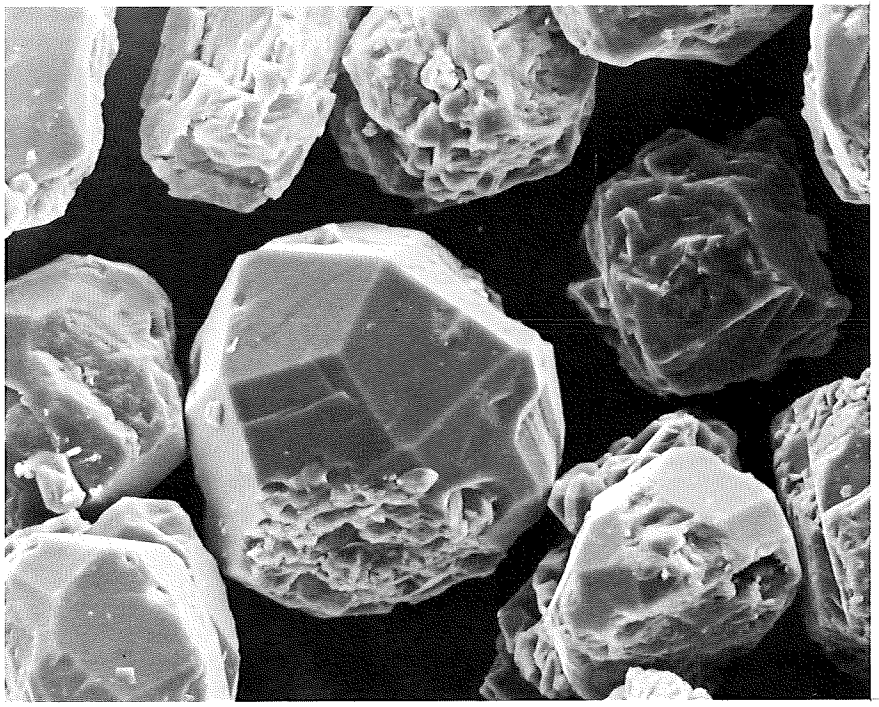

Note: The crystals in the center are morphologically like analcime. There is some feldspar at the lower right and next to the upper left and quartz grains may be present. The grains at the left edge, the center, and the bottom next to the grain at the lower right all appear to be similar in crystal habit and like analcime.

Figure 77. Scanning electron micrograph of analcime crystals from a dense particle of PARAHO retorted shale from a sample of 3/4-in. (19-mm) fragments at 770X

was opened, tiny white crystals of thenardite (Na_2SO_4) formed on the exposed surface overnight. X-ray diffraction examination of the three compressive strength samples (UC-L-28-13C (OD), UC-M-28-18B, and UC-S-28-8) showed patterns that were generally similar to those of unprocessed and of retorted shale. However, the general difference was that calcite was much more abundant than had been in the unprocessed shale. There were weak peaks in the X-ray diffraction pattern of the UC-L-28-13C (OD) sample at 7.9 and 7.6 A units (0.79 and 0.76 nanometres), respectively, that were not present in the raw shale. The 7.9 A peak was not identified; the 7.6 A peak was possibly gypsum.

The X-ray diffraction patterns of PARAHO retorted shale from the Franklin slake tests were not appreciably different from the other X-ray diffraction patterns of this material.

The chemical compositions of a sample of unprocessed shale and of a retorted compressive strength specimen are shown in Table 20. The losses in weight at 900°C for unprocessed and retorted shale, 34.45 and 17.20 percent, respectively, should include both hydrocarbons and carbon dioxide from the carbonate minerals, since 900°C is about 810°C above the decomposition temperatures, as shown by DTA, due to hydrocarbons and carbonates. Ignition at an intermediate temperature of 500°C for two hours gave losses of 17.23 and 3.35 percent by weight for the unprocessed and retorted samples, respectively. These values should essentially represent the amounts of oil or hydrocarbons that were present in each sample.

Discussion of cementation. The strength gain observed in compacted specimens of retorted shale is attributed to recementation by carbonates that were at least partially decomposed during the retorting process to remove hydrocarbons. This breakdown of the carbonates occurred from 700° to 810°C in the present DTA work. The lower than usual temperatures are probably due to the fine-grain size of these minerals in this rock. Decomposition of calcite and dolomite by removal of carbon dioxide results in the formation of calcium oxide from calcite and calcium and magnesium oxide from dolomite. These oxides can then alter to hydroxides or to calcite and magnesite ($MgCO_3$) or dolomite in the presence of moisture and carbon dioxide. Calcium oxide is much more active than magnesium oxide of the same crystallite size. Efforts to identify these oxides or their hydroxides in the present retorted samples were generally unsuccessful although MgO was tentatively identified. This failure could be due to the general masking effect of the original constituents on the reaction products in X-ray diffraction patterns or to the fact that the retorted material had had adequate time for the oxides to carbonate before this study was made, or to a combination of these factors.

The evidence to support the hypothesis that destruction and reformation of the carbonates has occurred includes the following:

a. Examination of thin sections of unprocessed and PARAHO retorted shale showed a larger grain size for the carbonate minerals in the retorted rock.

Table 20

Chemical Composition of Unprocessed and PARAHO Oil Shale

Dried to Constant Weight at 105°C Before Analysis

Chemical Components	Raw Shale - Composite of Pieces 1-6, %		PARAHO Oil Shales from Compressive Strength Specimen UC-S-28-8, %	
Silica as SiO_2	31.48	48.02*	42.44	51.26*
Calcium as CaO	12.05	18.38	13.50	16.30
Magnesium as MgO	7.73	11.79	6.85	8.27
Aluminium as Al_2O_3	6.83	10.42	9.46	11.42
Iron as Fe_2O_3	2.84	4.33	3.98	4.81
Titanium as TiO_2	0.54	0.82	0.66	0.80
Sodium as Na_2O	2.83	4.31	3.18	3.84
Potassium as K_2O	1.56	2.38	2.90	3.50
Ignition loss (900°C)	34.45	--	17.20	--
Total	100.31	100.45	100.17	100.20

* Recalculated on basis of material remaining after ignition at 900°C.

b. Calcite was often more abundant than dolomite in the retorted rock, whereas it was missing or less abundant than dolomite in the six pieces of unprocessed rock that were examined by X-ray diffraction.

c. Study of the scanning electron micrographs of dense and vesicular PARAHO retorted rock and of the retorted rock after compaction suggests a fusing and rounding of grains in the vesicular rock and a secondary growth of vermicular material in the compacted rock.

The DTA patterns indicated that the hydrocarbons present in the rock can be removed at a temperature of about 460°C.

Franklin slake durability tests (Franklin and Chandra, 1972). Table 21 summarizes the results of Franklin slake durability tests on raw and PARAHO retorted oil shale. These results show that the raw shale is extremely resistant to slaking with practically no weight loss observed. The 1-1/2-in. (38-mm) and 3/4-in. (19-mm) fragments of PARAHO retorted shale are also quite durable and resistant to slaking in water, but the smaller fragments are slightly less durable. However, the unconfined compression specimen exhibited a marked decrease in slaking durability. This dramatic reduction in durability suggests that the cementitious products formed by curing are weak cements when exposed to wetting and drying.

Table 21

Summary of Franklin Slake Durability Tests on Raw and PARAHO Oil Shales

Material/Description	Sample No.	Slake Durability Index, %*	Classification
Raw shale	1	99.0	Extremely high
	2	99.5	Extremely high
PARAHO 1-1/2 in.	1	92.5	Very high
	2	91.5	Very high
	3	82.5	High
	4	90.0	Very high
PARAHO 3/4 in.	1	94.0	
	2	94.0	
	3	93.5	
	4	94.0	
Unconfined compression UC-M-28-18B (PARAHO)	1	57.0	Medium
	2	55.5	Medium

* Average of two tests.

CHAPTER 5: CONCLUSIONS AND RECOMMENDATIONS

Conclusions

Based upon the materials tested, the laboratory equipment and test procedures used, and other results reported in the literature, the following conclusions are made:

Physical properties

a. The raw shale from which the PARAHO material was retorted is very hard and durable. After 18 months of soaking it still remained nonplastic. The durability of this material is further attested to by LAA and Franklin slake durability tests, which provided LAA values of 12-18 percent and a slake durability index value of 99.

b. The retorted shale from the PARAHO retort is classified as a nonplastic poorly graded sandy gravel, GP, with a trace of fines, by the Unified Soil Classification System. Retorting causes a loss in abrasion resistance as evidenced by LAA values of 67-80 percent and increased fines due to mechanical agitation by the sieve shakers. However, the material is resistant to water as the PI only increased from 0 to 5 after 18 months of soaking, and slake durability index values were 90-95 percent.

c. The retorted shale from the TOSCO retort is classified by the Unified Soil Classification System as silty sand (SM). Like PARAHO, TOSCO is resistant to water with the PI only increasing from 0 to 5 after 18 months of soaking.

Engineering properties

a. PARAHO can be compacted in the laboratory to dry densities of 95, 98, and 104 pcf under low, standard, and modified compaction efforts. Whether compacted in an air-dried or wetted condition, dry densities are essentially equal, hence water is not essential to achieving a desired density. The maximum density achieved by the laboratory vibratory table method was significantly less, only 89 pcf; however, WCC (1976) reports that field vibratory compaction is the best method of compaction, and vibratory densities ranging from 98 to 110 percent of standard were achieved depending upon lift thickness, number of passes, etc. Particle breakage increases with compacted effort and breakage values of 11, 16, and 25 percent resulted under low, standard, and modified compaction efforts, respectively. Modeling the full-scale gradations by scalping and replacement, parallel, or scalping techniques underestimates laboratory compacted densities of full-scale material.

b. TOSCO can be compacted in the laboratory to dry densities of 97, 99, and 104 pcf under low, standard, and modified compaction efforts, respectively. In the case of this material, optimum

water contents range from 22 to 17 percent, and water is required to achieve maximum dry density.

c. The compressibility of compacted PARAHO and TOSCO is comparable to that for dense rockfill or sands. The percent compression for a vertical stress of 800 psi (5.5 MPa) was 5-10 percent for PARAHO and 5-8 percent for TOSCO with lower compression observed for higher densities. Compression index values C_c ranged from 0.10 to 0.15 and 0.10 to 0.12 for PARAHO and TOSCO, respectively. Both PARAHO and TOSCO suffer particle breakage during consolidation, with both experiencing breakage values of approximately 28 percent for standard effort densities.

d. Both PARAHO and TOSCO possess self-cementing characteristics producing additional strength with time. However, PARAHO satisfies recommended criteria (Thompson, 1970) for assessing stabilization reactivity, while TOSCO does not. Increasing density produces higher strength gains, hence in critical areas requiring increased strength, additional compaction may be warranted. PARAHO is more reactive than TOSCO, exhibiting 3- to 8-fold strength gains over 28-day curing, while TOSCO only exhibits a 1.5- to 3-fold strength increase for comparable conditions. Cementing reactions under normal conditions are slow for PARAHO, with strength gains still indicated after 28 days, while TOSCO gains most of its strength within 3 days following compaction.

e. The shear strengths of both PARAHO and TOSCO are comparable to those for gravelly sands with respective effective internal friction angles of 33 and 37-43 deg. Corresponding cohesion values are less than 2.0 kg/cm^2 for both materials. Attempts to model gradations of PARAHO by scalping and replacement techniques resulted in unconservative overestimates of internal friction angles. Despite high densities, both materials generally exhibit positive pore pressure generation when sheared.

f. Compacted PARAHO can be considered as semipervious with permeability values of 10^{-3} and 10^{-4} cm/sec depending upon compaction effort. On the other hand, the finer grained TOSCO can be considered as semipervious to impervious with permeability values of 10^{-6} to 10^{-7} cm/sec depending upon compaction effort.

g. Despite significant strength gains with curing time for compacted PARAHO and TOSCO, K_o test results on specimens cured 13 and 19 months, respectively, showed no appreciable increase in stiffness. Poisson's ratio values for PARAHO ranged from 0.16 to 0.29, while those for TOSCO ranged from 0.24 to 0.30. The results also showed that K_o values increased with axial stress level (overburden pressure) and overconsolidation ratio.

k. Special interface shear tests investigating the angle of internal friction of raw shale and PARAHO against different surfaces showed the order of decreasing friction was rubber belting, rusty steel, and stainless steel. For unprocessed shale these values ranged from 31 to 14 deg, while for PARAHO the values ranged from 39 to 24 deg.

i. The dynamic characteristics of compacted PARAHO are good and comparable to those for dense sand and gravel.

j. Based upon the tests mentioned previously, these materials exhibited geotechnical properties characteristic of a GP and SM. They behaved as a moderately dense gravel or sand depending upon the applied compaction effort and exhibited adequate strength. In addition, their self-cementing characteristic enhances strength. The materials are pervious to semipervious and as such will not perform as an impermeable barrier. In this context, properly engineered waste embankments of these materials should perform satisfactorily.

Compositional properties

a. The unprocessed rock is yellowish-gray colored and composed of quartz, feldspar, clay-mica, dolomite, iron sulfide, calcite, analcime, and hydrocarbons. The only clay mineral, clay-mica, is a very minor constituent, hence the rock is not properly described as shale, but rather a carbonate rock.

b. Retorting by the PARAHO process to remove the hydrocarbons also causes decomposition of the carbonate minerals. Subsequent reformation of carbonates involves cementation which is responsible for the time-dependent strength gain observed in unconfined compression tests.

Recommendations

Although the unprocessed shale may vary from deposit to deposit and the method of operation may vary daily for the PARAHO or TOSCO processes, both of which will cause a variety of properties for spent shale, this report and that of WCC (1976) provide considerable information concerning the geotechnical properties of spent shale. In this context, unless a different retort process is used, additional laboratory research to identify typical geotechnical properties is unwarranted. This does not mean, however, for site-specific cases, that laboratory characterization is not necessary.

It is recommended that analytical studies of various disposal schemes be initiated. Specifically, typical embankment geometries for disposing of spent shale should be designed and analyzed using the properties of both PARAHO and TOSCO. Effects of internal drainage on seepage forces and seismic assessment should be included. Performance and design predictions could subsequently be verified by geotechnical centrifuge models.

REFERENCES

Al-Hussaini, M. M, and Townsend, F. C. 1975. "Investigation of K_o Testing in Cohesionless Soils," Technical Report S-75-16, U. S. Army Engineer Waterways Experiment Station, CE, Vicksburg, Miss.

_____. 1975a. "Stress-Deformation of Sand Under K_o Conditions," Fifth Panamerican Conference on Soil Mechanics and Foundation Engineering, Buenos Aires, Argentina.

American Society for Testing and Materials, (ASTM) Annual Book of Standards. 1979. "Soil and Rock, Building Stones, and Peats," Part 19, Philadelphia, Pa.

Becker, E., Chan, C. K., Seed, H. B. 1972. "Strength and Deformation Characteristics of Rockfill Materials in Plane Strain and Triaxial Compression Tests," Report No. TE 72-3, Department of Civil Engineering, University of California, Berkeley, Calif.

Dames and Moore. 1974. "Processed Shale Studies; Environmental Impact Analysis, Appendix 5, Colony Development Operation, Rifle, Colo."

Department of the Army, Office, Chief of Engineers. 1970. "Laboratory Soils Testing," Engineering Manual 1110-2-1906, Washington, D. C.

Donaghe, R. T, and Cohen, M. W. 1978. "Strength and Deformation Properties of Rockfill," Technical Report S-78-1, U. S. Army Engineer Waterways Experiment Station, CE, Vicksburg, Miss.

Donaghe, R. T., and Townsend, F. C. 1973. "Compaction Characteristics of Earth-Rock Mixtures, Report 1, Vicksburg Silty Clay and DeGray Dam Clayey Sandy Gravel," Miscellaneous Paper S-73-25, U. S. Army Engineer Waterways Experiment Station, CE, Vicksburg, Miss.

_____. 1975. "Scalping and Replacement Effects on the Compaction Characteristics of Earth-Rock Mixtures," American Society for Testing and Materials, Special Technical Publication 599, Soil Specimen Preparation for Laboratory Testing.

Drnevich, V. P. 1977. "Resonant Column Testing-Problem and Solutions," American Society for Testing and Materials, Special Technical Publication 654, Dynamic Geotechnical Testing.

_____. 1978. "Resonant Column Test, Miscellaneous Paper S-78-6, U. S. Army Engineer Waterways Experiment Station, CE, Vicksburg, Miss.

Dunlap, W. A. et al. 1975. "United States Air Force Soil Stabilization Index System-A Validation," Technical Report 73-150, Air Force Weapons Laboratory, Kirtland AFB, N. Mex.

Franklin, J. A. and Chandra, R. 1972. "The Slake-Durability Test," International Journal of Rock Mechanics and Mining Science, Vol 9, pp 325-341.

Hardin, B. O. and Black, W. L. 1969. Closure to "Vibration Modulus of Normally Consolidated Clay," Journal of the Soil Mechanics and Foundation Division, American Society of Civil Engineers, Vol 95, No. SM6, pp 1531-1537.

Hay, R. L. 1966. "Zeolites and Zeolitic Reactions in Sedimentary Rocks," Geologic Society of America, Special Paper No. 85, New York.

Heady, H. H. 1952. "Differential Thermal Study of Colorado Oil Shale," The American Mineralogist, Vol 37, pp 804-811.

Jaky, J. 1948. "State of Stress at Great Depth," Proceedings, Second International Conference on Soil Mechanics and Foundation Engineering, Rotterdam, Holland, Vol 1, pp 103-107.

Marachi, D. N. et al. 1969. "Strength and Deformation Characteristics of Rockfill Materials," Report No. TE-69-5, Department of Civil Engineering, University of California, Berkeley, Calif.

Marsal, R. J. 1967. "Large Scale Testing of Rockfill Materials," Proceedings of Journal of Soil Mechanics and Foundation Engineering Division, American Society of Civil Engineers, Vol 93, No. 2, pp 27-43.

National Research Council. 1963. "Rock-Color Chart," The Rock-Color Chart Committee, Washington, D. C.

Nicholson, G. A. 1979. "Determination of Shear Strength Parameters of Rock Masses" (in preparation), U. S. Army Engineer Waterways Experiment Station, CE, Vicksburg, Miss.

Parkin, A. K. 1977. "The Compression of Rockfill," Australian Geomechanics Journal, Vol G7.

Peterson, R. W., Townsend, F. C., and Bloomfield, R. A. 1978. "Geotechnical Properties of a Fine-Grained Spent Shale Waste," Proceedings, Eleventh Annual Oil Shale Symposium, Colorado School of Mines, Denver, Colo.

Seed, H. B. and Idriss, I. M. 1970. "Soil Moduli and Damping Factors for Dynamic Response Analyses," Report No. EERC 70-10, College of Engineering, University of California, Berkeley, Calif.

Silver, M. L. et al. 1976. "Cyclic Triaxial Strength of Standard Test Sand," Journal of Geotechnical Engineering Division, American Society of Civil Engineers, Vol 102, No. GT5.

Snethen, D. R., Farrell, W. J., and Townsend, F. C. 1978. "A Review of the Physical and Engineering Properties of Raw and Retorted Oil Shales from the Green River Formation," Miscellaneous Paper S-78-3, U. S. Army Engineer Waterways Experiment Station, CE, Vicksburg, Miss.

Thompson, M. R. 1970. "Suggested Method for Mixture Design Procedure for Lime Treated Soils," American Society for Testing and Materials, Special Technical Publication 479, Special Procedures for Testing Soils and Rock for Engineering Purposes.

Townsend, F. C. 1972. "Comparisons of Vibrated Density and Standard Compaction Tests on Sands with Fines," Miscellaneous Paper S-72-29, U. S. Army Engineer Waterways Experiment Station, CE, Vicksburg, Miss.

_____. 1977. "A Review of Factors Affecting Cyclic Triaxial Tests," American Society for Testing and Materials, Special Technical Publication 654, Dynamic Geotechnical Testing.

Woodward-Clyde Consultants. 1975. "Research and Development Program on the Disposal of Retorted Oil Shale-PARAHO Oil Shale Project; Phase IV, Interim Report No. 1 on Shale Retorted in Semi-Works Plant by Direct Heating Method," Prepared for Development Engineering, Inc.

_____. 1976. "Research and Development Program on the Disposal of Retorted Oil Shale-PARAHO Oil Shale Project," Final Report; Prepared for U. S. Department of Interior, Bureau of Mines, Contract No. J0255004.

_____. 1976a. "Raw Shale Tests, Research and Development Program on the Disposal of Retorted Oil Shale, PARAHO Oil Shale Project; Phase VII, Interim Report"; Prepared for U. S. Department of Interior, Bureau of Mines.

Wong, R. T., Seed, H. B., and Chan, C. K. 1975. "Cyclic Loading Liquefaction of Gravelly Soils," Journal, Geotechnical Engineering Division, American Society of Civil Engineers, Vol 101, No. GT6.

APPENDIX A: A REVIEW OF THE PHYSICAL AND ENGINEERING PROPERTIES OF RAW AND RETORTED OIL SHALES FROM THE GREEN RIVER FORMATION

(Published in March 1978 as Miscellaneous Paper S-78-3, U. S. Army Engineer Waterways Experiment Station, CE)

PREFACE

This study of the physical and engineering properties of retorted oil shales is a 2-year investigation funded by the Bureau of Mines, U. S. Department of the Interior, under Interagency Agreement H0262064. Mr. Roger A. Bloomfield, Spokane Mining Research Center, Bureau of Mines, was the Technical Project Officer.

The investigation was initiated during October 1976 by the Soils and Pavements Laboratory (S&PL) of the U. S. Army Engineer Waterways Experiment Station (WES). Dr. Frank C. Townsend, Research Group, Soil Mechanics Division (SMD), S&PL, was principal investigator during this phase of the study. The work reported herein was performed by Dr. Donald R. Snethen, Research Group, SMD, and Mr. Warren J. Farrell, Geology Branch, Engineering Geology and Rock Mechanics Division, S&PL. The report was prepared by Dr. Snethen. The investigation was accomplished under the general supervision of Mr. Clifford L. McAnear, Chief, SMD and Mr. James P. Sale, Chief, S&PL.

Director of WES during the conduct of this portion of the study and preparation and publication of this report was COL J. L. Cannon, CE. Technical Director was Mr. F. R. Brown.

CONTENTS

CONVERSION FACTORS, U. S. CUSTOMARY TO METRIC (SI) UNITS OF MEASUREMENT

U. S. customary units of measurement used in this report can be converted to metric (SI) units as follows:

Multiply	By	To Obtain
inches	25.4	millimetres
feet	0.3048	metres
square miles	2.589988	square kilometres
acres	4046.856	square metres
pounds (mass)	0.4535924	kilograms
tons (short)	907.1847	kilograms
pounds (mass) per cubic foot	16.01846	kilograms per cubic metre
pounds (force) per square inch	6.894757	kilopascals
gallons per ton	0.0000041	cubic metres per kilogram
foot-pounds per cubic foot	47.88017	joules per cubic metre
degrees (angle)	0.01745329	radians
Fahrenheit degrees	5/9	Celsius degrees or Kelvins*

* To obtain Celsius (C) temperature readings from Fahrenheit (F) readings, use the following formula: $C = (5/9)(F - 32)$. To obtain Kelvin (K) readings, use: $K = (5/9)(F - 32) + 273.15$.

A REVIEW OF THE PHYSICAL AND ENGINEERING PROPERTIES OF RAW AND RETORTED OIL SHALES FROM THE GREEN RIVER FORMATION

PART I: INTRODUCTION

1. Oil shale is a fine-grained, usually dark-colored (brown, gray, or black) sedimentary rock containing kerogen, a complex organic matter that decomposes on heating to yield oil. In the United States, the principal concentration of oil shale is in the Green River Formation in the three-state region of Colorado, Utah, and Wyoming. The Green River Formation shows the greatest promise for commercial shale oil production in the immediate future. The oil shale of the Green River Formation occurs beneath 25,000 square miles* (16 million acres) of land in the tristate area. Of the total amount, some 17,000 square miles (11 million acres) are estimated to contain oil shale suitable for commercial development (i.e., deposits at least 10 ft thick and averaging yields of 25 or more gallons of oil per ton). To be commercially feasible and operate economically an oil shale retort plant should process an estimated 25,000 to 50,000 tons of raw shale per day. Most of the currently used surface retort processes and materials produce retorted shale (spent shale, ash, etc.) at about 80 to 85 percent of total raw weight. In other words, for each ton of raw shale entering the retort plant, approximately 1600-1700 lb of retorted shale exists.

2. A major problem arises involving the efficient and safe disposal of extremely large amounts of the retorted or spent shale (over 40,000 tons per day for 50,000-ton plant). Several options are available for the disposal of retorted oil shales: (a) filling the deep, narrow canyons of the oil shale mine area with the spent shale; (b) backfilling the mine with spent shale as the raw shale is removed; and

---

* A table of factors for converting U. S. customary units to metric (SI) units of measurement is presented on page 4.

(c) using the spent shale for such productive uses as aggregate in asphalt or concrete mixtures, roadway base and subbase material, drilling mud, cement production, building bricks, and mineral filler. All of these options involve a determination and working knowledge of the geotechnical properties of the retorted oil shale.

3. The purpose of this report is to summarize the published geotechnical properties of raw and retorted oil shales from the Green River Formation. The data summary provides a basis for comparison with adddi-tional laboratory and field determination of geotechnical properties. The data are limited to that published on the Green River Formation of Colorado, Utah and Wyoming.

4. Possible sources of published geotechnical data were obtained through personal contacts with Federal and state agencies involved in oil shale development and through two computer based information retrieval systems: the National Technical Information Service, McLean, Virginia, and the Smithsonian Science Information Exchange, Washington, D. C.

PART II: PHYSICAL AND ENGINEERING PROPERTIES OF OIL SHALES

5. Serious interest in the production of shale oil dates back to 1920, with the interest fluctuating with the economy of the time and variations in and concern over the estimates of the domestic petroleum resources. During this period, several pilot studies and semiworks plants produced varying amounts of retorted shale; however, concern over the disposal of retorted shales and the corresponding need for quantifying the geotechnical properties did not arise until the middle 1960's. This roughly corresponds to the time frame for the major environmental protection legislation. Prior to about 1967, few, if any, geotechnical properties were determined for the retorted shale and only limited data were measured on the raw shales. Since the published data prior to this date was for raw shales only, the summary tables presented in this report were divided between raw and retorted shales with the data presented in chronological order. A survey of the information from personal contacts and computer information services resulted in 27 references[1-27] containing data pertinent to geotechnical properties of raw and retorted shales. Table 1 summarizes general information pertinent to the entries in the tables of properties for specific references. Tables 2 and 3 summarize the physical and engineering properties of raw oil shales. Table 4 summarizes physical and engineering properties of retorted oil shales. In subsequent paragraphs, data for both raw and retorted shales will be discussed in detail with emphasis on retorted shale properties.

Physical Properties

6. The physical properties of interest to geotechnical engineers are specific gravity, gradation, and Atterberg limits. Of equal importance but not considered to be a physical property is the classification of the material using either the Unified Soil Classification System (USCS) or the American Association of State Highway and Transportation Officials (AASHTO) system.

Specific gravity

7. The specific gravity may be expressed in three forms: (a) the specific gravity of solids, which is applied to soils finer than those passing a No. 4 sieve; (b) the apparent specific gravity; and (c) the bulk or mass specific gravity. Both the apparent and mass specific gravities are applied to soils coarser than the No. 4 sieve with the apparent specific gravity routinely used when dealing with coarser materials. The average value of the apparent specific gravity of raw oil shale (Tables 2 and 3) varied from 2.02 to 2.36. The apparent specific gravity was generally greater for the low-kerogen content shales and decreased with increasing kerogen content. No significant difference was noted between the samples taken parallel and perpendicular to the shale bedding planes. Mass specific gravity, available from only one reference,[26] and ranged between 1.99 and 2.20. For the retorted shales, the apparent specific gravity ranged between 2.11 and 2.59 with the majority of the values between 2.52 and 2.59. Mass specific gravity available from two references ranged between 1.80 and 1.85. These specific gravity values are quite low in comparison with sandstone, limestone, basalt and granite rockfill materials with values reported ranging from 2.29 to 2.84 for mass specific gravity and 2.65 to 2.87 for apparent specific gravity.

Gradation

8. The gradation of raw shale provides very little useful information since the gradation is dependent on mining operations and the type of crusher and amount of crushing the material undergoes prior to retorting. Of greater significance is the gradation of retorted shales, since it is helpful in classifying the material and thus qualitatively indicating the suitability of the material for engineering purposes. The influence of the retorting process on gradation is evident in Figure 1, which shows the gradation of a raw and retorted shale. As would be expected, the retorting process breaks down the raw shale. For example, the < No. 40 fractions for the raw and retorted shales are 43 and 62 percent, respectively. The < No. 200 fractions for the raw and retorted shales are 11 and 37 percent, respectively. Appendix A gives a

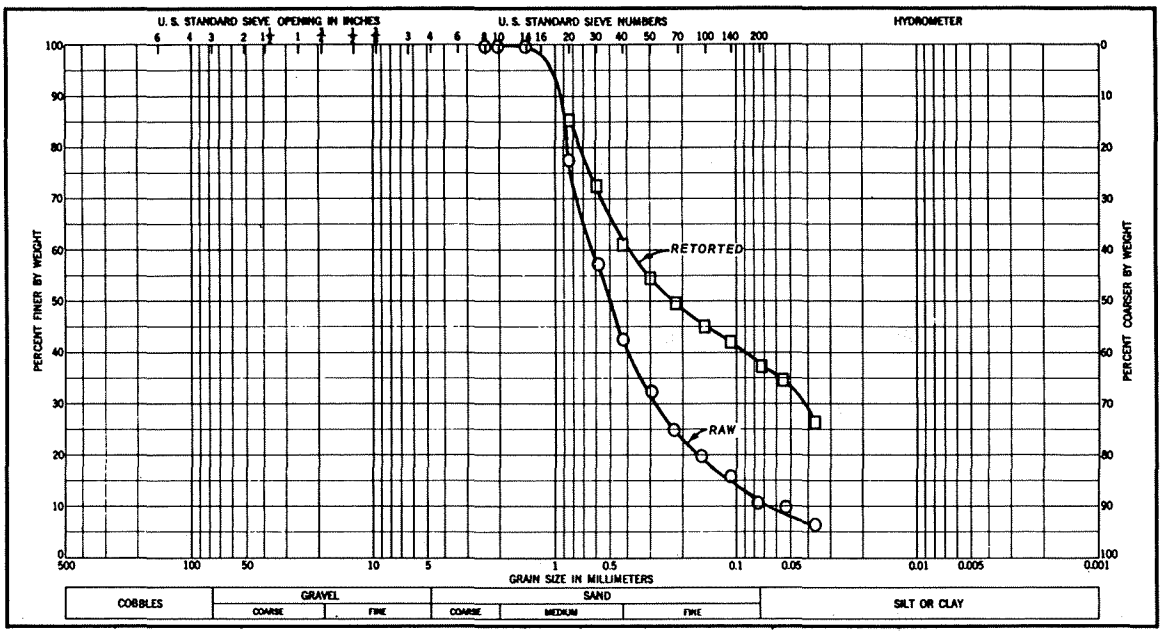

Figure 1. Comparison of raw and retorted oil shale gradations (from Reference 10)

detailed description of several different retorting processes. A fundamental difference in the raw shale gradations of the gas-combustion process (Paraho process) and the Tosco process exists. Specifically, the Paraho process uses the material between the 3- and 3/8-in. particle sizes while the Tosco process operates on <3/8-in. particle sizes. In the Paraho Study[26] the raw shale retort feed, raw shale reject, and three combinations of the two raw shale gradations were tested to obtain geotechnical properties of the raw materials. Figure 2 shows the two basic gradations (A and C) and the combinations (gradations B, D, and E). The raw shale feed, as screened, was 100 percent gravel-size particles. The raw shale reject contained 45 percent gravel-size, 48 percent sand-size, and 7 percent silt- and clay-size particles. The variability of the gradation for various retorted shales is evident in Table 4. The gravel-size particles ranged from zero to 79 percent and the silt and clay size from zero to 63 percent. Samples in which the percent <0.005 mm (clay) was determined ranged from zero to 12 percent. The uniformity coefficients for nearly all of the retorted samples were high with values beginning at 4.7 and going up to as high as 1822. The higher

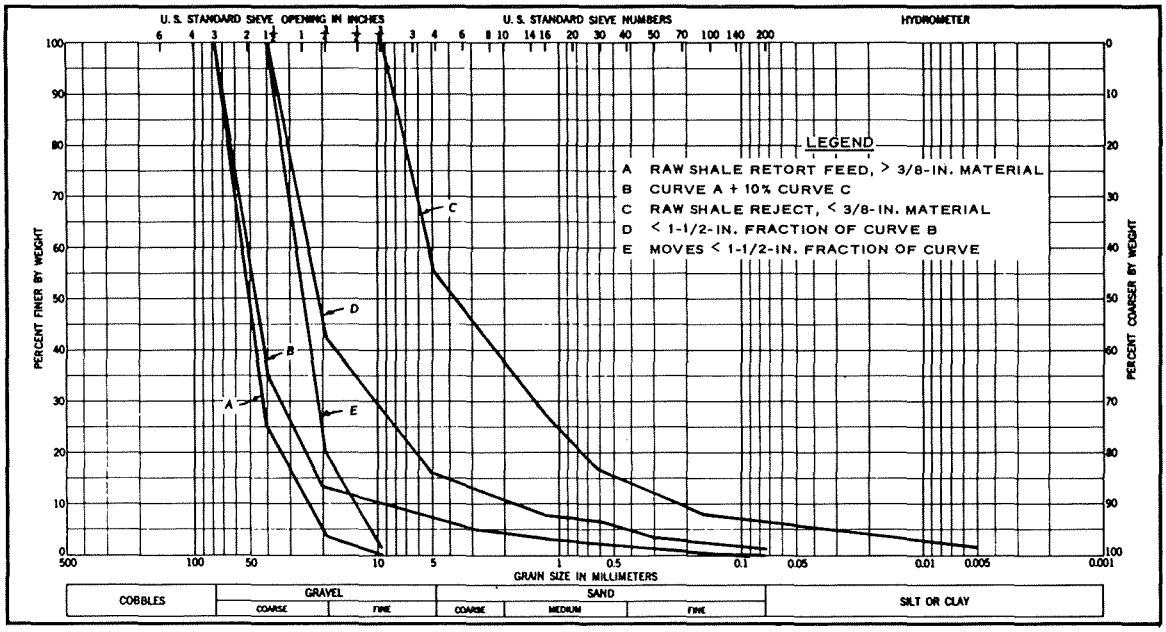

Figure 2. Gradations of raw shale samples used on Phase VII of Paraho Oil Shale Project (from Reference 26)

uniformity coefficients indicate a well-graded (or nonuniform for the geologist) sample, which is generally more desirable when compaction and strength properties are important.

Atterberg limits

9. Atterberg limits represent the end points and range of water contents over which the consistency of the material varies. No Atterberg limit data are available on the raw shales, and only a very limited amount is available for the retorted shales. Generally, the retorted materials are nonplastic. The two reported values of Atterberg limits showed liquid limits of 30 and 33 and plasticity indexes of 6 and 3, respectively.

Soil classification

10. Under the USCS, the retorted shales would be classified as GM, SM, or ML depending on the amount of gravel present in a specific sample and the plasticity of the fines. Under the AASHTO system, the retorted shales would be classified as A-1 or A-3 materials. In general, the classifications indicate good compaction characteristics, slight to medium compressibility, good to excellent strength values, and overall, a

good foundation material. Classification of the raw shale is of little consequence since it is considered to be rock in its in situ state, and classification based on gradation is meaningless because of the man-made variability of the gradation (i.e., different crushers and amount of crushing).

Engineering Properties

11. The major engineering properties pertinent to geotechnical engineers are compaction, permeability, consolidation or settlement, durability, and strength. As previously noted, engineering properties were not determined for retorted materials prior to the middle 1960's. In addition, the engineering tests that were conducted were run primarily on undisturbed cores with the data being used to determine mine roof and pillar strength and stability. Only one reference reported test data on raw crushed shale.[26] Beginning in the middle 1960's, disposal of retorted oil shale became a major concern. Disposal and/or alternative uses of spent shale necessitated the characterization of the material from an engineering viewpoint. The following discussions of engineering properties will be presented in the same chronological order: undisturbed raw shale, crushed raw shale, and retorted shale.

Compaction

12. Only one reference reported laboratory compaction characteristics for crushed raw shale.[26] Two of the gradations shown in Figure 2 (curves D and E) were tested at two different compaction energies (one half the American Society for Testing and Materials (ASTM) Standard[28] D 698 or 6,200 ft-lb/ft^3, and ASTM D 698, or 12,375 ft-lb/ft^3. The resulting optimum moisture contents and maximum dry densities were 6.0 percent and 88.3 pcf for the low compaction and 8.3 percent and 90.3 pcf for the standard compaction for gradation curve D. Corresponding values for curve E were 1.0 percent and 77.5 pcf for the low compaction and 1.0 percent and 80.1 pcf for the standard compaction. As would be expected for compaction of granular or gravelly materials, the variation of dry density through the range of moisture content tested was very small; dry

density varied from 89 to 91 pcf for a 10 percent change (0 to 10 percent) in moisture content.

13. Considerable effort has been expended in developing the laboratory compaction characteristics of retorted oil shales since the importance of compaction on the evaluation of disposal alternatives has been determined. In addition, compaction of the retorted shales influences the other engineering properties. The major variable in establishing the compaction characteristics was compaction energy, with five levels of compaction energy reported. The five levels and their corresponding ranges of optimum moisture content and maximum dry density are presented in the following tabulation:

Compaction Energy ft-lb/ft^3	ASTM Standard	Optimum Moisture Content, percent	Maximum Dry Density, pcf
6,200	D 698 (50 percent)	18.5-27.2	77.0-99.2
12,375	D 698	15.5-31.0	78.6-103.2
19,700	D 1557 (35 percent)	22.0	93.2-94.0
33,750	D 1557 (60 percent)	17.4	106.7
56,250	D 1557	14.2-22.0	88.8-109.2

Other trends not obvious in this tabulation but apparent in Table 4 include (a) the obvious trend of lower optimum moisture content and higher maximum dry density with increasing compaction energy and (b) the accepted trend of higher optimum moisture contents and lower maximum dry densities with decreasing maximum particle size (i.e., more sands, silts, and clays). The characteristic of small dry density changes over the molding moisture content range exhibited by the crushed raw shale is also predominant for the retorted materials. The range of maximum dry densities of the compacted retorted shales under standard compaction energy is somewhat less than would normally be anticipated for a GW soil, which would normally range from 120 to 135 pcf.

14. Laboratory compaction data provide extensive insight into the

behaviorial characteristics of compacted soils. However, because of the limited knowledge of the engineering properties of retorted oil shales, the effectiveness of field compaction equipment in achieving the desired density conditions is a question of considerable concern. To determine this effectiveness, the Paraho Oil Shale Project undertook the construction of an extensive compacted test fill.[25] The major variables in the test fill study were moisture added, loose lift thickness, type of compaction equipment, and number of passes. Table 5 summarizes the test fill study. The results tabulated in Table 5 are shown graphically in Figure 3. For the 8-in. loose lift thickness with moisture added at the test fill, the highest percent compaction was achieved with the vibrating drum compactor (6 passes) followed by the vibrating pad (5 passes), tractor (6 passes), rubber tire (6 passes), and sheepsfoot (6 passes) compactors. Combinations of the compaction equipment provided significant percent compactions, i.e., vibrating pad plus vibrating drum (4 passes each) and sheepsfoot plus rubber tire (4 and 6 passes, respectively). For the 12-in. loose lift thickness, the vibrating compactors were significantly better than the conventional compactors. The same percent compaction was achieved as was obtained using the vibrating compactors on the 8-in. lift; however, twice as many passes had to be made on the 12-in. thickness. For the test fill with no moisture added and an 8-in. loose lift thickness, the highest percent compaction was achieved with the vibrating drum compactor (6 passes) followed by the tractor (6 passes) and the remaining three compactors resulting in the same percent compaction (98 percent). Other than the one high point (104 percent) and one low point (92 percent) at 6 passes, the remainder of the compaction data (without moisture) fall within a fairly narrow band of percent compaction between 95 and 102 percent. This indicates that without adding water, the density of retorted shale cannot be significantly increased by varying the type of compactor or increasing the number of passes for a particular compactor. Based on these field data, the most economical compaction would be obtained using a vibrating drum compactor with either 8- or 12-in. lifts with increasing lift thickness requiring additional passes. Slightly higher densities can be obtained

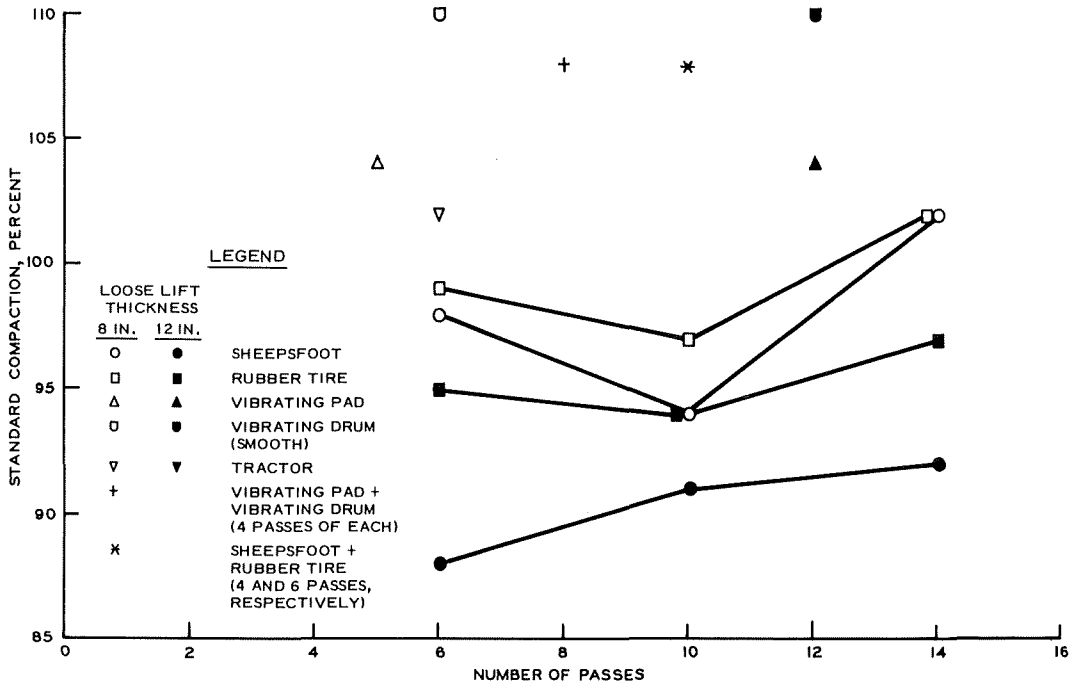

a. MOISTURE ADDED AT FILL

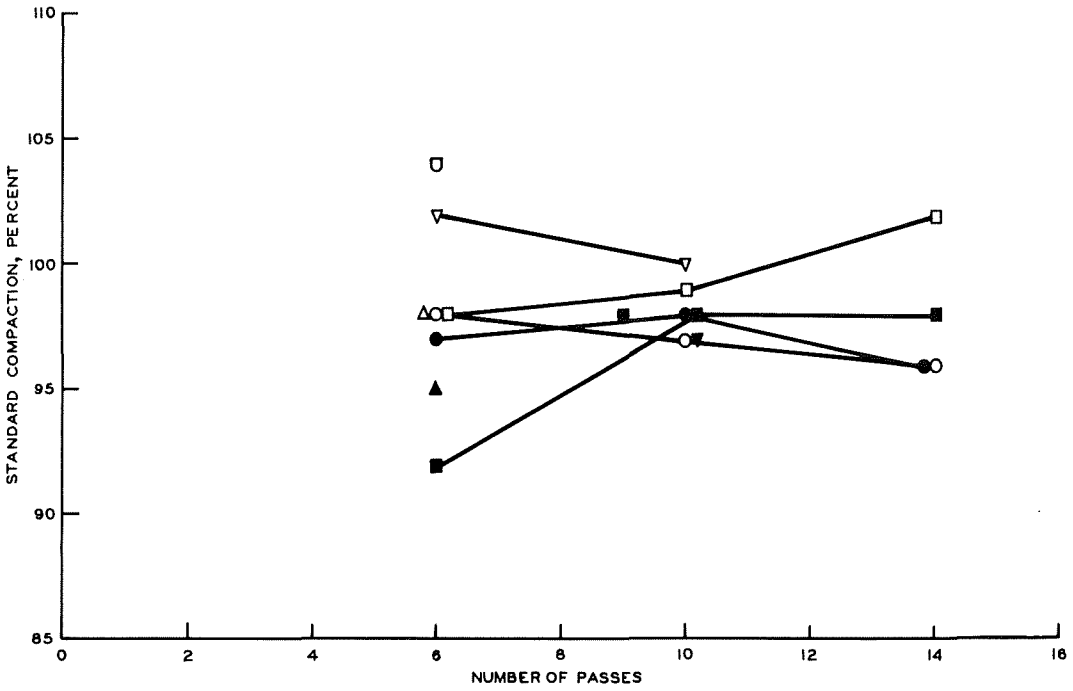

b. NO MOISTURE ADDED AT FILL

Figure 3. Summary of results of compacted test for study, Paraho Oil Shale Project (from Reference 25)

by adding water; however, the cost of hauling and distributing water may be prohibitive.

15. Table 5 shows the breakdown of the retorted shale by the various compactors. Based on an average of all tests conducted, 10 percent of the gravel-sized particles were broken down into the sand-, silt-, and clay-size fractions. Particle breakdown was less for the wet fill than for the dry fill construction.

16. Based on results of the test fill study, the filtration test pond lining (Pond No. 1) was compacted using a vibrating drum compactor. An average percent compaction of 98 percent was achieved. A discussion of the filtration test ponds will be presented in subsequent sections.

Permeability

17. The permeability of raw oil shale is an important property when considering in situ retorting of the shale. Permeability during in situ retorting is dependent on the temperature and pressure applied during the process.[13,20] Permeability values for compacted raw shales, reported in one reference,[26] ranged from 10,500 to 14,500 ft per year (uniaxial loading = 4 psi) for 3/8- and 1-1/2-in. maximum particle sizes, respectively. For retorted shales, the permeability is important when considering the stability of embankments constructed of the material and the pollution potential of rainwater leaching chemicals out of the disposed shale. Under various loadings, the permeability varied as indicated in the following tabulation. No definite trends were obvious from these data, which show that considerable variation exists in permeability values. However, accepted trends such as decreasing permeability with increasing density and increased percent of fines were verified. The amount of carbonate decomposition during retorting appeared to have a significant influence on permeability: the higher the decomposition, the greater the permeability. Since engineers are more familiar with permeability presented in units of centimetres per second, the values in the following tabulation and Tables 3 and 4 can be converted by multiplying feet per year by 0.97×10^{-6} to obtain centimetres per second.

Load (uniaxial) psi	Permeability ft per year	Dry Density pcf
50	0.3-71	98.9-93.9
100	0.25-52	98.9-93.9
200	0.08-30	98.7-93.9
70	1.5-2088	96.7-77.0
145	1.19-1016	96.7-77.0
300	0.3-480	96.7-77.0
1000	4.72-14.5	96.6-80.2

18. Field studies of the permeability of retorted oil shales were conducted during the Paraho Oil Shale Project[27] (Phase VII). In two filtration ponds, one with a compacted lining and the other with an uncompacted lining, the seepage and evaporation were monitored. The uncompacted lining was found to have an average permeability of 2039 ft per year while the compacted lining was found to have an average permeability of only 4.24 ft per year. For comparison, laboratory permeabilities on 6-in.-diam cores from the compacted lining ranged from 0.16 to 1.18 ft per year.

Settlement (consolidation)

19. Settlement (consolidation) properties are of minor consequence for raw oil shales, but are very important in assessing the stability of an embankment constructed of retorted shales since excessive settlement could cause such an embankment to become unstable. In addition, consolidation of retorted shale influences its permeability and strength characteristics as well as the total volume required in a disposal site.

20. One reference reported settlement properties on compacted raw shales[26] with several references reporting on retorted shale.[18,22-24] The percent settlement for the various applied loads (ASTM D 698 energy) is summarized in the following tabulation:

Material	Applied Load psi	Settlement percent	Dry Density pcf
Paraho	50	0.7-2.8	95.5-88.0
	100	0.8-3.4	95.5-98.3
	200	0.8-4.8	95.5-98.3

(Continued)

Material	Applied Load psi	Settlement percent	Dry Density pcf
Paraho	70	0.4-3.4	88.8-102.5
	145	0.7-4.8	85.0-97.4
	300	0.8-5.6	85.0-97.4
	1000	5.3-10.7	80.2-96.6
Tosco	100	0-15.5	86.6-56.5
	200	0.5-18.0	86.6-56.5
	1000	1.0-23.0	86.6-56.5

The common trend of decreasing settlement with increasing density was not apparent for the ranges of settlements obtained for the Paraho material; however, the trend was obvious for the Tosco material. This is probably a result of the limited range of densities tested for Paraho samples compared with that of the Tosco samples. Quantitatively, the minimum percent settlements are well within tolerable limits for nearly any application. In general, the maximum percent settlements up to about 5 percent are tolerable if an adequate design is prepared to accommodate the settlements. In other words, for both materials, settlement can be effectively minimized by adequate compaction. No detectable difference was noted between the materials retorted by the direct or indirect heating modes. In the Paraho Oil Shale Study, the low carbonate decomposition retorted shales settled roughly 1-1/2 to 2 times as much as the high carbonate decomposition shales.[23] Adding raw shale reject material (<3/8 in.) to different carbonate decomposition samples reduced overall magnitude of settlement; however, the same trend of increasing settlement with decreasing carbonate decomposition was evident.

Soundness

21. The soundness of an aggregate material is a measure of its ability to resist degradation from an applied force. Generally, soundness is quantified using the Los Angeles Abrasion (LAA) test. For the raw shale feed, the LAA value was 14 percent (material loss), which indicates a high degree of soundness. Many State Highway Agencies require maximum loss values for concrete and base course aggregate of 40 percent. The LAA values for retorted shales varied from 21.5 to 70 percent loss. The sample with the 21.5 percent loss was taken from the

U. S. Bureau of Mines (USBM) Demonstration Plant Stockpile and had been exposed to the climate for several years. The suggested reason for the low LAA value was that the softer particles deposited in the stockpile had probably broken down, leaving only the hard, sound rocks that were eventually tested. The more recent samples probably still include these softer materials within the gradation normally tested in the LAA device; hence, the high values of degradation.

Strength

22. The strength characteristics are most important in determining the stability or load-carrying capacity of the raw or retorted oil shale. Strength has been quantified using several parameters and tests: modulus values, unconfined compressive strength q_u, and triaxial shear strength ϕ, C. Prior to the mid-1960's, no strength tests were conducted on retorted shale. The only strength determinations made were on undisturbed cores of raw shale to determine the size and stability of underground mine openings.

23. Intact raw shale. The average q_u of undisturbed raw shale cores varied between 9,660 and 25,700 psi. The major variables investigated in the strength determinations were kerogen content and core sample orientation (parallel or perpendicular to bedding). Compressive strength was greater for the low-kerogen-content shales, with the ratio of low- to high-kerogen-content compressive strengths in excess of two. Differentiation on the basis of core sample orientation was not as evident; however, in most cases the horizontally oriented (parallel to bedding) cores yielded slightly higher strengths. During the Paraho Oil Shale Project, q_u values were determined on core samples taken from large mine-run blocks. Values of q_u varied from 7,540 to 10,027 psi.

24. Leps[30] classified rockfill on the basis of unconfined compressive strength of rock cores in the following manner:

q_u, psi	Strength Classification
500-2,500	Weak rock particles
2,500-10,000	Average rock particles
10,000-30,000	Strong rock particles

Based on this classification, most of the raw shale would be considered strong rock particles. The raw Paraho material exhibits the strength of average rock particles.

25. Modulus values were determined for use in the roof and pillar designs; however, the modulus of elasticity was the one most used and most easily identifiable. The average modulus of elasticity for undisturbed core samples varied from 0.83×10^6 to 6.025×10^6 psi. As expected, trends identical to those set for the compressive strength were obtained for the modulus of elasticity, namely, increasing modulus values with lower kerogen contents and horizontally oriented samples. The other modulus values, rupture and rigidity, along with Poisson's ratio ν for raw shale are summarized in Tables 2 and 3. Modulus of elasticity values ranged from 0.56×10^6 to 0.82×10^6 psi, and ν varied from 0.28 to 0.36 (values determined using shear wave tests).

26. Compacted raw shale. For crushed raw shale, in particular the <1-1/2-in. shale feed reject compacted at ASTM D 698 and one half ASTM D 698 compactive efforts, the friction angle ϕ values were 39 and 35 deg, respectively. Cohesion c values for the ASTM D 698 and one half ASTM D 698 efforts were 19.4 psi (13.9 psi for saturated specimens) and 22.9 psi (15.3 psi for saturated specimens), respectively.

27. Compacted retorted shale. Strength characteristics are most significant from an engineering viewpoint when considering the disposal of retorted shales. The parameters used to quantify the strength characteristics in the reported data were ϕ, c, and q_u.

28. Retorted materials compacted at 10 percent ASTM D 698 compaction energy were tested in unconsolidated, undrained (Q) triaxial and unconfined compression tests by the University of Denver.[15] The results of the unconfined compressive testing program are shown in Figure 4 and the triaxial testing program in Figure 5. The q_u increased with storage or curing time, increasing storage or preconsolidation pressure for constant curing time, and increasing molding water content. This latter trend is contrary to accepted trends for this general type of material (i.e., GW, ML); however, it may be explained on the basis of one of two arguments. The first argument involves the more extensive development

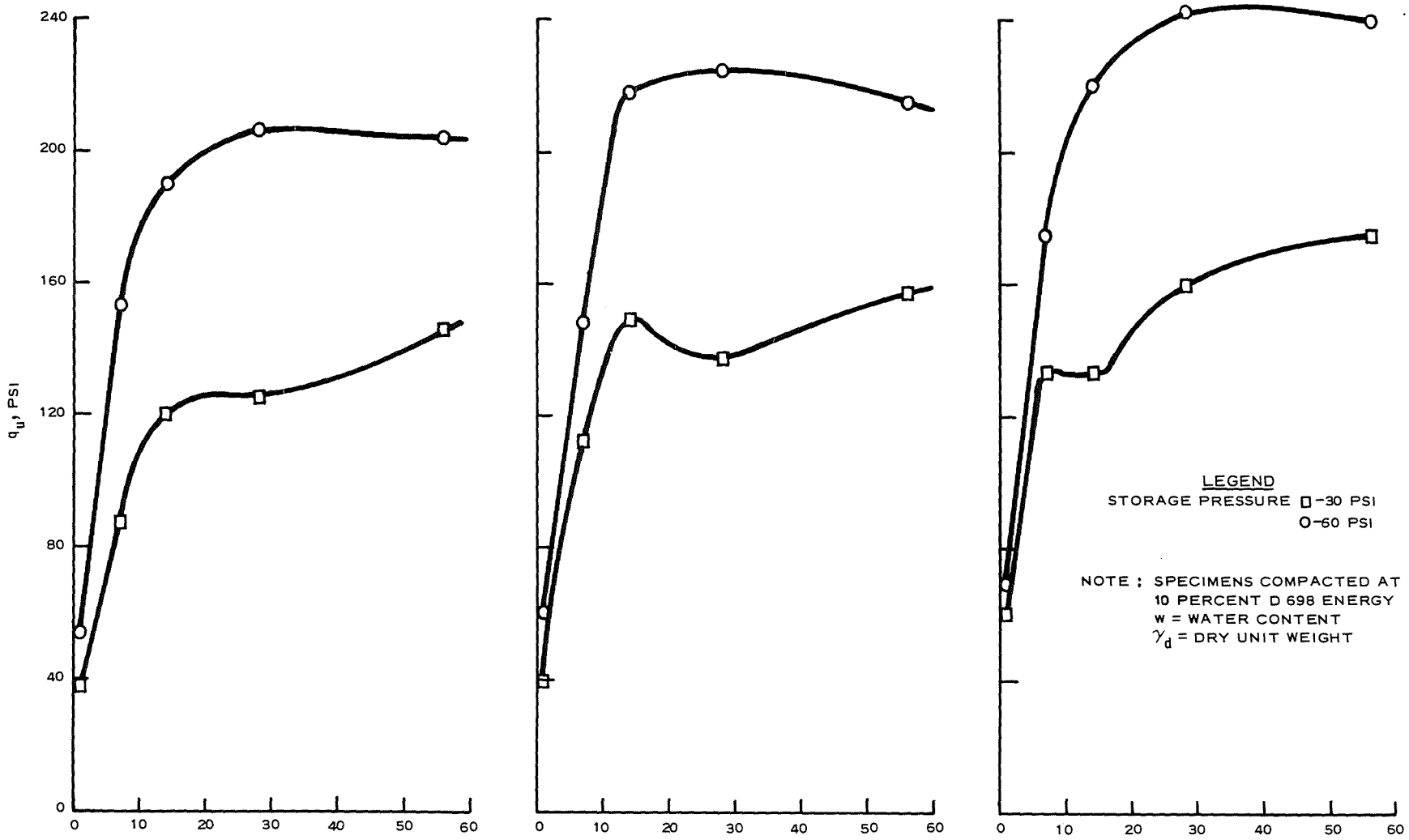

Figure 4. Influence of water content, storage time and storage pressure on q_u (from Reference 15)

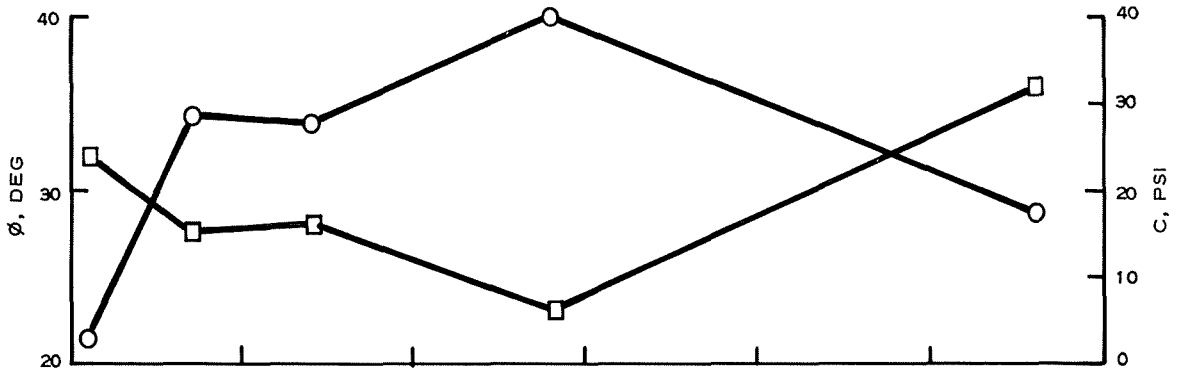

a. MOLDING W = 5 PERCENT; γ_d = 66.4 – 69.5 PCF

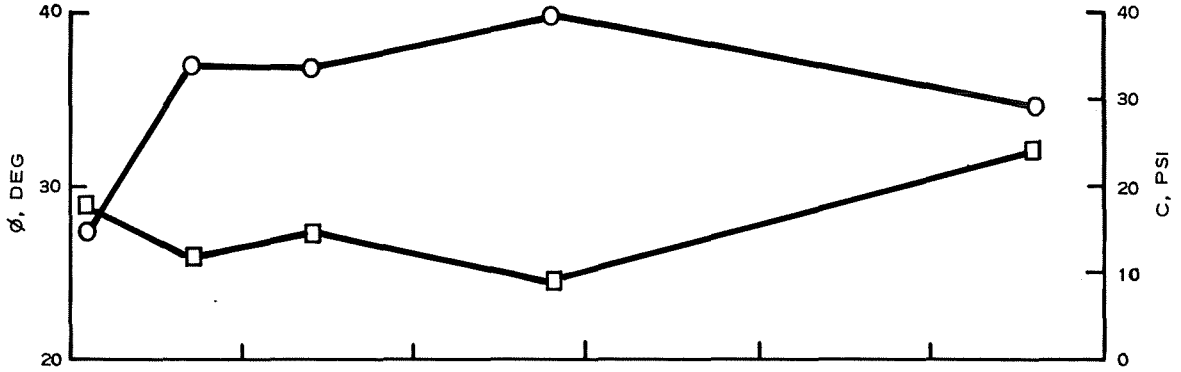

b. MOLDING W = 10 PERCENT; γ_d = 61.1 – 67.4 PCF

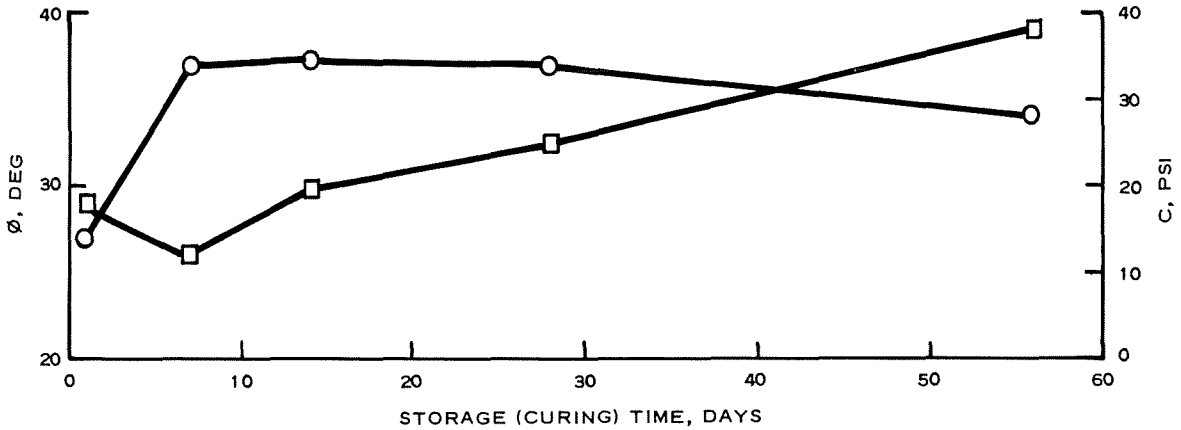

c. MOLDING W = 20 PERCENT; γ_d = 58.7 – 62.4 PCF

Figure 5. Influence of water content, storage time, and storage pressure on shear strength parameters (from Reference 15)

of cementitious reaction products as a result of the extra water made available to the material. The second argument involves apparent cohesion resulting from the surface tension effects of the increased water content. A simple way to determine which argument is valid is to inundate the q_u specimens prior to testing. If the soaked specimens maintain their strength, then the cementing reaction products argument is valid; if the specimens crumble during soaking, then the apparent cohesion argument is valid. During the laboratory testing program, none of the specimens were soaked prior to testing; however, some of the additional chemical tests indicated that cementing reaction products did develop in a somewhat similar process to lime stabilization. A second and less obvious possible indication of the cementing reaction product is shown in Figure 5. With increasing curing time, particularly at the higher molding water contents, the role of cohesion in determining the shear strength increases (i.e., the curves cross).

29. In a series of Q triaxial tests to develop strength parameters for a stability analysis,[18] ϕ and c were measured on compacted samples from the Tosco process with varying moisture contents and dry densities. The results showed that $\phi = 35$ deg for all tests and that c varied between 6.3 and 19.4 psi, with c increasing with increasing density. In a series of consolidated undrained (R) triaxial tests, back-pressure saturated, the results were $\phi = 20$ deg and $c = 0$.

30. In Phase II of the Paraho Oil Shale Project,[22] retorted shale that had been stockpiled for several years was tested. R triaxial test results on two different gradations compacted at optimum water content and maximum dry density were $\phi = 32.4$ deg and $c = 17.4$ psi for the 3/16-in. maximum size and $\phi = 34.2$ deg and $c = 2.2$ psi for the 1-1/2-in. maximum size. In an attempt to determine the stabilization potential of retorted shales and the influence of rapid curing at 125°F, 5 percent hydrated calcium lime was added to the material and q_u values measured versus curing time. The results are shown in Figure 6. A small increase in q_u was noted for the 28-day cure at 125°F for specimens containing no lime. Addition of the lime resulted in extremely large strength gains, which is most unusual because soils with

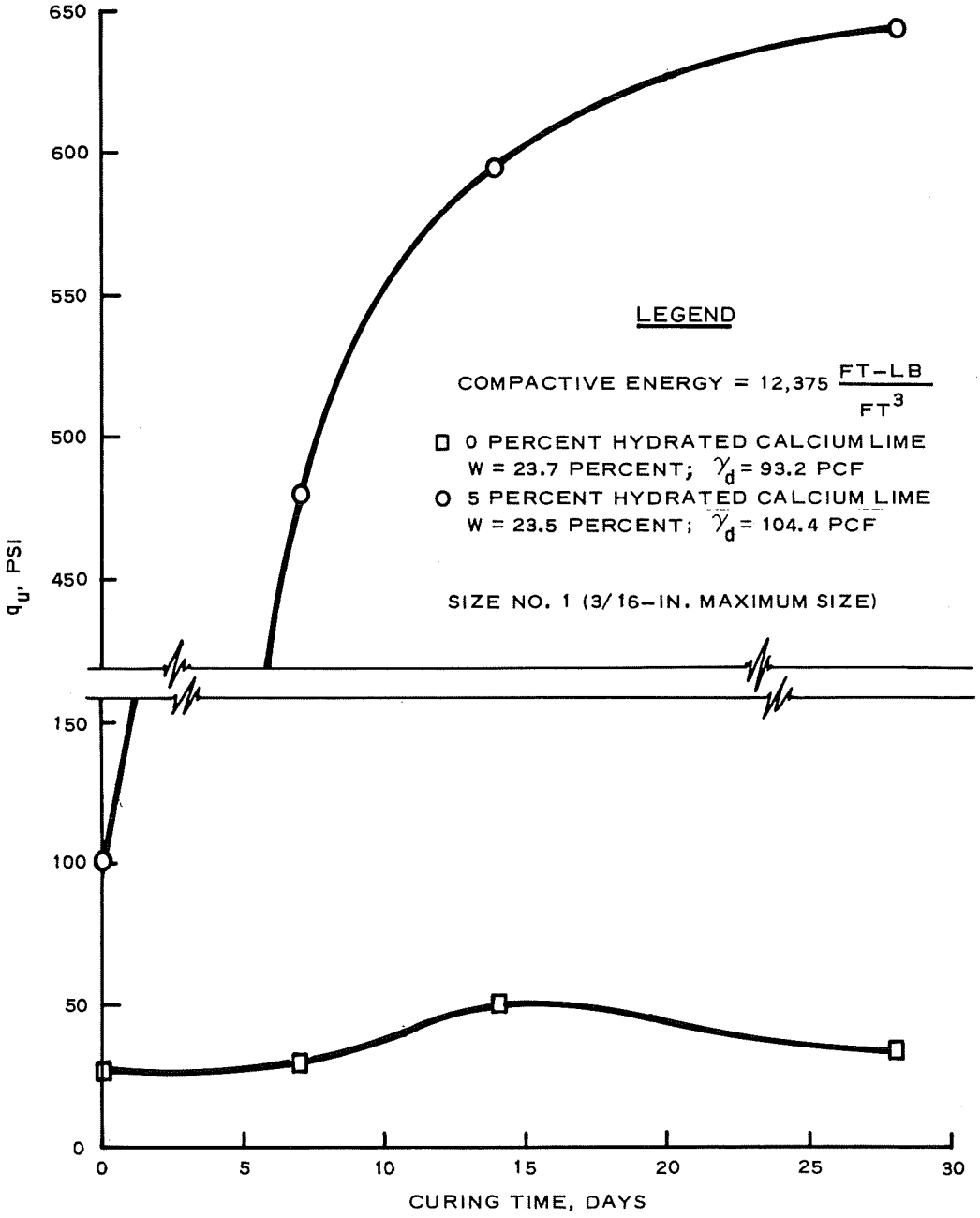

Figure 6. Influence of curing time and lime treatment on q_u (from Reference 22)

plasticity indexes less than 10 do not respond to lime treatment. The strength gains obtained would far exceed any of the generally accepted criteria for quantifying stabilization potential; however, the results should be viewed with some reservation. Rapid-cure procedures generally consist of curing specimens at elevated temperatures for shorter time periods (i.e., 30-90 hours) to simulate multiple-day curing (i.e., 7, 14, 21 days). It would appear that the procedure was incorrectly applied in this reference since apparently the samples were cured at 125°F for periods up to 28 days; therefore, it is not actually a true rapid-cure procedure. In addition, the 125°F temperature is generally considered to be too high since the type and amount of reaction products are dependent on the curing temperature. A more realistic temperature would be in the range of 100-105°F.

31. In Phase III of the Paraho Oil Shale Project,[23] consolidated, drained (S) triaxial and unconfined compression tests were run on three gradations at different compaction energies for shales having two different amounts of carbonate decomposition. Values of ϕ and c ranged between 35.0 and 37.6 deg and 12.5 and 13.9 psi, respectively, for the high carbonate decomposition without curing. For the low carbonate decomposition without curing, ϕ and c ranged between 34.2 and 42.9 deg and 9.7 and 13.2 psi, respectively. Comparable ϕ and c values were obtained for both materials with the low carbonate decomposition shale showing slightly higher ϕ values. Curing comparable specimens at ASTM D 698 compaction energy resulted in a decrease in ϕ and a considerable increase in c , which supports the cementing reaction product argument. The q_u values likewise support this argument, as shown in Figure 7. A significant increase in q_u with time is evident for the high carbonate decomposition shale, while the q_u increase is much less dramatic for the low carbonate decomposition shale.

32. In Phase IV[24] of the Paraho Oil Shale Project, S and K_o triaxial and unconfined compression tests, where K_o is the ratio of lateral stress developed to vertical stress applied, were run on retorted shales produced by direct and indirect heating modes of the retort plant. The variables studied during the testing program were

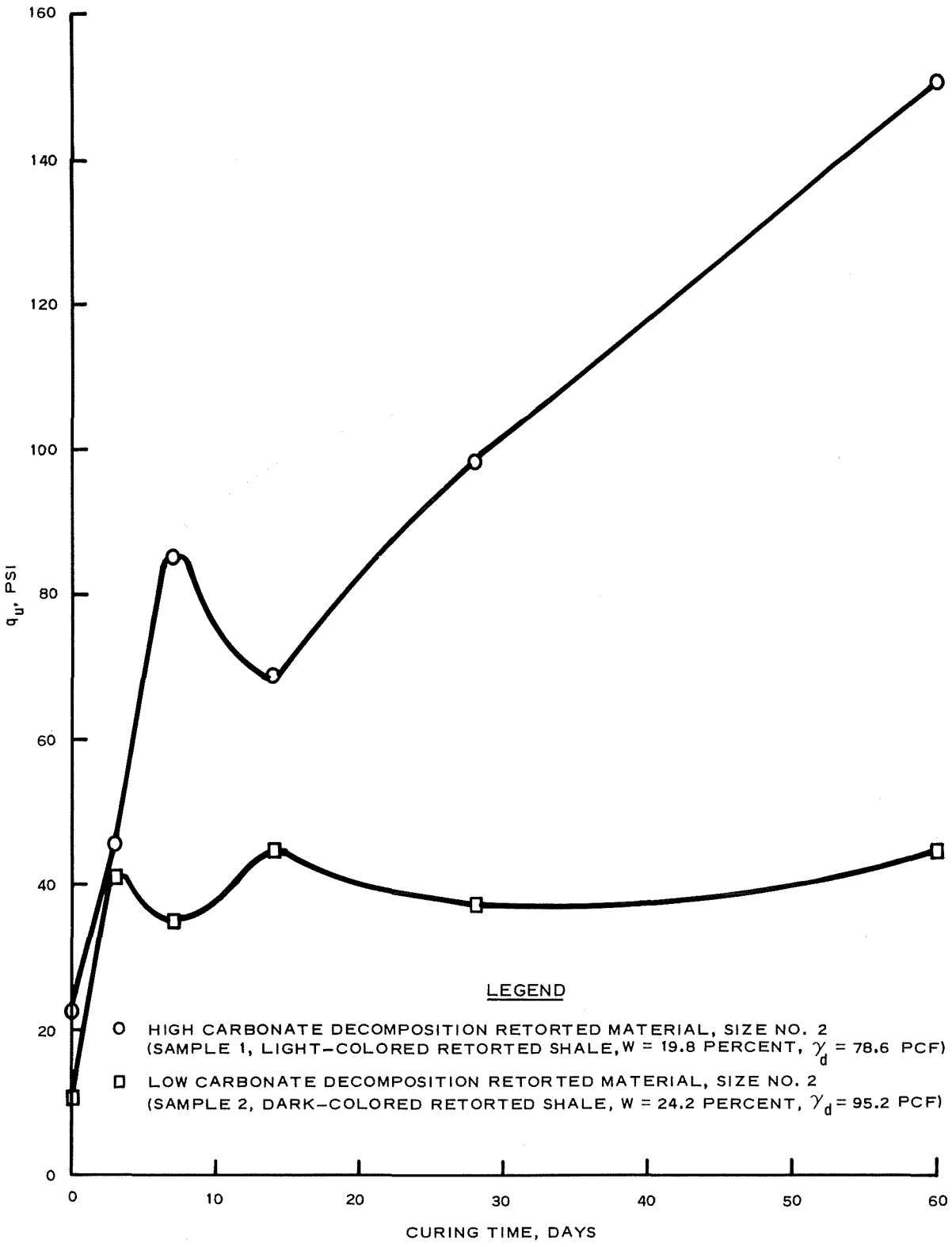

Figure 7. Influence of curing time on q_u for high and low carbonate decomposition materials (from Reference 23)

molding water content, curing time, compaction energy, and seasoning (mellowing) time. For the direct-heat retorted shale at optimum water content and maximum dry density for each of three compaction energies, ϕ and c ranged between 34.2 and 34.6 deg and 19.4 and 36.1 psi, respectively. For the indirect-heat retorted shale at ASTM D 698 optimum water content and maximum dry density, ϕ and c values were 29.2 deg and 3.0 psi, respectively. The q_u results corresponding to the previously described variables of water content, curing time, and seasoning time are shown in Figures 8, 9, and 10, respectively. The previously

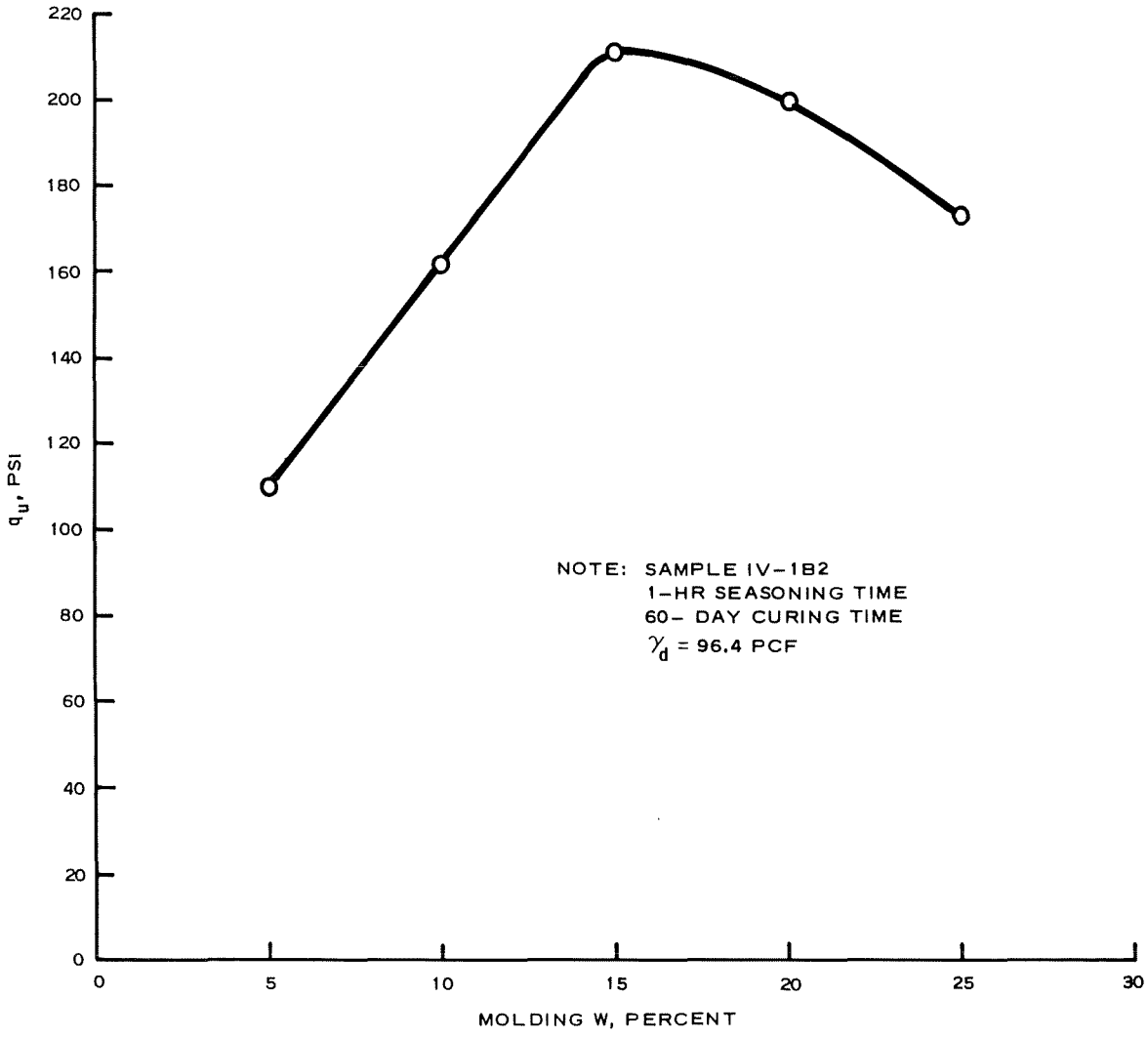

Figure 8. Effect of molding water content on q_u (from Reference 24)

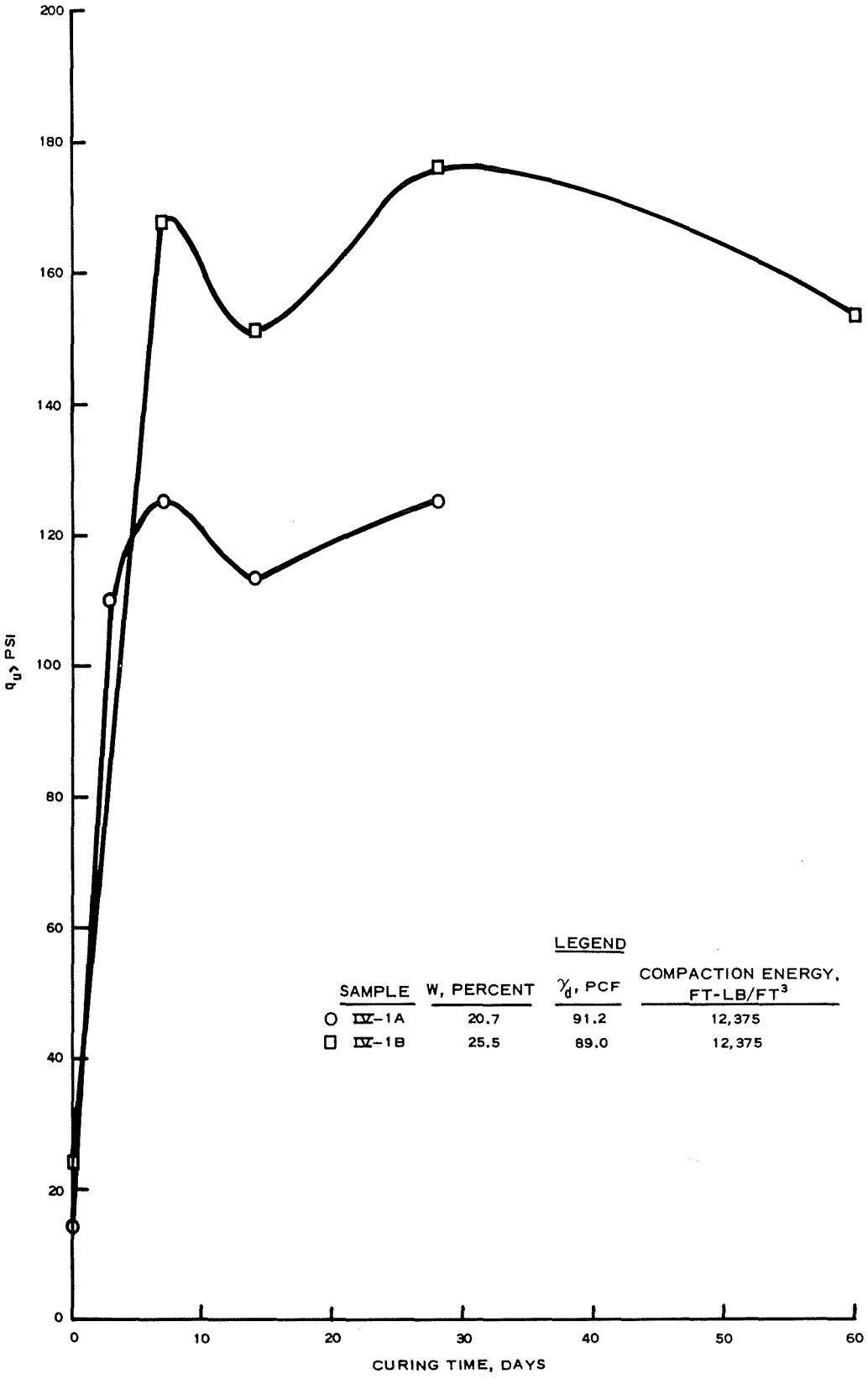

Figure 9. Influence of curing time on q_u (from Reference 24)

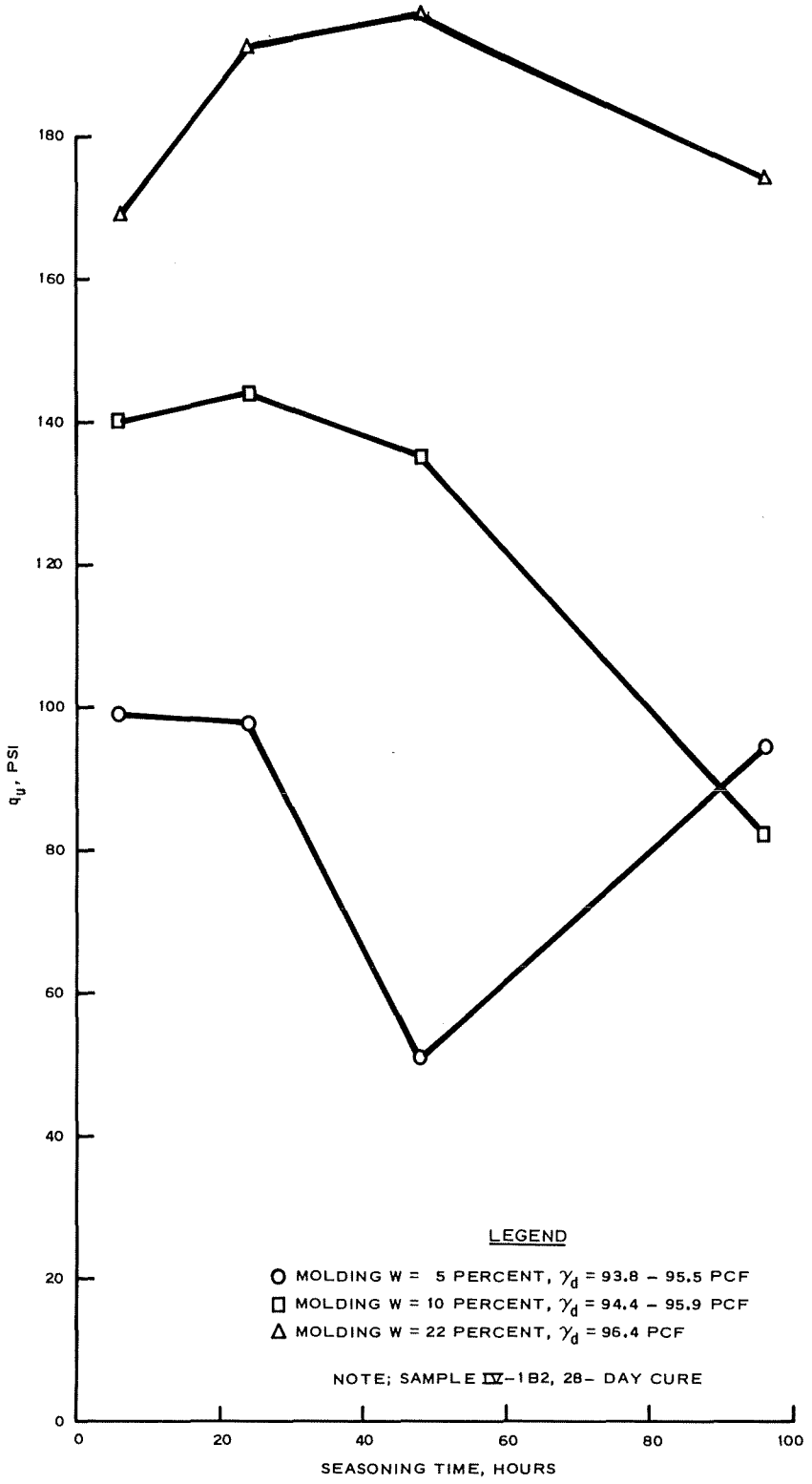

Figure 10. Influence of seasoning time and molding water content on q_u (from Reference 24)

described trend for retorted shales of increasing q_u with increasing water content was again evident up to a molding water content of 15 percent. Above 15 percent, the strength began to decrease, probably due to the fact that excess water was available in the specimen. The cementing reaction product effect is again evident in Figure 9 as the strength increased with time.

Influence of mellowing time

33. In lime stabilization, the development of pozzolanic (cementing) reaction products occurs at the contact points between particles when the lime reacts with surfaces of the individual particles and forms the cementing agent. This reaction and the corresponding cementing action occurs relatively fast, requiring that the particles be in close proximity (i.e., compacted) within a reasonably short time (i.e., 24 to 48 hours) after the lime is introduced into the soil. The influence of seasoning or mellowing time for retorted oil shales is comparable to that of lime-stabilized soils (Figure 10). At the lower molding water contents, the strength drops off rapidly after approximately 24 hours if the specimens are not compacted by that time. With increasing molding water content, q_u increases and the seasoning time before strength begins to decrease is extended. This is the result of the additional water being available to enhance the amount of the reaction and extend the reaction time. In other words, at the lower water contents the amount of development of reaction products and length of time for development is less because sufficient water is not available.

K_o tests

34. During the K_o triaxial testing program,[24] duplicate specimens were prepared and tested in unconfined compression. The major variables investigated in the testing program were gradation, compaction energy, and addition of additives (1 and 3 percent lime and cement). The purpose of the testing program was to compare modulus of deformation E_d values with such properties as q_u, K_o, and ν. The results of the K_o and q_u tests are summarized in Table 4 and shown graphically versus the previously mentioned properties in Figures 11, 12, and 13. Although the q_u values for the 60-day cure specimens did

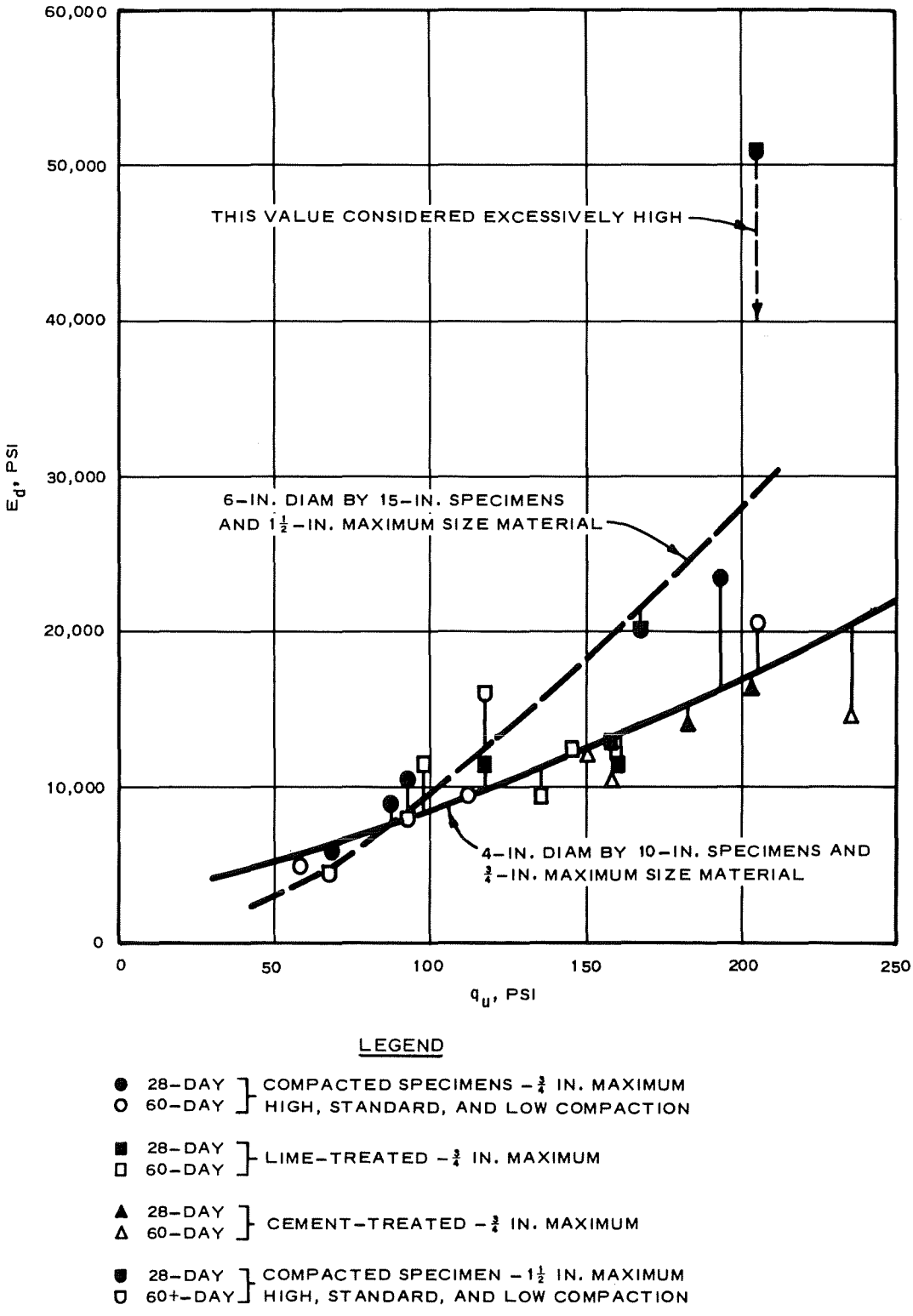

Figure 11. Trends of comparisons between E_d and q_u (from Reference 24)

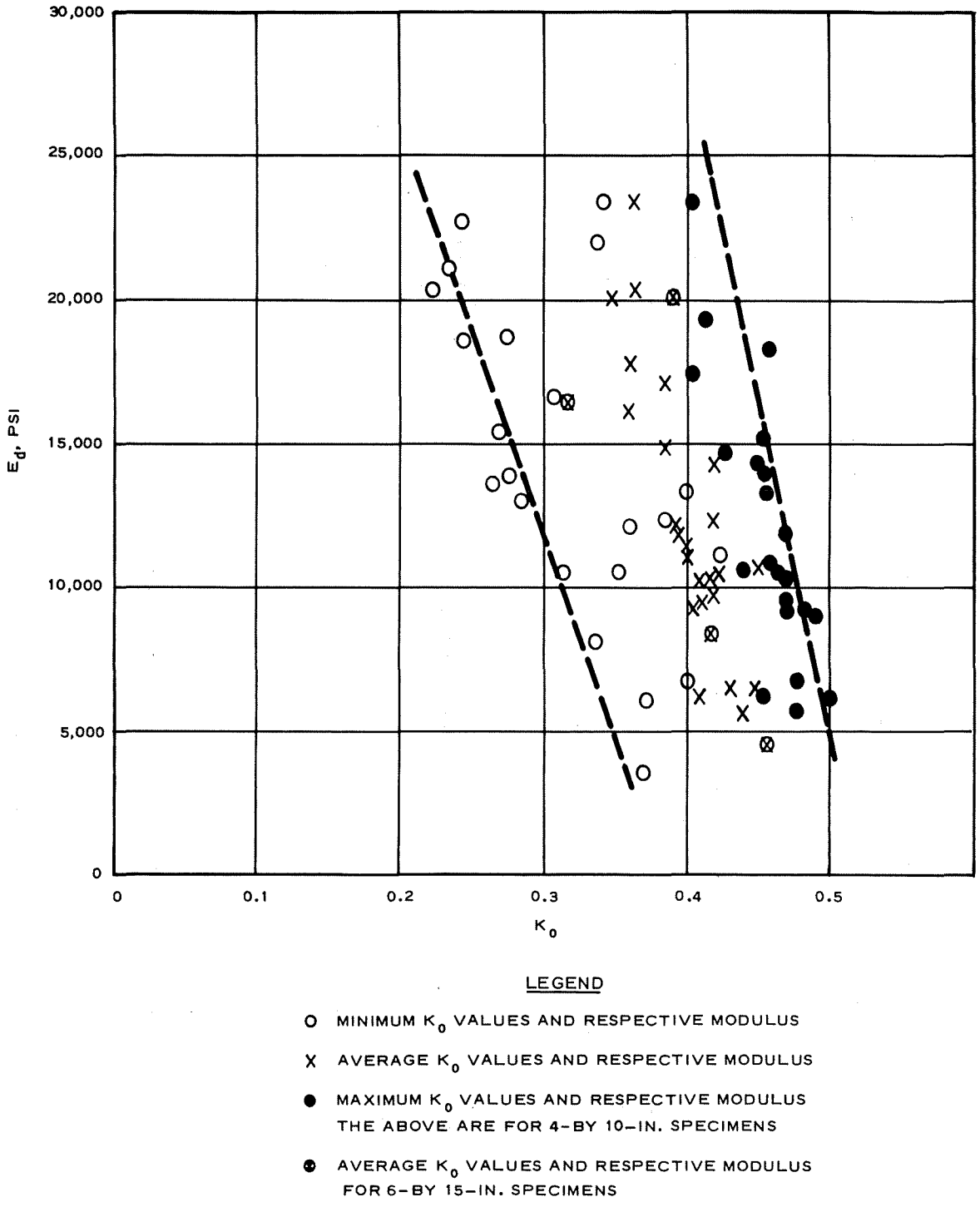

Figure 12. Summary of K_o results (from Reference 24)

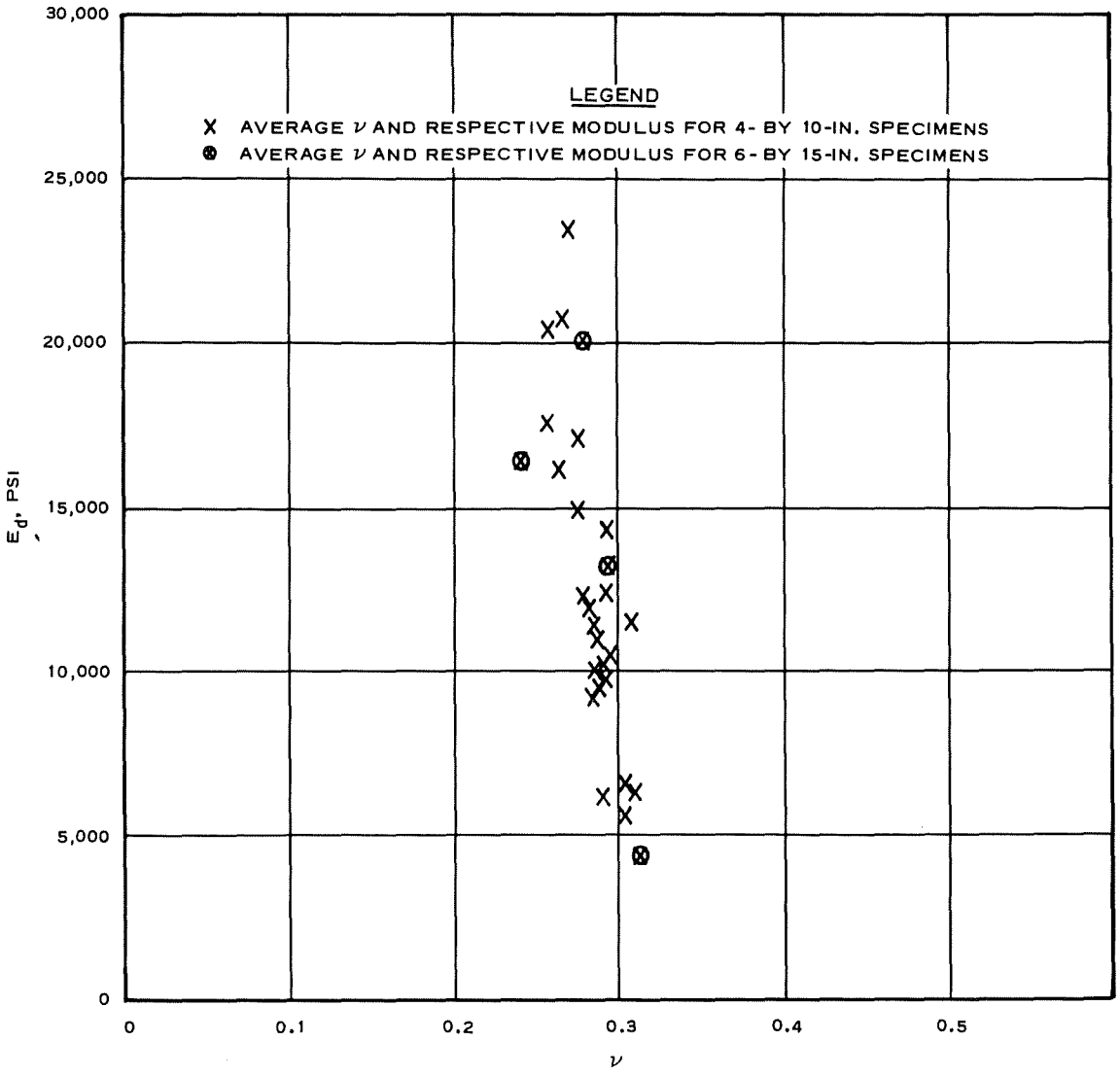

Figure 13. Summary of average values of Poisson's ratio ν (from Reference 24)

show some slight increase over the 28-day cure specimens, on the whole there was very little discernible difference. This would indicate that the cementing action that develops with time is essentially developed prior to the 28-day cure limit. This finding is consistent with all of the previous testing results. As expected, increased compaction energy resulted in higher q_u values. Addition of 1 percent hydrated lime resulted in a distinct improvement in q_u, i.e., 159.2 psi and 136.2 psi for 28- and 60-day cures, respectively, as compared with 88.2 psi and 103.1 psi for the 30- and 60-day cures, respectively, without lime. Addition of 3 percent lime actually resulted in a decrease in q_u values, i.e., 117.9 psi and 122.3 psi for 28- and 60-day cures, respectively. The probable explanation for this decrease is the hydration of the excess lime, which reduces the water available to the retorted material for its own cementing reaction and reaction with the usable lime. Addition of 1 percent cement significantly increased q_u, i.e., 183.6 psi and 154.3 psi at 28- and 60-day cures, respectively. Further increases were obtained by adding 3 percent cement, i.e., 203.0 psi and 234.8 psi for 28- and 60-day cures, respectively. Although the q_u testing program on 1-1/2-in. maximum size particles was limited compared with the 3/4-in. maximum size previously described, the q_u values were higher for the larger particle sizes.

35. The basic parameters obtained from the K_o testing were E_d, ν, and K_o. The E_d values are indicators of strength and compression property variations. Values of E_d, ν, and K_o from the testing program are summarized in Table 4 and shown graphically as a function of one another and of q_u in Figures 11, 12, and 13. Modulus values, as expected, increased with increasing compaction effort; however, no distinct differences were noted between the 28- and 60-day cure specimens. Adding lime increased the modulus values, but consistent with the q_u test results, the higher percentage of lime resulted in a lower strength as compared with the lower lime percentage. Adding cement significantly increased the modulus values, following the same trends set by the q_u tests. Higher modulus values were obtained for specimens molded from 1-1/2-in. maximum size particles. Average K_o

values varied from 0.35 to 0.45 over the range of modulus values obtained. Average ν values ranged between 0.25 and 0.31 over the range of modulus values obtained.

36. A total of four specimens, two K_o and two q_u, were saturated prior to testing. In both q_u tests the strengths were higher for the saturated specimens compared with those of specimens molded at the same conditions and not saturated. Higher modulus and lower K_o values were obtained for the saturated specimens versus their unsaturated counterparts.

PART III: CONCLUSIONS

37. Whether disposal of retorted oil shales involves filling the surface canyons in the oil shale mine area, backfilling oil shale mines, or a productive use such as aggregates, the geotechnical properties of the shales will determine the performance of the disposal structure (i.e., embankment) or product (i.e., aggregates). During previous discussions, the important physical and engineering properties of raw and retorted oil shales from available sources have been defined and briefly discussed via available published information. Although the properties exhibited considerable variability, the data did provide insight into the behaviorial characteristics from a geotechnical point of view. Pertinent conclusions regarding the geotechnical properties are discussed in the following paragraphs with emphasis on the properties of retorted oil shale.

38. Published physical property data show that the apparent specific gravity of retorted oil shales generally range between 2.5 and 2.6. Retorted oil shales are generally well-graded materials regardless of the particle size (i.e., gravel, sand, silt, and clay) predominant in the gradation. Retorted oil shales are classified as GM, SM, or ML materials by the USCS depending on the amount of gravel present and plasticity of the fines. In the AASHTO System, retorted shales are classified as A-1 or A-3 materials. Retorted oil shales are generally nonplastic; however, measured plasticity indexes are less than 10 percent.

39. Compaction characteristics of crushed raw shale indicated optimum moisture contents between 1 and 8 percent and maximum dry densities between 77 and 90, pcf depending on the gradation and compaction energy. For retorted shales over the same compaction energy range, the optimum moisture content ranged between 18 and 31 percent and maximum dry density ranged between 77 and 103 pcf. The crushed raw shale and most of the retorted shales tested exhibited a generally flat S-shaped compaction curve in which the density decreased in the lower end of the moisture content range and then increased to the maximum value and began decreasing again.

40. Field compaction can be effectively achieved using routine compaction procedures and equipment. Vibrating compactors, either pad or drum, obtain maximum percent compaction with fewer passes than do conventional compaction equipment. Water added at the compaction site increases the efficiency of most compaction equipment. Adding water also reduces particle breakdown compared with compaction of dry material.

41. Permeability of retorted oil shales is variable and, like most material, is dependent on gradation, amount of compaction, and applied load. Field studies show that compaction significantly reduces the permeability when leaching of chemicals by rainwater is considered a potential environmental hazard.

42. As with permeability, the settlement or consolidation properties are variable. The material follows the accepted trends of lower densities resulting in larger settlements. Settlement properties were distinctly affected by the amount of carbonate decomposition of the retorted shales with low-carbonate decomposition shales settling 1-1/2 to 2 times as much as high-carbonate decomposition shales.

43. Retorted oil shales are not relatively hard materials since their resistance to degradation by external force, i.e., soundness, is generally less than minimum accepted values for concrete or base course aggregates.

44. Reported compressive strength of undisturbed raw shales ranged between 9,000 and 25,000 psi, with the lower strengths corresponding to low-kerogen content shales and increasing as the kerogen content increased. Sample orientation (i.e., parallel or perpendicular to bedding) had a slight effect on strength with the parallel to bedding samples yielding slightly higher strength. Reported modulus of elasticity values ranged between 0.83×10^6 and 6.025×10^6 psi and exhibited trends similar to those for compressive strength, kerogen content, and sample orientation.

45. Reported data on strength of compacted retorted shales showed that strength increases with (a) increasing molding water content, (b) increasing storage or curing time, and (c) decreasing seasoning or mellowing time. The combination of these factors and their variations

indicates that the strength of retorted shales is analogous to that developed in lime-stabilized soils: the strength is dependent on the development of pozzolanic reaction products or cementing agents between individual particles. Increasing strength with increasing water content indicates that the water is being used by the material to form the cementing agents; however, one data source[24] did show that strength decreases after reaching a molding water content (Figure 8) of approximately 15 percent. The rapid increase in strength with time is typical of strength that is dependent on cementing agents. In nearly all reported cases, the major portion of the strength was developed by or prior to the 14-day curing time.

46. Additives such as lime and cement showed distinct effects on strength characteristics. One percent hydrated lime increased the strength compared with that of the untreated material, but addition of 3 percent lime resulted in a decrease compared with the 1 percent strengths. This would indicate an excess of lime, which would have a tendency to reduce the water available to the shale to develop its own cementing agent or to react with the usable lime. Addition of cement at the 1 and 3 percent level resulted in continued strength gain with increasing percent cement.

47. K_o testing of retorted oil shales indicated that E_d values varied between 5,000 and 24,000 psi, depending on the gradation and compaction energy. Average K_o values ranged between 0.35 and 0.45 over the range of modulus values obtained. Average V values ranged between 0.25 and 0.31 over the same range.

REFERENCES

1. Windes, S. L., "Physical Properties of Mine Rock," Report RI 4727, Part II, Sep 1950, U. S. Bureau of Mines, Washington, D. C.

2. Stanfield, K. E. et al., "Properties of Colorado Oil Shale," Report RI 4825, Nov 1951, U. S. Bureau of Mines, Washington, D. C.

3. Wells, W. E. and Ruark, J. R., "Pilot-Plant Batch Retorting of Colorado Oil Shale," Report RI 4874, May 1952, U. S. Bureau of Mines, Washington, D. C.

4. U. S. Bureau of Mines, "Synthetic Liquid Fuels, Part II--Oil from Oil Shale," Report RI 4866 (Annual Report of the Secretary of the Interior), Jul 1952, Washington, D. C.

5. _____, "Synthetic Liquid Fuels, Part II--Oil from Oil Shale," Report RI 4943 (Annual Report of the Secretary of the Interior), Jan 1953, Washington, D. C.

6. _____, "Synthetic Liquid Fuels, Part II--Oil from Oil Shale," Report RI 5044 (Annual Report of the Secretary of the Interior), Apr 1954, Washington, D. C.

7. Merrill, R. H., "Design of Underground Mine Openings, Oil-Shale Mine, Rifle, Colorado," Report RI 5089, Dec 1954, U. S. Bureau of Mines, Washington, D. C.

8. Blair, B. E., "Physical Properties of the Mine Rock," Report RI 5130, Part III, Jun 1955, U. S. Bureau of Mines, Washington, D. C.

9. U. S. Bureau of Mines, "Synthetic Liquid Fuels, Part II-Oil from Oil Shale," Report RI 5237 (Annual Report of the Secretary of the Interior), Jul 1956, Washington, D. C.

10. Sohns, W. W., Jukkola, E. E., and Murphy, W. I. R., "Development and Operation of an Experimental, Entrained-Solids, Oil-Shale Retort," Report RI 5522, 1959, Washington, D. C.

11. Matzick, A., Danneberg, R. O., and Guthrie, B., "Experiments in Crushing Green River Oil Shale," U. S. Bureau of Mines Report RI 5563, 1960, Washington, D. C.

12. Tisot, P. R. and Murphy, W. I. R., "Physical Structure of Green River Oil Shale from Colorado," U. S. Bureau of Mines Report RI 6184, 1963, Washington, D. C.

13. East, J. H., Jr., and Gardner, E. D., "Oil-Shale Mining, Rifle, Colorado, 1944-56," U. S. Bureau of Mines Bulletin 611, 1964, Washington, D. C.

14. Haugan, S. E., "Initial Evaluation of the Physical Properties of Oil Shale Ash," Master of Science Thesis, Aug 1967, University of Denver, Denver, Colo.

15. Straek, J. M., "An Investigation of the Shear Strength Characteristics of Oil Shale Ash," Master of Science Thesis, Jun 1969, University of Denver, Denver, Colo.

16. Nevens, T. D., Culbertson, W. J., Jr., and Hollingshead, R., "Disposal and Uses of Oil Shale Ash," Final Report, U. S. Bureau of Mines Project No. SWD-8, Apr 1970, Denver Research Institute, University of Denver, Denver, Colo.

17. Tisot, P. R. and Sohns, H. W., "Structural Deformation of Green River Oil Shale as It Relates to In Situ Retorting," U. S. Bureau of Mines Report RI 7576, 1971, Washington, D. C.

18. Atlantic Richfield Company, "Processed Shale Studies," Environmental Impact Analysis, Appendix 5, Colony Development Operation, Feb 1974.

19. Schmidt, R. A. and Schuler, K. W., "Mechanical Properties of Oil Shale from Anvil Point Under Conditions of Uniaxial Compression," Report SAND-74-0035, Sandia Laboratories, Aug 1974, Albuquerque, N. Mex.

20. Burwell, E. L., Tihen, S. S., and Sohns, H. W., "Permeability Changes and Compaction of Broken Oil Shale During Retorting," U. S. Bureau of Mines Report RI 7860, 1974, Washington, D. C.

21. Gromko, G. J., "A Preliminary Investigation of the Feasibility of Spent Oil Shale as Road Construction Material," paper presented at 54th Annual Meeting of the Transportation Research Board, Jan 1975, Washington, D. C.

22. Holtz, W. G., "Research and Development Program on the Disposal of Retorted Oil Shale - Paraho Oil Shale Project," Phase II, Interim Report, U. S. Bureau of Mines, Feb 1975, Washington, D. C.

23. _____, "Research and Development Program on the Disposal of Retorted Oil Shale - Paraho Oil Shale Project," Phase III, Interim Report on Oil Shale Retorted in Pilot Plant, Apr 1975, Woodward-Thorfinnson & Associates, Inc., Denver, Colo.

24. _____, "Research and Development Program on the Disposal of Retorted Oil Shale - Paraho Oil Shale Project, " Phase IV, Interim Report No. 1 on Shale Retorted in Semi-Works Plant by Direct Heating Method, Aug 1975, Woodward-Thorfinnson & Associates, Inc., Denver, Colo.

25. _____, "Research and Development Program on the Disposal of Retorted Oil Shale - Paraho Oil Shale Project," Phase V, Interim Report on Field Compaction Studies on Shale Retorted in Semi-Works Plant by Direct Heating Method, Feb 1976, Woodward-Clyde Consultants, Rocky Mountain Region, Denver, Colo.

26. _____, "Research and Development Program on the Disposal of Retorted Oil Shale - Paraho Oil Shale Project," Phase VII, Interim Report on Raw Shale Tests, Jul 1976, Woodward-Clyde Consultants, Rocky Mountain Region, Denver, Colo.

27. _____, "Research and Development Program on the Disposal of Retorted Oil Shale - Paraho Oil Shale Project," Final Report, Dec 1976, Woodward-Clyde Consultants, Rocky Mountain Region, Denver, Colo.

28. American Society for Testing and Materials, Standard Test Methods for Moisture-Density Relations of Soils, Using 5.5-lb (2.5-kg) Rammer and 12-in. (304.8-mm) Drops, Designation D698-70, 1977 Annual Book of ASTM Standards, Part 19, 1977, Philadelphia, Pa.

29. American Society for Testing and Materials, Standard Test Methods for Moisture-Density Relations of Soils, Using 10-lb (4.5-kg) Rammer and 18-in. (457-mm) Drop, Designation D1557-70, 1977 Annual Book of ASTM Standards, Part 19, 1977, Philadelphia, Pa.

30. Leps, T. M., "Review of Shearing Strength of Rockfill," Journal of the Soil Mechanics and Foundations Division, Vol 96, No. SM 4, ASCE, 1970, New York, N. Y.

Table 1

Summary of Material and Sample Description and Location Information

Reference No.	Date	Material	Location	Sample Description/Designation	Remarks
1	1950	Green River Formation	Rifle Oil Shale Mine, Rifle, Colo.	Raw shale, Designated Group No. 29 in Reference	Tests run on cores from vertical and horizontal core holes for high- and low-kerogen materials
2	1951	Green River Formation, Mahogany Ledge	USBM Oil Shale Demonstration Plant, Rifle, Colo.	Raw shale, 16 samples designated in two groups - "Six Selected Colorado Oil Shales" (6) and "Mineable Bed Samples" (10)	Tests run on core samples (3/4-in.)
3	1952	Green River Formation, Mahogany Ledge	USBM Oil Shale Demonstration Plant, Rifle, Colo.	Raw shale, retort feed	Gradation of crushed raw shale only data presented
4	1952	Green River Formation	USBM Oil Shale Demonstration Plant, Rifle, Colo.	Raw shale, retort feed	Gradation of crushed raw shale only data presented
5	1953	Green River Formation	USBM Oil Shale Demonstration Plant, Rifle, Colo.	Raw shale, retort feed	Gradation of crushed raw shale only data presented
6	1954	Green River Formation, Mahogany Ledge	USBM Oil Shale Demonstration Plant, Rifle, Colo.	Raw shale, retort feed	Gradations of raw shale for different crushers and mine run
7	1954	Green River Formation, Mahogany Ledge	USBM Oil Shale Demonstration Plant, Rifle, Colo.	Raw shale	Tests run on core parallel and perpendicular to bedding on roof and pillars by 3 different laboratories
8	1955	Green River Formation, Mahogany Ledge	USBM Oil Shale Mine, Rifle, Colo. (near Book Cliffs)	Raw shale, Designated Group No. 41 in Reference	Tests run on cores from vertical and horizontal core holes for high- and low-kerogen materials
9	1956	Green River Formation, Mahogany Ledge	USBM Oil Shale Demonstration Plant, Rifle, Colo.	Raw shale, retort feed	Gradation of mine run shale only data presented
10	1959	Green River Formation, Mahagony Ledge	USBM Anvil Points Mine, Rifle, Colo.	Raw and retorted shale	Gradation of shale feed and retorted shale only data presented
11	1960	Green River Formation, Mahogany Ledge	USBM Oil Shale Mine, Rifle, Colo.	Raw shale	Tests run on cores from vertical and horizontal core holes. Most information on crushers and corresponding gradations
12	1963	Green River Formation, Mahogany Ledge	USBM Oil Shale Mine, Rifle, Colo.	Raw shale	Tests run on shales following removal of organic constituents. Data include particle size distribution, specific surface area and, pore sizes
13	1964	Data same as presented in Reference 7 with some additional discussion			
14	1967	Green River Formation, Mahogany Ledge	Not specified in Reference	Retorted shale	Tests run on reheated retorted shales using 1-in.-diam. × 2-in.-high remolded specimens. Data not included in summary table because too many variables and too few samples were used.
15	1969	Green River Formation, Mahogany Ledge	Not specified in Reference	Retorted shale	Tests run on reheated retorted shales using 1-in.-diam. × 2-in.-high remolded specimens

(Continued)

Table 1 (Concluded)

No.	Date	Material	Location	Sample Description/Designation	Remarks
16	1970	Green River Formation, Mahogany Ledge	Below Mahogany Marker, Colony Mine Above Mahogany Marker, USBM Mine	Retorted shale, Designated BM Raw and retorted shale, Designated AM	Majority of data is taken from References 14 and 15. Remaining data include numerous variables. Data not included in summary tables
17	1971	Green River Formation, Mahogany Ledge	USBM Experimental Mine, Rifle, Colo.	Raw shale	Tests run on 3/4-in.-diam. × 1-1/2-in.-high cores of high pressures and temperatures to simulate insitu retorting. Data not included in summary tables
18	1974	Green River Formation	Parachute Creek Oil Shale Plant, Colony Development Operation	Retorted shale	Test data on parts 2, 4, and 5
19	1974	Green River Formation	USBM Anvil Points Mine, Rifle, Colo.	Raw shale	Tests run on low-, moderate-, and high-Kerogen shales
20	1974	Green River Formation	Various locations	Raw shale	Tests run at high temperatures and pressures to simulate insitu retorting. Data not included in summary tables
21	1975	Green River Formation	USBM Laramie Energy Research Center, Laramie, Wyo.	Retorted shale	Test run to evaluate use of retort shale as highway construction material
22	1975 (Feb)	Green River Formation	USBM Demonstration Plant Stockpile, Anvil Point, Colo.	Retorted shale (Phase II of Paraho Oil Shale Study). Designated: Size 1. < No. 4 Size 2. < 3/4 in. Size 3. < 1-1/2 in.	Tests run on remolded specimens blended to reproduce the original gradation of stockpiled material
23	1975 (Apr)	Green River Formation, Mahogany Member	USBM Experimental and Demonstration Facility, Paraho Oil Shale Project (Phase III), Anvil Points, Colo.	Retorted shale from pilot plant. Designated: Size 1. < 1-1/2 in. Size 2. < 3/4 in. Size 3. < No. 4 Samples taken from exit conveyor belt	Tests run on remolded specimens for high and low degrees of carbonate decomposition
24	1975 (Oct)	Green River Formation, Mahogany Member	USBM Experimental and Demonstration Facility, Paraho Oil Shale Project (Phase IV)	Retorted shale from semi-works plant. Designated: IV-1A, IV-1B, IV-1B2: Discharge Conveyor (Direct) IV-S1: Stockpile (Direct) IV-SC1: Stocking Conveyor (Direct) IV-1IH: Discharge Conveyor (Indirect)	Tests run on remolded specimens representing direct and indirect heating modes of the retort plant
				Raw shale	Tests run on cores cut from block samples
25	1976 (Feb)	Green River Formation Mahogany Member	USBM Experimental and Demonstration Facility, Paraho Oil Shale Project (Phase V)	Compacted test fill using retorted shale from Semi-Works Plant	Percent compaction determined for various equipment and coverage combinations See sample IV-1B for lab properties
26	1976 (Jul)	Green River Formation Mahogany Member	USBM Experimental and Demonstration Facility, Paraho Oil Shale Project (Phase VII)	Raw shale Sample designations VII-1. Raw shale feed VII-2. Block samples (Feb 75) VII-3. Block samples (Dec 75)	Tests run on different gradations blended to meet desired conditions. Tests run on cores cut from block samples
27	1976 (Dec)	Green River Formation Mahogany Member	USBM Experimental and Demonstration Facility, Paraho Oil Shale Project (Phase VI)	Retorted shale. Infiltration ponds constructed of discharge conveyor material	Infiltration tests run to determine permeabilities

(Note: Separate report not prepared. Data appear in Chapter 10 of Reference 27.)

Table 2

Summary of Physical and Engineering Properties of Raw Oil Shale

Reference Number	Material/Sample Description or Designation	Apparent Specific Gravity	Moisture Content Percent	Density pcf	Apparent Porosity Percent	Modulus of Elasticity 10^6 psi	Poisson's Ratio ν	Modulus of Rupture 10^3 psi	Modulus of Rigidity 10^6 psi	Unconfined Compressive Strength, q_u 10^3 psi
1	Green River Formation									
	Vertical core hole									
	Low kerogen (2 observations)	2.31			3.2	3.77	0.16	1.9	1.645	21.75
		(2.31-2.31)			(1.5-4.9)	(3.61-3.93)	(0.11-0.21)	(1.8-2.0)	(1.61-1.68)	(21.6-21.9)
	High kerogen (2 observations)	2.13			1.35	2.295	0.10	0.985	0.985	12.75
		(2.02-2.24)			(0.51-2.2)	(1.89-2.7)	(0.02-0.18)	(0.87-1.1)	(0.84-1.13)	(12.5-13.0)
	Horizontal core hole									
	Low kerogen (2 observations)	2.355			8.6	6.025	0.265	4.45	2.375	25.7
		(2.26-2.45)			(5.2-12.0)	(5.0-7.05)	(0.25-0.28)	(4.1-4.8)	(1.94-2.81)	(23.2-28.2)
	High kerogen (2 observations)	2.17			1.35	3.723	0.657	3.40	1.14	11.13
		(2.08-2.25)			(0.24-2.1)	(2.87-4.47)	(0.45-0.94)	(2.0-4.6)	(1.0-2.42)	(9.6-13.4)
				(Bulk)						
2	Six selected Colorado oil shales	2.02	1.18	74.65						
		(1.673-2.504)	(0.38-2.93)	(60.4-98.8)						
7	Green River Formation, Mahogany Ledge									
	Lab 1, College Park, Md.									
	Roof cored parallel to bedding	2.18				3.1	0.58	3.0	0.98	--
	Roof cored perpendicular to bedding	2.25				1.8	-0.10	0.36	1.0	16.6
	Pillar cored perpendicular to bedding	--				--	--	--	--	22.7
	Lab 2, Columbia University									
	Roof and pillar cored perpendicular to bedding					1.869		4.38		12.78
						(0.51-3.56)		(3.35-6.59)		(7.35-19.0)
	Lab 3, Pittsburgh, Pa.									
	Roof and pillar cored perpendicular to bedding					1.35		1.43		11.7
	Roof and pillar cored parallel to bedding									9.66
8	Green River Formation, Mahogany Ledge									
	Vertical core hole									
	High kerogen	2.025			1.0	0.83	0.18	4.0	0.465	10.0
	Low kerogen	2.25			1.1	3.575	0.145	1.13	1.535	15.3
	Horizontal core hole									
	Low kerogen	2.36				5.95	0.33		2.22	25.0
11	Green River Formation, Mahogany Ledge									
	Vertical core	2.25				3.66	0.12		1.59	15.1
	Horizontal core	2.36				5.95	0.30		2.22	25.0
19	Green River Formation									
	Low kerogen			139.6		3.80				24.9
	Moderate kerogen			140.0		1.47				10.9
	High kerogen			124.6		1.02				10.6

Table 3

Summary of Physical and Engineering Properties of Raw Paraho Study Oil Shale

Reference Number	Material/Sample Description or Designation	Specific Gravity		Gradation								Atterberg Limits		Compaction					Relative Density		Permeability, ft/yr				Settlement, % (Co		
																					At Loading, psi				At Loading,		
		Apparent	Mass	Maximum Particle Size, in.	>No. 4 (Gravel)	<No. 4, >No. 200 (Sand)	<No. 200 (Silt & Clay)	<0.005 mm (Clay)	D_{60}, mm	D_{10}, mm	C_u	Liquid Limit	Plasticity Index	Compaction Energy ft-lbs/ft^3	Optimum Moisture, %	Maximum Dry Density at Optimum, pcf	Maximum Dry Density at Half Optimum, pcf	Maximum Dry Density at Air Dry, pcf	Density (100%) pcf	Loose (0%) pcf	50	100	200	1000	50	100	
24	Green River Formation, Paraho Oil Shale Project																										
	Block 1 (Specimen 1-6)																										
	Block 2 (Specimen 2-2)																										
	Block 3 (Specimen 3-4)																										
26	Green River Formation, Paraho Oil Shale Project																										
	Sample VII-1																										
	1-1/2 - 3 in. (shale feed)	2.11	1.99	3	100	0	0	0	--	--	--																
	3/8 - 3 in. (shale feed), Curve A			3	100	0	0	0	55	22	2.5																
	3/4 - 1-1/2 in. (shale feed)		2.20	1-1/2	100	0	0	0	--	--	--																
	-3/4 in. (shale feed +10% of -3/8 in.)			3/4	50	43	7	--	--	--	--																
	-3/8 in. (shale feed reject), Curve C	2.12		3/8	45	48	7	2	5.2	0.2	26										10,500*						
	-1-1/2 in. (shale feed +10% of -3/8 in.), Curve D			1-1/2	84	14	2	0	23.0	1.5	15			6,200 12,375	6.0 8.3	88.3 90.3			84.8	72.6	14,500**						
	3/8 - 1-1/2 in. (shale feed), Curve E	2.15		1-1/2	100	0	0	0	28	14	2			6,200 12,375	1.0 1.0	77.5 80.1			80.5	62.4					1.0 2.0	2.0 3.0	
	Sample VII-3																										
	Raw shale cores from block sample (Avg. of 9 samples)																										

Note: D_{60} = Grain-size diameter at 60 percent passing.

D_{10} = Grain-size diameter at 10 percent passing.

C_u = Coefficient of uniformity, D_{60}/D_{10}.

* δ_d = 79 pcf; Loading = 4 psi.

** δ_d = 80.7 pcf; Loading = 4 psi.

Table 3

Summary of Physical and Engineering Properties of Raw Paraho Study Oil Shale

Compaction					Relative Density		Permeability, ft/yr				Settlement, % (Consolidation)				Triaxial Shear				Unconfined Compression			Los Angeles Abrasion	Comments
							At Loading, psi				At Loading, psi				Friction		Cohesion psi						
Compaction energy ft-lbs/ft^3	Optimum Moisture, %	Maximum Dry Density at Optimum, pcf	Maximum Dry Density at Half Optimum, pcf	Maximum Dry Density at Air Dry, pcf	Density (100%) pcf	Loose (0%) pcf	50	100	200	1000	50	100	200	1000	ϕ	tan ϕ	C	C' (Saturated)	Moisture Content, %	Density, pcf	Unconfined Compressive Strength, psi		
																					10,027		Modulus of Elasticity 10^6 psi 0.58; ν 0.32
																					7,563		0.82; 0.36
																					10,027		0.56; 0.28 (25% of failure load)
																						14	Angle at repose = 40°
										10,500*									8.3	90.3	9.7		Average of 3 specimens
,200	6.0	88.3			84.8	72.6				14,500**					35	0.70	22.9	15.3					
,375	8.3	90.3													39	0.81	19.4	13.9					
,200	1.0	77.5			80.5	62.4					1.0	2.0	4.5	20.0									
,375	1.0	80.1									2.0	3.0	6.0	17.5									
																			1.3 (0.8-2.5)	126.2 (109.1-1385)	7540 (6320-9720)		

Table 4

Summary of Physical and Engineering Properties of Retorted Oil Shales

Reference Number	Material/Sample Description or Designation	Specific Gravity: Apparent	Specific Gravity: Mean	Gradation: Maximum Particle Size, in.	Gradation: >No. 4 (Gravel)	Gradation: <No. 4, >No. 200 (Sand)	Gradation: <No. 200 (Silt & Clay)	Gradation: <0.005 mm (Clay)	Gradation: D_{60}, mm	Gradation: D_{10}, mm	Gradation: C_u	Atterberg Limits: Liquid Limit	Atterberg Limits: Plasticity Index	Compaction: Compaction Energy ft-lbs/ft3	Compaction: Optimum Moisture, %	Compaction: Maximum Dry Density at Optimum, pcf	Compaction: Maximum Dry Density at Half Optimum, pcf	Compaction: Maximum Dry Density at Air Dry, pcf	Relative Density: Density (100%) pcf	Relative Density: Loose (0%) pcf	Permeability, ft/yr: At Loading, psi: 50	100	200	1000	Settlement, % (Consolidation): At Loading, psi: 50	100	200	1000	Triaxial Shear: Friction: ϕ	tan ϕ	Cohesion psi: C	C' (Saturated)	Unconfined Compression: Moisture Content, %	Density, pcf	Unconfined Compressive Strength, psi	Los Angeles Abrasion	Comments
15	Green River Formation Reheated retorted shale																												21.4 27.3 26.8	0.39 0.52 0.51	24 18 18	5 10 20		69.5 67.4 62.1	See Figures 4 & 5 for curving time effect		
18 (Part 2)	Green River Formation Colony Development Operation Semi-works Plant (Avg of 14 observations unless otherwise noted)			3/8 (1/4-1/2)	8.2 (1.5-19.0)	59.9 (42.2-76.2)	31.1 (17.1-47.0)	--	0.71 (0.2-2.11)	0.032 (.014-0.05)	29 (4.7-111)			12,375 33,750 56,250	19.4 (15.7-21.8) 17.4 (16.6-18.1) 15.7 (14.2-17.2)	95.8 (88.2-100.4) 106.7 (106.5-106.8) 108.5 (107.8-109.2)																							12 observations for std compaction, 2 observations for 60 percent modified and modified compaction
18 (Part 4)	Green River Formation Colony Development Operation Semi-works Plant	2.525		3/16	0	47	53	--	0.095	0.0065	15	30	6	56,250	17.0	100.0			32.0 52.5 86.5 63					-- -- -- -- 15.5 10.5 0 0.5 18.0 13.0 .5 1.0 23.0 19.0 1.0 2.0 Final specimen tested at $W_{molding}$ - no inundation														Consolidation specimens δ_{dry} = 56.5 pcf = 65.0 pcf = 86.6 pcf = 71.0 pcf
18 (Part 5)	Green River Formation Colony Development Operation Semi-works Plant																												35° 35° 35° 20°	6.3 12.5 19.4 0	Q-test R-test (Back-pressure saturated)						w = 5-20%, δ_d = 85 pcf w = 5-20%, δ_d = 90 pcf w = 10%, δ_d = 95 pcf δ_d = 85-90 pcf
21	Green River Formation Laramie Energy Research Center		1.85	3/4	53	47	0	0	7	0.074	95	--	NP																							48.5	
22	Green River Formation, USBM Experimental and Demonstration Facility, Parahо Oil Shale Project As received Size 1	2.53		3/16	0	37	63	--	0.060	0.0024	25	--	--	6,200 12,375 56,250	23.7 23.7 19.9	91.3 93.2 99.5	84.9 90.5 96.1	85.9 91.1 95.0			1.57	1.04	0.72	--	1.3	1.8	2.2	12.8	32.4	0.635 (Q-test)	17.4	12.5	--	--	26.7		
	Size 2	2.13		3/4	26	30	44	--	0.50	.0034	147	--	--	6,200 12,375 56,250	20.0 20.2 15.3	95.8 98.3 104.6	92.5 95.8 102.5	92.8 94.2 99.2			0.56	0.53	0.61	--	2.8	3.4	4.8	--									
	Size 3	2.11		1-1/2	42	22	36	--	5.8	.0034	1705	--	--	6,200 12,375 56,250	18.5 15.5 14.4	99.2 103.2 108.4	94.4 95.8 104.0	93.8 95.8 104.2			1.32	1.07	0.87	--	1.8	2.2	3.7	--	34.2	0.68 (Q-test	2.2	--				21.5	LAA Run on 1/2 - 1-1/2-in. material
23	Green River Formation, USBM Experimental and Demonstration Facility, Paraho Oil Shale Project																																			
	High Carbonate Decomposition As received	2.56		3	76	17	7	2	13	0.21	62	--	NP																								
	Low Carbonate Decomposition As received	2.58		3	73	20	7	3	12	0.033	364	--	NP																								
	High Carbonate Decomposition Size 1	2.56		1-1/2 1-1/2 1-1/2 1-1/2 1-1/2	79 54 50 48 52	14 28 31 32 36	7 18 19 20 12	-- -- -- --						0 6,200 12,375 56,250 12,375	22.0 19.8 22.0 21.8	77.0 80.2 88.8 80.2	76.5 80.0 87.0 --	73.6 79.8 88.1 --	82.3	59.2	(70 psi)* 2088 157 51.0 828	(145 psi)* 1016 713 40.1 307	(300 psi)* 480 40.6 16.1 146	14.5	(70 psi)* 1.6 1.1 0.4 0.5	(145 psi)* 2.4 1.3 1.2 0.8	(300 psi)* 2.8 1.4 1.3 1.1	5.3	35.8 35.0 37.6 30.1	0.72 0.70 0.77 0.58 (S-tests)	13.2 12.5 13.9 48.6	9.0 3.5 18.7 38.2	-- --	-- --	22.6 64.8		Shear and permeability placement w = 0% 14-day cure
	Low Carbonate Decomposition Size 1	2.58		1-1/2 1-1/2 1-1/2 1-1/2 1-1/2	72 49 45 35 52	16 25 19 27 24	12 26 36 38 24	-- -- -- --						0 6,200 12,375 56,250 12,375	22.0 22.0 22.0 24.0	93.0 96.6 102.5 96.6	87.7 94.6 96.9 --	91.1 96.1 102.4 --	85.3	76.3	199.0 167.6 2.10 2.30	118.3 140.4 1.76 1.52	75.8 80.6 1.07 1.36	4.72	2.8 3.0 3.4 0.4	3.4 4.1 3.6 1.2	4.4 5.5 3.9 1.5	10.7	37.2 34.2 42.9 29.7	0.76 0.68 0.93 0.57 (S-tests)	13.2 9.7 13.2 22.9	5.6 9.7 13.2 13.9	-- --	-- --	10.4		Shear and permeability placement w = 0% 14-day cure
	High-Carbonate Decomposition Size 2			3/4	70	20	10	--						12,375	19.8	78.6	--																--	--	22.6		

(Continued)

Note: D_{60} = Grain-size diameter at 60 percent passing.
D_{10} = Grain-size diameter at 10 percent passing.
C_u = Coefficient of uniformity, D_{60}/D_{10}.
* Loading conditions for Reference 23 only.

Table 4 (Continued)

Reference Number	Material/Sample Description or Designation	Specific Gravity: Apparent	Specific Gravity: Mass	Gradation: Maximum Particle Size, in.	Gradation: >No. 4 (Gravel)	Gradation: <No. 4, >No. 200 (Sand)	Gradation: <No. 200 (Silt & Clay)	Gradation: <0.005 mm (Clay)	Gradation: D_{60}, mm	Gradation: D_{10}, mm	Gradation: C_u	Atterberg Limits: Liquid Limit	Atterberg Limits: Plasticity Index	Compaction: Compaction Energy ft-lbs/ft³	Compaction: Optimum Moisture, %	Compaction: Maximum Dry Density at Optimum, pcf	Compaction: Maximum Dry Density at Half Optimum, pcf	Compaction: Maximum Dry Density at Air Dry, pcf	Relative Density: Density (100%) pcf	Relative Density: Loose (0%) pcf	Permeability, ft/yr: At Loading, psi: 50	100	200	1000	Settlement, % (Consolidation): At Loading, psi: 50	100	200	1000	Triaxial Shear: Friction: ϕ	tan ϕ	Cohesion psi: C	C' (Saturated)	Unconfined Compression: Moisture Content, %	Density, pcf	Unconfined Compressive Strength, psi	Los Angeles Abrasion	Comments
23	(Continued)																				(70 psi)	(145 psi)	(300 psi)		(70 psi)	(145 psi)	(300 psi)										
	Low Carbonate Decomposition Size 2			3/4	64	22	14	--						12,375	24.2	95.2	--	--															--	--	10.4		
	High Carbonate Decomposition Size 3			3/16	0	67	33	--						12,375	31.0	80.0	--	--										12.5	30.1	0.58 (S-test)	131.9	52.1					
	Low Carbonate Decomposition Size 3			3/16	0	48	52	--						12,375	24.0	90.5	--	--							1.8	2.5	3.7	12.1	32.2	0.63 (S-test)	45.1	20.8					
	High Carbonate Decomposition Size 1 crushed			3/16	0	76	24	4																													
	80 percent size 1 + 20 percent size 1 crushed			1-1/2	55	33	12	--						12,375	19.5	85.0	--	--			6.5	2.6	1.8	--	0.7	0.7	0.8	--									
	Raw shale			3/8	43	50	7	3																													
	80 percent size 1 + 20 percent raw shale			1-1/2	73	20	7	--						12,375	17.5	82.7	--	--			130.0	56.0	49.2	--	0.8	1.0	1.2	--									As received reject
	Low Carbonate Decomposition Size 1 crushed			3/16	0	34	46	5																													
	80 percent size 1 + 20 percent size 1 crushed			1-1/2	56	27	17	--						12,375	24.2	96.7	--	--			1.5	1.19	0.30	--	1.5	1.8	2.2	--									
	Raw shale			3/8	42	51	7	2																													
	80 percent size 1 + 20 percent raw shale			1-1/2	68	22	10	--						12,375	19.0	97.4	--	--			147.3	29.0	17.4	--	2.4	4.8	5.6	--									As received reject
24	Green River Formation Paraho Semi-works Plant-Direct Heating Mode																																				
	Sample IV-1A			2	66	21	13	2				--	NP																								
				3/4	33	34	33	--						12,375	20.7	91.2																	22.0	--	17		
	Sample IV-1B	2.59		2	55	23	22	2				--	NP																								
				3/4	23	41	36	--						12,375	25.5	89.0																	22.0	--	24		
				1-1/2	43	26	31	2																											68.0		
				1-1/2	43	28	29	--						6,200	23.7	88.0	85.8	85.8			15.0	5.5	1.7	--	2.8	3.0	3.2	--	34.6	0.69	19.4	15.3					
				1-1/2	42	29	29	--						12,375	22.0	92.5	89.5	89.9			7.0	1.4	0.8	--	1.4	1.6	1.7	--	34.2	0.68	27.8	24.3	22.0	89.0			Shear and permeability placement w = 0% 28-day cure on q_u
				1-1/2	33	31	36	--						56,250	22.0	98.7	96.4	96.4			1.1	0.6	0.08	--	0.9	1.0	1.1	--	34.6	0.69 (S-tests)	36.1	29.2					
	Sample IV-1B Initial			1-1/2	45	31	24	3																													
	After permeability			--	32	36	32	5						12,375	22.0	95.5					0.8	0.4	0.3	--	0.8	0.8	0.8	--									
	Initial			1-1/2	54	22	24	2																													
	After compaction			--	43	28	29	--						12,375	22.0	92.5					7.0	1.4	0.8	--	1.4	1.6	1.7	--									
	Initial			1-1/2	65	19	16	2																													
	After permeability			--	48	27	25	4						12,375	22.0	95.5					1.6	0.6	0.4	--	0.7	0.8	0.9	--									
	Initial			3/4	45	30	25	3																													
	After compaction			--	36	36	28	4						12,375	22.0	91.0																	22.0	91.0	161.8		28-day cure
	Initial			3/4	55	25	20	3																													
	After compaction			--	42	35	23	4						12,375	22.0	88.6																	22.0	88.6	168.1		28-day cure
	Initial			3/4	65	19	16	3																													
	After compaction			--	43	29	28	--						12,375	22.0	90.5																	22.0	90.5	163.5		28-day cure
	Initial			3/16	0	56	44	6																													
				--	0	53	47	7						12,375	25.5	89.5																	22.0	--	297.2		28-day cure
	Sample IV-1B2	2.59	1.83	2	52	35	13	4																													
				1-1/2	51	37	12	3						0																								
					33	52	15	--						6,200	22.0	87.5	86.2	86.5																			
					32	52	16	--						12,375	22.0	94.8	91.2	92.2																			
					26	58	16	--						20,000	22.0	94.0	92.8	93.8																			
					24	59	17	--						56,250	22.0	98.9	96.1	97.6																			
																					0.3	0.25	0.15	--	0.8	0.9	1.0	--									0-day cure
																					0.75	0.75	1.7	--	0.15	0.25	0.5	--									28-day cure
				3/4	38	46	16	3						0																								
					28	56	16	--						6,200	27.2	85.5																						
					22	63	15	--						12,375	25.2	90.2																						
					21	64	15	--						20,000	22.0	93.2																						
					18	68	14	--						56,250	22.0	96.4																	22.0	--	142.4		7-day cure
																																		24.0	--	206.9		28-day cure
																																		24.0	--	218.8		60-day cure

(Continued)

Table 4 (Concluded)

Reference Number	Material/Sample Description or Designation	Specific Gravity: Apparent	Specific Gravity: Mass	Gradation: Maximum Particle Size, in.	Gradation: >No. 4 (Gravel)	Gradation: <No. 4, >No. 200 (Sand)	Gradation: <No. 200 (Silt & Clay)	Gradation: <0.005 mm (Clay)	Gradation: D_{60}, mm	Gradation: D_{10}, mm	Gradation: C_u	Atterberg Limits: Liquid Limit	Atterberg Limits: Plasticity Index	Compaction: Compaction Energy ft-lbs/ft3	Compaction: Optimum Moisture, %	Compaction: Maximum Dry Density at Optimum, pcf	Compaction: Maximum Dry Density at Half Optimum, pcf	Compaction: Maximum Dry Density at Air Dry, pcf	Relative Density: Density (100%) pcf	Relative Density: Loose (0%) pcf	Permeability, ft/yr: At Loading, psi: 50	100	200	1000	Settlement, % (Consolidation): At Loading, psi: 50	100	200	1000	Triaxial Shear: Friction: ϕ	Friction: tan ϕ	Cohesion psi: C	Cohesion psi: C' (Saturated)	Unconfined Compression: Moisture Content, %	Unconfined Compression: Density, pcf	Unconfined Compression: Unconfined Compressive Strength, psi	Los Angeles Abrasion	Comments
24	(Continued)																																			
	Paraho Semi-works Plant-Indirect Mode																																			
	Sample IV-I-1H	2.55	1.80	2	70	18	12	3				--	NP																							
				1-1/2	68	21	11	2						0																							
				--	47	40	13	2						6,200	22.0	93.9	90.5	89.0			71	52	30	--	2.1	2.7	4.2	--									
					42	44	14	2						12,375	18.0	98.8	94.9	94.4			3.8	3.7	2.9	--	1.2	2.0	3.8	--	29.2	0.56 (S-test)	3.0	2.9					
					38	43	19	--						56,250	18.0	105.8	101.6	102.1			2.0	2.5	2.4	--	1.0	1.6	2.2	--									
				3/4	55	29	16	3						0																							
					49	36	15	3						12,375	22.0	99.2																					
																																	24.0	--	11.8		28-day cure
																																24.0	--	15.3		60-day cure
																																24.0	--	10.8		120-day cure
	Paraho Semi-works Plant-Direct Heating Mode																																			
	IV-S1			3/4										12,375																						1-hour seasoning time
				3/4										12,375																			22.0	91.0	26.6	70%	28-day cure
				3/4										56,250																			24.0	92.5	26.8		28-day cure
				3/4										56,250																			24.0	95.0	27.8		28-day cure
				3/4										56,250																			24.0	95.0	28.5		60-day cure
																																24.0	95.0	65.3		120-day cure
	IV-SC1			3/4										56,250																			24.0	95.0	42.0		28-day cure
				3/4										56,250																			24.0	95.0	45.9		60-day cure
				3/4										56,250																			24.0	95.0	66.7		120-day cure
	IV-1B2																																			1-hour seasoning time
	+3 percent cement			3/4										56,250																			23.0	96.4	314.9		28-day cure
	+3 percent lime			3/4										56,250																			23.0	96.4	280.6		28-day cure
	IV-1B2 (K_o tests)			3/4	32	53	15	4	2.74	0.043	64			0																							
				3/4										6,200	27.2	85.5																					
				3/4										12,375	25.2	90.2																					
				3/4										56,250	22.0	96.4																					
				3/4		(plus 1 percent lime)								12,375	26.2	90.2																					
				3/4		(plus 3 percent lime)								12,375	28.2	90.2																					
				3/4		(plus 1 percent cement)								12,375	26.2	90.2																					
				3/4		(plus 3 percent cement)								12,375	28.2	90.2																					
				1-1/2	46	42	12	3	6.66	0.055	121			0																							
				1-1/2										6,200	22.0	87.5																					
				1-1/2										12,375	22.0	94.8																					
				1-1/2										56,250	22.0	98.9																					

Deformation Modulus, psi	μ	K_o	Number of Tests	Curing Time Days	Comments
6,370	0.296	0.420	2	28	Column headings pertaining to K_o test series
5,894	0.306	0.442	2	60	Specimens molded at W_{opt} and δ_{max}
11,185	0.268	0.374	1	36	Saturated prior to testing
9,680	0.289	0.406	2	30	
9,867	0.293	0.416	1	60	
23,996	0.273	0.381		40	Saturated prior to testing
22,122	0.267	0.364	2	28	
20,348	0.259	0.349	1	60	
12,037	0.300	0.429	2	28	
10,092	0.292	0.415	2	60	
11,760	0.282	0.395	2	28	
11,357	0.283	0.398	1	60	
13,166	0.289	0.406	2	28	
10,379	0.293	0.417	1	60	
16,953	0.261	0.356	2	28	
16,048	0.275	0.383	2	60	
4,765	0.311	0.453	1	28	
8,478	0.293	0.417	1	60	
20,084	0.279	0.389	1	30	
16,358	0.240	0.317	1	100	
51,427	0.203	0.256	1	37	

Table 5

Summary of Field Compaction Test Results Paraho Semi-Works Plant Retorted Shale Research, Phase V

Direct Heat Retorting (from Reference 25)

Identification	Test Section Number	Layer Number	Roller Type	Number of Roller Passes	Laboratory Compaction		Field Compaction			Gradation									Remarks
										% No. 200 Sieve			% No. 200 to No. 4 Sieves			% >No. 4 Sieve			
					Moisture %	Dry Density pcf	Moisture %	Dry Density pcf	Percent Compaction (D 698)	Before Compaction	After Compaction	Change	Before Compaction	After Compaction	Change	Before Compaction	After Compaction	Change	
Laboratory Tests																			
Pilot Plant			Drop	D-698	0	96.1				12	36	+24	16	19	+3	72	45	-27	
Phase III			Hammer	D-698	22.0	96.6													
(Sample 2, Dark)			(ASTM Standard)	D-1557	22.0	102.5				12	38	+26	16	27	+11	72	35	-37	
Semi-Works				D-698	0	89.9				24	29	+5	22	29	+7	54	42	-12	
Plant				D-698	22.0	92.5													
Phase IV (Sample 1-B)				D-1557	22.0	98.7				24	36	+12	22	31	+9	54	33	-21	
Field Tests																			
Semi-Works	A	1-4	Speeps-	6	20.0	93.5	17.3	91.2	98	11	24	+13	42	34	-8	47	42	-5	
Plant	B		foot	10	20.0	95.2	15.4	89.6	94	--	26	--	--	37	--	--	37	--	
Phase V	C			14	20.0	93.6	17.5	96.1	102	19	15	--	31	39	--	50	46	--	
Moisture added	D	1-4	Rubber	6	20.0	96.7	15.6	95.7	99	20	12	--	35	29	--	45	59	--	
at fill	E		tire	10	20.0	94.7	16.0	91.5	97	15	24	--	30	36	--	55	40	--	
	F			14	20.0	90.9	19.3	92.8	102	24	21	--	17	40	--	59	39	--	
8-in. loose layer	O-1	1-4	Vibrator pad	5	18.0	94.3	18.0	97.8	104	16	23	+7	41	44	+3	43	33	-10	
thickness	P-1	1-4	Vibrator smooth	6	20.0	90.9	20.0	99.7	110	14	19	+5	41	42	+1	45	39	-6	
	M-1	1-4	Vibrator pad	4	18.7	91.9	18.7	99.5	108	15	17	+2	38	49	+11	47	34	-13	
			Vibrator smooth	4															
	N-1	1-4	Sheeps-foot	4	19.8	89.4	19.8	96.6	108	16	23	+7	40	45	+5	44	32	-12	
			Rubber tire	6															

(Continued)

Notes: Laboratory compaction and field percent compaction based on standard test compactive effort of 12.375 ft-lb/ft^3.

Field densities and "after compaction" gradations taken in layers 2 and 3 for 8-in. layer compaction and layer 6 for 12-in. layer compaction, unless otherwise noted.

Layer 2 'before compaction" gradations not representative and not included in averages. Others are layers 2 and 3 or layer 6, unless otherwise noted.

Table 5 (Continued)

Identification	Test Section Number	Layer Number	Roller Type	Number of Roller Passes	Laboratory Compaction		Field Compaction			Gradation									Remarks
										% No. 200 Sieve			% No. 200 to No. 4 Sieves			% >No. 4 Sieve			
					Moisture %	Dry Density pcf	Moisture %	Dry Density pcf	Percent Compaction (D 698)	Before Compaction	After Compaction	Change	Before Compaction	After Compaction	Change	Before Compaction	After Compaction	Change	
							Field Tests (Continued)												
	R-1	1-4	Tractor	6	21.7	95.5	21.7	97.4	102	12	23	+11	34	44	+10	54	33	-21	
	POND 1	1-15	Vibrator smooth	7	--	--	22.1	100.6	--	--	25	--	--	42	--	--	33	--	
12-in. loose layer thickness	A	5-7	Sheeps-foot	6	20.0	94.4	13.3	83.7	88	23	19	--	44	39	--	33	43	--	
	B			10	20.0	95.0	11.8	86.5	91	24	24	0	42	40	-2	34	36	+2	
	C			14	20.0	88.5	14.1	81.2	92	18	22	+4	33	48	+15	49	30	-19	
	D	5-7	Rubber tire	6	20.0	94.2	13.0	89.6	95	18	23	+5	36	41	+5	46	36	-10	
	E			10	20.0	93.2	15.2	87.6	94	19	23	+4	34	45	+11	47	32	-15	
	F			14	20.0	90.9	15.8	87.9	97	20	22	+2	37	45	+8	43	33	-10	
	0-3	1-3	Vibrator pad	12	20.0	90.1	20.0	93.9	104	17	18	+1	42	48	+6	41	34	-7	
	P-3	1-3	Vibrator smooth	12	17.6	91.3	17.6	100.4	110	17	23	+6	45	43	-2	38	34	-4	
No moisture added to fill	G	1-4	Sheeps-foot	6	6.2	96.6	6.2	94.5	98	31	24	--	21	44	--	48	32	--	
	H			10	3.7	97.2	3.7	94.6	97	30	25	--	13	41	--	57	34	--	
	I			14	6.8	95.1	6.8	91.7	96	36	27	--	15	40	--	49	33	--	
8-in. loose layer thickness	J	1-4	Rubber tire	6	1.7	98.6	1.7	96.7	98	40	16	--	14	41	--	46	43	--	
				10	1.9	98.9	1.9	98.1	99	38	19	--	19	40	--	43	41	--	
				14	1.0	99.4	1.0	101.6	102	23	14	-9	21	36	+15	56	50	-6	
	0-2	1-2	Vibrator pad	6	6.5	93.9	6.5	92.2	98	17	18	+1	42	41	-1	31	31	0	Only 2 of 4 layers completed.
	P-2	1-4	Vibrator smooth	6	0	97.5	0	101.4	104	18	18	0	33	36	+3	49	46	-3	Layers 1 and 2 tested
	R-2	1-4	Tractor	6	4.6	92.7	4.6	94.2	102	10	22	+12	23	43	+20	67	35	-32	Very coarse material
	S-1	1-2	Tractor	10	5.2	92.4	5.2	92.3	100	13	24	+11	35	46	-11	52	30	-22	
	POND	1-16	Haul-spread	--	3.7	93.5	3.7	91.5	98	15	21	+6	30	40	+10	55	39	-16	4 truck passes and 2 loader passes on bottom lining. 2 loader passes on side lining plus travel
	G	5-7	Sheeps-foot	6	0.7	92.2	0.7	89.1	97	19	17	-2	44	42	-2	37	41	+4	
	H			10	0.4	91.6	0.4	89.8	98	13	16	+3	35	42	+7	52	42	-10	
	I			14	0.5	92.0	0.5	88.1	96	18	16	-2	32	41	+9	50	43	-7	

(Continued)

Table 5 (Concluded)

Identification	Test Section Number	Layer Number	Roller Type	Number of Roller Passes	Laboratory Compaction		Field Compaction			Gradation									Remarks
										% No. 200 Sieve			% No. 200 to No. 4 Sieves			% >No. 4 Sieve			
					Moisture %	Dry Density pcf	Moisture %	Dry Density pcf	Percent Compaction (D 698)	Before Compaction	After Compaction	Change	Before Compaction	After Compaction	Change	Before Compaction	After Compaction	Change	
Field Tests (Continued)																			
	J	5-7	Rubber tire	6	0.5	91.5	0.5	84.1	92	13	16	+3	31	46	+15	56	38	-18	
	K			10	0.7	94.5	0.7	92.4	98	14	18	+4	31	42	+11	55	40	-15	
	L			14	1.9	96.7	1.9	94.4	98	12	20	+8	30	41	+11	58	39	-19	
	O-4	1-2	Vibrator pad	6	2.1	96.2	2.1	91.7	95	17	16	-1	38	36	-2	45	48	+3	Only 2 of 4 layers completed. Layers 1 and 2 tested for gradation. Only 1 density test made in layer 2
	P-4	1-3	Vibrator smooth	9	3.5	92.3	3.5	90.7	98	15	20	+5	27	36	+9	58	44	-14	
	S-2	1-3	Tractor	10	3.8	96.7	3.8	93.3	97	12	22	+10	33	41	+8	55	37	-18	
					--	93.9	--	93.0	99	16	20	+4	36	42	+6	48	38	-10	Average of all tests
	Summary of all field tests				19.8	92.8	17.1	93.0	100	16	21	+5	38	42	+4	46	37	-9	Average for all tests in wetted area
					2.8	95.0	2.8	93.1	98	15	19	+4	34	41	+7	51	40	-11	Average for all tests in non-wetted area

APPENDIX A: OIL SHALE RETORTING PROCESSES

1. Three retorting processes are used to extract oil from oil shale:

a. Solid to solid heat transfer (Tosco process).

b. U. S. Bureau of Mines gas combustion method.

c. Gas to solid heat transfer (Petrosix process).

Tosco Process

2. Figure A1 shows a flow diagram of the Tosco process. In this process the shale is mixed with preheated balls in a horizontal rotating kiln. The gas produced is of high quality and can be refined for its valuable components. The process can take a large amount of finely crushed shale particles. The process efficiency is further increased by the reduction of particle size by the crushing action of the balls. One disadvantage of this process is that it produces a large amount of fine waste material which may increase disposal problems.

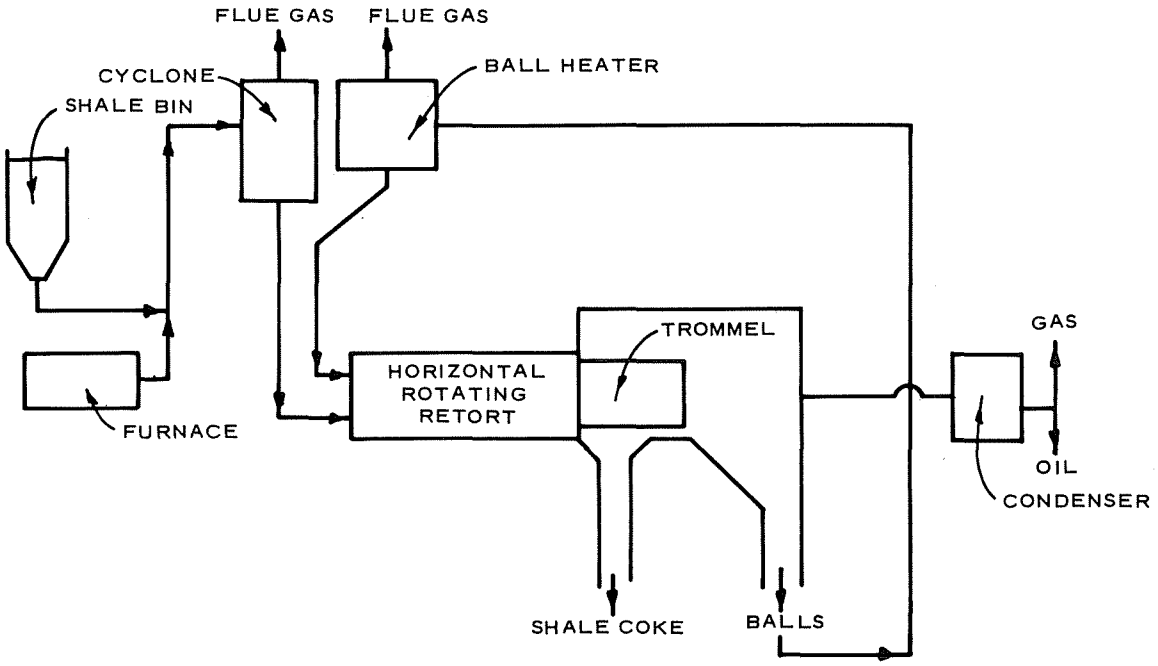

Figure A1. Tosco process

Gas Combustion Process (Paraho)

3. Figure A2 shows a flow diagram of the U. S. Bureau of Mines gas combustion process. A stream of crushed shale enters at the top and is preheated by the combustion gases. Air and recycling gas are injected at the midpoint and are burned, bringing the oil shale above this point to retorting temperature. Some of the spent shale is consumed as fuel in the burning process. The gas entering at the bottom is heated by the burnt shale before it is ignited.

4. Major disadvantages of this process are that it produces a low Btu gas product and it is not able to process the fines that result from crushing the shale. It has the advantage of producing a waste material in the form of a soft friable rock containing approximately 2 to 3 percent carbon.

Petrosix Process

5. Figure A3 shows a flow diagram of the gas to solid heat transfer system for extraction of oil from oil shale. This process has many of the same features as the gas combustion process except that no actual burning takes place inside the kiln. The oil shale is fed in at the top and cold gas at the bottom. The temperature increases toward the middle of the kiln where a preheated gas is injected. This process produces a gas that is not contaminated with combustion products. It is possible to recover sulfur, ammonia, and other valuable components from the high-Btu gas product.

6. A major disadvantage of this process is that the facility cannot process the fines that result from crushing the shale because the gas pressure drop across the kiln would increase excessively. The waste products contain enough carbon so that they can be burned and used for heating of the recycling gas.

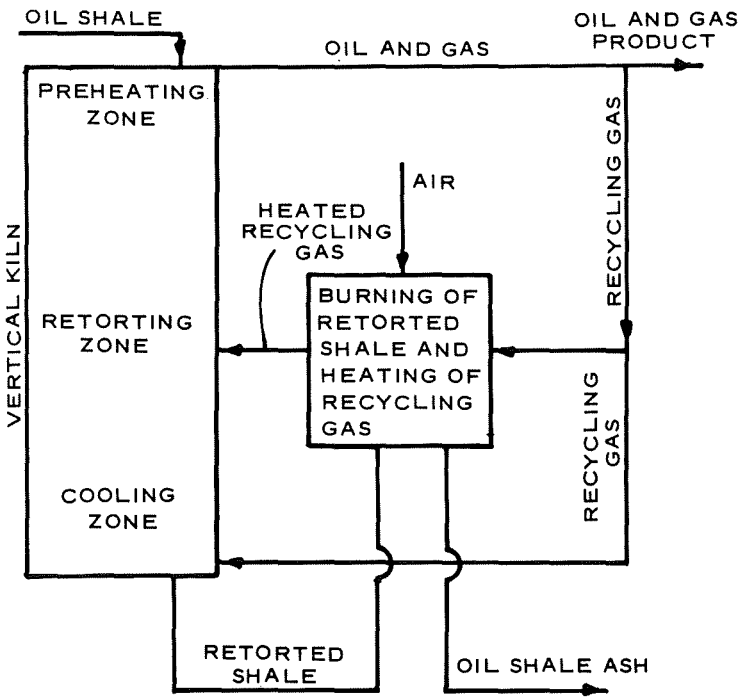

Figure A2. Gas combustion process

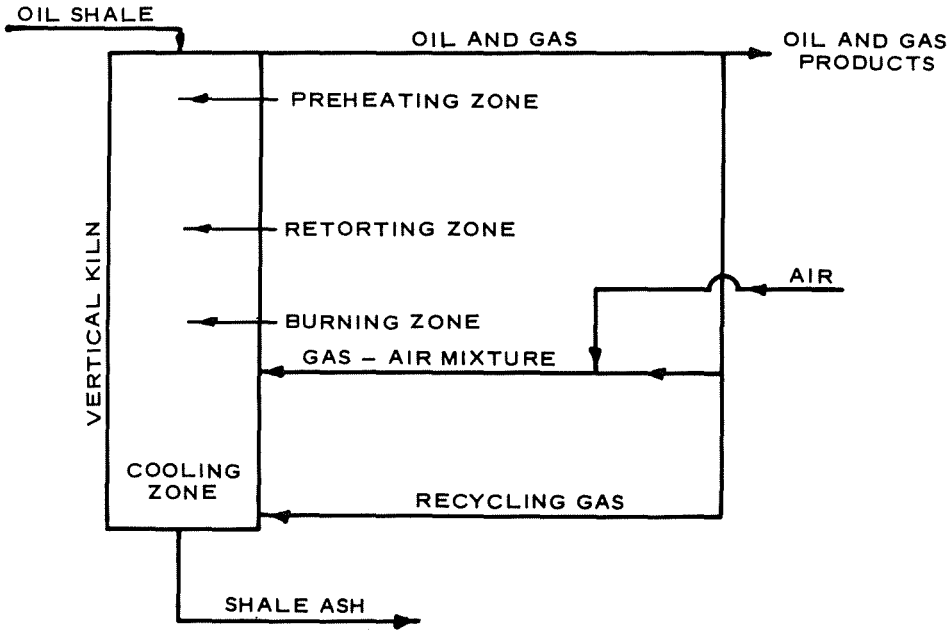

Figure A3. Petrosix process

APPENDIX B: RESULTS OF BIN AND HOPPER TESTS AND RECOMMENDATIONS FOR RAW OIL SHALE STORAGE BINS

(Prepared Under WES Purchase Order No. DACW 39-77-M-2633 (4/5/77))

by

Jenike and Johanson, Inc.,
No. Billerica, Mass.

SELECTION OF BIN TYPE AND FEEDER SIZE

Types of bins

In the process of selection of a bin [1,2]*, the first step is to decide on the type of bin. From the standpoint of flow, there are three types of bins: mass-flow, funnel-flow and expanded-flow.

Mass-flow bins are particularly suitable for powders, cohesive solids, solids which degrade with time, and when segregation needs to be minimized. Mass-flow bins give a uniform feed density often permitting the use of volumetric feed control in place of gravimetric control. Low level indicators work reliably in mass-flow bins.

Examples of mass-flow bins are shown in Figures 1a and 1b. In mass-flow bins, the hopper, i.e. the converging part of a bin, is sufficiently steep and smooth to cause flow of all the solid without stagnant regions whenever any solid is withdrawn. This produces uniform flow and a feed density which is practically independent of the head of solid in the bin. Segregation is minimized because, while a solid may segregate at the point of charge into the bin, continuity of flow enforces remixing of the fractions within the hopper [1,3]. Mass-flow bins have a first-in first-out flow sequence. This is useful in the storage of solids which degrade with time and of powders which thus deaerate with a minimum of residence time. Powders do not flush as long as a sufficient head of solid is maintained and the gravity flow rate is not exceeded; air locks are not needed [4,5,6].

Fig. 1a defines the outlet width for oval outlets and the hopper slope angles for transition hoppers.

Fig. 1b defines the outlet diameter and the hopper slope angle for circular, conical hoppers.

The minimum outlet dimensions are given in "Results of Flow Tests," Sections I-A and I-B. The length of an oval outlet should be at least

* Numbers in brackets designate references listed on page 5.

three times its width. The maximum slope angles (measured from the vertical) are given in Section III for the specified wall materials and conditions of storage. For some solids and wall materials, the slope angles vary with the size of the outlet.

Valleys are not permitted. Ledges and protrusions into a mass-flow channel are not allowed. If a hopper is equipped with a shut-off gate, the gate must be fully open for mass flow to be possible.

Mass-flow bins of special design can be used for in-bin blending by circulation of solid [7].

Funnel-flow bins are suitable for coarse, free-flowing or slightly cohesive, non-degrading solids when segregation is unimportant. Examples of funnel-flow bins are shown in Figures 2a, 2b and 2c. Funnel flow occurs when the hopper is not sufficiently steep and smooth to allow material to slide along the walls or when the outlet of a mass-flow bin is not fully effective (see "Feeders" below). In these bins, solid flows toward the outlet through a channel that forms within stagnant solid. The diameter of that channel approximates the largest dimension of the effective outlet. When the outlet is fully effective, this dimension is the diameter of a circular outlet, or the diagonal of a square or rectangular outlet. As the solid within the channel flows out, layers slough off the top of the stagnant mass into the channel. This spasmodic behavior is particularly pronounced with cohesive solids and with powders. A powder, sloughing off the top, aerates as it falls into the channel and may flush out if the level of solid in the bin is low. With a cohesive solid, a channel may empty out completely (rathole) and powder charged into the bin then flushes through. A rotary valve is often used under these conditions to contain the material, but a uniform flow rate cannot be ensured with this arrangement because flow into the valve is erratic. These bins are more prone to cause arching of cohesive solids than are mass-flow bins and, hence, frequently require larger outlets for dependable flow.

Such a large outlet may preclude the use of a rotary valve. These bins also cause segregation of solids [1,3] and are unsuitable for solids which degrade with time because of the stagnant regions.

Figures 2a and 2b define the outlet dimensions for rectangular outlets. Fig. 2c defines the outlet dimension for circular outlets.

The minimum dimensions are listed in Sections I-A and I-B. The length of a slot should be either not less than D_f, Fig. 2a, or equal to the full diameter of the bin, Fig. 2b. Usually D_f is much larger than B_f and a long rectangular (slot) outlet is more advantageous than a circular or square one.

Clean out of a funnel-flow bin is often uncertain because solid in the stagnant regions may pack hard and cake. Mass-flow bins should be specified when clean out is mandatory.

Expanded-flow bins are recommended for the storage of large quantities of non-degrading solids. This design is also useful as a modification of existing funnel-flow bins to correct erratic flow caused by arching, rat-holing or flushing. The concept can be used with single or multiple outlets.

Examples of expanded-flow bins are shown in Figures 3a and 3b. The lower part of such a bin is designed for mass-flow. The mass-flow outlet usually requires a smaller feeder than would be the case for a funnel-flow bin. The mass-flow hopper expands the flow channel to a diagonal or diameter equal to or greater than D_f, thus eliminating the likelihood of rat-holing. In the case of powders, the volume of the mass-flow hopper should ensure sufficient residence time for deaeration.

Feeders

The specified outlet must be fully effective. If flow from the bin is controlled by means of a feeder, the feeder must be so designed as to draw uniformly through the entire cross-section of the outlet [1,2].

Vibrating equipment

Vibration has two effects: on the one hand it tends to break up the arches that obstruct flow, on the other it packs so stagnant solid

gains greater strength. In order to allow for this packing, the outlet dimensions for flow with vibration are often larger than those for gravity flow without vibration.

Many fine and wet materials tend to pack severely when vibrated, and vibrating equipment is not recommended for them. The applicability of vibrating equipment can be judged from Section I-B of the "Results of Flow Tests" which lists the minimum outlet dimensions required for flow with vibrating equipment. These dimensions refer to the outlet dimensions of a static bin that discharges into vibrating equipment.

External vibrators are particularly suitable for materials which are free-flowing under conditions of continuous flow, but set up and gain strength when stored at rest for hours or days. Hoppers for these materials should always be equipped with pads for the mounting of external vibrators.

Flow rate of powders

The rate at which a coarse solid discharges through an outlet [8] is usually sufficient to satisfy the requirements of the process. The situation is different with powders. Density changes which occur within a flowing mass, combined with the low permeability of a powder, cause air pressure gradients within the mass and these gradients critically affect the rate of powder discharge from a bin. Depending on the fineness of the powder, its volumetric rate of gravity discharge may be one hundredth or one thousandth that of a coarse solid.

If the flow rate tests have been run, conservative estimates of the maximum rate for mass-flow hoppers are shown in Section IV of the "Results of Flow Tests." They are based on material discharging onto a belt feeder.

These flow rates can be increased significantly using an air permeation technique (patent pending). Examples of the application of air permeation are given in references [4,5,6].

Calculation of effective consolidating head h_e

The critical rathole diameter D_f (Section I), bulk density (Section II), wall friction angle φ' (Section III), and fine powder flow rate (Section IV) are functions of the consolidation pressure of the solid in the pertinent regions of the bin. To calculate the critical rathole diameter and fine powder flow rate, this pressure is specified by the effective head of solid in the bin h_e as follows:

$$h_e = \frac{R}{\mu K}\left[1 - e^{-\mu K \frac{h}{R}}\right] \qquad (1)$$

or $h_e = 2R$ whichever is larger

where

R = hydraulic radius of the cylinder (cross-sectional area/circumference)
R = D/4 for a circular cylinder of diameter D
R = W/2 for a long rectangular cylinder of width W

μ = coefficient of friction on the cylinder walls
$\mu = \tan \phi'$

K = ratio of horizontal to vertical pressures = 0.4

h = height of vertical bin section

To calculate the bulk density and wall friction angle at the outlet of a mass flow bin,

$h_e = B_p$ for transition hopper
$= B_c/2$ for conical hopper

References

1. Jenike, A. W., "Storage and Flow of Solids," Engineering Experiment Station, University of Utah, Salt Lake City, Utah, Bulletin No. 123, Nov 1964.
2. Johanson, J. R., "Feeding," CHEMICAL ENGINEERING, Deskbook Issue, Oct 13, 1969, pp 75-83.
3. Jenike, A. W., "Why Bins Don't Flow," MECHANICAL ENGINEERING, Vol 86, No 5, May 1964, pp 40-43.
4. Bruff, W. and Jenike, A. W., "A Silo for Ground Anthracite," POWDER TECHNOLOGY, Vol 1, 1967/68, pp 252-256.
5. Reed, G. B. and Johanson, J. R., "Feeding Calcine Dust with a Belt Feeder at Falconbridge," ASME, JOURNAL OF ENGINEERING FOR INDUSTRY, Vol 95, Ser B, No 1, Feb 1973, pp 72-74.
6. Valji, S. E., Wilkinson, C. L., and Jenike, A. W., "Georgia Kaolin Company Solves Calciner Feed Problems," ASME Paper No 72-MH-26 presented at the Second Symposium on Storage and Flow of Solids, Chicago, Illinois Sep 17-20, 1972.
7. Johanson, J. R., "In-Bin Blending," CHEMICAL ENGINEERING PROGRESS, Vol 66, No 6, June 1970, pp 50-55.
8. Johanson, J. R., "Method of Calculating Rate of Discharge from Hoppers and Bins," SME of AIME, TRANSACTIONS, Vol 232, Mar 1965, pp 69-80.

Glossary of terms and symbols

Arching - a no-flow condition in which material forms a stable dome (or arch) across the bin

Bin - container for bulk solids with outlets for withdrawal of solids either by gravity alone or by gravity assisted by flow-promoting devices

Cylinder - vertical part of a bin

Expanded flow - flow pattern which is a combination of mass flow and funnel flow

Feeder - device for controlling the rate of withdrawal of bulk solid from a bin

Flow channel - space in bin through which a bulk solid is actually flowing during withdrawal

Funnel flow - flow pattern in which solid flows in a channel formed within stagnant material

Hopper - converging part of a bin

Mass flow - flow pattern in which all solid in a bin is in motion whenever any of it is withdrawn

Piping - a no-flow condition in which material forms a stable vertical hole within the bin

Ratholing - same as piping

B_c - minimum diameter of a circular outlet in a mass-flow bin to prevent arching, ft

B_f - minimum width of a rectangular outlet in a funnel-flow bin to prevent arching, ft

B_p - minimum width of an oval outlet in a mass-flow bin to prevent arching, ft

D_f - critical piping or ratholing dimension, ft

F - unconfined compressive force, lb; equal to 1/13 times the unconfined compressive strength, psf

H - total height of bin, ft

h - height of cylinder, ft

h_e - effective consolidating head, ft

L - length of hopper outlet, ft

Glossary (cont.)

S	- shearing force applied to a shear cell, lb
V_1	- major consolidating force, lb; equal to 1/13 times the major consolidating pressure, psf
V	- normal force applied to a shear cell, lb
δ	- effective angle of internal friction of a solid during flow, degree
θ_c	- maximum recommended angle (from vertical) of conical hoppers and end walls of transition hoppers for mass flow, degree
θ_p	- maximum recommended angle (from vertical) of side walls of transition hoppers for mass flow, degree
ϕ'	- kinematic angle of friction between a solid and a wall, degree
ϕ_t	- angle of internal friction of a solid for incipient flow, degree

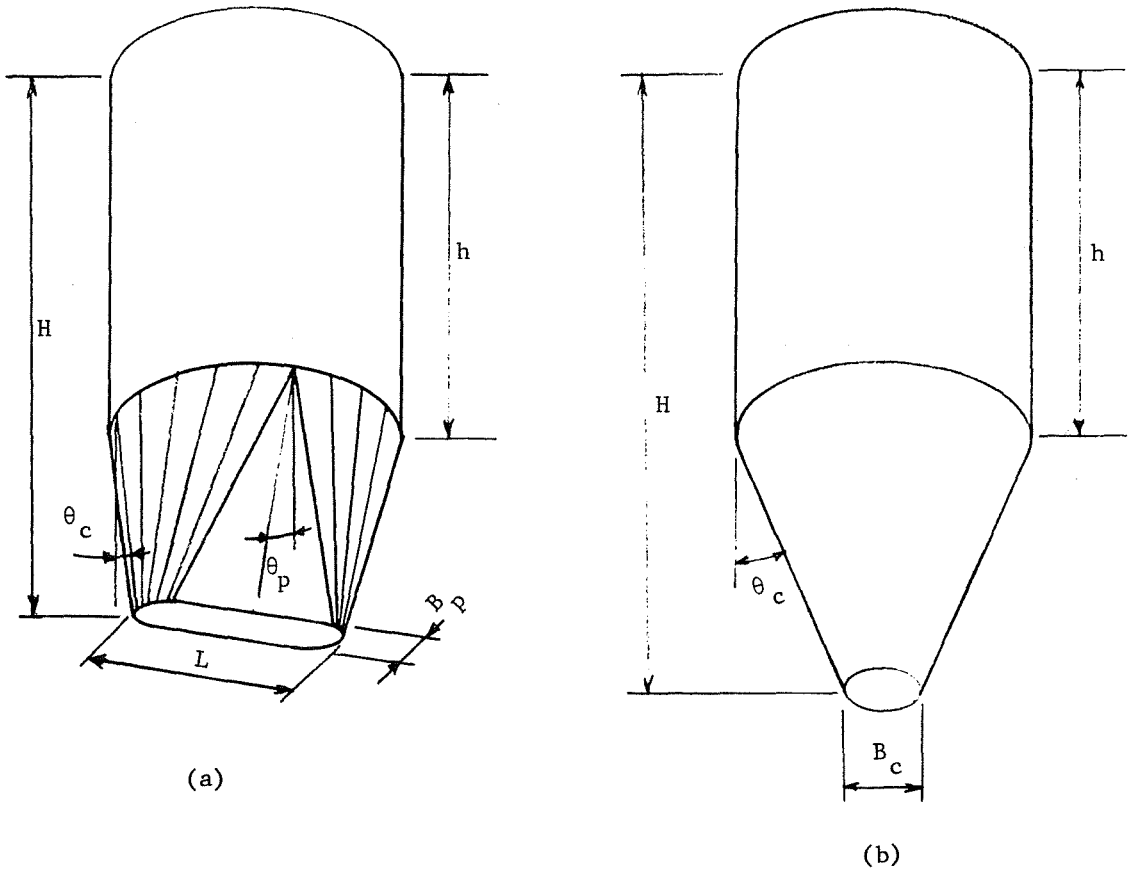

MASS-FLOW BINS

FIG. 1

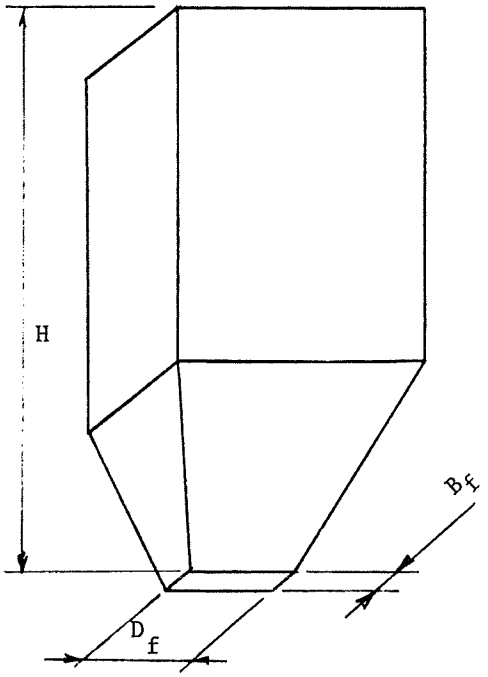

(a)

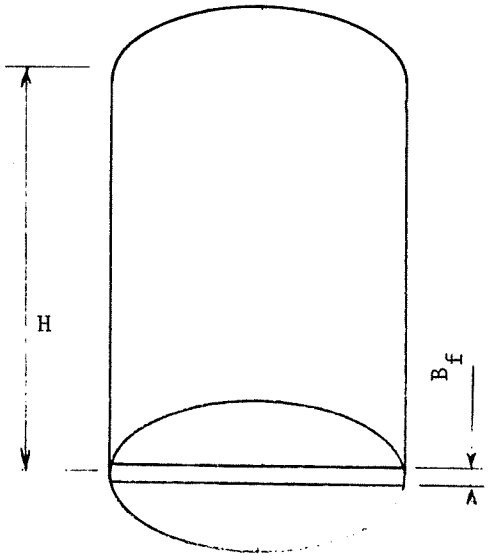

(b)

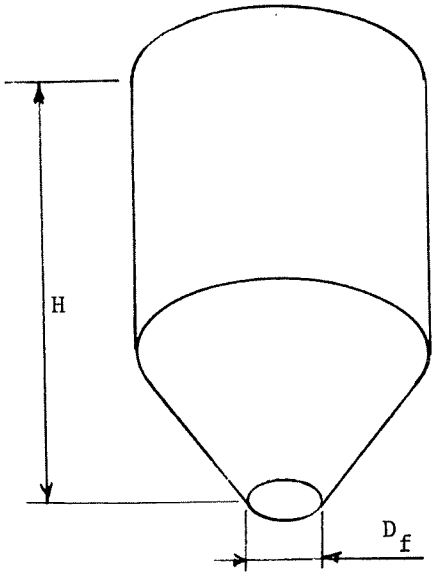

(c)

FUNNEL-FLOW BINS

FIG. 2

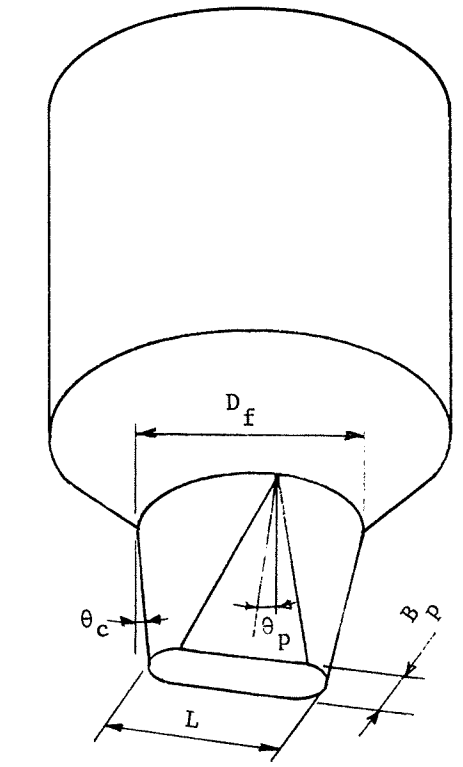

EXPANDED-FLOW BINS

FIG. 3

RESULTS OF FLOW TESTS

Material(s) tested: Oil shale

For each material, results are presented in the following order:

Section I	Minimum outlet dimensions for dependable flow
	A. Gravity flow
	B. With vibrating equipment
Section II	Bulk density as a function of head of solid
Section III	Maximum allowable hopper slope angles
Section IV	Maximum solids flow rate (if tested)

Material Oil shale

Section I. Minimum outlet dimensions for dependable flow

A. Gravity flow

Storage time at rest	Water content, % wet weight	Temperature, °	Mass-flow		Funnel-flow			Ref. Fig.
			Circular outlet diameter B_c, ft	Oval outlet width B_p, ft	Rectangular outlet width B_f, ft	Critical rathole diameter h_e	D_f	
Continuous flow	As Received (1.0)	Amb.	*	*	*	5′	4	4 - 6
						10	7	
						20	15	
						40	29	
3 Days			*	*	*	5′	4	
						10	7	
						20	15	
						40	29	
Continuous flow	5.9		1.3	0.7	0.8	5	7	8 - 10
						10	10	
						20	17	
3 Days			1.3	0.7	0.8	5	7	
						10	10	
						20	17	
Continuous flow	10.7		1.6	0.8	0.9	5	7	12 - 14
						10	12	
						20	22	
3 Days			1.6	0.8	0.9	5	7	
						10	12	
						20	22	

* No minimum dimensions given from tests. Minimum outlet size set by consideration of particle interlocking, flow rate, etc.

Material Oil shale

B. With vibrating equipment

☐ Material not suited to vibration

Water content, % wet weight	Temperature, °	Mass-flow: Circular outlet diameter B_c, ft	Mass-flow: Oval outlet width B_p, ft	Funnel-flow: Rectangular outlet width B_f, ft	Funnel-flow: Critical rathole diameter h_e	D_f	Ref. Fig.
As Received (1.0)	Amb.	*	*	*	5′	5	4 - 6
					10	11	
					20	22	
					40	44	
5.9		1.7	0.8	1.1	5	7	8 - 10
					10	10	
					20	17	
10.7		2.2	1.1	1.9	5	7	12 - 14
					10	12	
					20	22	

* No minimum dimensions given from tests. Minimum outlet size set by consideration of particle interlocking, flow rate, etc.

Section II. Bulk density as a function of effective consolidating head of solid

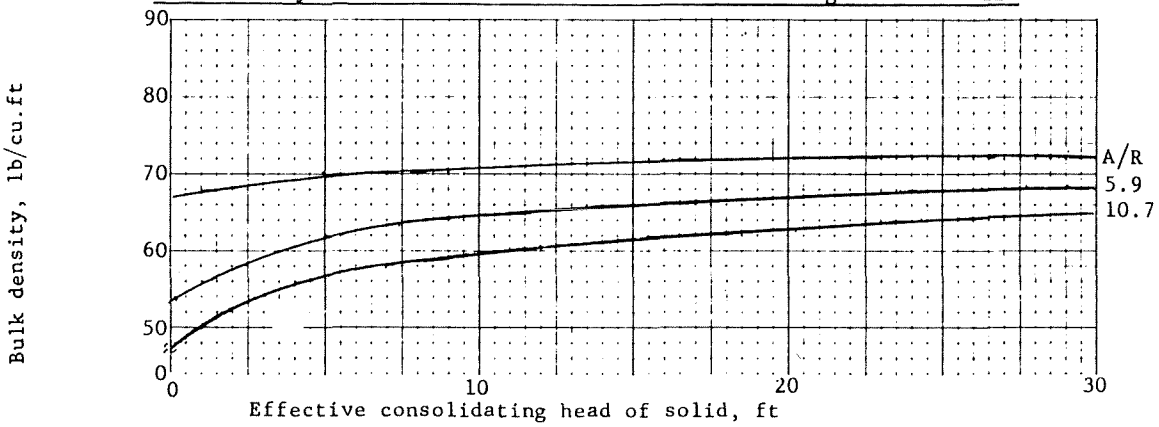

Material Oil shale as received (1.0%) moisture

Section III Friction test results for various wall materials and maximum recommended hopper angles (measured from the vertical) for mass flow

Effective consolidating head, ft		0.25	0.5	1.0	2.0	4.0	5.0
Width B_p of oval outlet, ft		0.25	0.5	1.0	2.0	4.0	5.0
Dia. B_c of Circular outlet, ft		0.5	1.0	2.0	4.0	8.0	10.0
Wall material	Angle deg.						
304 - 2B finish stainless steel	ϕ'	36*	27	20	17	15	15
	θ_c	2	14	23	27	29	29
	θ_p	13	24	34	38	41	41
304 - 2B finish stainless steel 3 day time test	ϕ'	36*	36*	30	21	17	17
	θ_c	2	2	9	21	26	27
	θ_p	13	13	20	32	38	39
304 #1 finish stainless steel	ϕ'	36*	36*	35*	32	31	31
	θ_c	2	2	2	6	8	9
	θ_p	13	13	13	17	19	19
304 #1 finish stainless steel 3 day time test	ϕ'	36*	36*	35*	32	31	31
	θ_c	2	2	2	6	8	9
	θ_p	13	13	13	17	19	19
Carbon steel	ϕ'	32	32	32	32	32	32
	θ_c	6	6	6	6	6	6
	θ_p	17	17	17	17	17	17

* Material may build up on hopper walls.

Material Oil shale 5.9% moisture

Section III Friction test results for various wall materials and maximum recommended hopper angles (measured from the vertical) for mass flow

Effective consolidating head, ft		0.25	0.5	1.0	2.0	4.0	5.0
Width B_p of oval outlet, ft		0.25	0.5	1.0	2.0	4.0	5.0
Dia. B_c of Circular outlet, ft		0.5	1.0	2.0	4.0	8.0	10.0
Wall material	Angle deg.						
304 - 2B finish stainless steel	ϕ'	21	21	21	21	21	21
	θ_c	21	21	21	21	21	21
	θ_p	32	32	32	32	32	32
304 - 2B finish stainless steel 3 day time test	ϕ'	24	24	24	24	24	24
	θ_c	18	18	18	18	18	18
	θ_p	29	29	29	29	29	29
304 #1 finish stainless steel	ϕ'	36*	34	32	31	31	31
	θ_c	2	4	7	8	8	8
	θ_p	13	15	17	18	19	19
304 #1 finish stainless steel 3 day time test	ϕ'	36*	34	32	31	31	31
	θ_c	2	4	7	8	8	8
	θ_p	13	15	17	18	19	19
Carbon steel	ϕ'	33	33	33	33	33	33
	θ_c	5	5	5	5	5	5
	θ_p	16	16	16	16	16	16

* Material may build up on hopper walls.

Material Oil shale 10.7% moisture

Section III Friction test results for various wall materials and maximum recommended hopper angles (measured from the vertical) for mass flow

Effective consolidating head, ft		0.25	0.5	1.0	2.0	4.0	5.0
Width B_p of oval outlet, ft		0.25	0.5	1.0	2.0	4.0	5.0
Dia. B_c of Circular outlet, ft		0.5	1.0	2.0	4.0	8.0	10.0
Wall material	Angle deg.						
304 - 2B finish stainless steel	ϕ'	28	24	22	22	21	21
	θ_c	13	17	19	20	21	21
	θ_p	26	30	31	31	32	32
304 - 2B finish stainless steel 3 day time test	ϕ'	28	24	23	23	23	23
	θ_c	13	17	19	19	19	19
	θ_p	26	30	30	30	30	30
304 #1 finish stainless steel	ϕ'	38*	38*	35	32	31	30
	θ_c	1	1	4	8	9	10
	θ_p	12	12	16	18	19	20
304 #1 finish stainless steel 3 day time test	ϕ'	38*	38*	35	32	31	30
	θ_c	1	1	4	8	9	10
	θ_p	12	12	16	18	19	20
Carbon steel	ϕ'	33	33	33	33	33	33
	θ_c	5	5	5	5	5	5
	θ_p	16	16	16	16	16	16

*Material may build up on hopper walls.

Material Oil shale as received (1.0%) moisture

Section IV. Maximum solids flow rate onto a belt feeder without air permeation

A. From a conical mass-flow hopper with an effective consolidating head h_e =

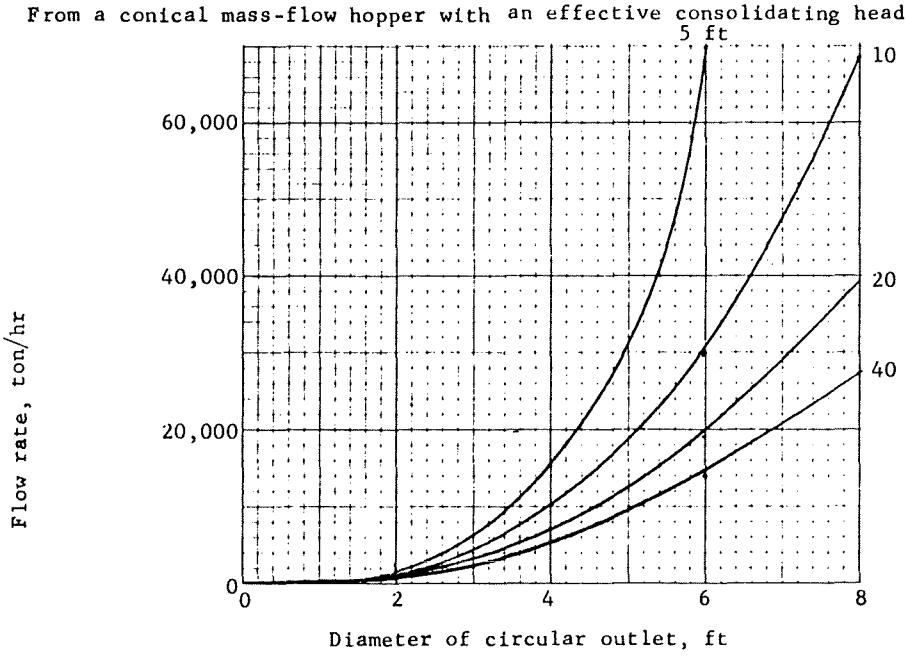

B. From a transition mass-flow hopper with an effective consolidating head h_e =

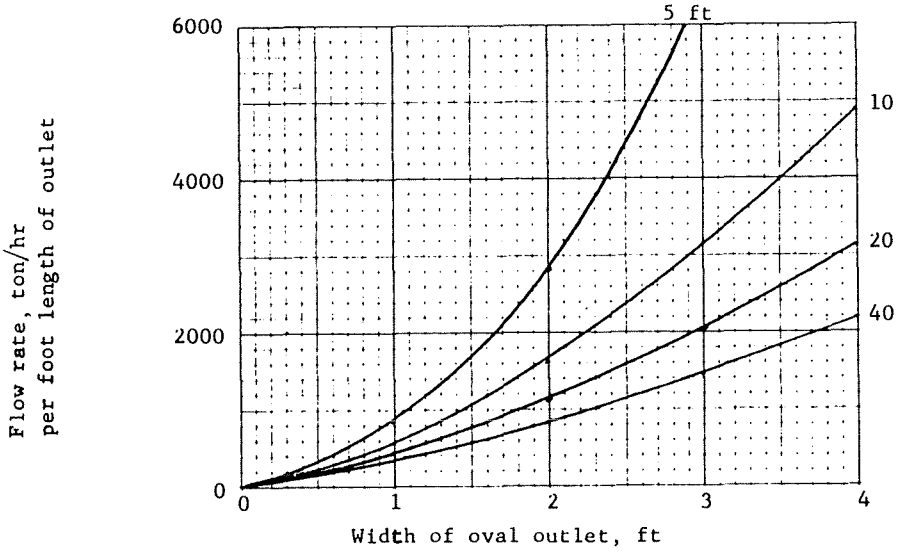

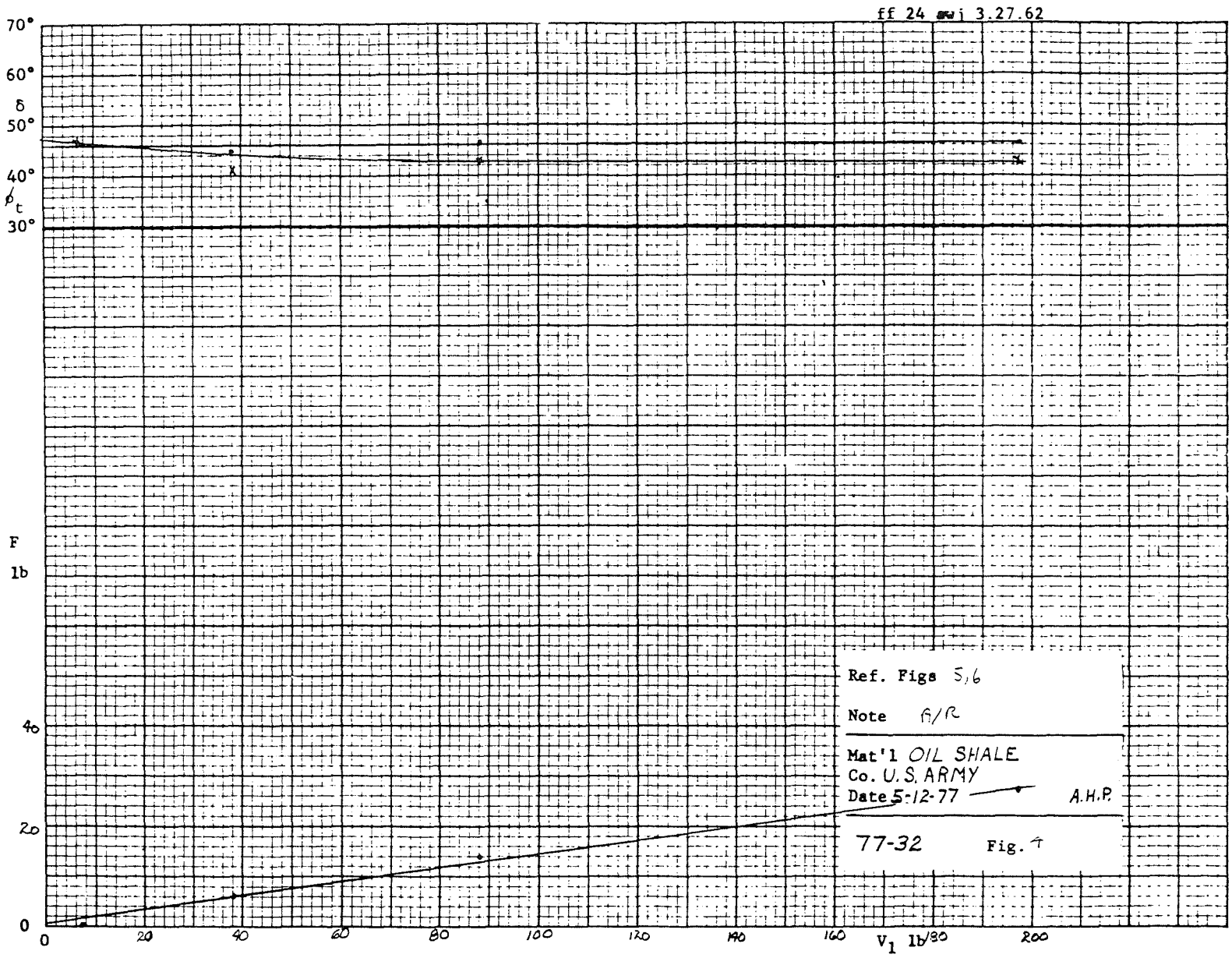
ff 24 ewj 3.27.62
70°
60°
δ
50°
40°
ϕ_t
30°
F
lb
40
20
0
0
20
40
60
80
100
120
140
160
200
V_1 lb/sec
Ref. Figs 5,6
Note A/R
Mat'l OIL SHALE
Co. U.S. ARMY
Date 5-12-77
A.H.P.
77-32
Fig. 4

yl 48 awj 3.27.62

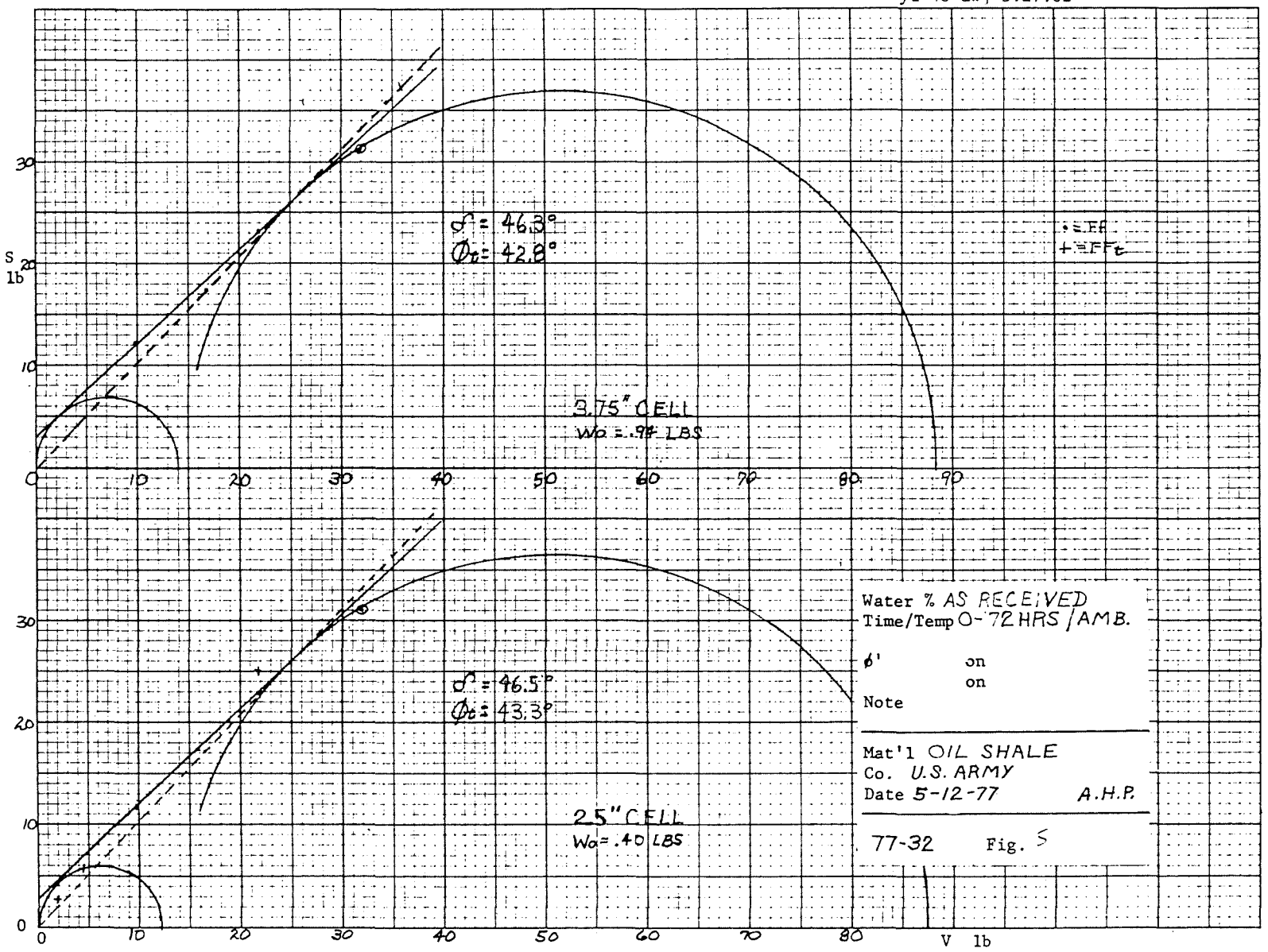

yl 48 awj 3.27.62

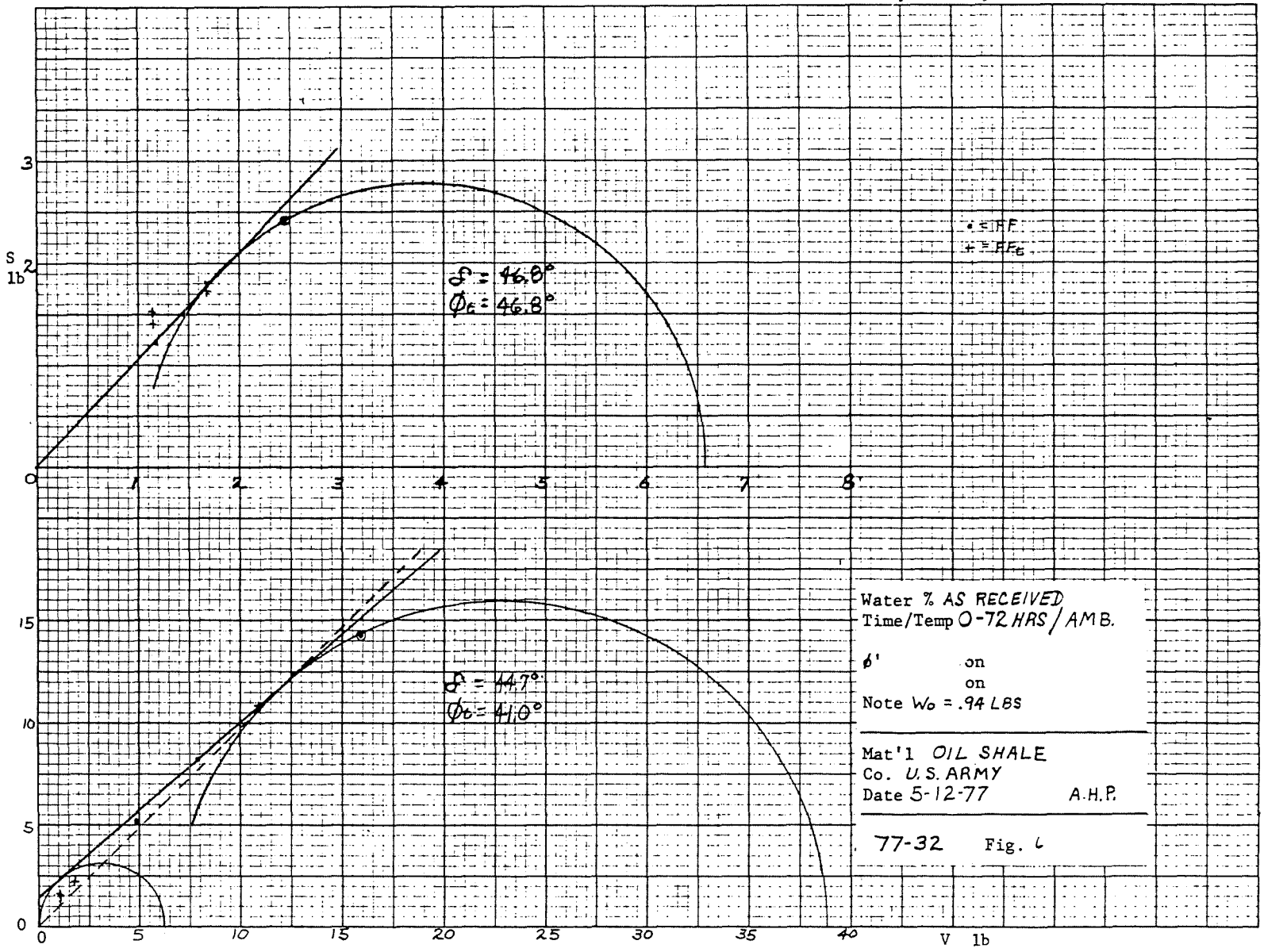

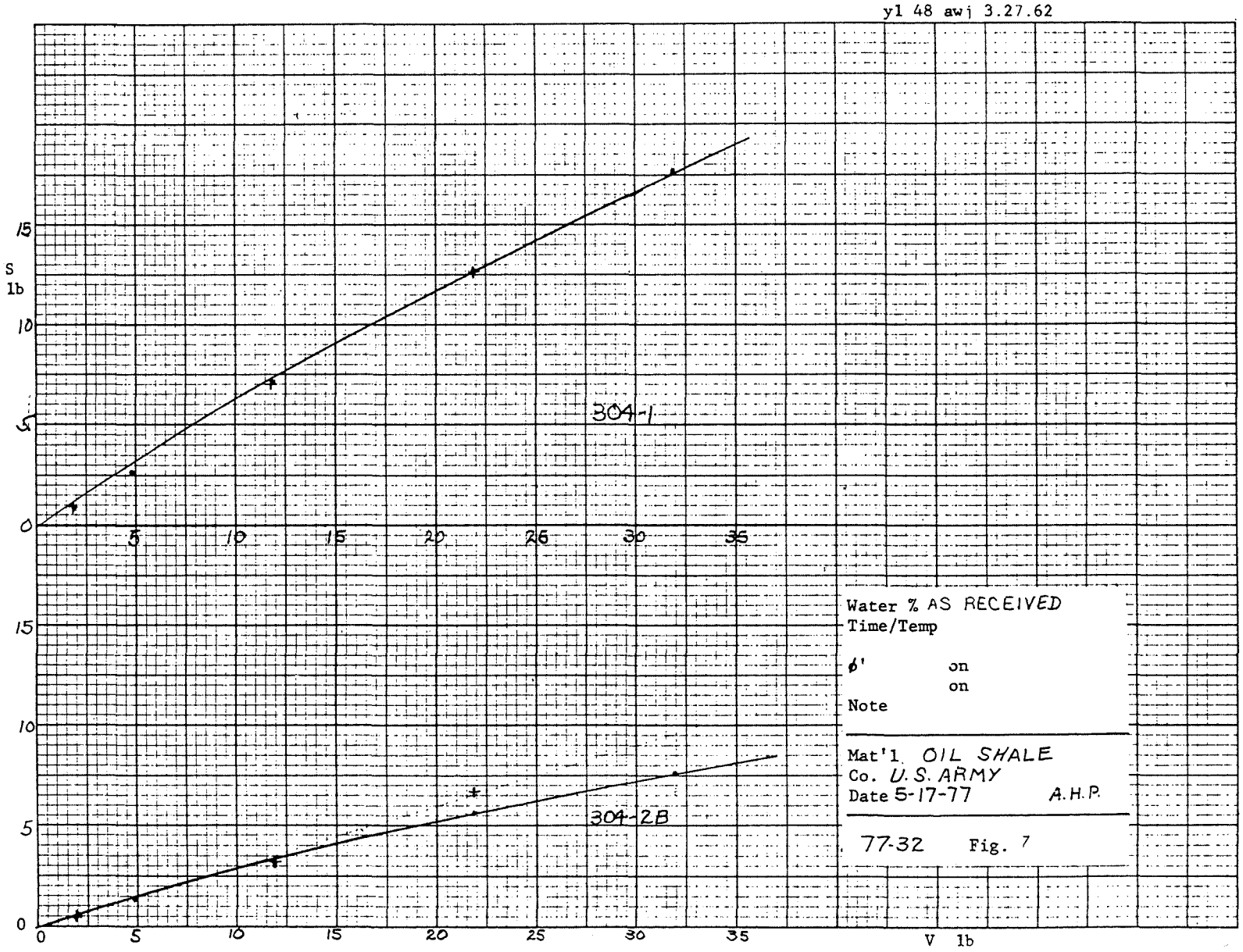
yl 48 awj 3.27.62
S
lb
15
10
5
0
304-1
304-2B
0
5
10
15
20
25
30
35
V lb
Water % AS RECEIVED
Time/Temp
ϕ' on
on
Note
Mat'l. OIL SHALE
Co. U.S. ARMY
Date 5-17-77 A.H.P.
77-32 Fig. 7

70°
60°
δ
50°
40°
ϕ_t
30°
F
lb
0
10
20
30
40
50
60
70
80
V_1 lb
Ref. Figs 9, 10
Note 3.9 gm H2O
Mat'l OIL SHALE
Co. U.S. ARMY
Date 5-12-77
A.H.P.
77-32
Fig. 8

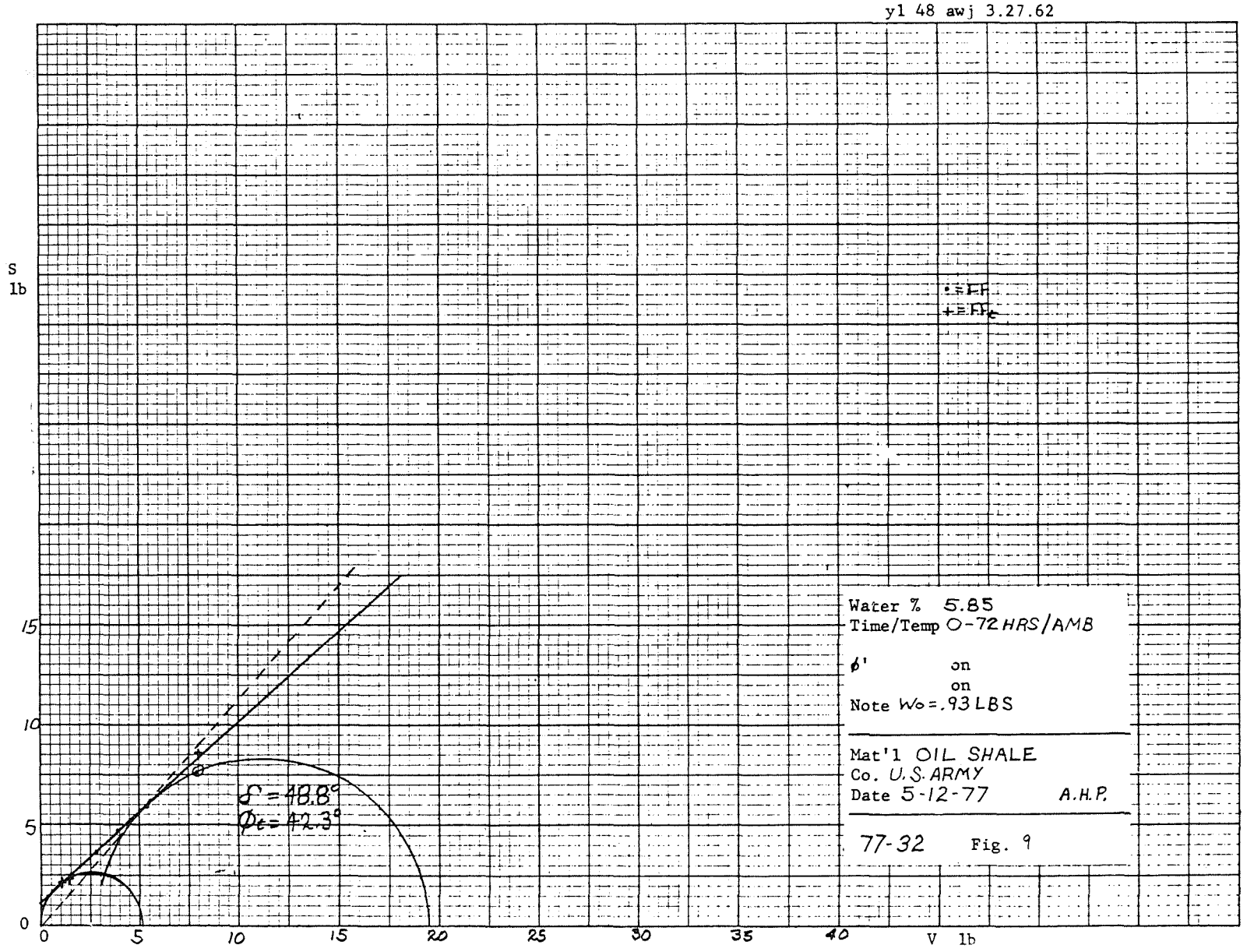
y1 48 awj 3.27.62
S
lb
0
5
10
15
0
5
10
15
20
25
30
35
40
V lb
δ = 48.8°
Øt = 42.3°
Water % 5.85
Time/Temp O-72 HRS/AMB
ø' on
on
Note Wo = .93 LBS
Mat'l OIL SHALE
Co. U.S. ARMY
Date 5-12-77 A.H.P.
77-32 Fig. 9

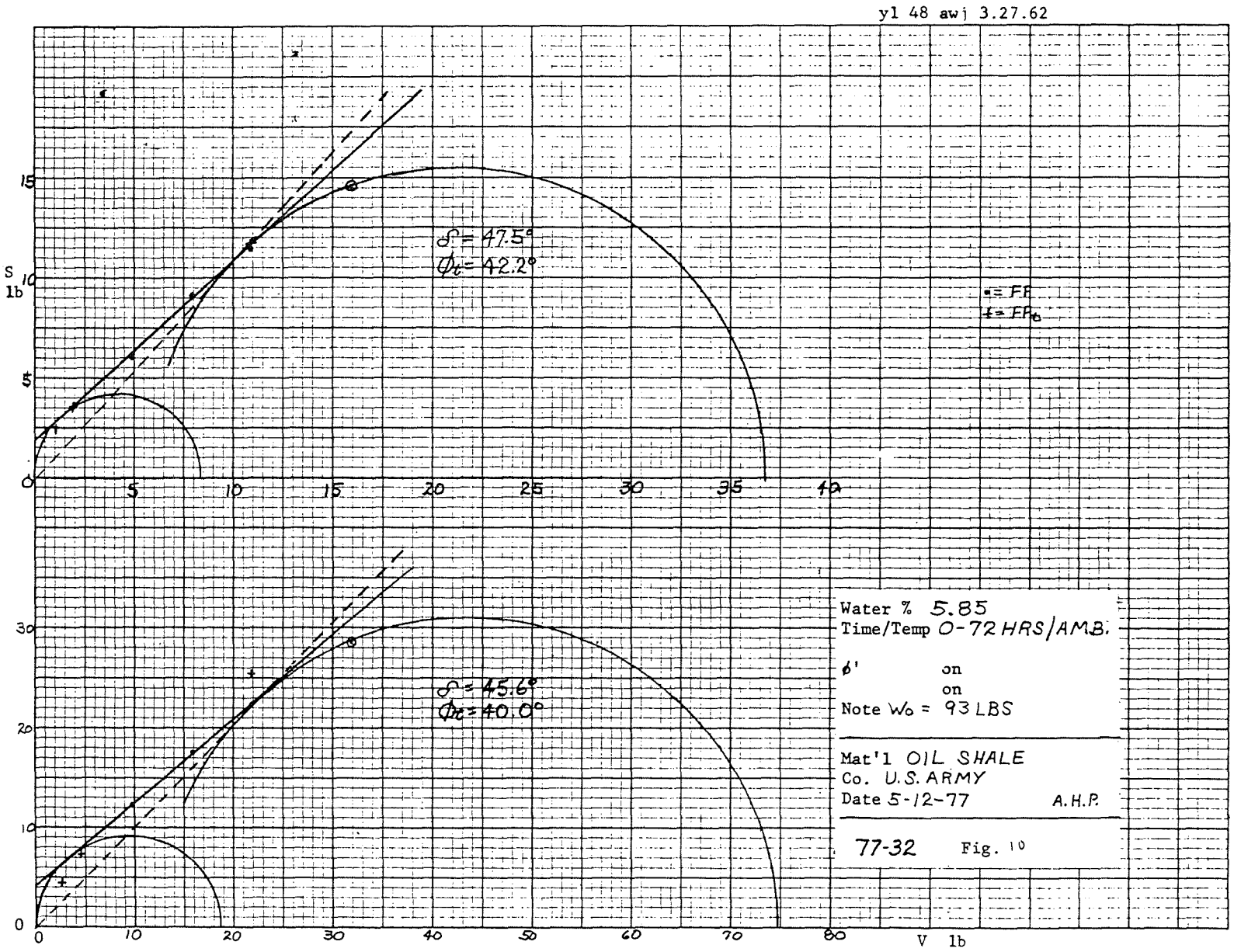
yl 48 awj 3.27.62
S lb
V lb
0
5
10
15
20
25
30
35
40
45
50
60
70
80
$\delta = 47.5°$
$\phi_t = 42.2°$
$\delta = 45.6°$
$\phi_t = 40.0°$
• = FF
+ = FF$_0$
Water % 5.85
Time/Temp O-72 HRS/AMB.
ϕ' on
on
Note W_o = 93 LBS
Mat'l OIL SHALE
Co. U.S. ARMY
Date 5-12-77 A.H.P.
77-32 Fig. 10

yl 48 awj 3.27.62

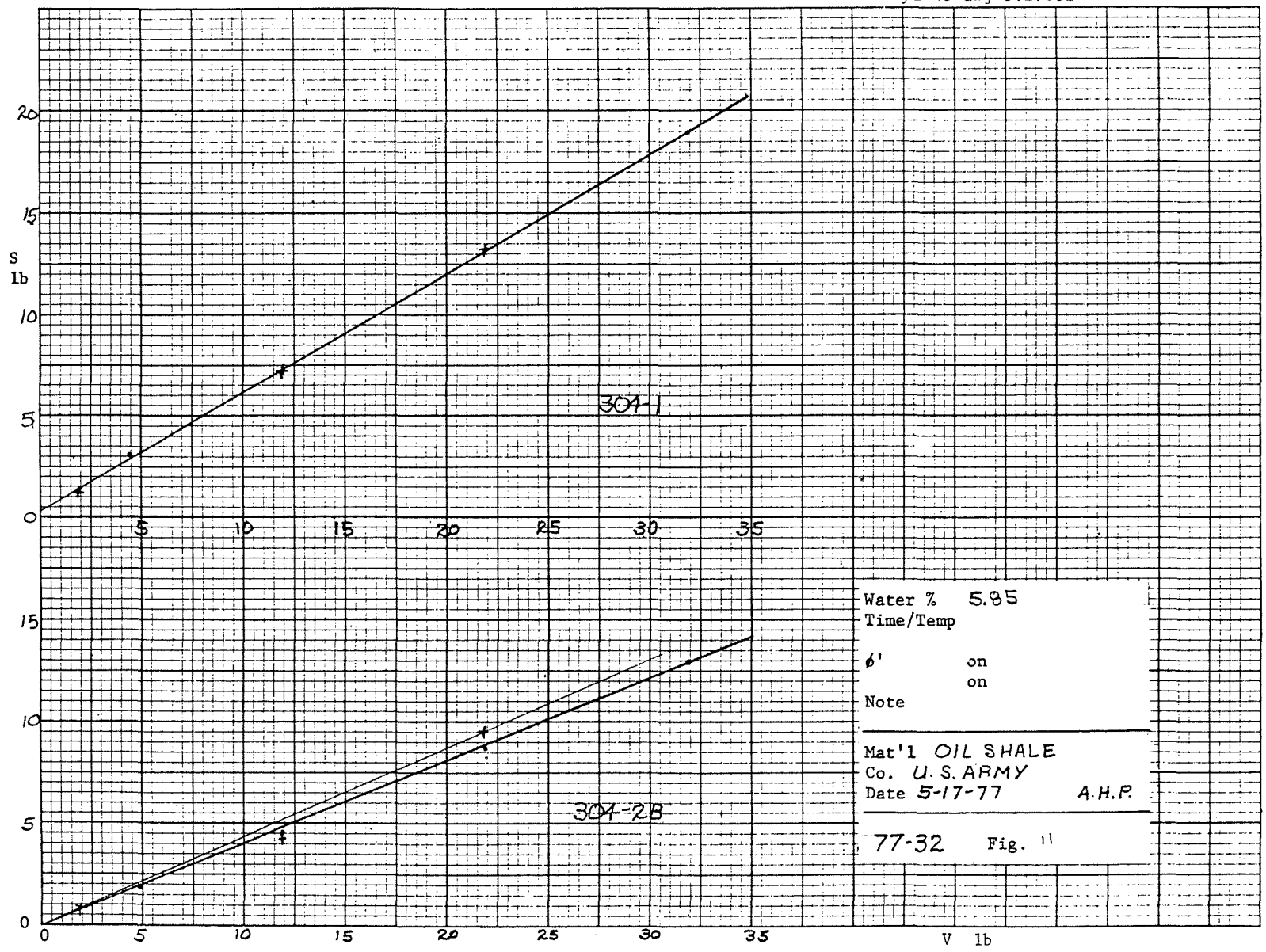

70°
60°
δ
50°
40°
ϕ_t
30°
F
lb
0
10
20
30
40
50
60
70
80
V_1 lb
Ref. Figs 13, 14
Note 10.7% H_2O
Mat'l OIL SHALE
Co. U.S. ARMY
Date 5-13-77
A.H.P.
77-32
Fig. 12

yl 48 awj 3.27.62

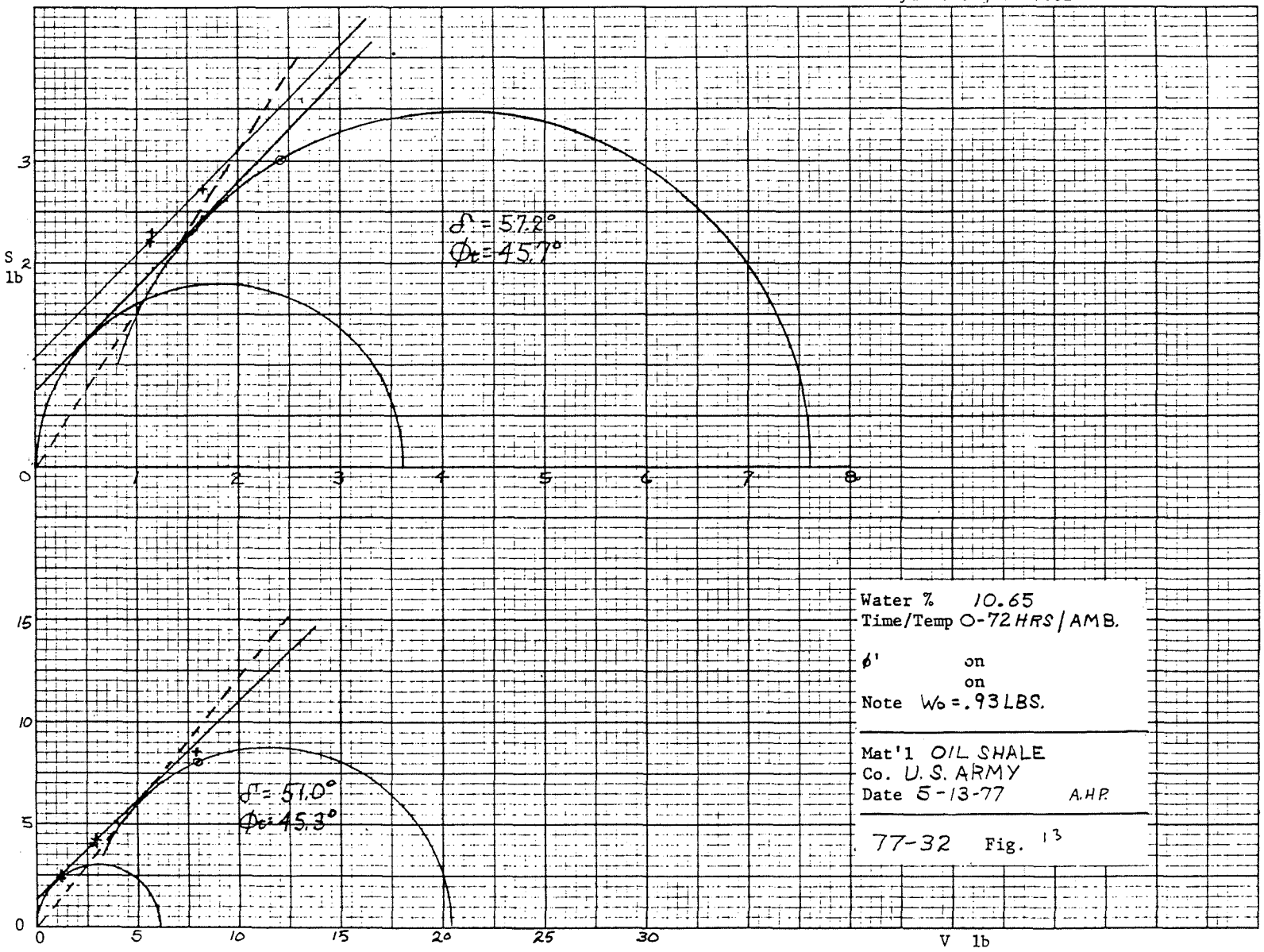

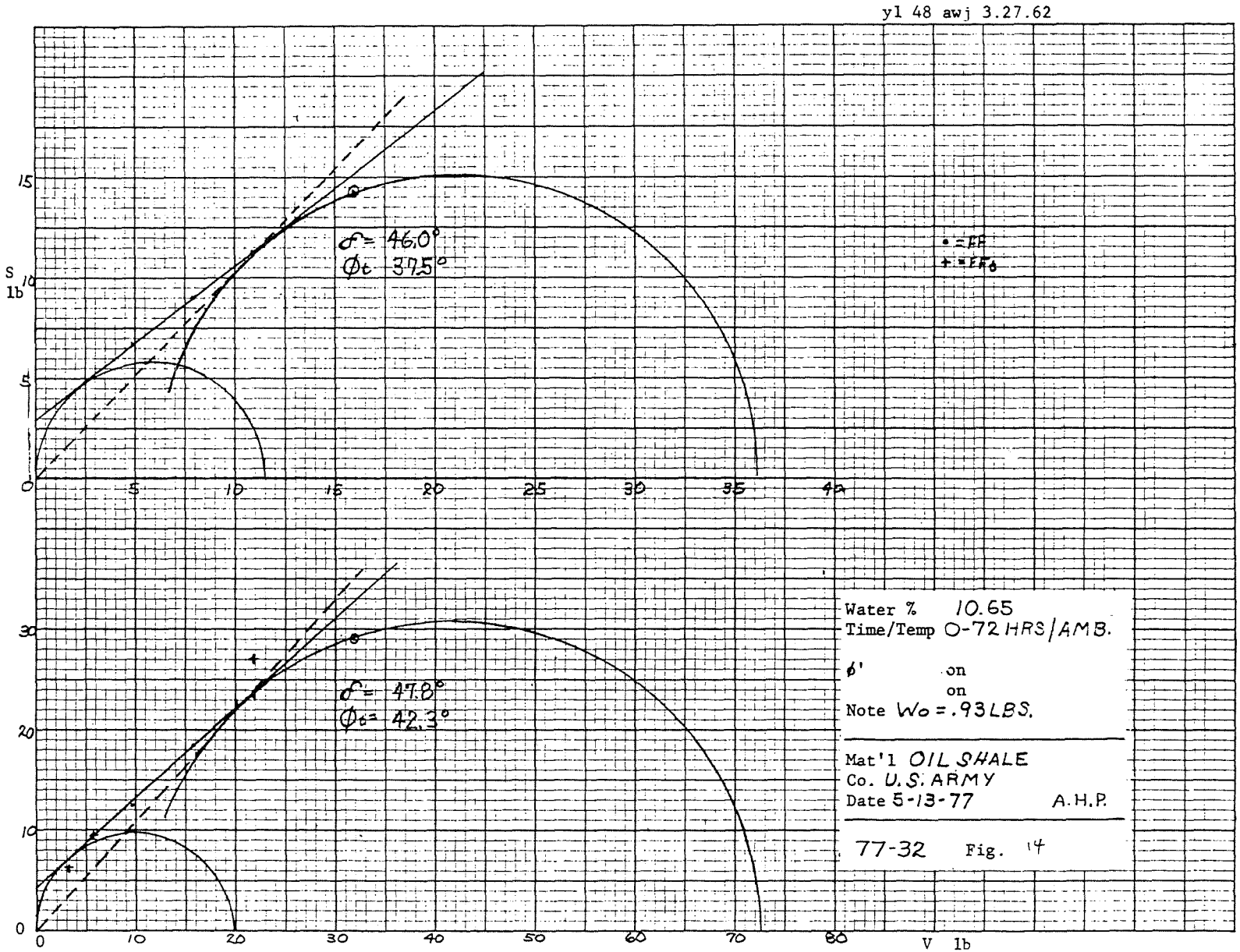
yl 48 awj 3.27.62
S lb
V lb
δ= 46.0°
φc 37.5°
• = FF
+ = FRφ
δ= 47.8°
φc= 42.3°
Water % 10.65
Time/Temp 0-72 HRS/AMB.
φ' on
on
Note Wo = .93 LBS.
Mat'l OIL SHALE
Co. U.S. ARMY
Date 5-13-77 A.H.P.
77-32 Fig. 14

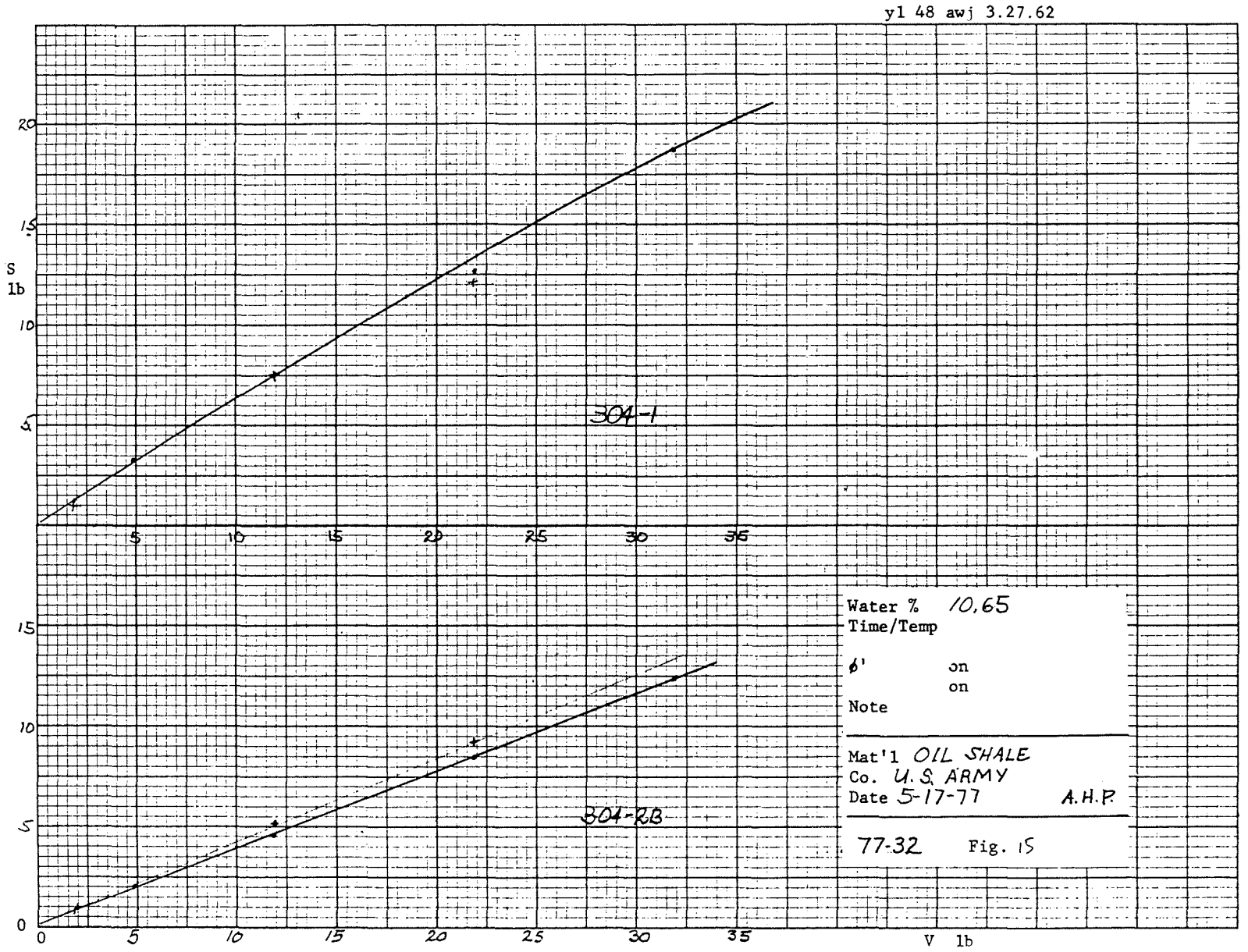
yl 48 awj 3.27.62
S
lb
20
15
10
5
0
5
10
15
20
25
30
35
V lb
304-1
304-2B
Water % 10,65
Time/Temp
ϕ' on
on
Note
Mat'l OIL SHALE
Co. U.S. ARMY
Date 5-17-77 A.H.P.
77-32 Fig. 15

12 August 1977

RECOMMENDATIONS FOR RAW OIL SHALE STORAGE BINS

U. S. ARMY

Introduction

The U. S. Army Waterways Experiment Station has been working with the Bureau of Mines in developing design data for an oil shale processing facility. One aspect of the problem is to design bins and feeders to store up to 25,000 tons of raw shale and feed it reliably to a retort at a rate up to 700 tons/hr.

Jenike & Johanson, Inc. has been asked to test a sample of raw shale at several moisture contents and to recommend bins and feeders for reliable flow.

Material properties

A sample of - 8 mesh shale was tested at ambient temperature for continuous flow and for flow after three days storage at rest at three moisture contents: "as received" (1%), 5.9%, and 10.7%. In addition, compressibility, wall friction, and flow rate tests were also run. Results are shown in Jenike & Johanson, Inc. Standard Test Report #77 - 32.

Up to 10.7% moisture, the material has a maximum critical outlet width in a mass flow bin of 0.8'. Funnel flow bins are not recommended because of the large stable ratholes which shale is capable of forming. Stainless steel is recommended for hopper walls in order to be assured of developing mass flow and to have a surface which will not deteriorate with time.

Recommendations

Bin and feeder design

Because of the volume of material which is to be stored, two bin designs are considered. One, shown in Fig. 1, has a capacity of approximately 26,000 cu.ft. Three such units are required for the storage of the total required volume. The other, shown in Fig. 2, is capable of storing the entire 25,000 tons in one bin.

Whichever bin is used, the design of the belt feeder and interface between the feeder and the bin will be the same. Details of these items are shown in Fig. 3.

Feeder loads

The force on that portion of the belt feeder which is under the bin can be resolved into a normal (vertical) and shear (horizontal) component:

normal load	650 F + 800 lb
shear load	500 F lb

where F is a dimensionless multiplier depending on flow conditions in the hopper.

When the feeder is running, F = 1.0. These loads will not change significantly if the feeder is restarted after it has been running or if the bin is refilled provided at least a 5 ft head of material is left in the bin before refilling.

Considerably larger loads may occur when the feeder is started after the bin has been filled from empty with the feeder stopped. These larger loads are due to the difference in deflection between the feeder and hopper outlet, the initial stress field in the solid, and the expansion of material which accompanies the initiation of a shear plane.

There are several ways to minimize these overloads. Running the feeder - even at a slow rate - while the bin is being filled is the most effective. For this condition we recommend F = 1.3 for initial starting loads. If the feeder is suspended from the lower portion of the hopper so that the two deflect in unison and the feeder is stopped during filling, use F = 2.5 for initial starting loads. And, finally, providing elastic supports under the feeder will reduce F to approximately 1.5 for initial starting loads, provided these supports maintain the feeder in its proper position when running (F = 1) but deflect 1¼" when an additional load of 900 lb is applied. This can also be accomplished by mounting the feeder on hydraulic or pneumatic cylinders which are designed to hold the feeder in its normal vertical position. If starting problems occur, the pressure in the cylinders is reduced and the feeder is lowered 1¼". As soon as the feeder is running, the feeder is raised to its usual normal position.

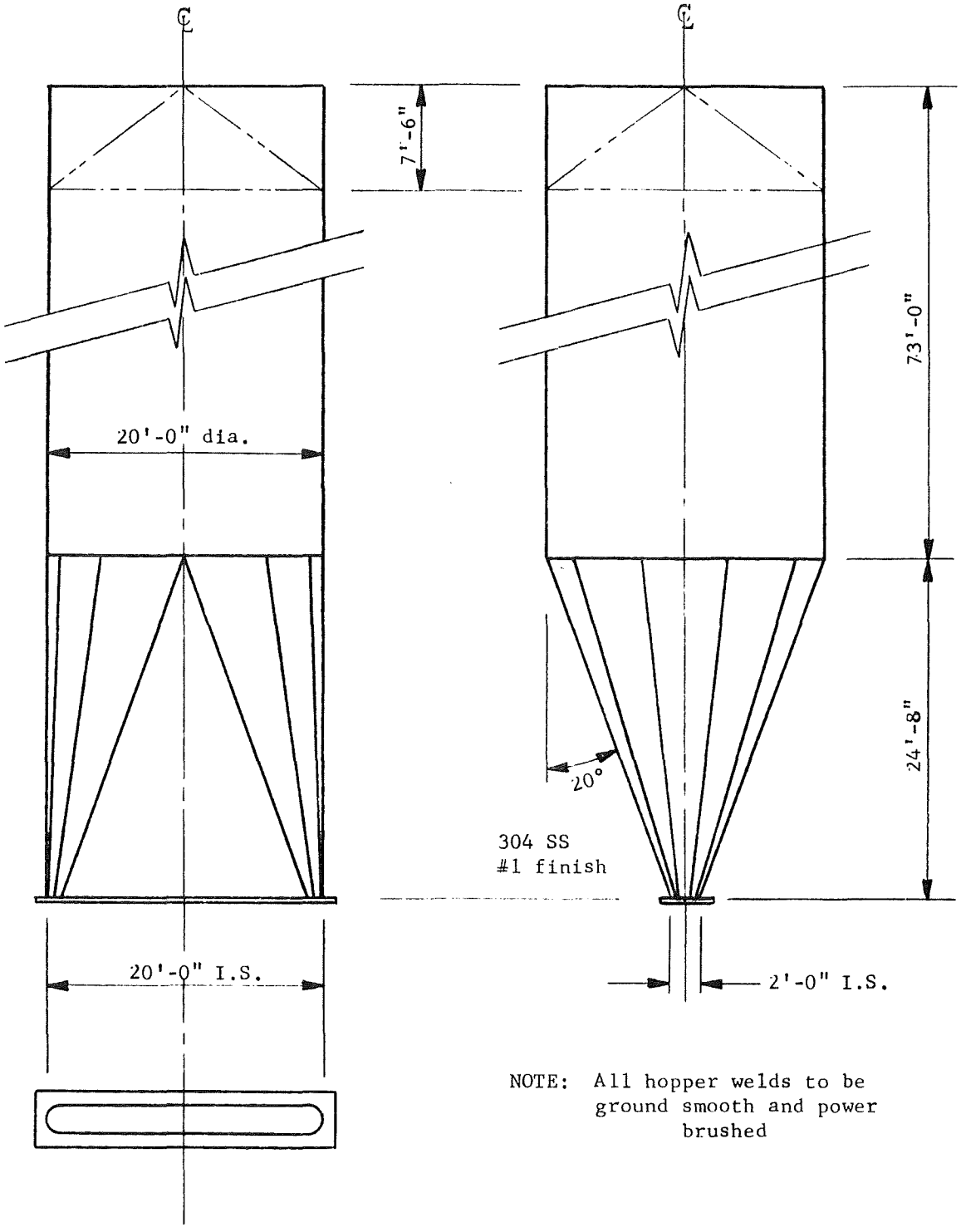

Fig. 1 Bin Design for 26,000 cu.ft Capacity

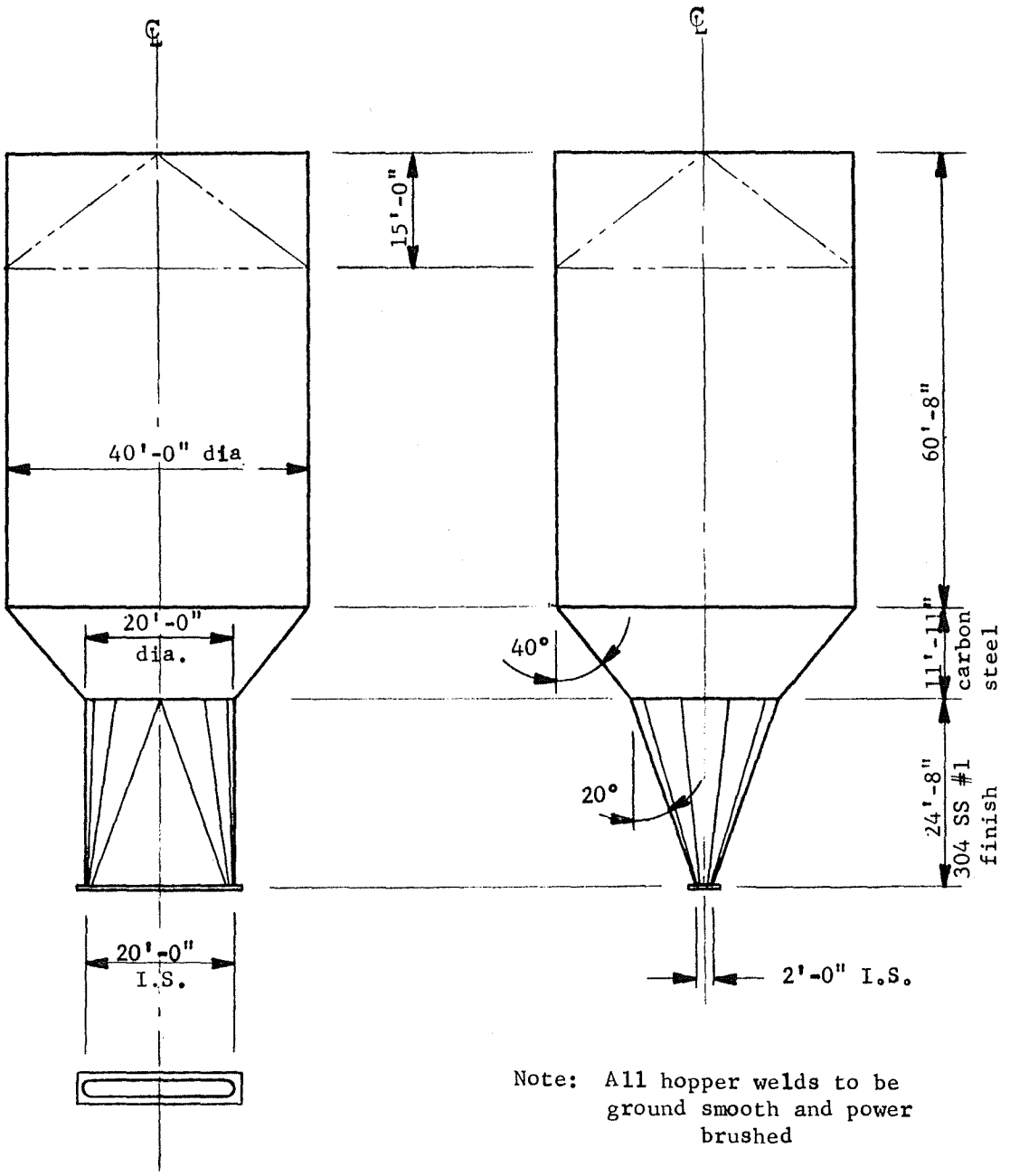

Fig. 2 Bin Design for 78,000 cu.ft capacity

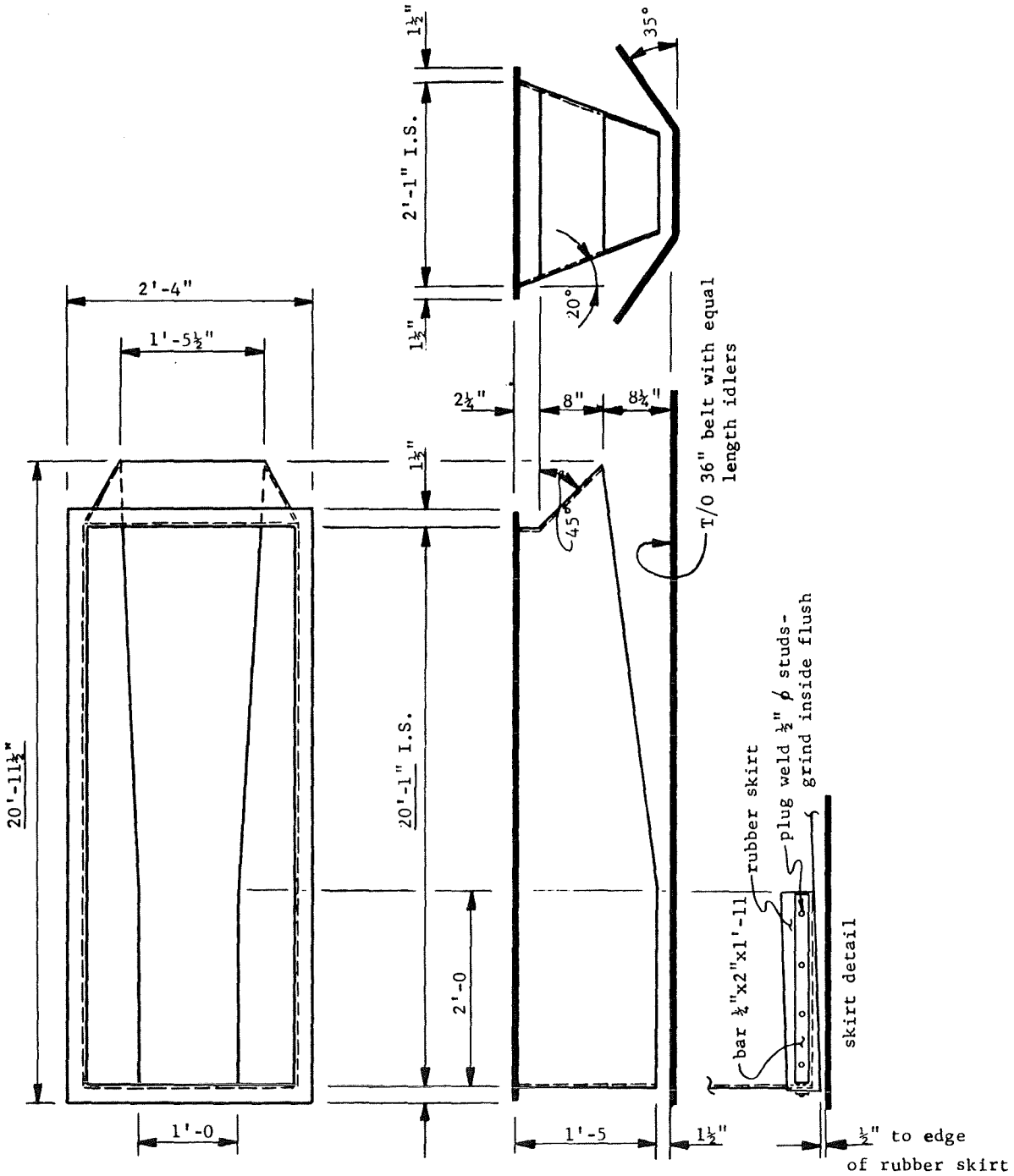

Fig. 3 Recommended Interface with Belt Feeder

APPENDIX C: SETTLEMENT-LOG TIME CONSOLIDATION-REBOUND CURVES FOR PARAHO AND TOSCO

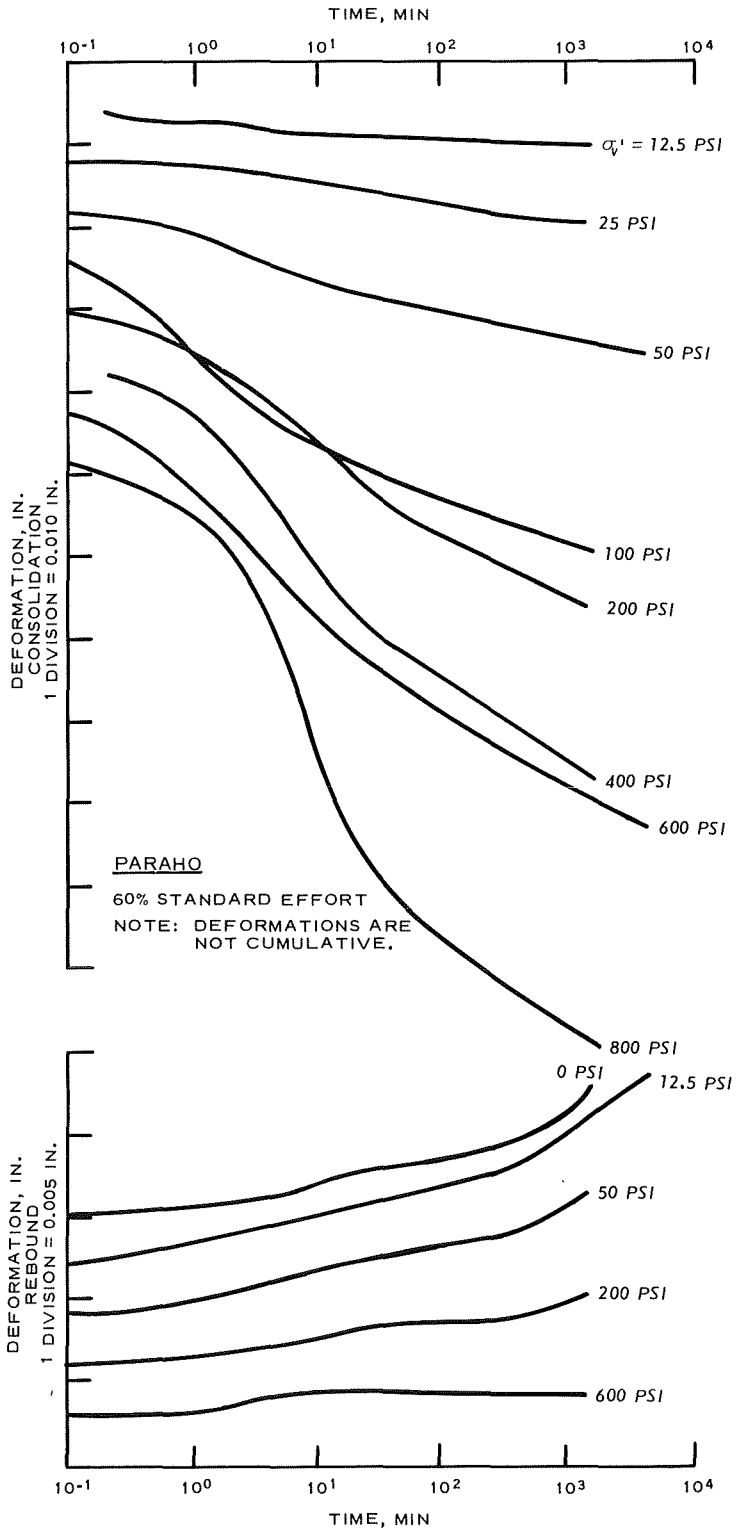

Figure C-1. Time-settlement relationships for consolidation tests on PARAHO compacted to 60 percent of standard effort

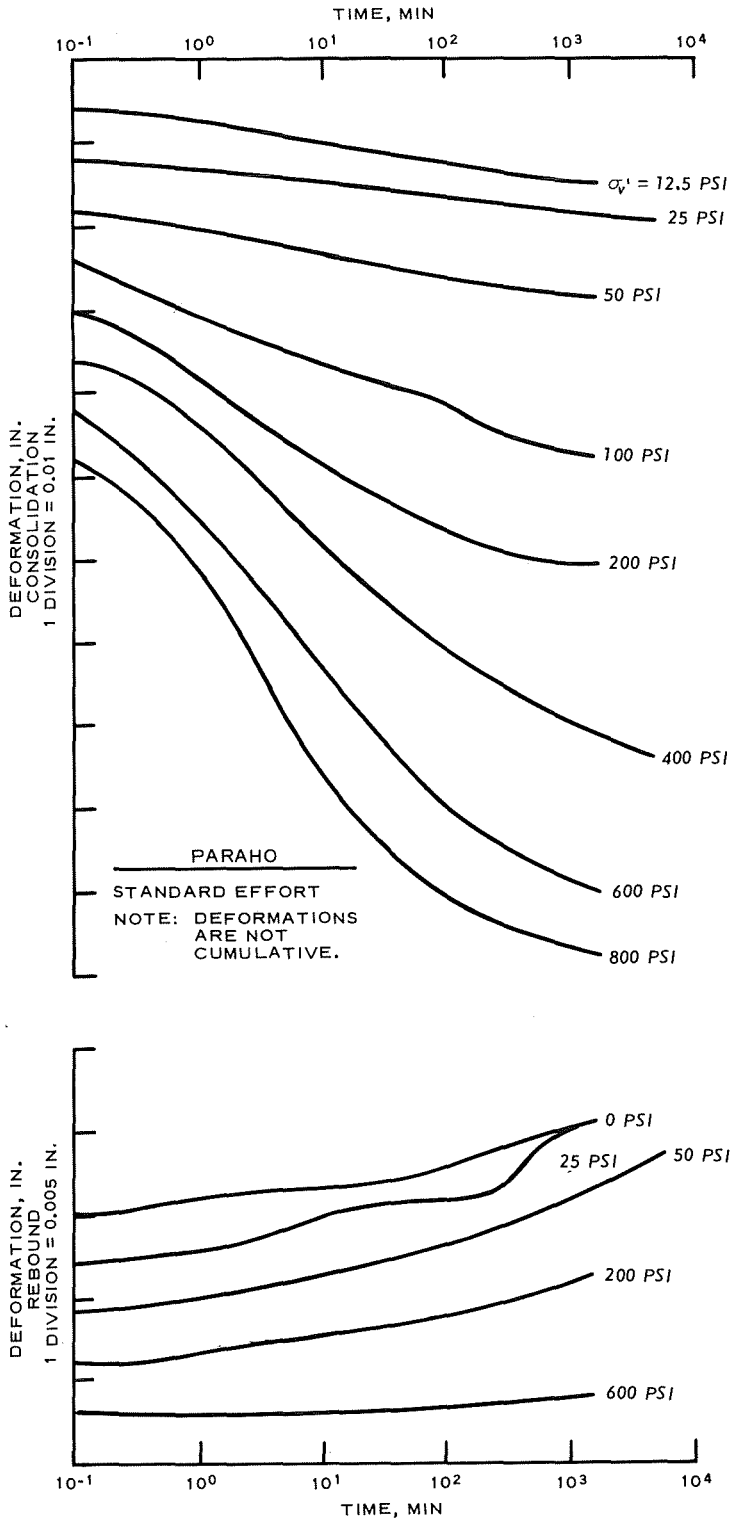

Figure C-2. Time-settlement relationships for consolidated tests on PARAHO compacted to standard effort

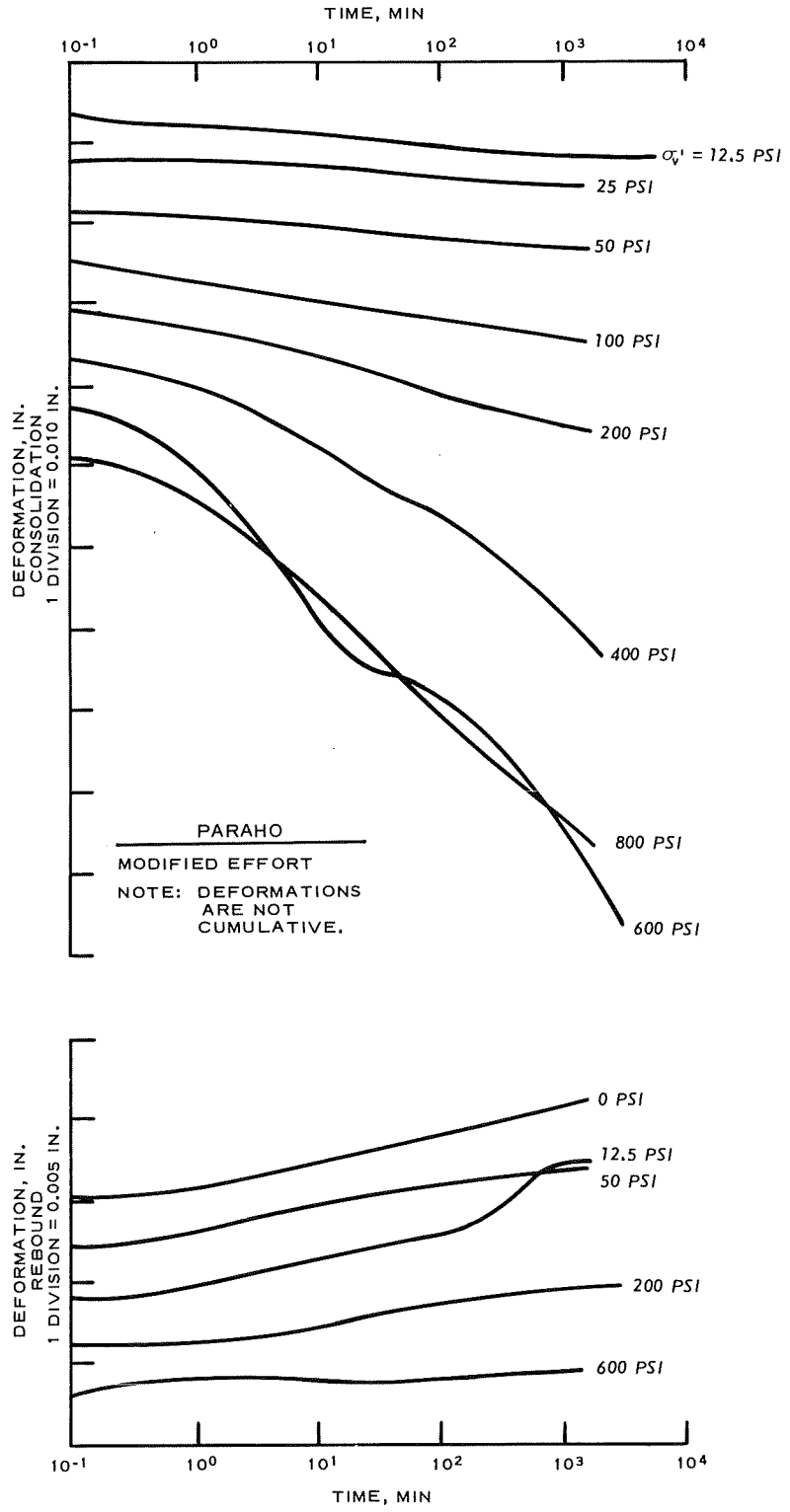

Figure C-3. Time-settlement relationships for consolidated tests on PARAHO compacted to modified effort

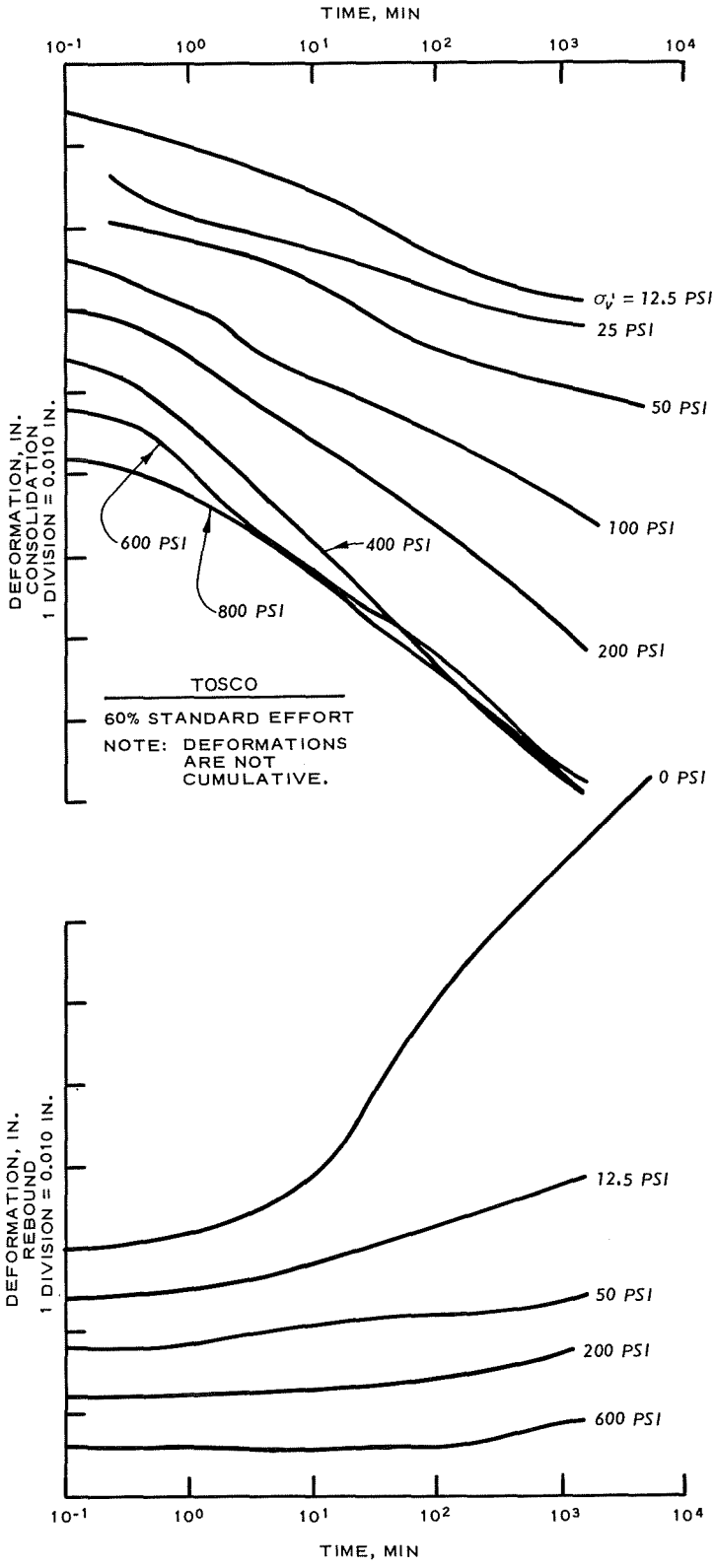

Figure C-4. Time-settlement relationships for consolidation tests on TOSCO compacted to 60 percent of standard effort

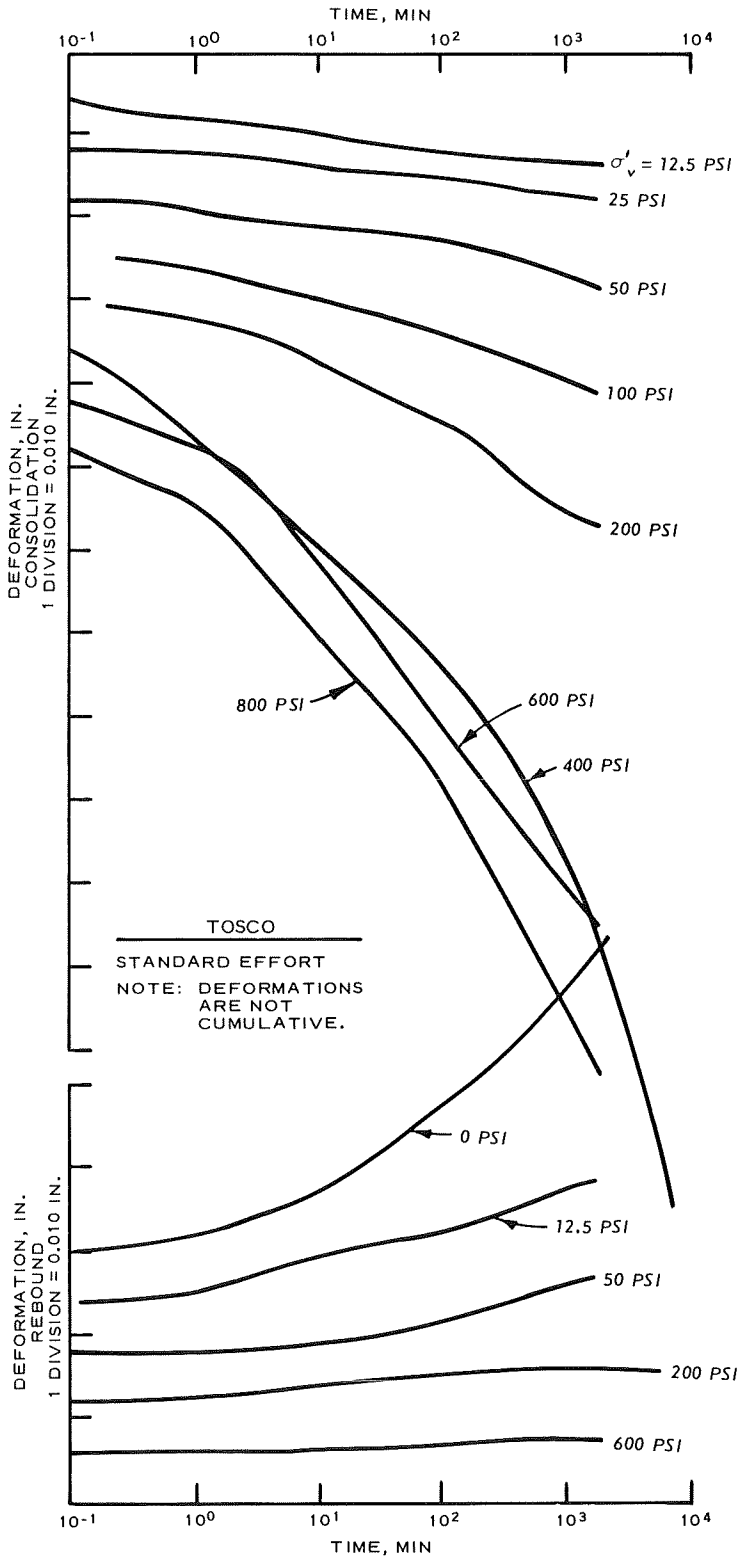

Figure C-5. Time-settlement relationships for consolidated tests on TOSCO compacted to standard effort

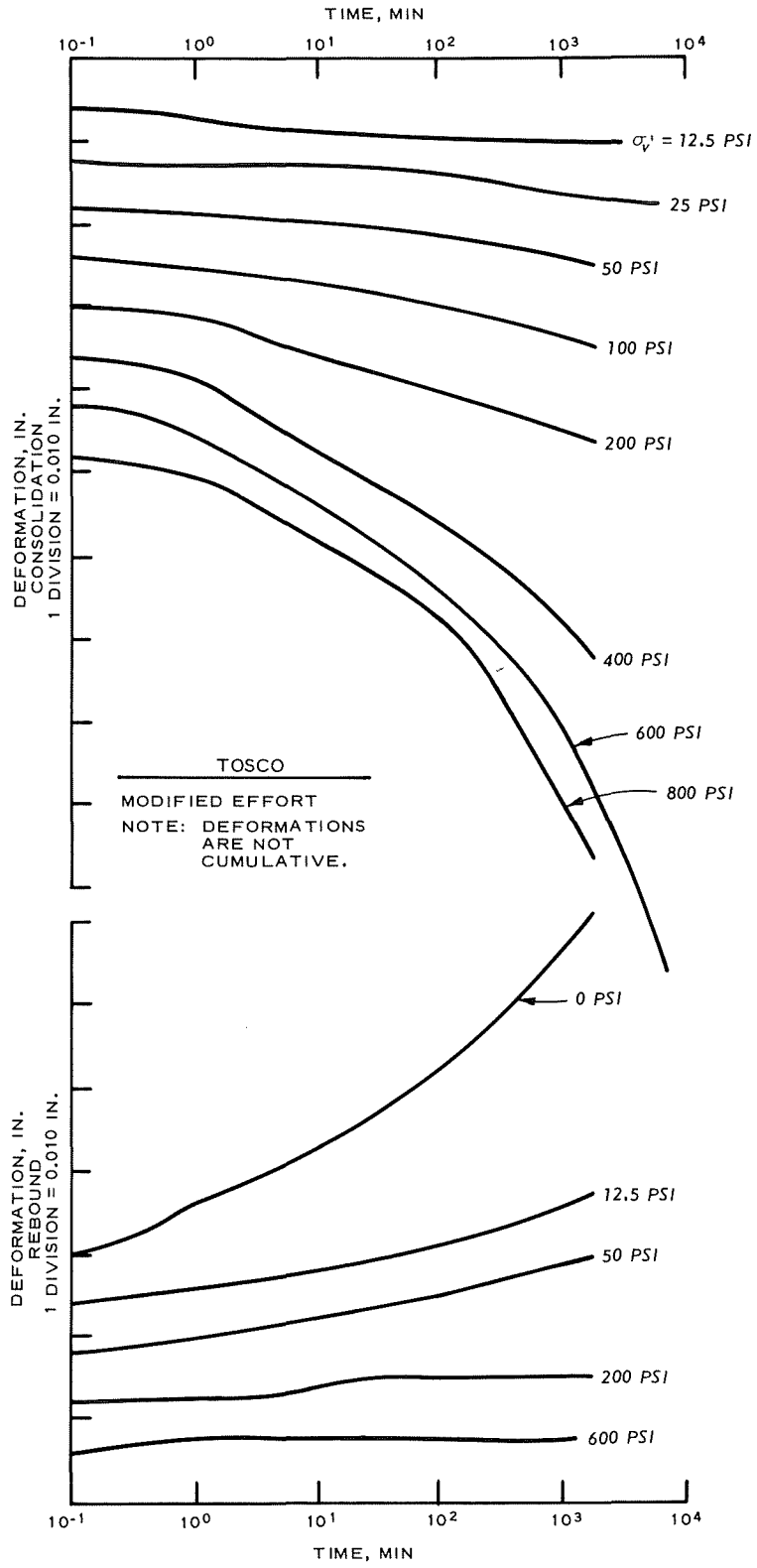

Figure C-6. Time-settlement relationships for consolidated tests on TOSCO compacted to modified effort

APPENDIX D: CONVERSION FACTORS, U. S. CUSTOMARY TO METRIC (SI) UNITS OF MEASUREMENT

U. S. customary units of measurement used in this report can be converted to metric (SI) units as follows:

Multiply	By	To Obtain
cubic feet	0.02831685	cubic metres
cubic yards	0.7645549	cubic metres
Fahrenheit degrees	5/9	Celsius degrees or Kelvins*
feet	0.3048	metres
foot-pounds (force)	1.355818	joules
gallons (U. S. liquid)	3.785412	cubic decimetres
inches	25.4	millimetres
pounds (force) per square foot	47.88026	pascals
pounds (force) per square inch	6894.757	pascals
pounds (mass)	0.4535924	kilograms
pounds (mass) per cubic foot	16.01846	kilograms per cubic metre
square feet	0.09290304	square metres
tons (2000 lb, mass)	907.1847	kilograms
tons (force) per square foot	95.76052	kilopascals

* To obtain Celsius (C) temperature readings from Fahrenheit (F) readings, use the following formula: $C = (5/9)(F - 32)$. To obtain Kelvin (K) readings, use: $K = (5/9)(F - 32) + 273.15$.

APPENDIX E: NOTATION

a_v	Coefficient of compressibility
B	Breakage factor; pore pressure parameter, $\Delta u/\Delta\sigma_3$
c, c'	Cohesion and effective cohesion, respectively
C_c	Compression index
C_u	Uniformity coefficient
C_v	Coefficient of consolidation
D	Constrained modulus
D_r	Relative density
e	Void ratio
E	Young's modulus
E_d	Young's modulus under K_o conditions
G	Shear modulus
G_a	Apparent specific gravity plus No. 4 fraction
G_s	Specific gravity of solids
k	Coefficient of permeability
K_o	Coefficient of earth pressure at rest, under conditions of lateral restraint, σ_3/σ_1
NP	Nonplastic
P	Pressure
PI	Plasticity index
$\bar{R}$	Consolidated-undrained tests with pore pressure measurements
S	Consolidated-drained tests
$u-u_o$	Induced pore pressure
w	Water content
w_{opt}	Optimum water content
γ	Shear strain
γ_d	Dry density
ε_a	Axial strain
ε_1, ε_3	Axial and radial strain, respectively
λ	Damping ratio
ν	Poisson's ratio
σ_{dc}	Cyclic deviator stress
σ_{ff}	Normal stress on failure plane
σ_n	Normal stress

$\bar{\sigma}_1$, σ_3	Major (overburden pressure) and minor principal stress, respectively
τ	Shear stress
τ_{ff}	Shear stress on failure plane
ϕ, ϕ'	Angle of internal friction and effective angle of internal friction, respectively

In accordance with letter from DAEN-RDC, DAEN-ASI dated 22 July 1977, Subject: Facsimile Catalog Cards for Laboratory Technical Publications, a facsimile catalog card in Library of Congress MARC format is reproduced below.

Townsend, Frank C
Geotechnical properties of oil shale retorted by the PARAHO and TOSCO processes / by Frank C. Townsend, Richard W. Peterson. Vicksburg, Miss. : U. S. Waterways Experiment Station ; Springfield, Va. : available from National Technical Information Service, 1979.
271 p. : ill. ; 27 cm. (Technical report - U. S. Army Engineer Waterways Experiment Station; GL-79-22)
Prepared for U. S. Department of the Interior, Bureau of Mines, Spokane Mining Research Center, Spokane, Wash., under Contract No. H0262064.
Includes bibliographies.

1. Compaction. 2. Compositions. 3. Consolidation. 4. Geotechnical engineering. 5. Oil shales. 6. Shear strength. I. Peterson, Richard W., joint author. II. United States. Bureau of Mines. Spokane Mining Research Center. III. Series: United States. Waterways Experiment Station, Vicksburg, Miss. Technical report ; GL-79-22.
TA7.W34 no.GL-79-22